Long-Term Evolution of High Earth Orbits: Effects of Direct Solar Radiation Pressure and Comparison of Trajectory Propagators

by

L. Anselmo and C. Pardini

(Luciano.Anselmo@isti.cnr.it & Carmen.Pardini@isti.cnr.it)

Technical Report

29 March 2007

Space Flight Dynamics Laboratory
Istituto di Scienza e Tecnologie dell'Informazione "A. Faedo"
CNR – Area della Ricerca di Pisa
Via G. Moruzzi 1, 56124 Pisa, Italy

TABLE OF CONTENTS

ABSTRACT

The recent observational discovery, in high Earth trajectories (for the most part in geosynchronous orbits), of artificial objects with extremely large area-to-mass ratios (up to ~ 25 m^2/kg) stimulated the revisit of direct solar radiation pressure models, in order to assess their long-term performances in such extreme situations. For this purpose, a comprehensive set of simulations and comparisons was carried out, mainly focusing the attention on the long-term evolution of objects characterized by high area-to-mass ratios in geosynchronous, GPS, Molniya and geosynchronous transfer orbits.

The topics specifically addressed in the study were the following: comparison of direct solar radiation pressure approximations and effects of the varying Sun-Earth distance (Section 2); comparison of several trajectory propagators (Section 2); dynamical effects of the Earth's shadow (Section 3); comparison of the relative importance of the relevant perturbations in geosynchronous orbit (Section 4).

1. INTRODUCTION

1.1 Study Outline

For objects in high Earth orbits, the perturbing acceleration due to direct solar radiation pressure cannot be ignored, in particular when the area-to-mass ratio (*A*/*M*) is relatively large and the trajectory evolution is investigated over several years, or more. In order to determine the relative performances and the accuracy of various orbit propagators available at ISTI/CNR, a comprehensive set of comparisons was carried out, mainly focusing the attention on the long-term evolution of objects with high area-to-mass ratios. In this way, the properties and the effects of direct solar radiation pressure modeling were more evident.

The following orbit propagators were used and compared: ASAP, LEGO, LOP, SATORB, SATRAP and WB1/COWELL. ASAP [1], SATORB [2], SATRAP [3] and WB1/COWELL [4] [5] are special perturbations propagators using high accuracy numerical integrators. Their force models include geopotential harmonics, luni-solar third body attraction, direct solar radiation pressure with eclipses and air drag, if applicable.

LEGO is a very fast ESA/ESOC software tool, based on the analytic theory developed by J.C. Van Der Ha [6]. It includes the main terms of the geopotential, luni-solar effects and solar radiation pressure. However, it is only applicable to the geosynchronous and near-geosynchronous orbital regimes.

LOP [7], finally, is a long-term orbit predictor based on the integration of the Lagrange's planetary equations. It uses the variation of parameters method in the formulation of the equations of motion. The perturbations taken into account are: the Earth's geopotential, the third body attraction of the Moon and the Sun, the air drag (when applicable) and the solar radiation pressure, including the eclipses. To expedite the computations, the terms including the mean anomaly (fast variable) are removed in the Earth's and third-body potentials before numerical integration (singly averaged method). On the other hand, when resonances occur between the orbital period and the Earth rotation, the terms containing the mean anomaly in the tesseral harmonics of the geopotential are retained, giving rise to resonant effects. To average the potential due to solar radiation pressure and air drag, a standard 8^{th} order Gaussian quadrature method is used. The resulting averaged equations are integrated numerically using a multi-step, variable step-size and variable order method. The computation time is maintained under control, without compromising the accuracy, due to the elimination of the fast variable and the possibility to use large step sizes (days).

In addition to the comparison of the propagators, the effects and the relative importance of the various perturbations was investigated. Concerning direct solar radiation pressure, the impact of different model options and Earth's shadowing was assessed as well. When needed, air drag was modeled with a simple exponential atmospheric density model, with the parameters

shown in Table 1.1.

Table 1.1

Parameters of the Exponential Atmospheric Density Model and Drag Perturbation

Termospheric Density Model	Jacchia-71
Exospheric Temperature	1000 K
Reference Altitude for Air Density	400 km
Scale Height of Air Density	55.92 km
Air Density at Reference Altitude	3.11 x 10^{-3} kg/km^3
Maximum Altitude to Include Drag	1000 km
Drag Coefficient	2.2

Concerning the geopotential, in general gravity harmonics up to the 8th degree and order were included, but LOP considered only the resonant tesserals and the resonance effects.

1.2 Solar Radiation Pressure Modeling

The perturbing acceleration of an Earth satellite due to direct solar radiation pressure is given by [2]:

$$\ddot{\vec{r}} = C_r P_s \frac{A}{M}\left[\frac{AU}{r_v}\right]^2 \frac{\vec{r}_v}{r_v}, \tag{1.1}$$

where $\vec{r}$ is the satellite position vector in the geocentric reference frame, A is the average satellite projected area in the Sun direction, M is the satellite mass, P_s is the radiation pressure (4.56316×10^{-6} N/m^2) on a perfectly absorbing surface at 1 astronomical unit (AU), $\vec{r}_v$ is the satellite position vector relative to the center of the Sun, r_v/AU represents the distance between the Sun and the satellite in astronomical units and C_r is a dimensionless radiation coefficient. C_r may vary between 0 and 2 ($C_r < 1$ for translucent materials; $C_r = 1$ for a perfectly absorbent material; $C_r = 2$ for a perfectly reflective material), but typically assumes values between 1 and 2. If $\vec{r}_s = \vec{r} - \vec{r}_v$ is the Sun position vector in the geocentric reference frame, then for orbiting objects it may be assumed that $\vec{r}_v \approx -\vec{r}_s$ ($r/r_v \approx 2.8 \times 10^{-4}$ for geosynchronous satellites and 1.8×10^{-4} for GPS satellites) and Eq. (1.1) becomes:

$$\ddot{\vec{r}} = -C_r P_s \frac{A}{M}\left[\frac{AU}{r_s}\right]^2 \frac{\vec{r}_s}{r_s}. \tag{1.2}$$

In this formulation of the radiation pressure acceleration, the satellite position coincides with the Earth center as seen from the Sun. A further simplification may be introduced, by

disregarding the small eccentricity of the Earth's orbit around the Sun (0.0167) and putting $r_s = 1\ AU$ in the $\left[AU/r_s\right]^2$ term:

$$\ddot{\vec{r}} = -C_r P_s \frac{A}{M} \frac{\vec{r}_s}{r_s}. \tag{1.3}$$

However, the correct evolution (i.e. including the small eccentricity of the Earth's orbit) of the Sun motion in the geocentric reference frame is retained in the computation of the running Earth-Sun direction ($\vec{r}_s / r_s$).

Concerning the modeling of the Sun eclipsed by the Earth as seen by the satellite, the following geometric conditions must be checked for shadowing [1]:

$$\vec{r} \cdot \vec{r}_s < 0 \tag{1.4}$$

and

$$r \sin\left[\cos^{-1}\left(\frac{\vec{r} \cdot \vec{r}_s}{r r_s} \right) \right] < R_a, \tag{1.5}$$

where R_a is the radius of the Earth plus the altitude of the obscuring atmosphere.

2. COMPARISON OF DIRECT SOLAR RADIATION PRESSURE MODELS

2.1 Comparison of Radiation Pressure Models in GEO

The aim of the analysis presented in this section was to compare the long-term evolution of geosynchronous orbits (GEO) predicted by various trajectory propagators with different models for the direct solar radiation pressure. The reference orbit adopted as initial conditions for the first set of computer runs is given in Table 2.1. The time span of the simulations was 100 years, C_r = 1 and A/M = 17 m^2/kg, in order to enhance the dynamical effects of solar radiation pressure.

Table 2.1

Initial Geosynchronous Orbit Used for the First Set of Runs

Epoch	2005.12.22 00:00 UTC
Orbital Elements	Mean Keplerian
Earth Centered Reference Frame	True of Date
Semimajor Axis	42164.465 km
Eccentricity	0.0001
Inclination	0.097 deg
Right Ascension of Ascending Node	50.00 deg
Argument of Perigee	220.00 deg
Mean Anomaly	301.22 deg

As benchmark cases, ASAP and SATRAP were used. The perturbations included were the geopotential, up to the 8th degree and order, luni-solar third body attraction and direct solar radiation pressure with eclipses. Both programs adopt a common core of force models and use the same special perturbations method for the integration of the equations of motion. Concerning the solar radiation pressure, however, ASAP adopts the simplified approach if Eq. (1.3) [1], while Eq. (1.2) was recently implemented in the last version of SATRAP.

As found by Stéphane Valk during a series of comprehensive orbital propagation comparisons between ISTI/CNR and the University of Namur, in Belgium, the adoption of Eq. (1.3), instead of Eq. (1.1) or (1.2), has a significant qualitative – and not only quantitative – effect on the long-term eccentricity evolution of high area-to-mass ratio objects in geosynchronous orbits [8]. This conclusion was immediately confirmed comparing ASAP with the last version of SATRAP, as shown in Figure 2.1 [9]. In addition, an impact, even though decidedly more limited, was found on the evolution of the inclination as well, as shown in Figure 2.2 [9]. Figure 2.3 presents, instead, the evolution of the semimajor axis.

The results obtained confirmed that the correct modeling of the Sun-Earth distance is very important to describe accurately the long-term evolution of geosynchronous objects, in particular if the area-to-mass ratio is large. A fixed value of the Sun-Earth distance, in fact, induces significant long period effects, mainly affecting the eccentricity, but also the orbital lifetime and the inclination [10] [11] [12].

The orbit of Table 2.1, with various force model combinations, was also propagated with other software codes available at ISTI/CNR, in order to compare their predictions and solar radiation pressure representations. This set of runs was carried out to assess the outputs of ASAP, LOP and WB1/COWELL [13]. The orbit propagations with the latter were shorter (about 60 years), because such a code requested a lot of CPU time.

The results obtained are summarized in the following figures, grouped in terms of the orbital perturbations considered:

1. Solar radiation pressure – Figure 2.4 (semimajor axis), Figure 2.5 (eccentricity) and Figure 2.6 (inclination);
2. J_2 + solar radiation pressure – Figure 2.7 (semimajor axis), Figure 2.8 (eccentricity) and Figure 2.9 (inclination);
3. Zonal harmonics + solar radiation pressure – Figure 2.10 (semimajor axis), Figure 2.11 (eccentricity) and Figure 2.12 (inclination);
4. Zonal and tesseral harmonics + solar radiation pressure – Figure 2.13 (semimajor axis), Figure 2.14 (eccentricity) and Figure 2.15 (inclination);
5. Sun (3^{rd} body) + solar radiation pressure – Figure 2.16 (semimajor axis), Figure 2.17 (eccentricity) and Figure 2.18 (inclination);
6. Moon (3^{rd} body) + solar radiation pressure – Figure 2.19 (semimajor axis), Figure 2.20 (eccentricity) and Figure 2.21 (inclination);
7. Moon and Sun (3^{rd} body) + solar radiation pressure – Figure 2.22 (semimajor axis), Figure 2.23 (eccentricity) and Figure 2.24 (inclination);
8. Zonal and tesseral harmonics + Moon and Sun (3^{rd} body) + solar radiation pressure – Figure 2.25 (semimajor axis), Figure 2.27 (eccentricity) and Figure 2.29 (inclination).

The last case (No. 8) was also repeated with the reference orbit given in Table 2.2. This time the duration of the simulations was 30 years, C_r = 1.2 and A/M = 17 m^2/kg. The results obtained are presented in Figure 2.26 (semimajor axis), Figure 2.28 (eccentricity) and Figure 2.30 (inclination).

Generally, the agreement between ASAP, LOP and WB1/COWELL was quite good. Concerning the direct solar radiation pressure modeling, it resulted quite clearly that all the codes neglect the varying Sun-Earth distance in the estimation of the perturbation magnitude.

The comparison was therefore extended to SATORB [14]. In ASAP, LOP and SATRAP the ephemerides of the Moon and the Sun are computed from analytic polynomials, which do not take into account the short period variations of the orbital elements [1]. This approximation, significant only for the Moon, is acceptable for the estimation of the third body perturbation and has the advantage of being applicable to any chosen time span. SATORB, on the other

hand, uses the more accurate JPL DE-200 ephemerides, which are, however, only available in a given time interval [2]. For this reason, and in order to maximize the time span of the comparisons, the initial elements listed in Table 2.3 were selected. The time span of the simulations was ~ 40 years, C_r = 1 and A/M = 17 m^2/kg. The perturbations included were the geopotential, up to the 8th degree and order (GEM-10B in ASAP and JGM-3 in SATORB), luni-solar third body attraction and direct solar radiation pressure with eclipses.

Table 2.2

Initial Geosynchronous Orbit Used for the Second Set of Runs

Epoch	1975.01.01 00:00 UTC
Orbital Elements	Mean Keplerian
Earth Centered Reference Frame	True of Date
Semimajor Axis	42164.465 km
Eccentricity	0.0001
Inclination	0.097 deg
Right Ascension of Ascending Node	50.00 deg
Argument of Perigee	220.00 deg
Mean Anomaly	301.22 deg

Table 2.3

Initial Geosynchronous Orbit Used for the Comparison with SATORB

Epoch	1981.01.01 00:00 UTC
Orbital Elements	Mean Keplerian
Earth Centered Reference Frame	True of Date
Semimajor Axis	42164.5 km
Eccentricity	0.0001
Inclination	0.01 deg
Right Ascension of Ascending Node	0.0 deg
Argument of Perigee	0.0 deg
Mean Anomaly	0.0 deg

The results obtained are presented in Figure 2.31 (semimajor axis), Figure 2.32 (eccentricity) and Figure 2.33 (inclination). Again, a quite good agreement between the propagators was observed. Regarding the direct solar radiation pressure modeling, it resulted quite clearly (see Figure 2.32) that also SATORB neglects the varying Sun-Earth distance in the estimation of the perturbation magnitude.

A final set of runs was carried out to compare ASAP and LOP with LEGO, adopting the initial conditions given in Table 2.4 [15]. The time span of the simulations was 100 years and area-to-mass ratios of 0.05, 1, 10 and 20 m^2/kg were considered. All relevant perturbations were included in the test, that is geopotential harmonics (8 × 8 in ASAP and LOP, 4 × 4 in

LEGO), luni-solar third body attraction and direct solar radiation pressure [16]. C_r was put equal to 1.2 in ASAP and LOP, but probably it is implicitly set equal to 2 inside the LEGO software (see the following discussion of the results). Moreover, the Earth's shadow was modeled in ASAP and LOP, but not in LEGO.

Table 2.4

Initial Geosynchronous Orbit Used for the Comparison with LEGO

Epoch	2005.05.01 00:00 UTC
Orbital Elements	Mean Keplerian
Earth Centered Reference Frame	True of Date
Semimajor Axis	42164.465 km
Eccentricity	0.0001
Inclination	0.097 deg
Right Ascension of Ascending Node	52.087 deg
Argument of Perigee	171.191 deg
Mean Anomaly	287.842 deg

The results obtained are summarized in Figures 2.34-2.45. Concerning the long-term evolution of semimajor axis and inclination, it was found a very good agreement between LEGO and the other two propagators for area-to-mass ratios of 0.05 and 1 m^2/kg (see Figures 2.34, 2.36, 2.37 and 2.39). For A/M = 10 m^2/kg, significant discrepancies were observed (see Figures 2.40 and 2.42), while, for $A/M \geq 20$ m^2/kg, the eccentricity computed by LEGO increased so much, in a few months or weeks, depending on the area-to-mass ratio, to induce an early orbital decay (see Figures 2.43, 2.44 and 2.45).

Regarding the eccentricity evolution, significant quantitative and qualitative differences were also found with low area-to-mass ratios (see Figures 2.35, 2.38 and 2.41), both short and long-term. However, the causes of the short and long-term discrepancies between LEGO and the other two software codes were probably different. In fact, focusing the attention on the first few years of the propagations, LEGO systematically predicted an amplitude of the yearly eccentricity oscillation larger by approximately a factor 2 with respect to that computed by ASAP and LOP. This may be explained by assuming that C_r is implicitly set equal to 2 (as for a perfectly reflective material) inside the LEGO software, as demonstrated by the very good agreement on the eccentricity short-term evolution obtained with a simulation based on such a hypothesis (see Figure 2.46).

Nevertheless, the assumption of C_r = 2 implicitly fixed inside LEGO was not able to remove the long-term eccentricity discrepancy with ASAP and LOP, as shown in Figure 2.47. The two latter codes, on the other hand, neglect the varying Sun-Earth distance in the estimation of the solar radiation pressure magnitude, introducing significant long period effects on resonant near-circular orbits, as repeatedly shown throughout Section 2. For this reason, LEGO was also compared with the last version of SATRAP, adopting the initial conditions given in Table 2.1 and a very high value of the area-to-mass ratio, in order to enhance the dynamical effects of solar radiation pressure.

The results obtained are presented in Figure 2.48 for the semimajor axis, Figure 2.49 for the eccentricity and Figure 2.50 for the inclination. In this case, a quite satisfactory long-term agreement was found, by assuming that $C_r = 2$ is implicitly set inside LEGO. Moreover, the LEGO eccentricity evolution was compatible with the predictions of the propagators, like the last version of SATRAP, which consider the varying Sun-Earth distance in the estimation of the solar radiation pressure magnitude.

2.2 Comparison of Radiation Pressure Models in GPS Orbit

The comparison of the long-term dynamical effects induced by different models of the direct solar radiation pressure was extended to other high Earth orbits, beginning with the near-circular 2:1 mean motion resonant orbits used by the Global Positioning System (GPS). Two trajectory propagators were employed: ASAP, adopting Eq. (1.3) for the modeling of the radiation pressure perturbation, and the last version of SATRAP, adopting Eq. (1.2), which considers the varying Sun-Earth distance to estimate the acceleration magnitude.

Table 2.5

Reference GPS Orbit (Initial Conditions)

Epoch	2005.07.12 07:06:39.28 UTC
Orbital Elements	Mean Keplerian
Earth Centered Reference Frame	True of Date
Semimajor Axis	26559.357 km
Eccentricity	0.0091107
Inclination	54.6752 deg
Right Ascension of Ascending Node	275.8354 deg
Argument of Perigee	107.7453 deg
Mean Anomaly	253.3161 deg

The reference orbit adopted as initial conditions is given in Table 2.5. The time span of the simulations was 100 years, $C_r = 1.2$ and $A/M = 10$ m^2/kg, in order to enhance the dynamical effects of solar radiation pressure. The perturbations included were the geopotential harmonics, up to the 8th degree and order, luni-solar third body attraction and direct solar radiation pressure with eclipses.

The results obtained are presented in Figure 2.51 for the semimajor axis, Figure 2.52 for the eccentricity and Figure 2.54 for the inclination. Figures 2.53 and 2.55 show, respectively, the expected long-term evolution of the eccentricity and inclination vectors. As in GEO, a near-circular 1:1 mean motion resonant orbit, also in this case the assumption of a fixed Sun-Earth distance, in the estimation of the solar radiation pressure magnitude, introduced significant spurious long period effects, mainly affecting the eccentricity evolution. The use of the more accurate model, exemplified by Eq. (1.2), is therefore mandatory for the long-term

propagations of objects with relatively high area-to-mass ratios.

2.3 Comparison of Radiation Pressure Models in Molniya Orbit

The long-term dynamical effects induced by different models of the direct solar radiation pressure were therefore investigated in Molniya orbit, a strongly elliptical 2:1 mean motion resonant orbit at the critical inclination, mainly used by Russian communications satellites. Again, two trajectory propagators were employed: ASAP, adopting Eq. (1.3) for the modeling of the radiation pressure perturbation, and the last version of SATRAP, adopting Eq. (1.2), which considers the varying Sun-Earth distance to estimate the acceleration magnitude.

The reference orbit adopted as initial conditions is given in Table 2.6. The time span of the simulations was several decades, $C_r = 1.2$ and $A/M = 1$ m^2/kg, in order to enhance, as much as possible, the dynamical effects of solar radiation pressure (higher values of the area-to-mass ratio induced too short orbital lifetimes). The perturbations included were the geopotential harmonics, up to the 8th degree and order, luni-solar third body attraction, direct solar radiation pressure with eclipses and air drag, according to the parameters given in Table 1.1.

Table 2.6

Reference Molniya Orbit (Initial Conditions)

Epoch	2005.07.12 18:29:20.47 UTC
Orbital Elements	Mean Keplerian
Earth Centered Reference Frame	True of Date
Semimajor Axis	26558.929 km
Eccentricity	0.6982377
Inclination	63.6525 deg
Right Ascension of Ascending Node	96.6475 deg
Argument of Perigee	273.7710 deg
Mean Anomaly	15.7838 deg

The results obtained are presented in Figure 2.56 for the semimajor axis, Figure 2.57 for the eccentricity, Figure 2.58 for the inclination and Figure 2.59 for the perigee altitude. For more than 30 years, the agreement between ASAP and SATRAP remained quite good. Later on, the discrepancies observed were basically a consequence of small numerical differences in the perigee altitude, leading to dissimilar apogee evolutions and orbital lifetimes. However, the evolution qualitatively remained the same with both propagators. In addition, similar numerical differences were also found using different trajectory predictors with the same solar radiation pressure model, like ASAP and LOP [15].

In this case, therefore, the assumption of a fixed Sun-Earth distance, in the estimation of the solar radiation pressure magnitude, did not introduce the significant spurious long period effects found in near-circular mean motion resonant orbits, like those used by GEO (1:1) and

GPS (2:1) satellites. The use of the more accurate solar radiation pressure model, exemplified by Eq. (1.2), is consequently not mandatory for Molniya orbits, even for relatively long propagations of objects with significantly high area-to-mass ratios.

2.4 Comparison of Radiation Pressure Models in GTO

The long-term dynamical effects induced by different models of the direct solar radiation pressure were finally investigated in geosynchronous transfer orbit (GTO). The reference trajectory selected, given in Table 2.7, was an Ariane V GTO, a strongly elliptical, and nearly resonant (2:1), orbit at low inclination. As for GPS and Molniya orbits, two trajectory propagators were employed: ASAP, adopting Eq. (1.3) for the modeling of the radiation pressure perturbation, and the last version of SATRAP, adopting Eq. (1.2), which considers the varying Sun-Earth distance to estimate the acceleration magnitude.

Table 2.7

Reference Ariane V GTO (Initial Conditions)

Epoch	2005.07.13 19:28:41.06 UTC
Orbital Elements	Mean Keplerian
Earth Centered Reference Frame	True of Date
Semimajor Axis	25932.231 km
Eccentricity	0.7289232
Inclination	7.5452 deg
Right Ascension of Ascending Node	3.9417 deg
Argument of Perigee	53.1657 deg
Mean Anomaly	353.7054 deg

The time span of the simulations was 100 years, C_r = 1.2 and A/M = 1 m^2/kg, in order to enhance, as much as possible, the dynamical effects of solar radiation pressure (higher values of the area-to-mass ratio induced too short orbital lifetimes). The perturbations included were the geopotential harmonics, up to the 8th degree and order, luni-solar third body attraction, direct solar radiation pressure with eclipses and air drag, according to the parameters specified in Table 1.1.

The results obtained are presented in Figure 2.60 for the semimajor axis, Figure 2.61 for the eccentricity, Figure 2.62 for the inclination and Figure 2.63 for the perigee altitude. For about 50 years, the agreement between ASAP and SATRAP remained very good. Later on, the discrepancies observed were basically a consequence of small numerical differences in the perigee altitude, leading to dissimilar apogee evolutions and orbital lifetimes. However, the evolution qualitatively remained the same with both propagators. In addition, similar numerical differences were also found using different trajectory predictors with the same solar radiation pressure model, like ASAP and LOP [15].

Even in this case, therefore, the assumption of a fixed Sun-Earth distance, in the estimation of the solar radiation pressure magnitude, did not introduce the significant spurious long period effects found in near-circular mean motion resonant orbits (see Sections 2.1 and 2.2). As for Molniya orbits (see Section 2.3), the use of the more accurate solar radiation pressure model, exemplified by Eq. (1.2), is consequently not mandatory for GTO, even for relatively long propagations of objects with significantly high area-to-mass ratios.

2.5 Summary

The long-term evolution of objects in high Earth orbits and with very high area-to-mass ratios was analyzed with various trajectory propagators, in order to investigate the performances of different models for the direct solar radiation pressure.

The results obtained clearly indicated that the correct modeling of the Sun-Earth distance, in the estimation of the solar radiation pressure magnitude, is very important to describe accurately the long-term evolution of objects in near-circular mean motion resonant orbits, as in the GEO (1:1) and GPS (2:1) cases. A fixed value of the Sun-Earth distance, in fact, induces significant spurious long period effects, mainly affecting the eccentricity evolution, but also the orbital lifetime (for very high A/M values) and the inclination. The use of the more accurate solar radiation pressure model, described by Eq. (1.2), is therefore mandatory in the long-term propagations of objects with relatively high area-to-mass ratios.

Concerning GTO and Molniya orbits, on the other hand, the assumption of a fixed Sun-Earth distance, in the estimation of the solar radiation pressure magnitude, as described by Eq. (1.3), did not introduce the significant spurious long period effects found in near-circular mean motion resonant orbits. In these cases, the use of the more accurate solar radiation pressure model is therefore not required, even for relatively long propagations of objects with significantly high area-to-mass ratios.

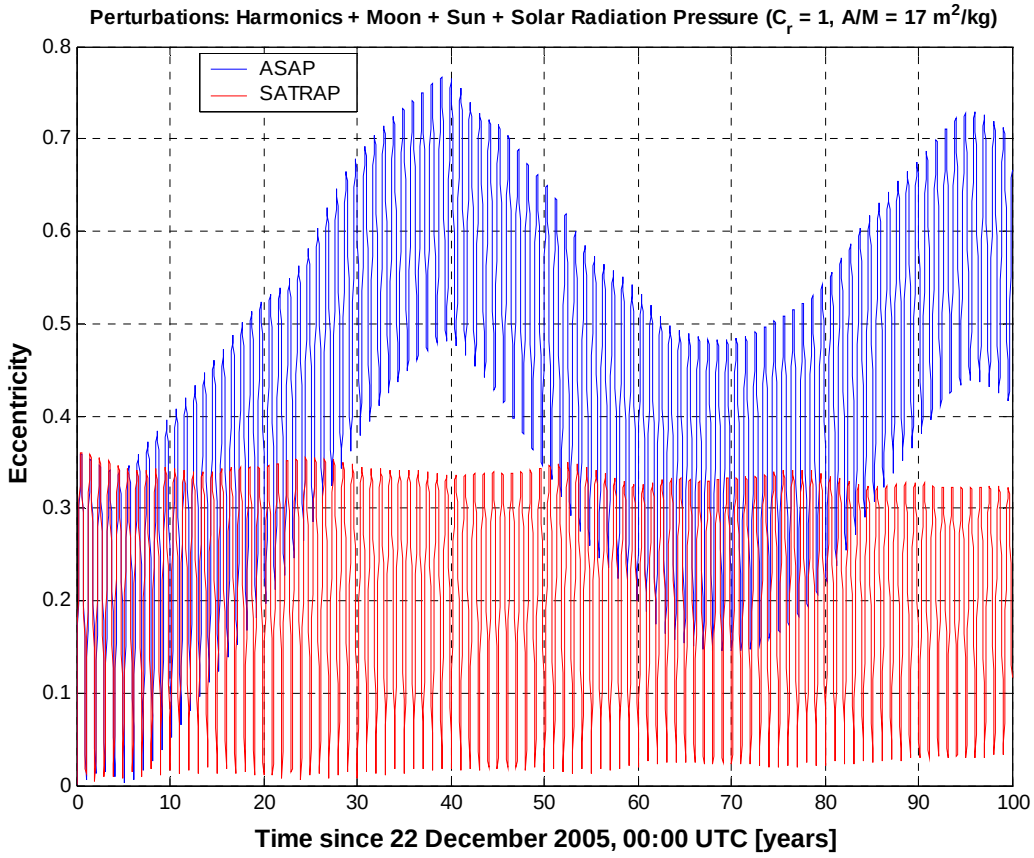

Figure 2.1

Long-term eccentricity evolution in GEO, taking into account all relevant perturbations. In ASAP, the radiation perturbation model neglected the varying Sun-Earth distance in the estimation of the radiation pressure magnitude, while in SATRAP the small eccentricity of the Earth's orbit was taken into account.

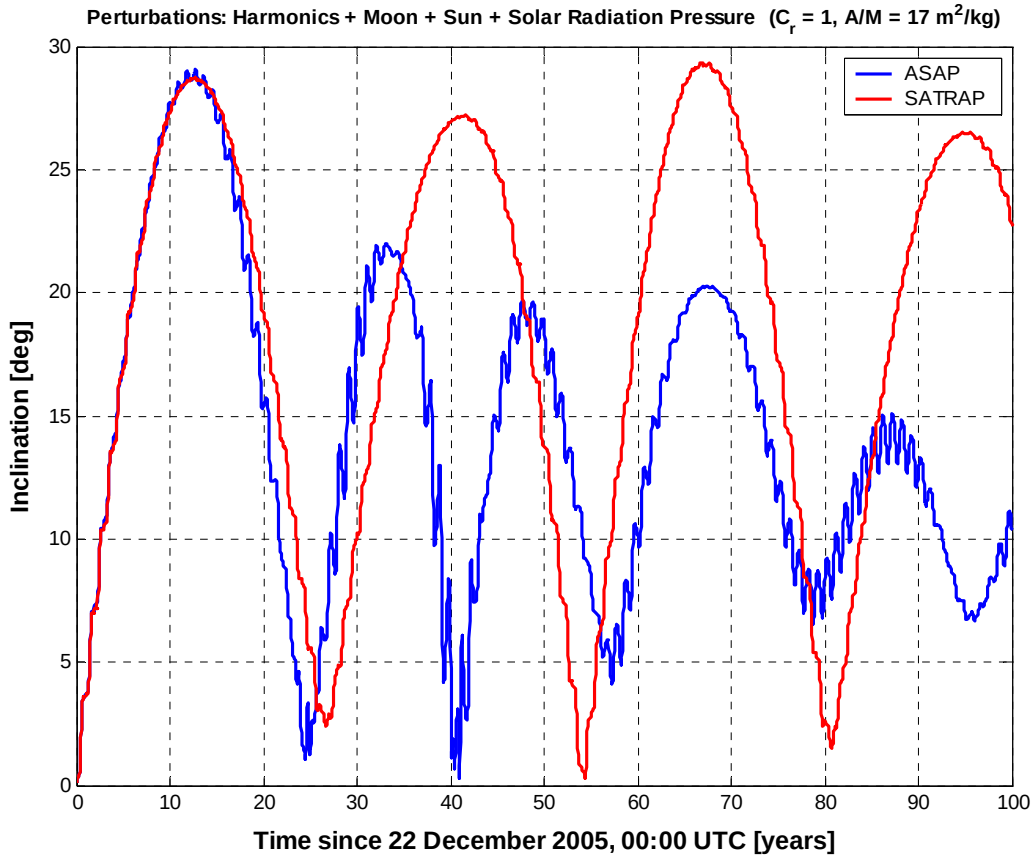

Figure 2.2

Long-term inclination evolution in GEO, taking into account all relevant perturbations. In ASAP, the radiation perturbation model neglected the varying Sun-Earth distance in the estimation of the radiation pressure magnitude, while in SATRAP the small eccentricity of the Earth's orbit was taken into account.

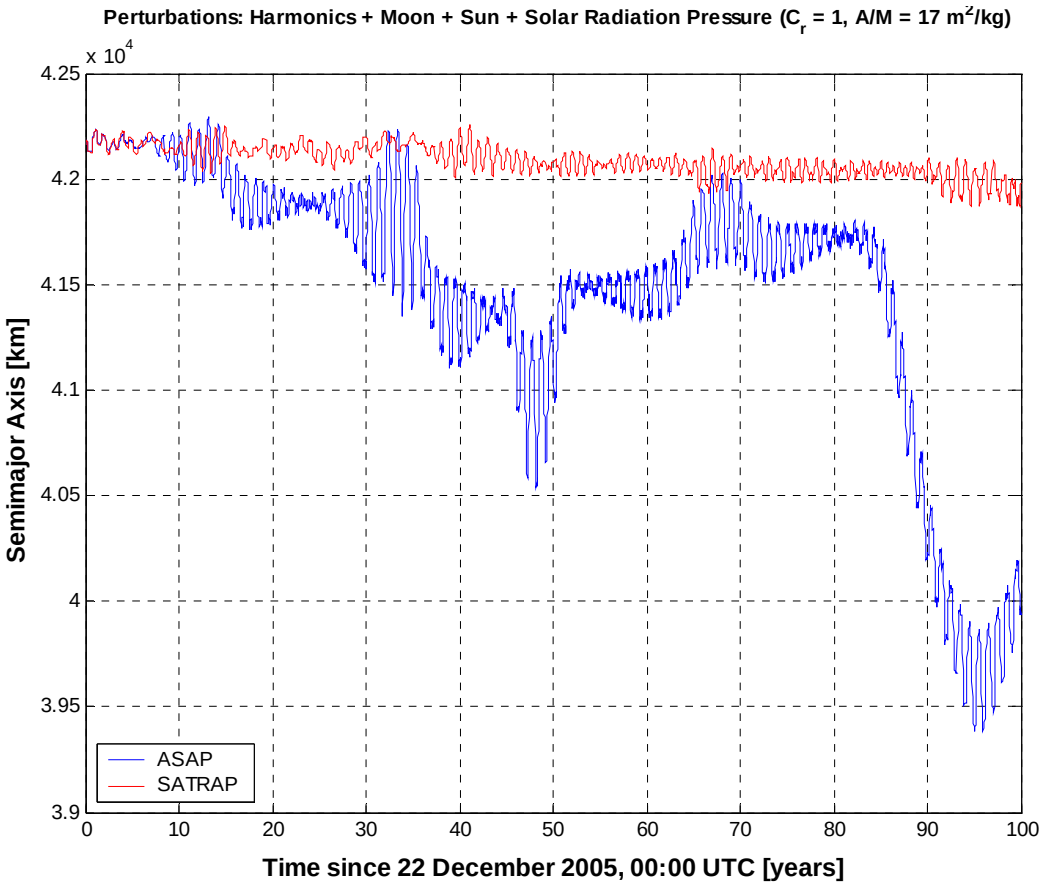

Figure 2.3

Long-term semimajor axis evolution in GEO, taking into account all relevant perturbations. In ASAP, the radiation perturbation model neglected the varying Sun-Earth distance in the estimation of the radiation pressure magnitude, while in SATRAP the small eccentricity of the Earth's orbit was taken into account.

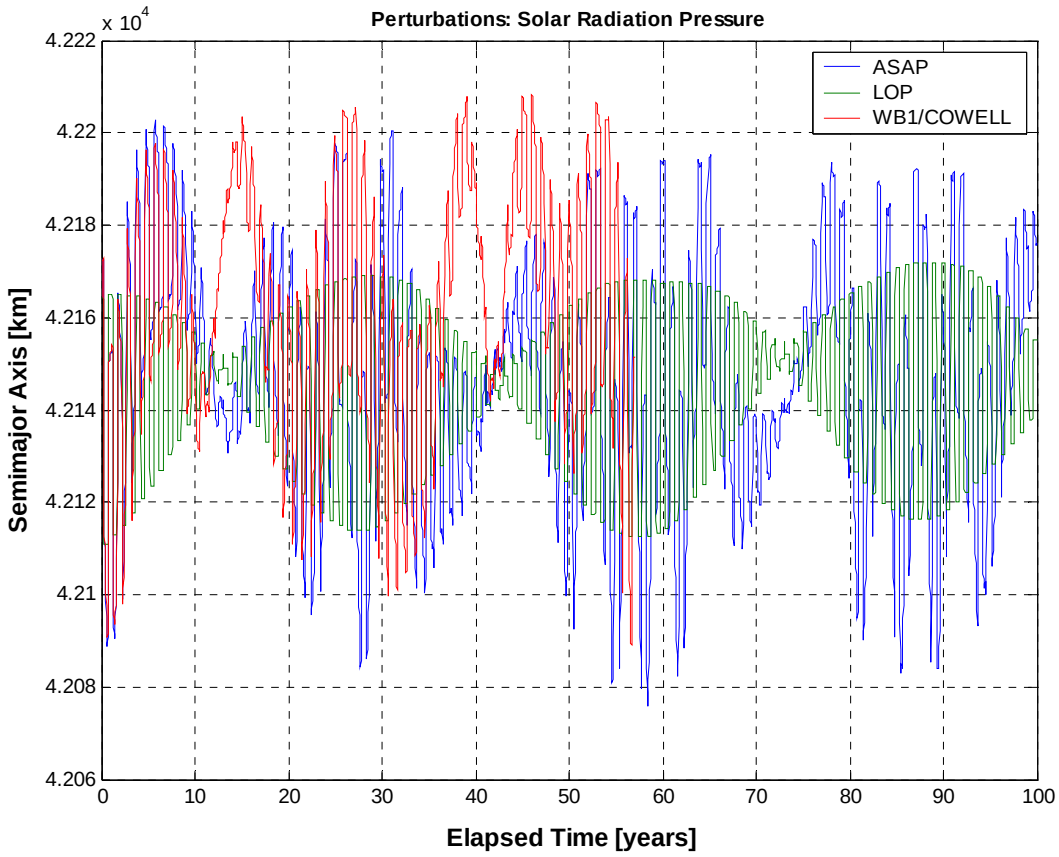

Figure 2.4

Long-term semimajor axis evolution in GEO, taking into account only solar radiation pressure. ASAP and WB1/COWELL, both numerical trajectory integrators, showed a better agreement.

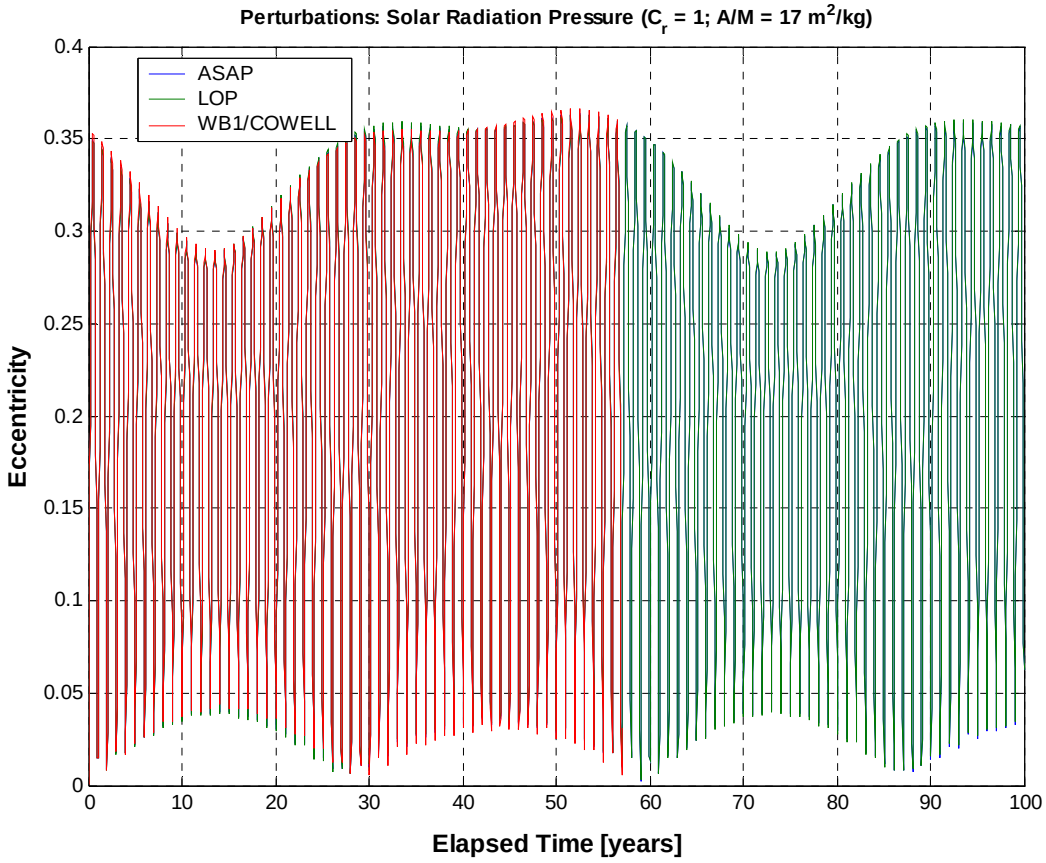

Figure 2.5

Long-term eccentricity evolution in GEO, taking into account only solar radiation pressure. The agreement between the three codes was very good.

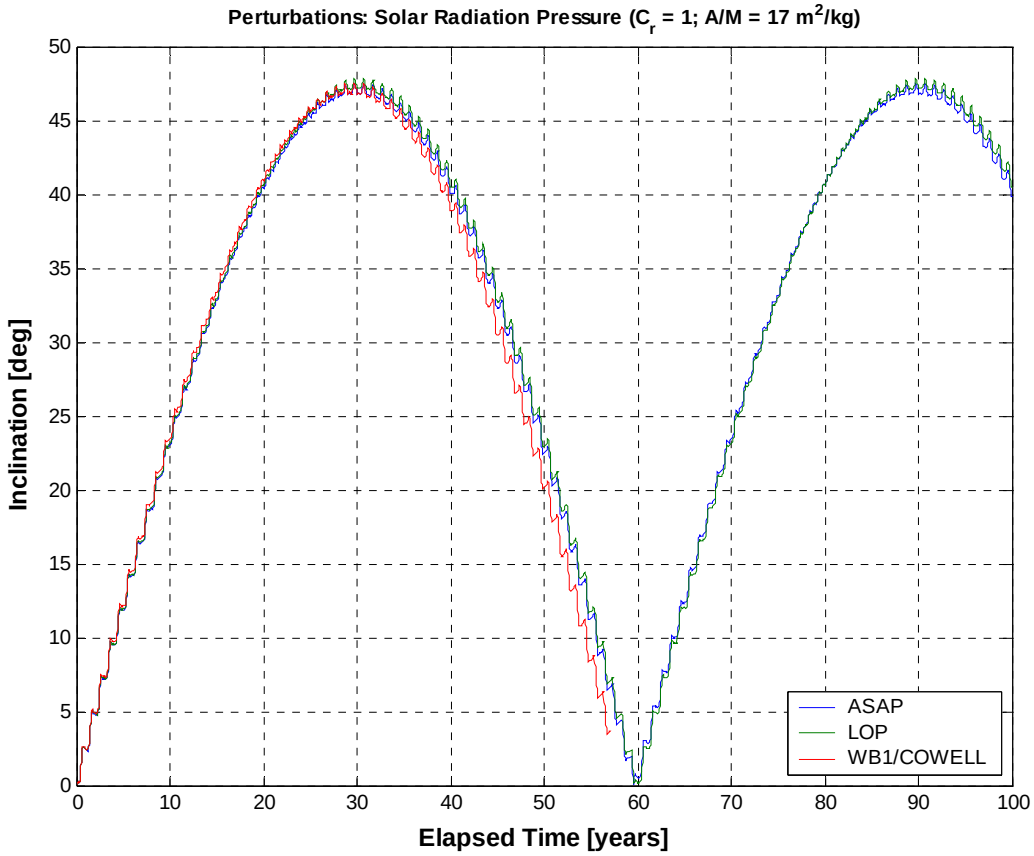

Figure 2.6

Long-term inclination evolution in GEO, taking into account only solar radiation pressure. The agreement between the three codes was very good, in particular between ASAP and LOP, which shared exactly the same reference frame, force model constants and options.

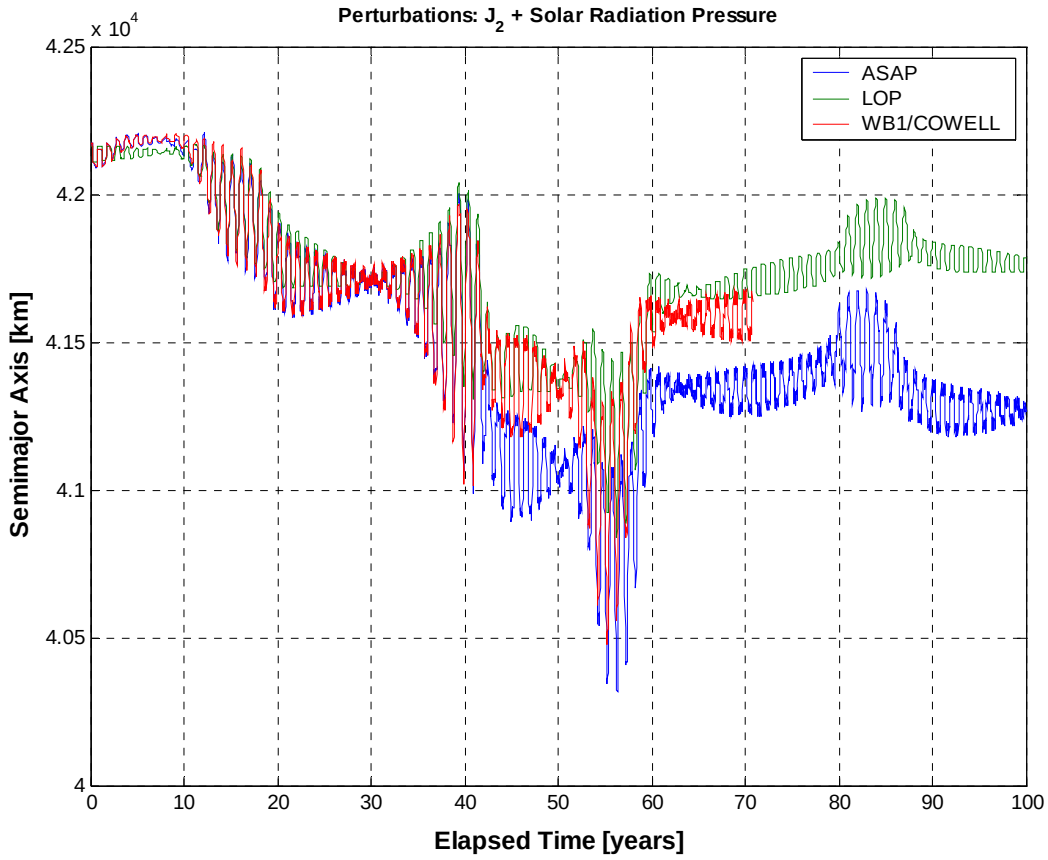

Figure 2.7

Long-term semimajor axis evolution in GEO, taking into account J_2 and solar radiation pressure. The three software codes showed a reasonable agreement, at least during the first 40 years.

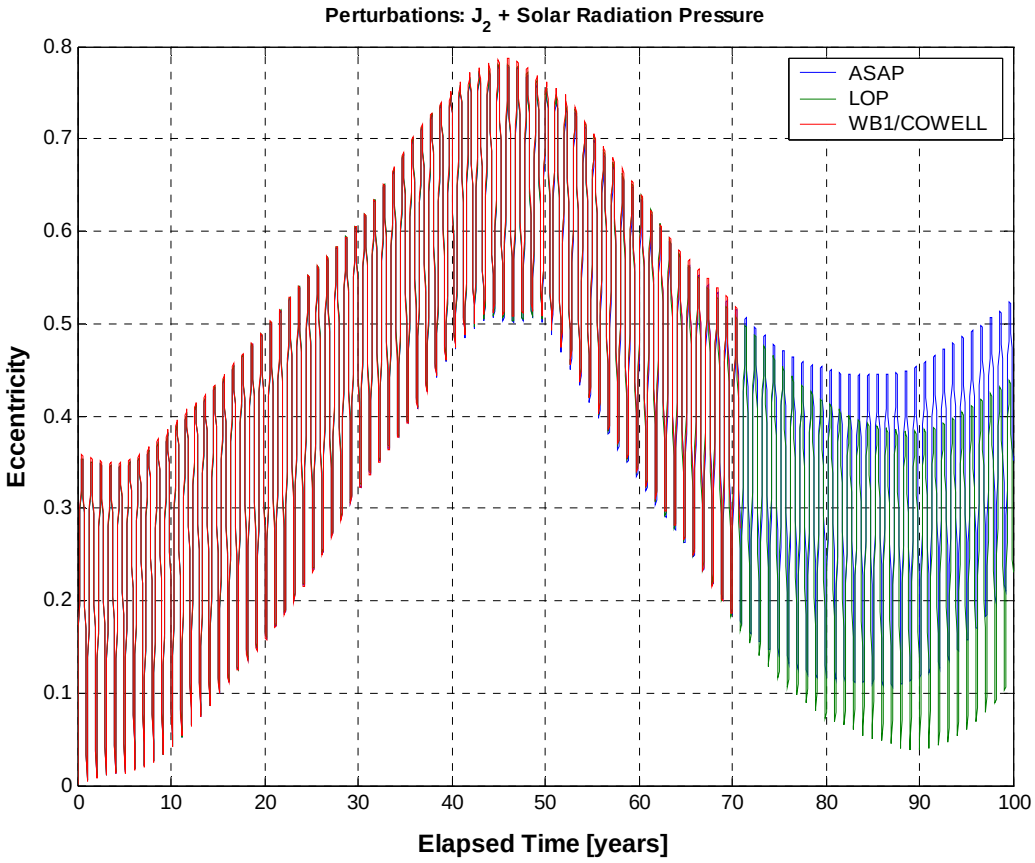

Figure 2.8

Long-term eccentricity evolution in GEO, taking into account J_2 and solar radiation pressure. In ASAP and LOP, the solar radiation perturbation model neglected the varying Sun-Earth distance in the estimation of the radiation pressure magnitude. The good agreement between such propagators and WB1/COWELL indicated that also the latter adopted a similar assumption.

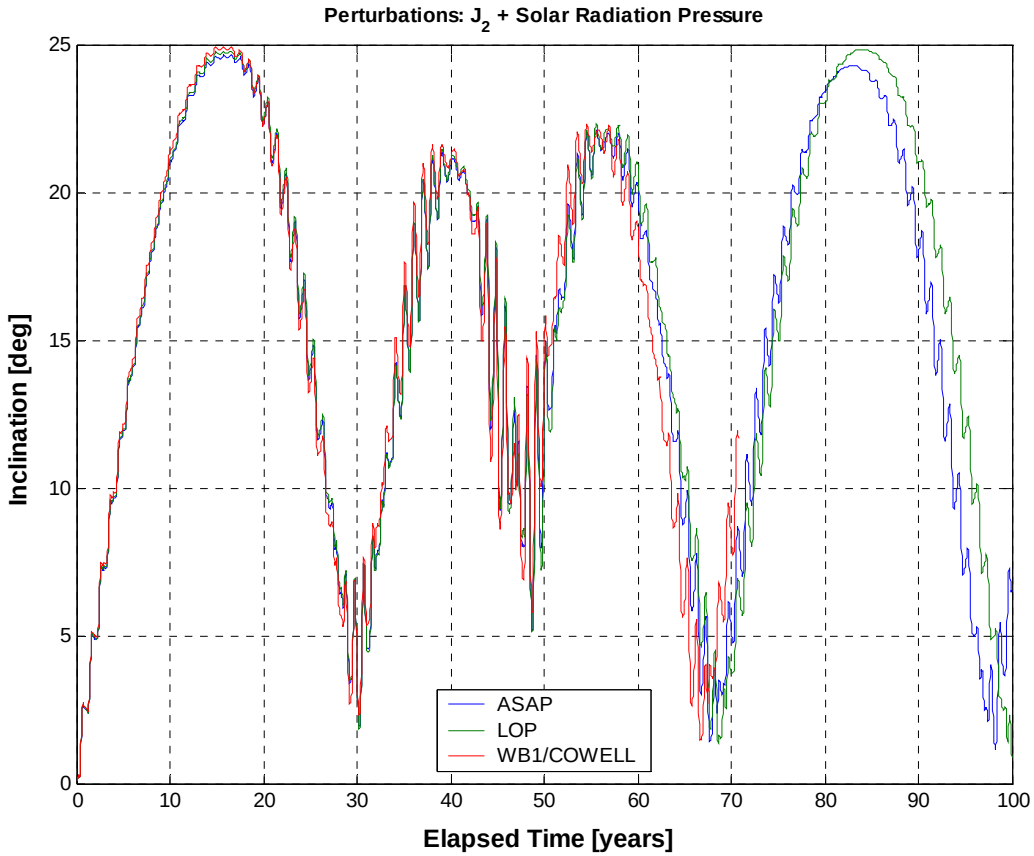

Figure 2.9

Long-term inclination evolution in GEO, taking into account J_2 and solar radiation pressure. In ASAP and LOP, the solar radiation perturbation model neglected the varying Sun-Earth distance in the estimation of the radiation pressure magnitude. The good agreement between such propagators and WB1/COWELL indicated that also the latter adopted a similar assumption.

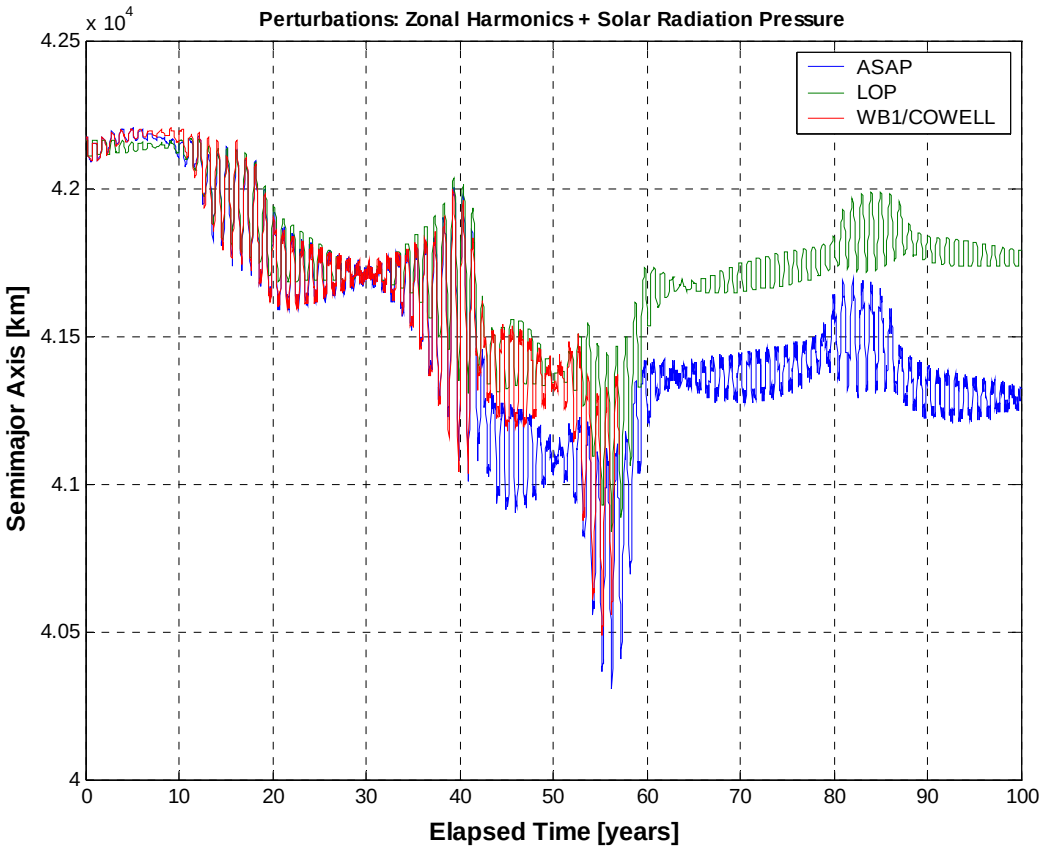

Figure 2.10

Long-term semimajor axis evolution in GEO, taking into account the zonal harmonics of the geopotential (up to the 8th degree in ASAP and LOP, up to the 6th degree in WB1/COWELL) and solar radiation pressure. The three software codes showed a reasonable agreement, at least during the first 40 years.

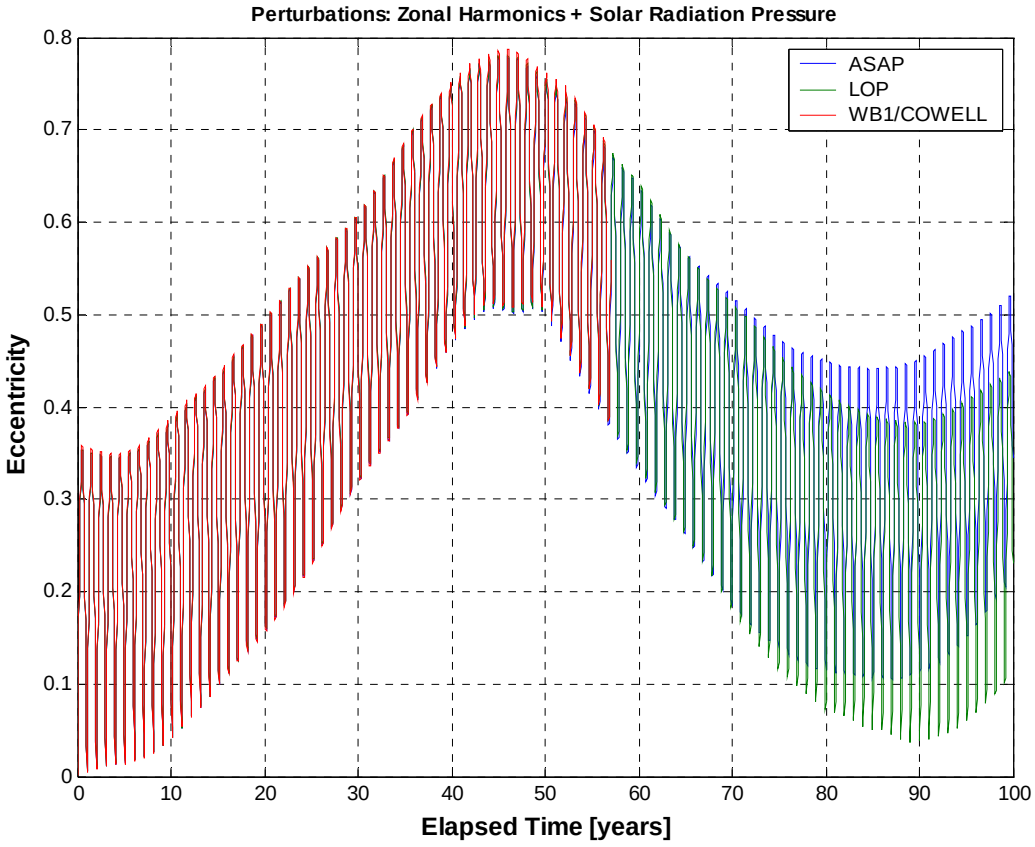

Figure 2.11

Long-term eccentricity evolution in GEO, taking into account the zonal harmonics of the geopotential (up to the 8th degree in ASAP and LOP, up to the 6th degree in WB1/COWELL) and solar radiation pressure. In ASAP and LOP, the solar radiation perturbation model neglected the varying Sun-Earth distance in the estimation of the radiation pressure magnitude. The good agreement between such propagators and WB1/COWELL indicated that also the latter adopted a similar assumption.

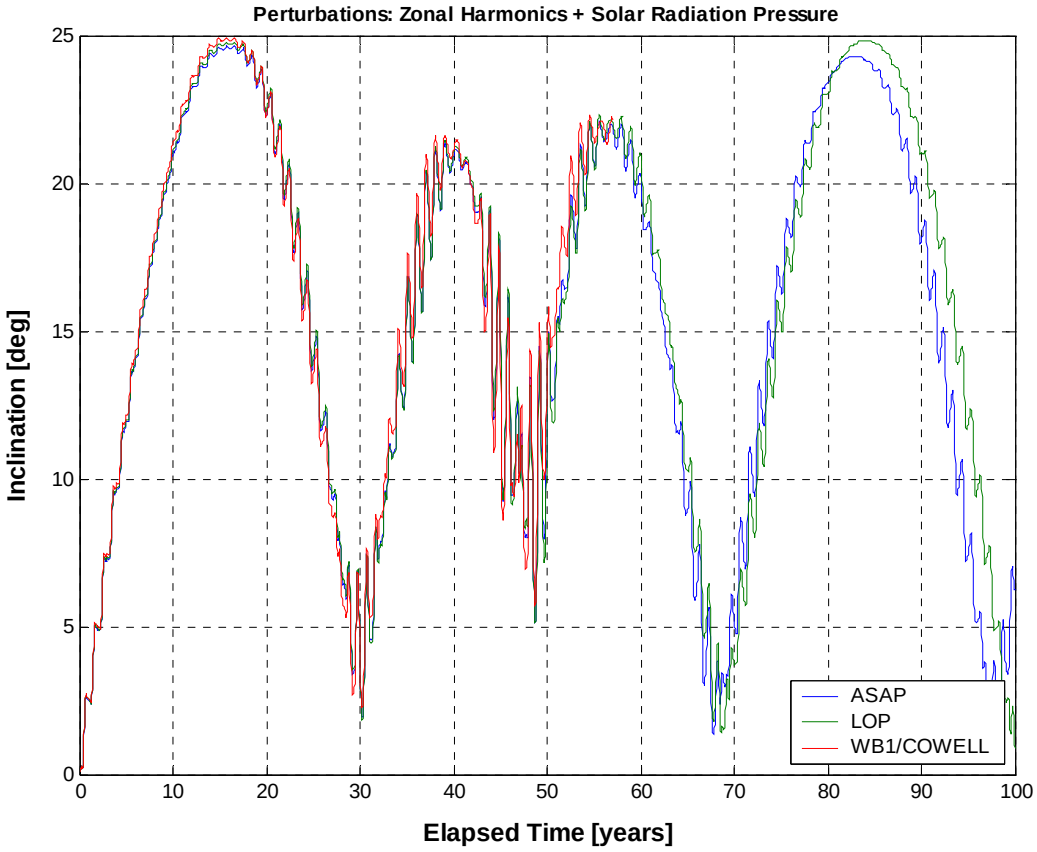

Figure 2.12

Long-term inclination evolution in GEO, taking into account the zonal harmonics of the geopotential (up to the 8th degree in ASAP and LOP, up to the 6th degree in WB1/COWELL) and solar radiation pressure. In ASAP and LOP, the solar radiation perturbation model neglected the varying Sun-Earth distance in the estimation of the radiation pressure magnitude. The good agreement between such propagators and WB1/COWELL indicated that also the latter adopted a similar assumption.

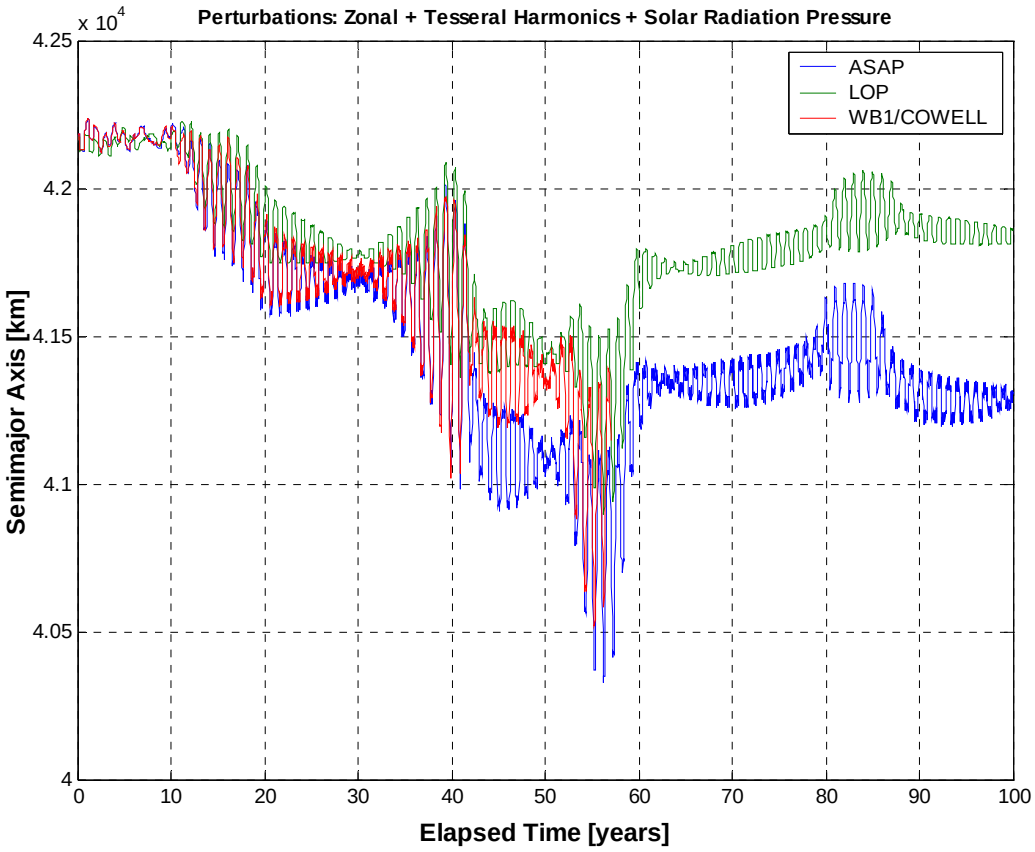

Figure 2.13

Long-term semimajor axis evolution in GEO, taking into account the harmonics of the geopotential (up to the 8th degree and order in ASAP and LOP, up to the 12th degree and order in WB1/COWELL) and solar radiation pressure. The three software codes showed a reasonable agreement, at least during the first 40 years.

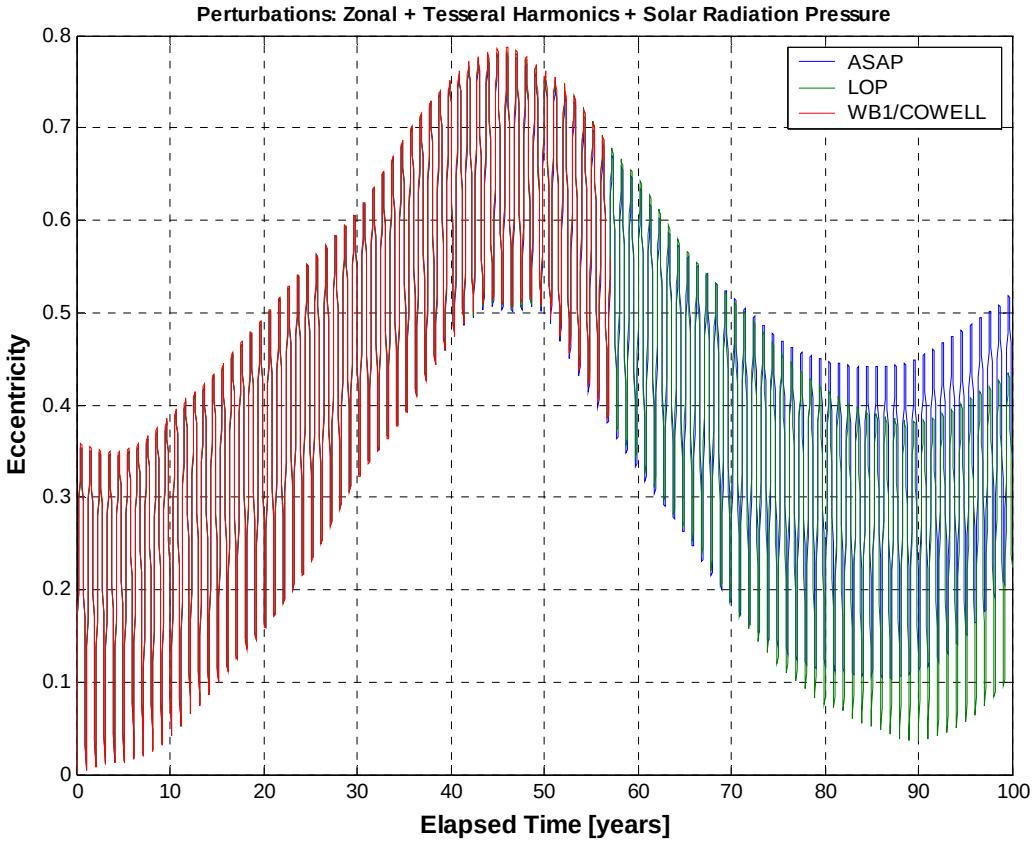

Figure 2.14

Long-term eccentricity evolution in GEO, taking into account the harmonics of the geopotential (up to the 8th degree and order in ASAP and LOP, up to the 12th degree and order in WB1/COWELL) and solar radiation pressure. In ASAP and LOP, the solar radiation perturbation model neglected the varying Sun-Earth distance in the estimation of the radiation pressure magnitude. The good agreement between such propagators and WB1/COWELL indicated that also the latter adopted a similar assumption.

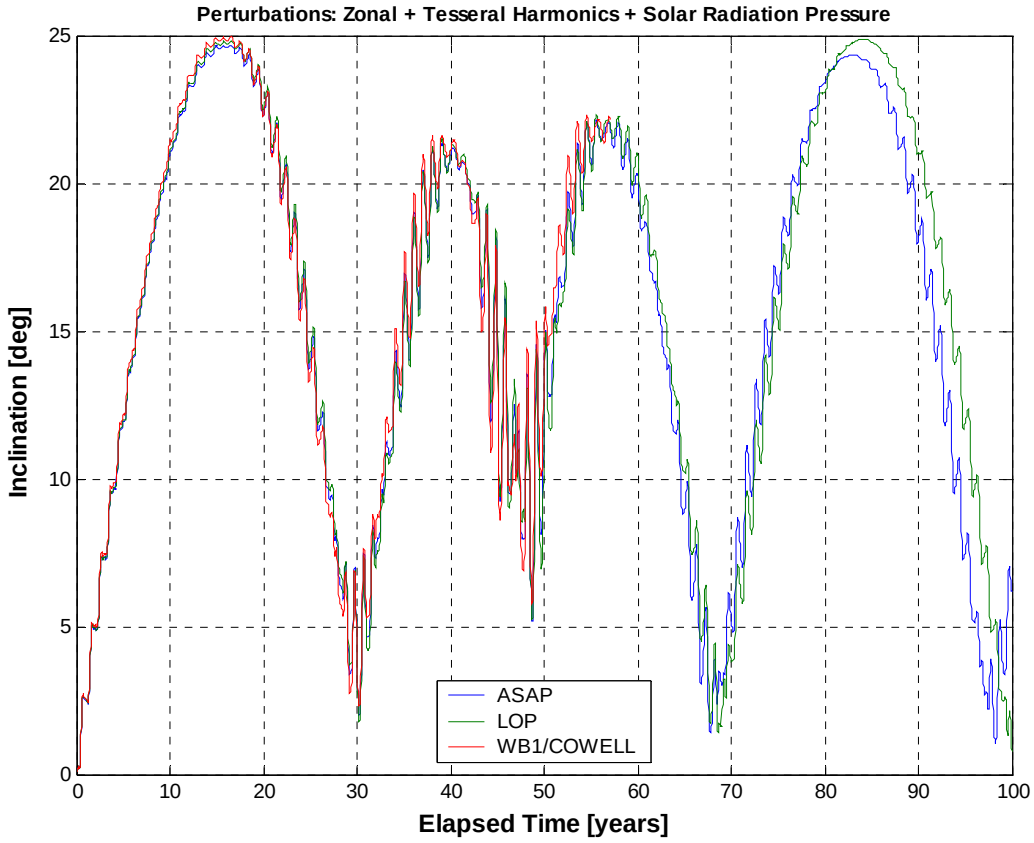

Figure 2.15

Long-term inclination evolution in GEO, taking into account the harmonics of the geopotential (up to the 8th degree and order in ASAP and LOP, up to the 12th degree and order in WB1/COWELL) and solar radiation pressure. In ASAP and LOP, the solar radiation perturbation model neglected the varying Sun-Earth distance in the estimation of the radiation pressure magnitude. The good agreement between such propagators and WB1/COWELL indicated that also the latter adopted a similar assumption.

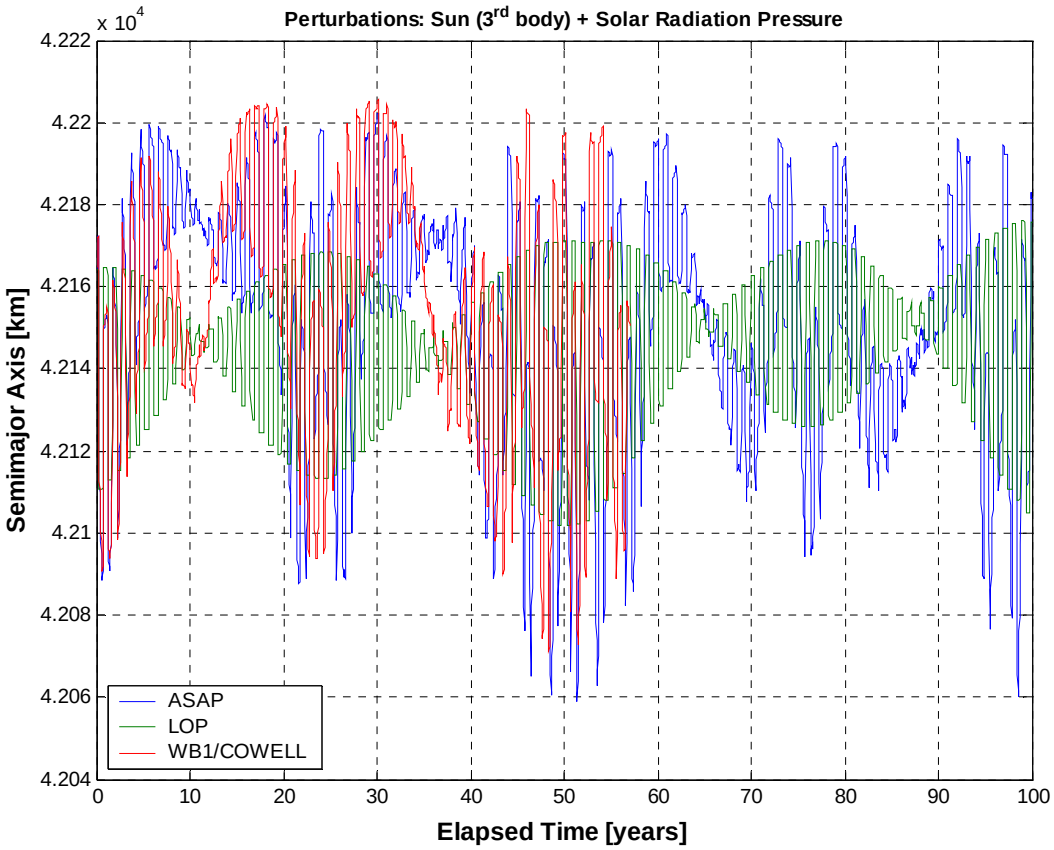

Figure 2.16

Long-term semimajor axis evolution in GEO, taking into account the Sun third body attraction and solar radiation pressure.

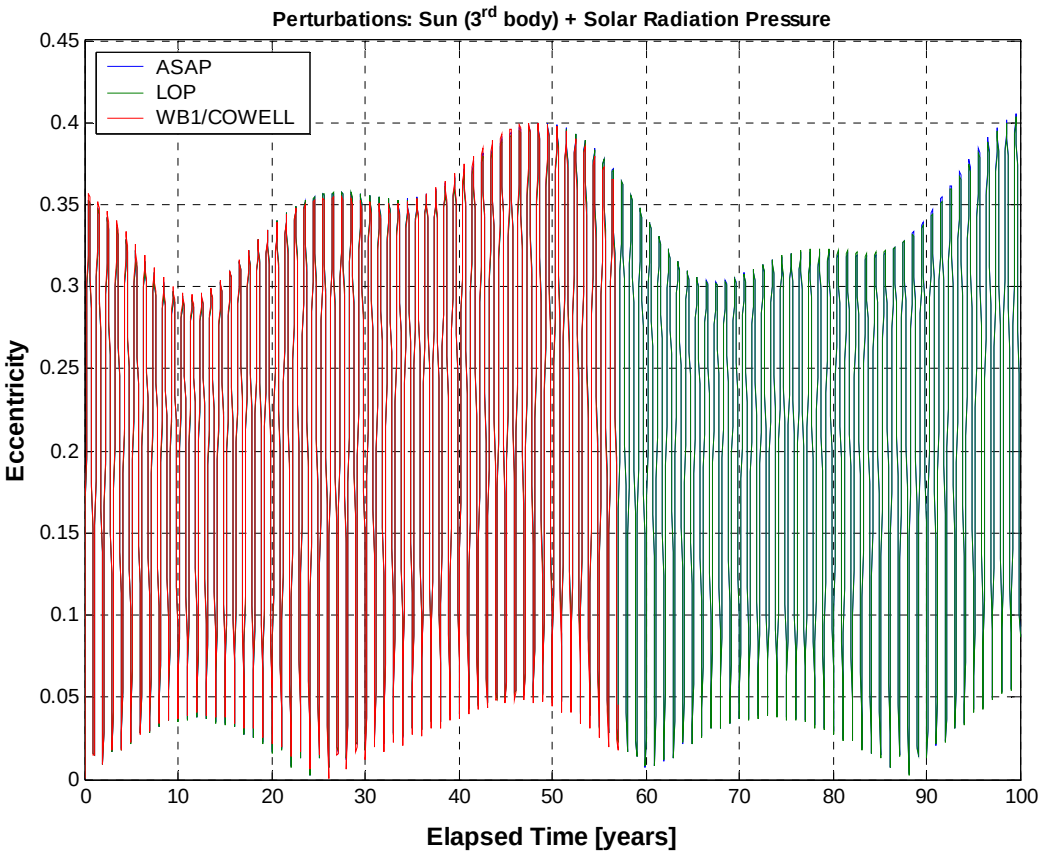

Figure 2.17

Long-term eccentricity evolution in GEO, taking into account the Sun third body attraction and solar radiation pressure. The agreement between the three orbit propagators was very good.

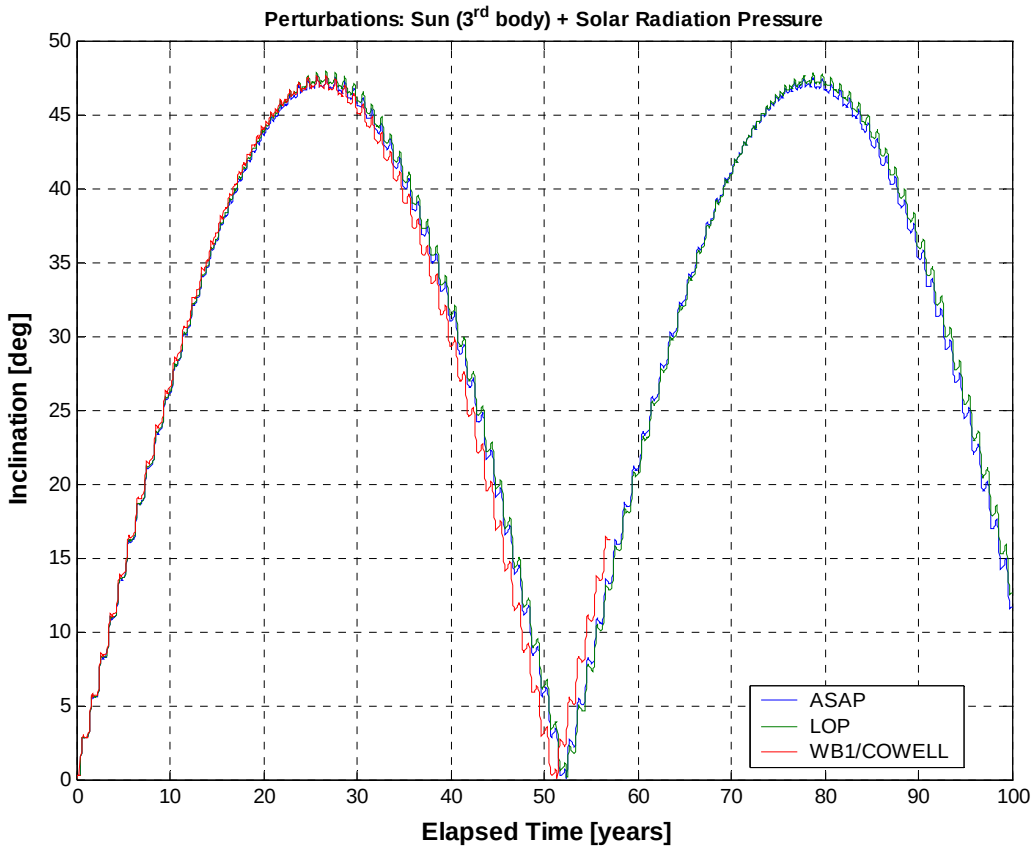

Figure 2.18

Long-term inclination evolution in GEO, taking into account the Sun third body attraction and solar radiation pressure. The agreement between the three orbit propagators was quite good.

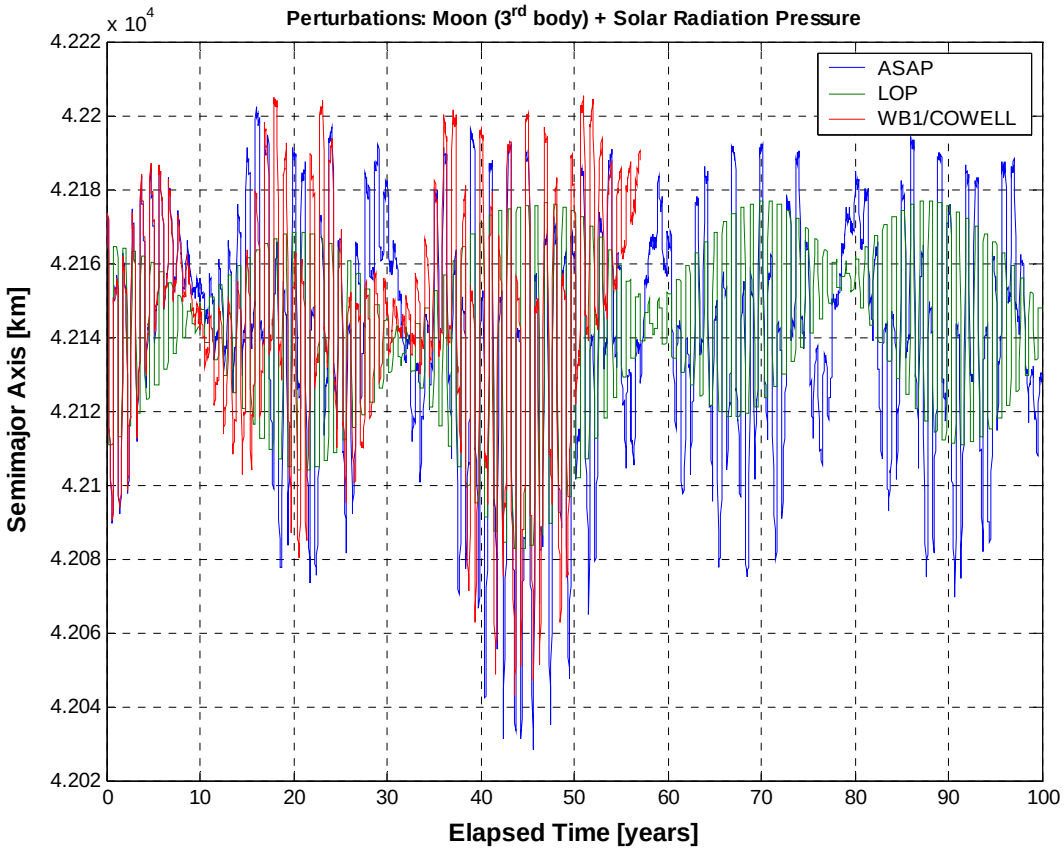

Figure 2.19

Long-term semimajor axis evolution in GEO, taking into account the Moon third body attraction and solar radiation pressure.

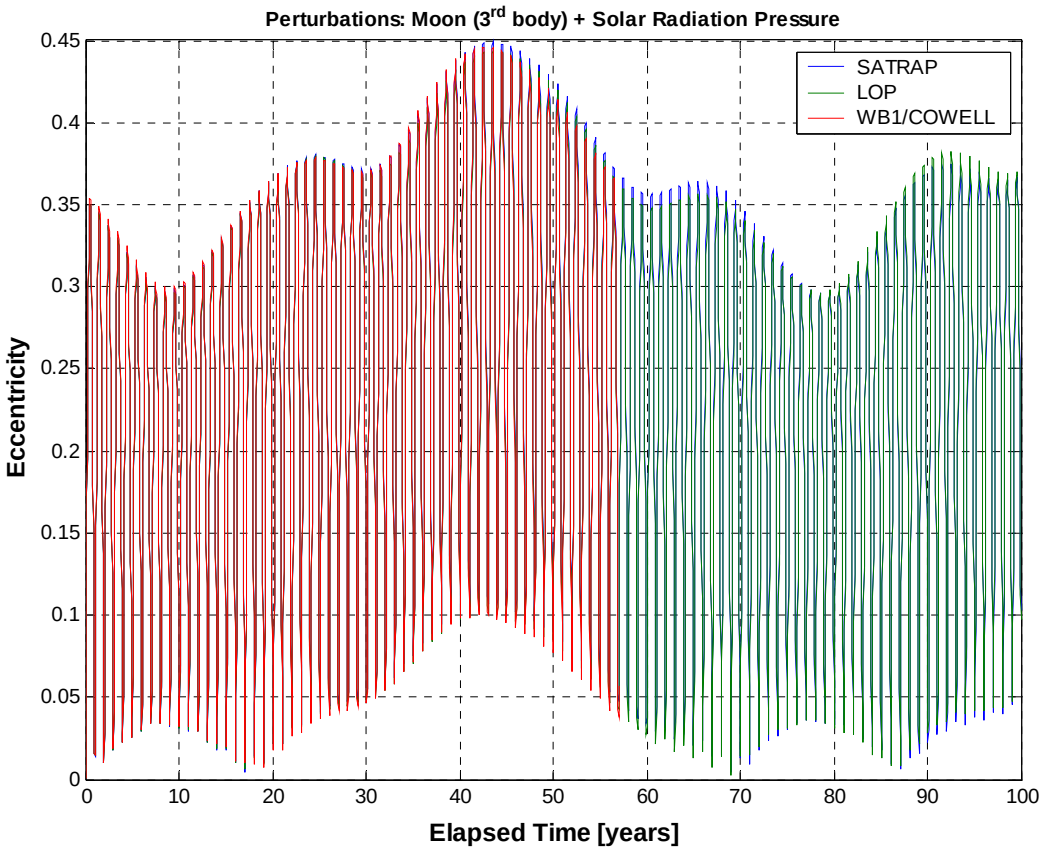

Figure 2.20

Long-term eccentricity evolution in GEO, taking into account the Moon third body attraction and solar radiation pressure. The agreement between the three orbit propagators was very good.

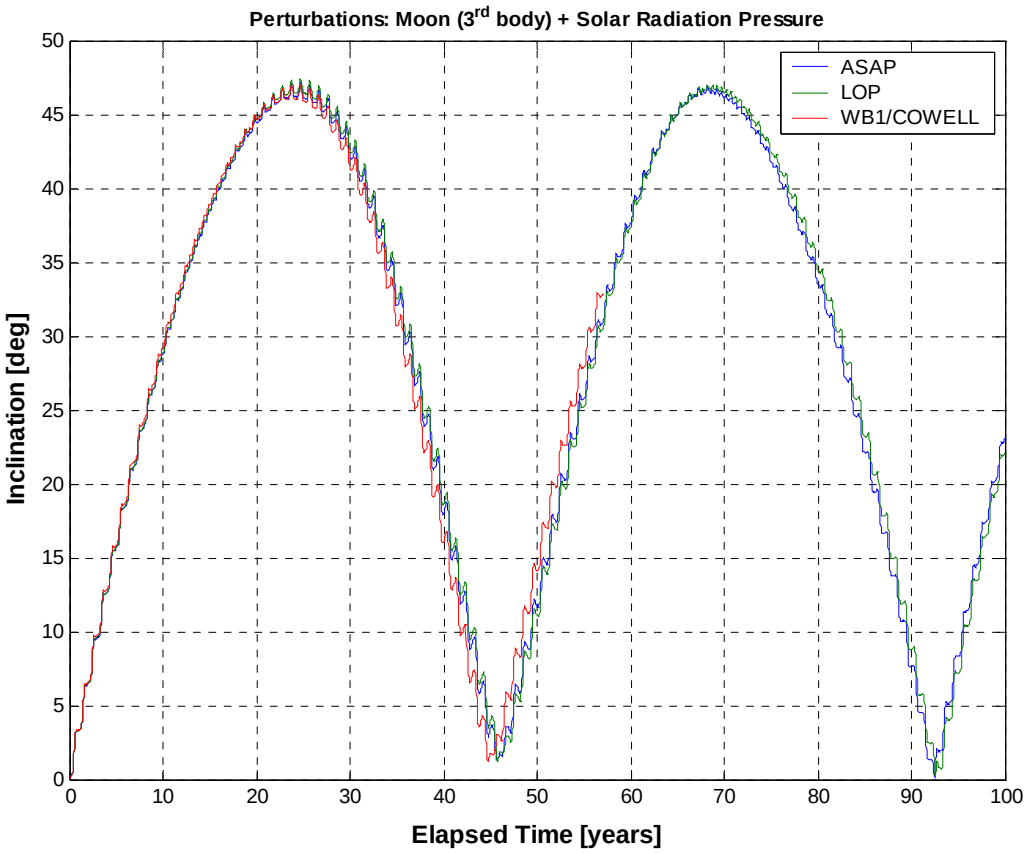

Figure 2.21

Long-term inclination evolution in GEO, taking into account the Moon third body attraction and solar radiation pressure. The agreement between the three orbit propagators was quite good.

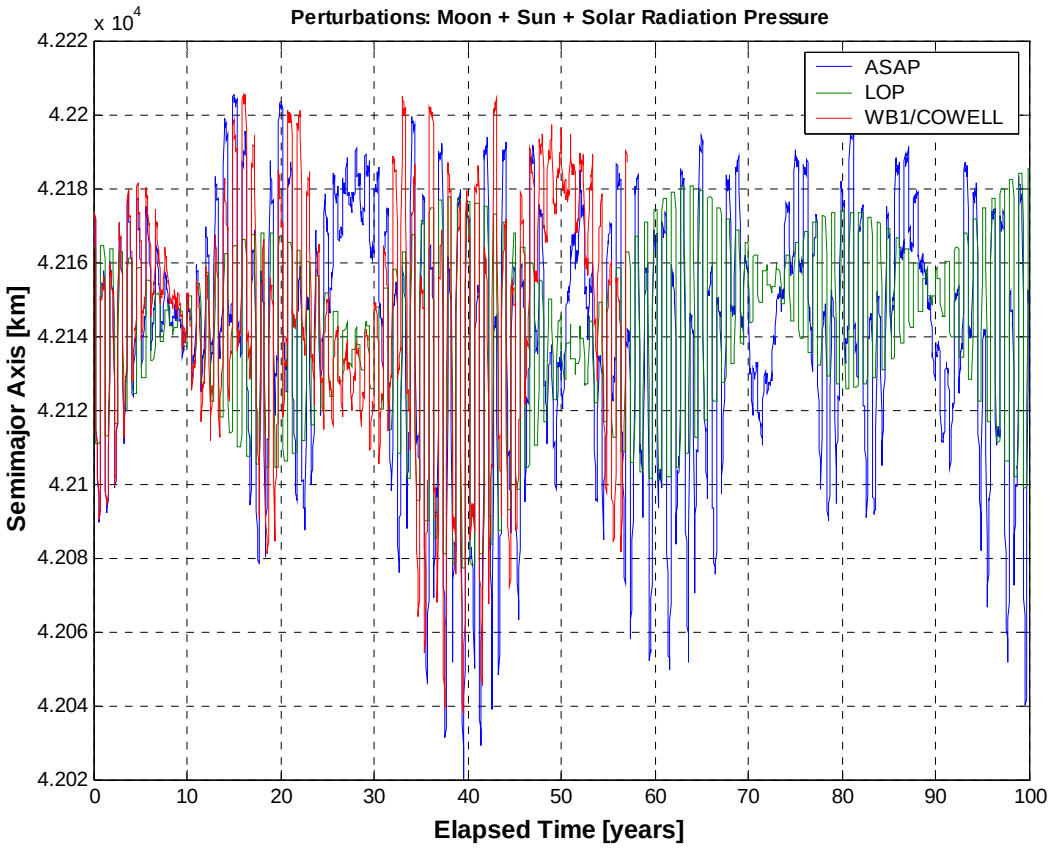

Figure 2.22

Long-term semimajor axis evolution in GEO, taking into account the luni-solar third body attraction and solar radiation pressure.

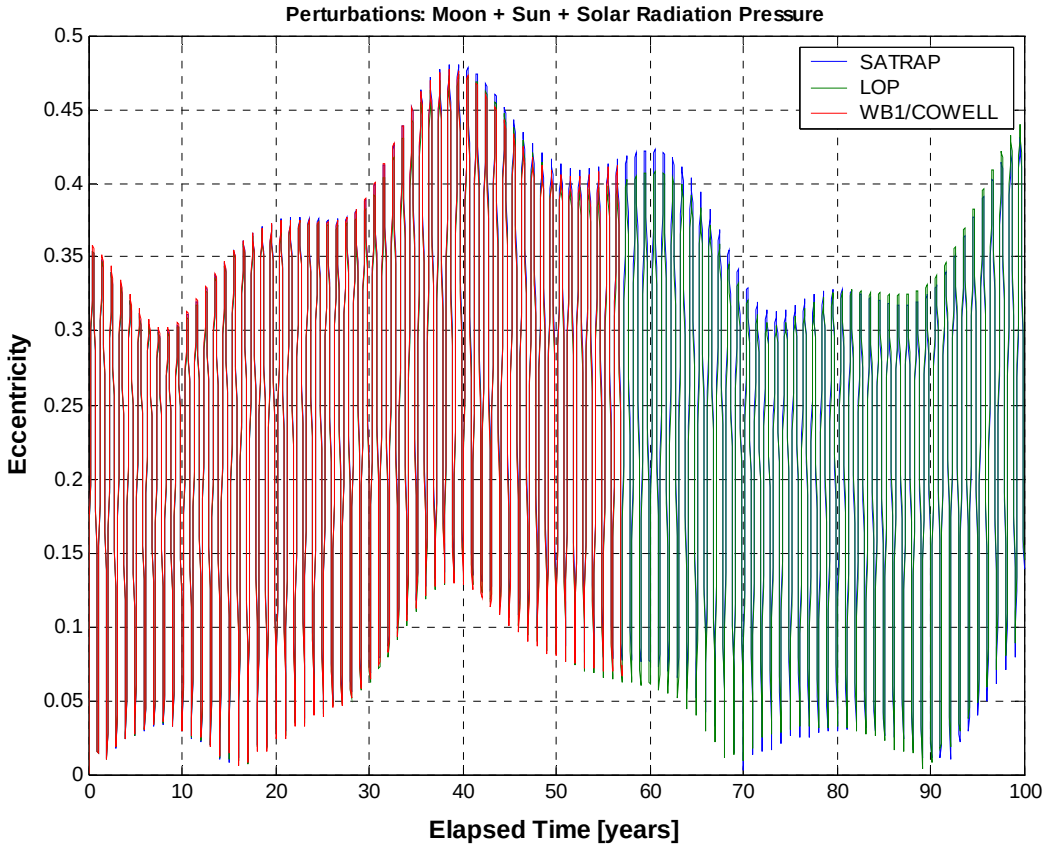

Figure 2.23

Long-term eccentricity evolution in GEO, taking into account the luni-solar third body attraction and solar radiation pressure. The agreement between the three orbit propagators was very good.

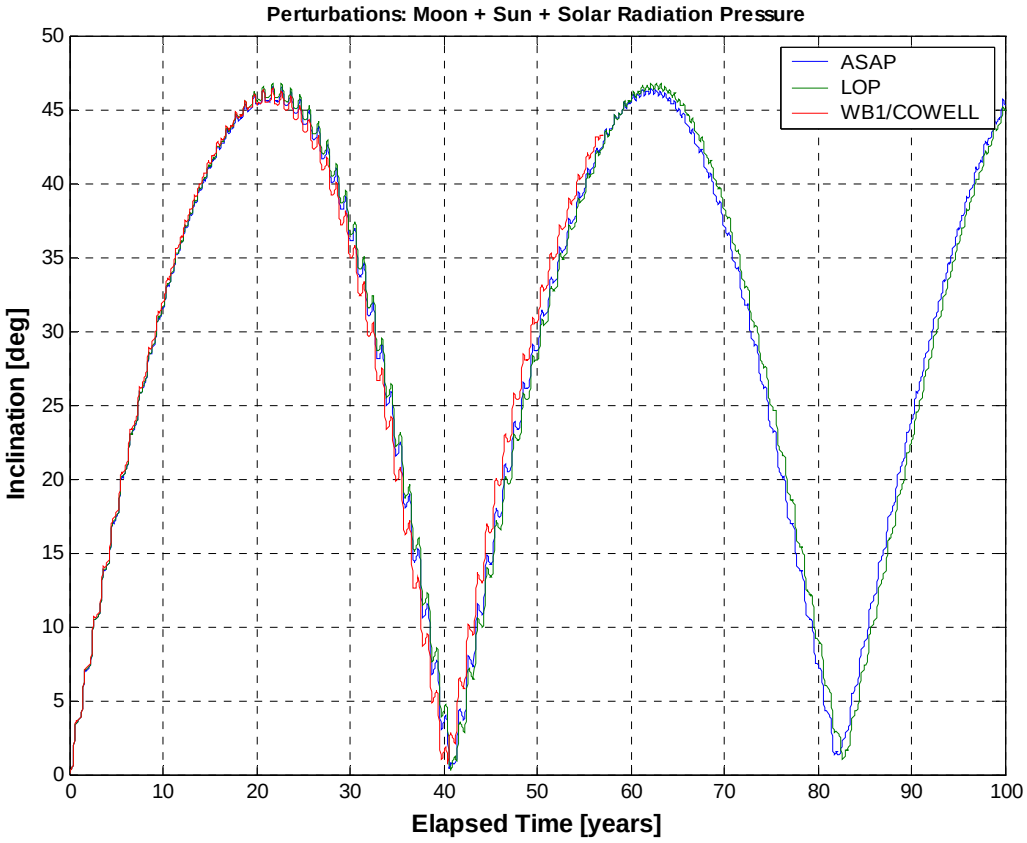

Figure 2.24

Long-term inclination evolution in GEO, taking into account the luni-solar third body attraction and solar radiation pressure. The agreement between the three orbit propagators was quite good.

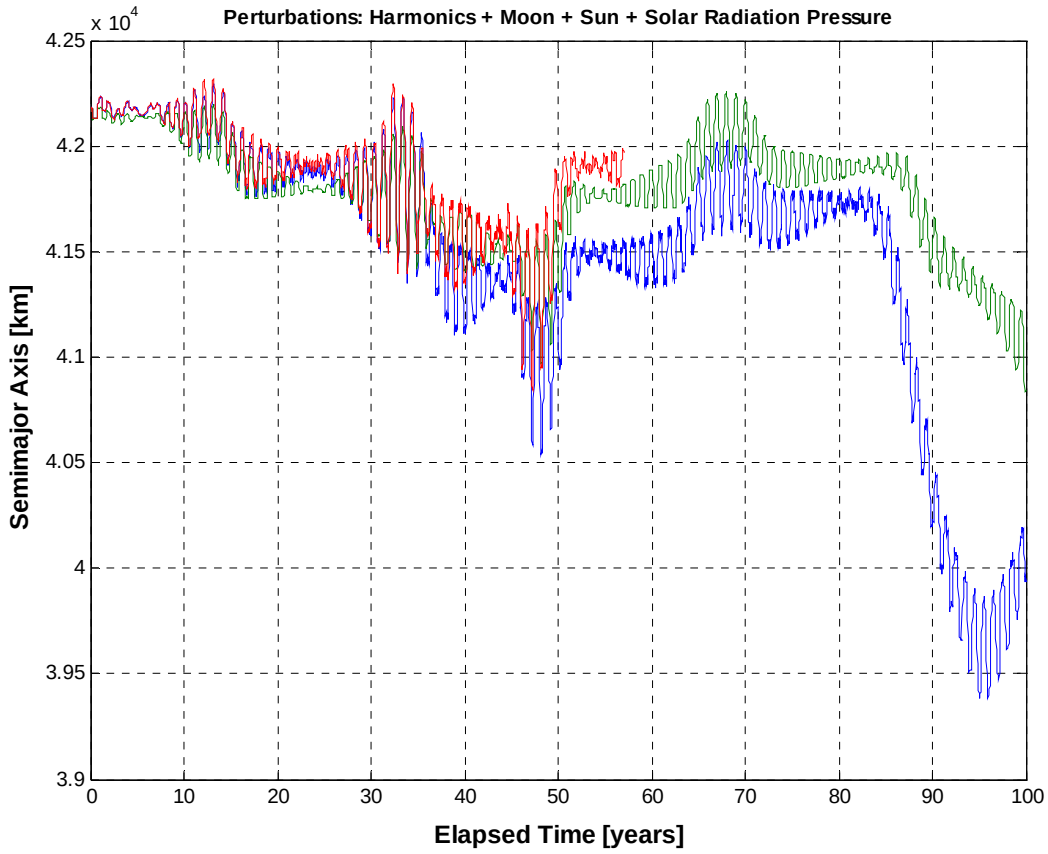

Figure 2.25

Long-term semimajor axis evolution in GEO, taking into account all relevant perturbations. The three software codes showed a reasonable agreement, at least during the first 40 years.

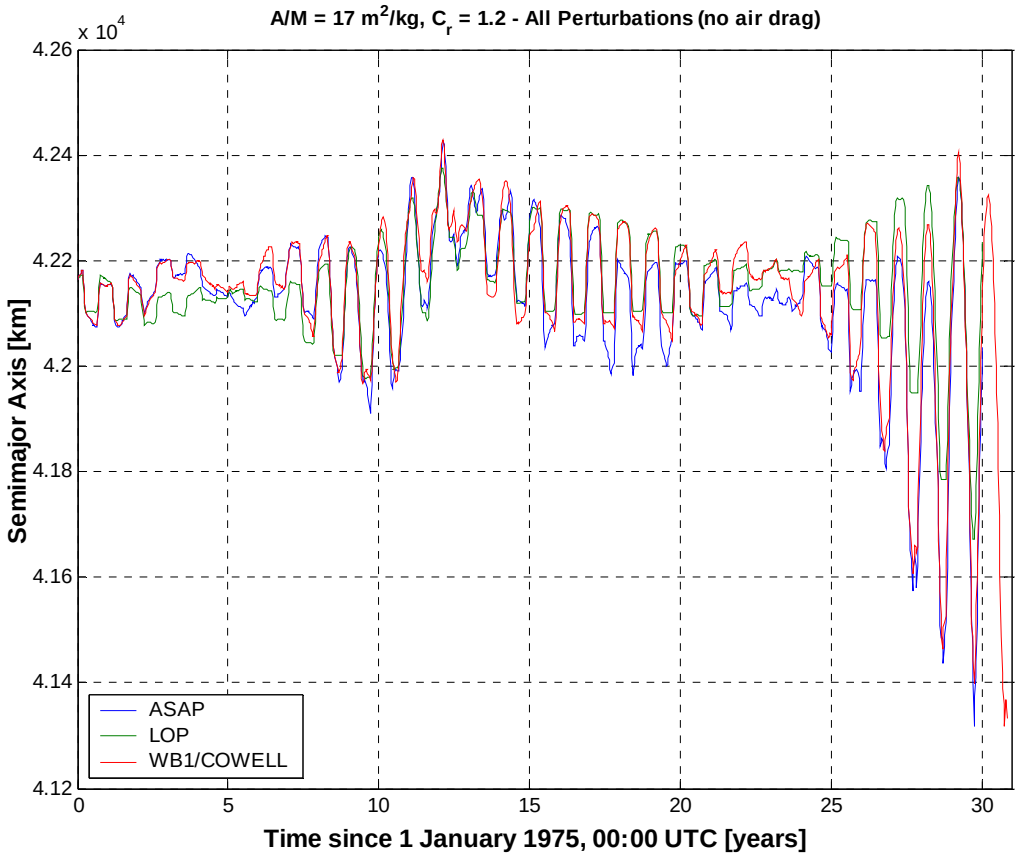

Figure 2.26

Semimajor axis evolution in GEO, over about 30 years, taking into account all relevant perturbations (see Table 2.2). The three software codes showed a quite good agreement.

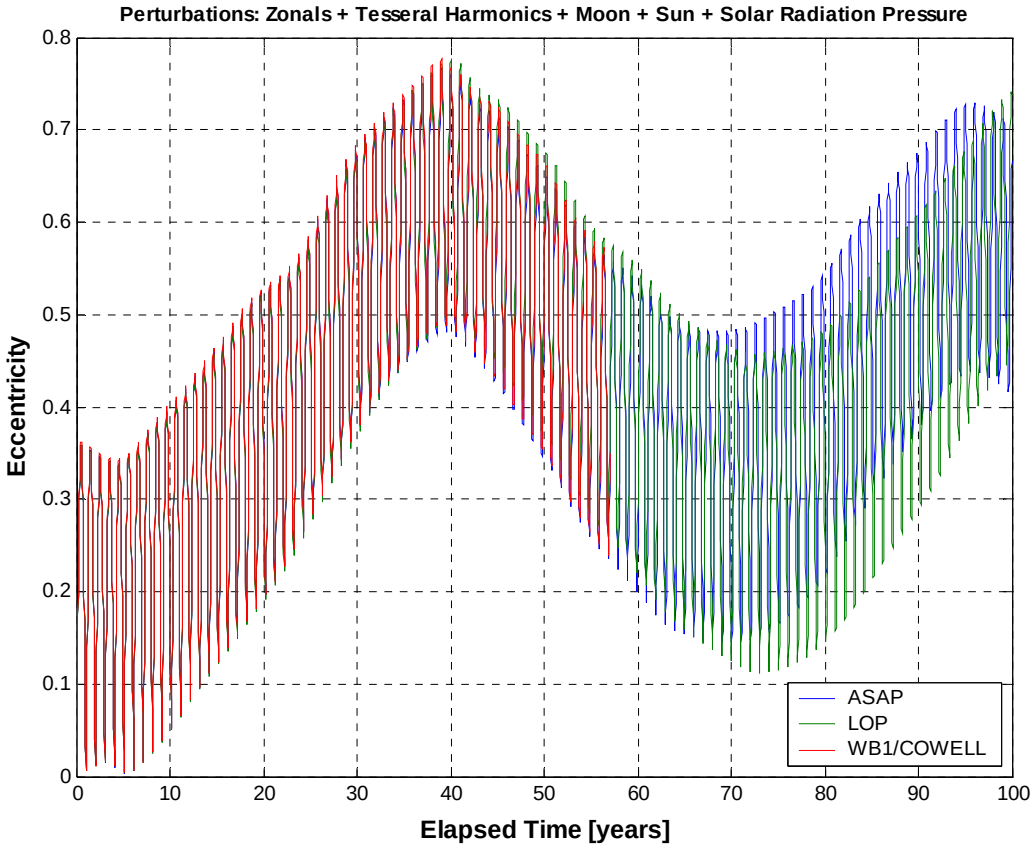

Figure 2.27

Long-term eccentricity evolution in GEO, taking into account all relevant perturbations. In ASAP and LOP, the solar radiation perturbation model neglected the varying Sun-Earth distance in the estimation of the radiation pressure magnitude. The good agreement between such propagators and WB1/COWELL indicated that also the latter adopted a similar assumption.

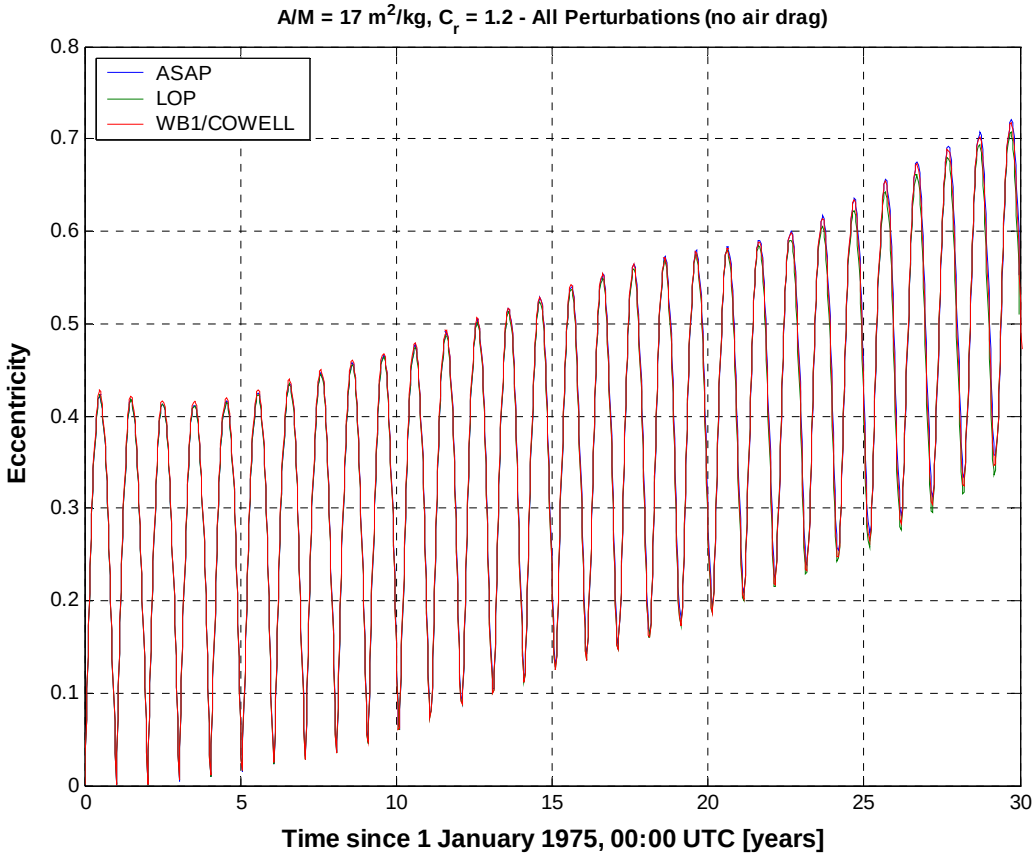

Figure 2.28

Eccentricity evolution in GEO, over about 30 years, taking into account all relevant perturbations (see Table 2.2). In ASAP and LOP, the solar radiation perturbation model neglected the varying Sun-Earth distance in the estimation of the radiation pressure magnitude. The good agreement between such propagators and WB1/COWELL indicated that also the latter adopted a similar assumption.

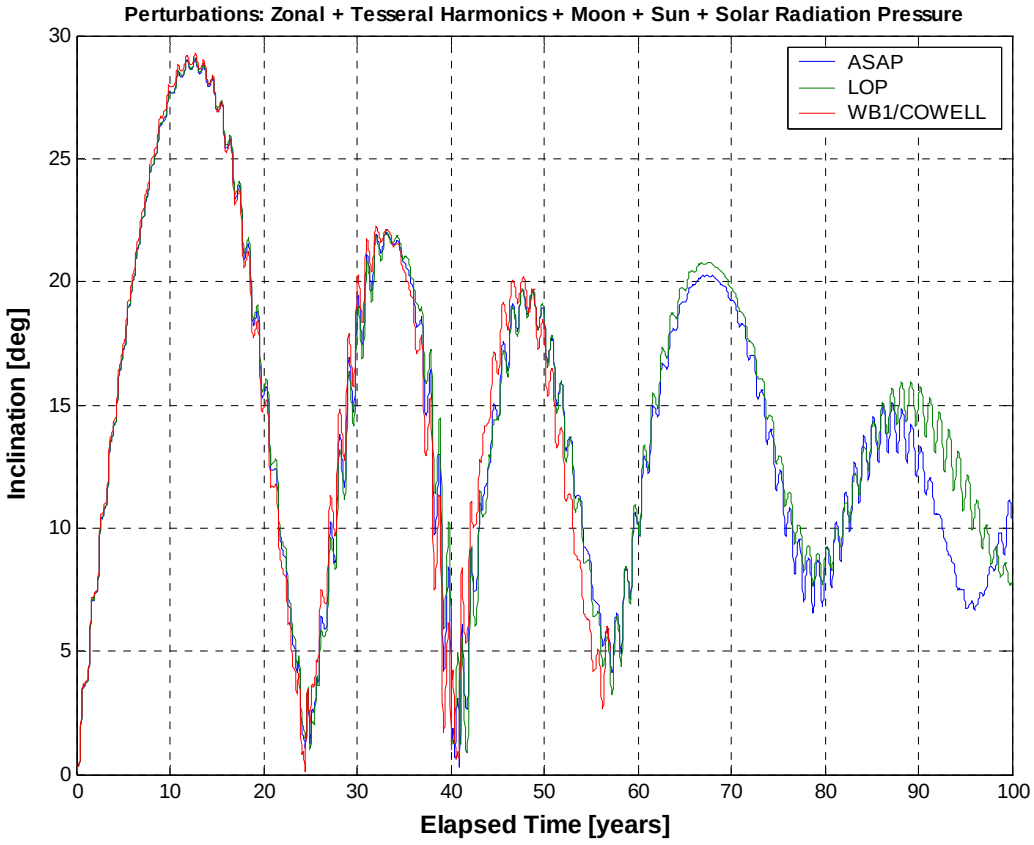

Figure 2.29

Long-term inclination evolution in GEO, taking into account all relevant perturbations. In ASAP and LOP, the solar radiation perturbation model neglected the varying Sun-Earth distance in the estimation of the radiation pressure magnitude. The good agreement between such propagators and WB1/COWELL indicated that also the latter adopted a similar assumption.

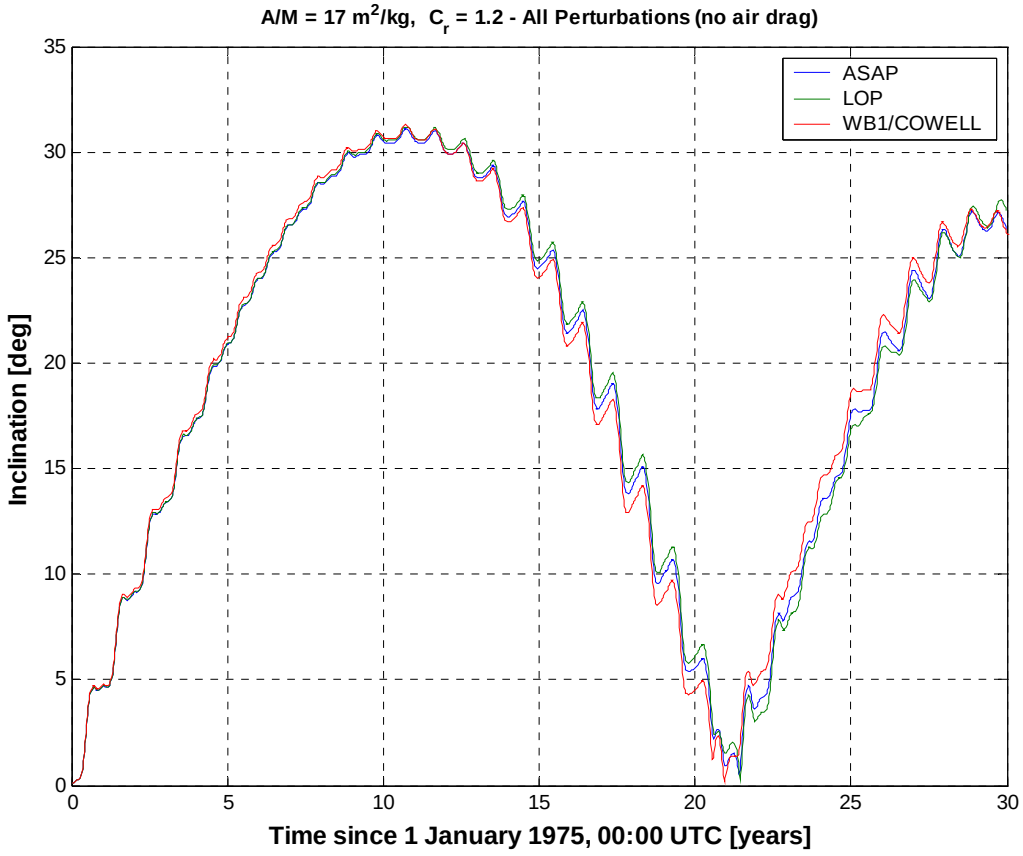

Figure 2.30

Inclination evolution in GEO, over about 30 years, taking into account all relevant perturbations (see Table 2.2). In ASAP and LOP, the solar radiation perturbation model neglected the varying Sun-Earth distance in the estimation of the radiation pressure magnitude. The quite good agreement between such propagators and WB1/COWELL indicated that also the latter adopted a similar assumption.

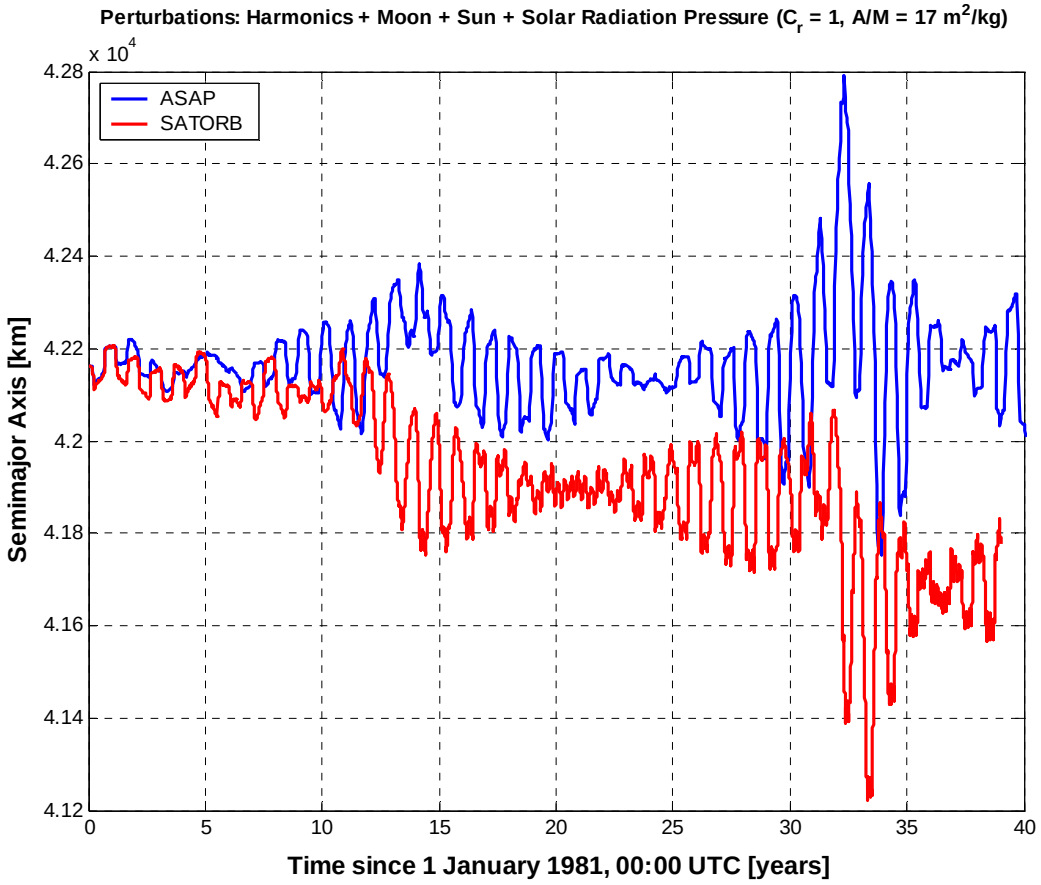

Figure 2.31

Long-term semimajor axis evolution in GEO, taking into account all relevant perturbations (see Table 2.3).

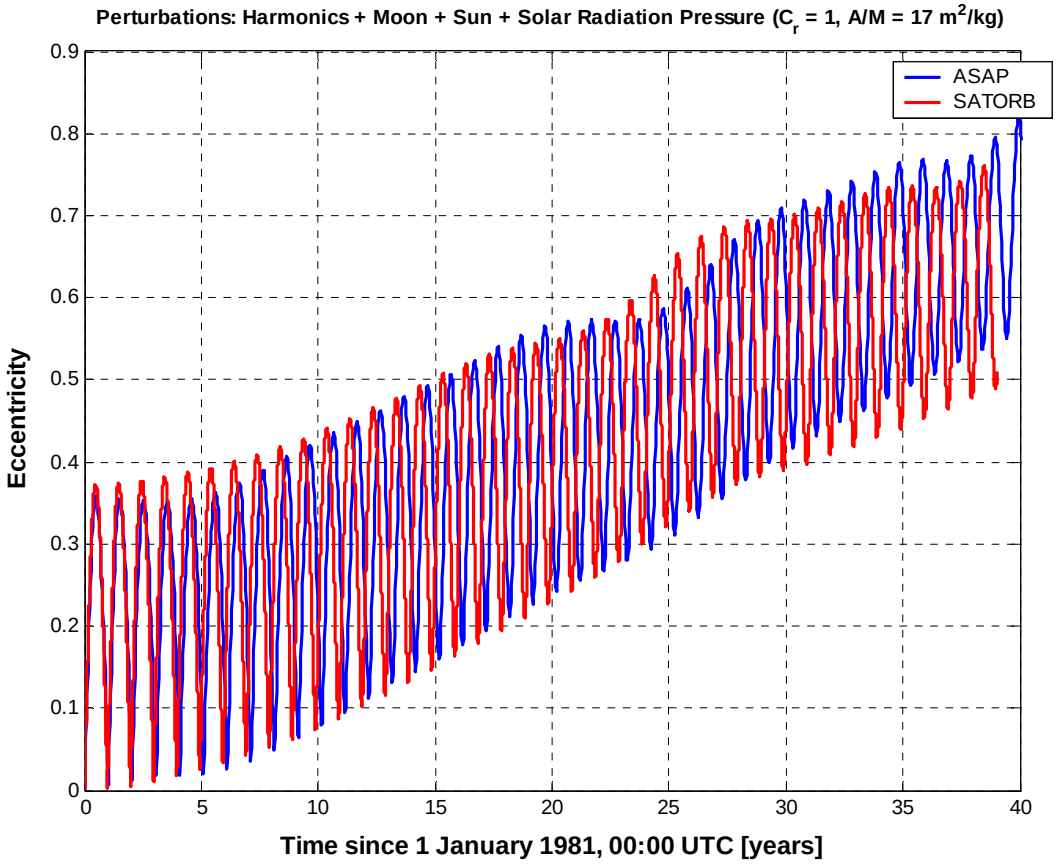

Figure 2.32

Long-term eccentricity evolution in GEO, taking into account all relevant perturbations (see Table 2.3). In ASAP, the solar radiation perturbation model neglected the varying Sun-Earth distance in the estimation of the radiation pressure magnitude. The good agreement between it and SATORB indicated that also the latter adopted a similar assumption.

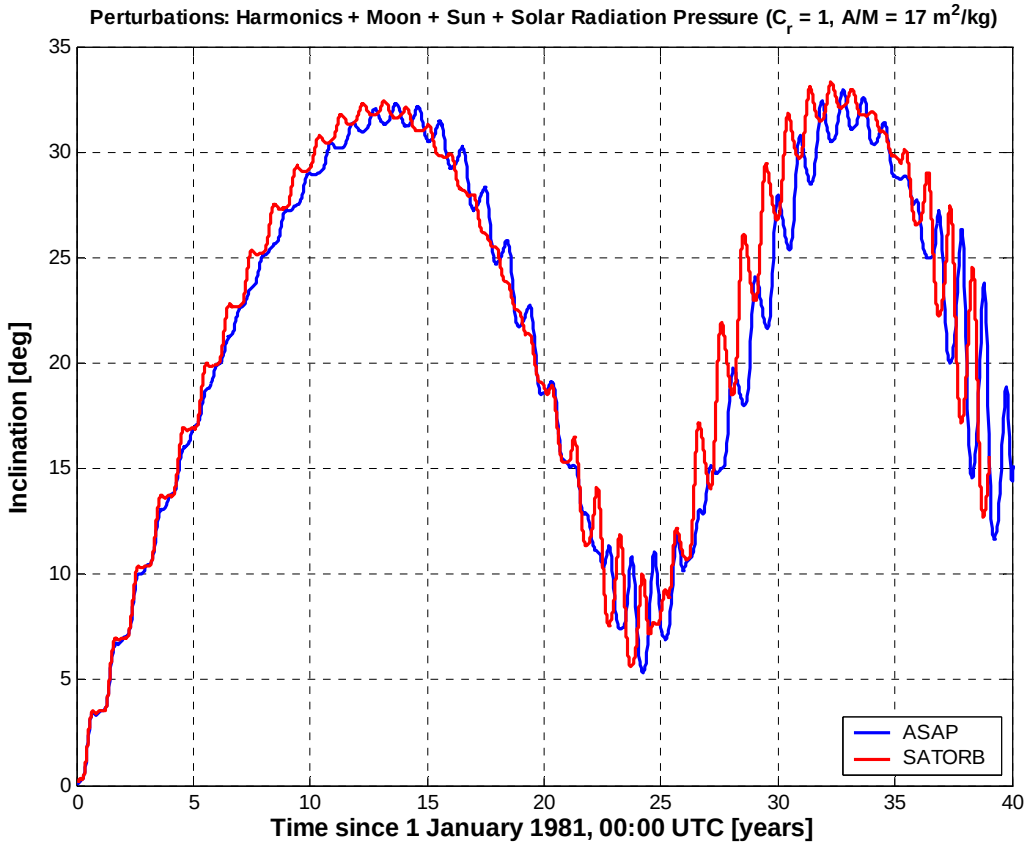

Figure 2.33

Inclination evolution in GEO, taking into account all relevant perturbations (see Table 2.3). In ASAP, the solar radiation perturbation model neglected the varying Sun-Earth distance in the estimation of the radiation pressure magnitude. The quite good agreement between it and SATORB indicated that also the latter adopted a similar assumption.

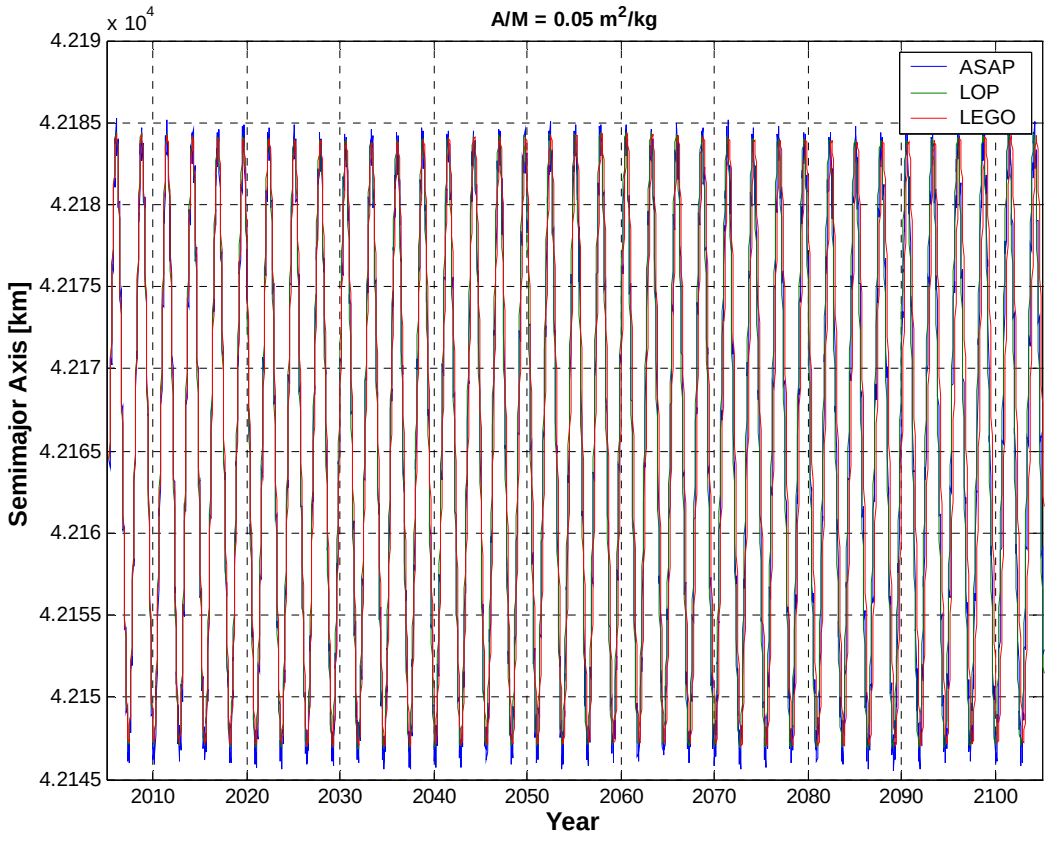

Figure 2.34

Long-term semimajor axis evolution in GEO, taking into account all relevant perturbations (A/M = 0.05 m^2/kg). The LEGO predictions were in good agreement with those of ASAP and LOP.

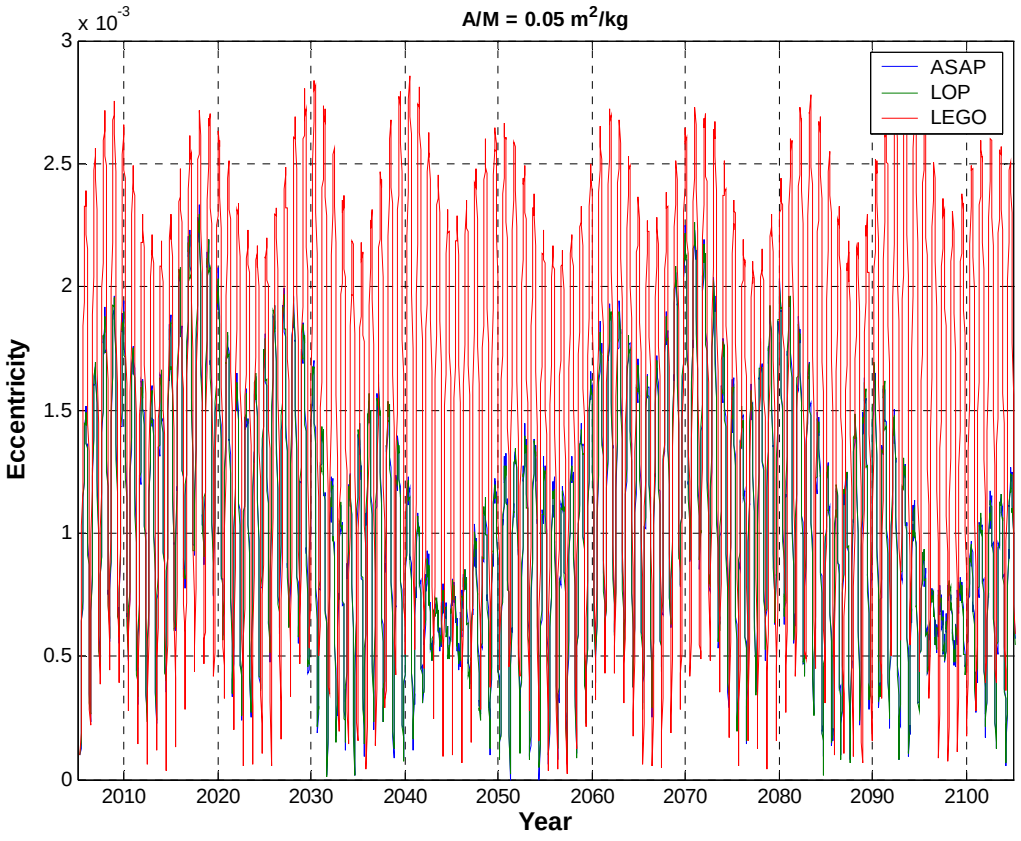

Figure 2.35

Long-term eccentricity evolution in GEO, taking into account all relevant perturbations (A/M = 0.05 m^2/kg). There were significant discrepancies, both qualitative and quantitative, between the predictions of LEGO and those of ASAP and LOP.

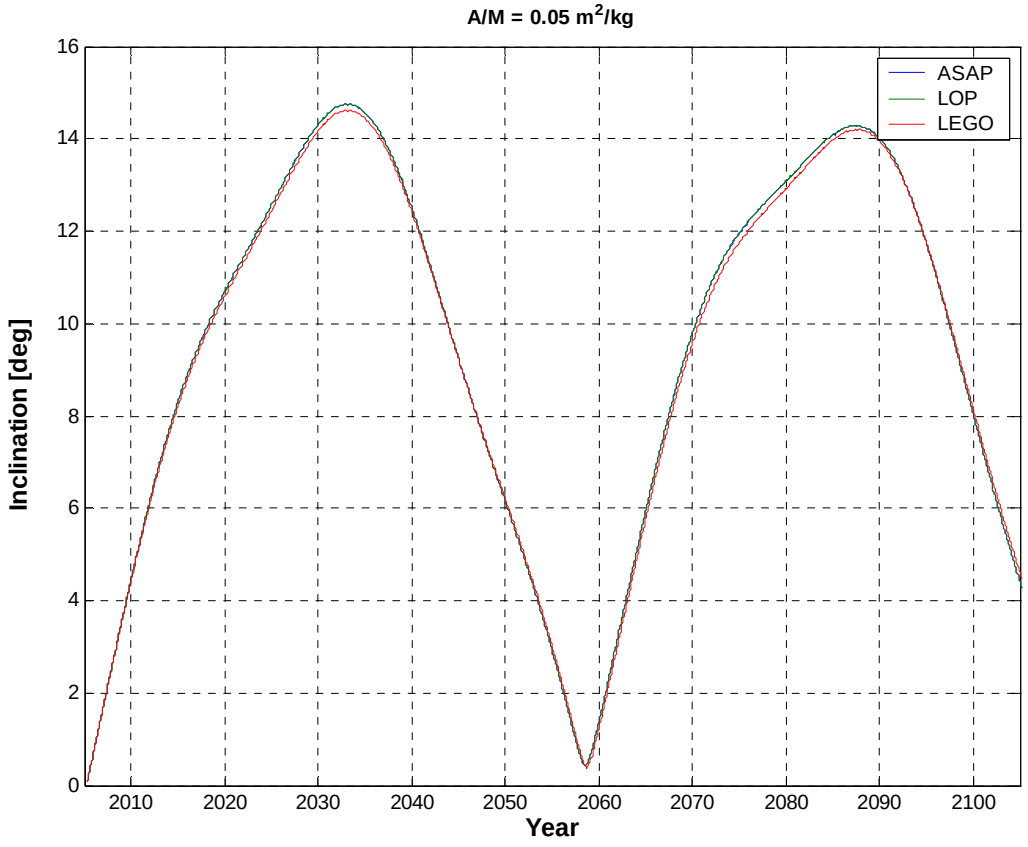

Figure 2.36

Long-term inclination evolution in GEO, taking into account all relevant perturbations (A/M = 0.05 m^2/kg). The LEGO predictions were in good agreement with those of ASAP and LOP.

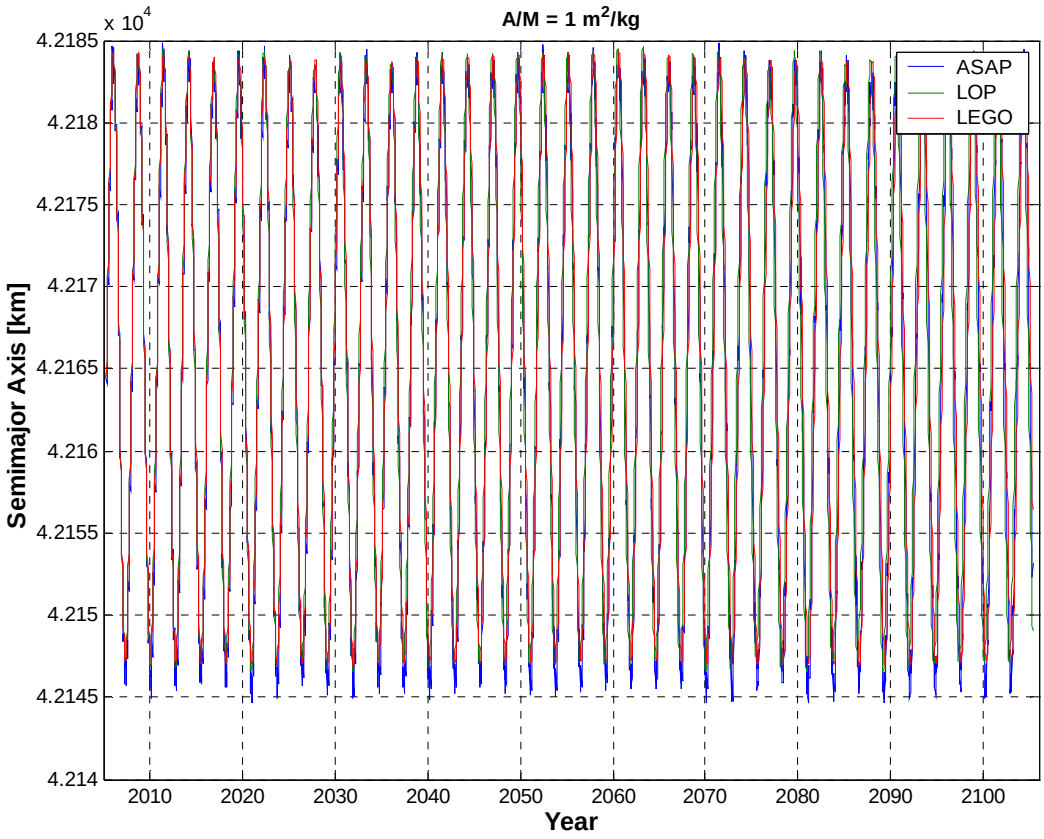

Figure 2.37

Long-term semimajor axis evolution in GEO, taking into account all relevant perturbations (A/M = 1 m^2/kg). The LEGO predictions were in good agreement with those of ASAP and LOP.

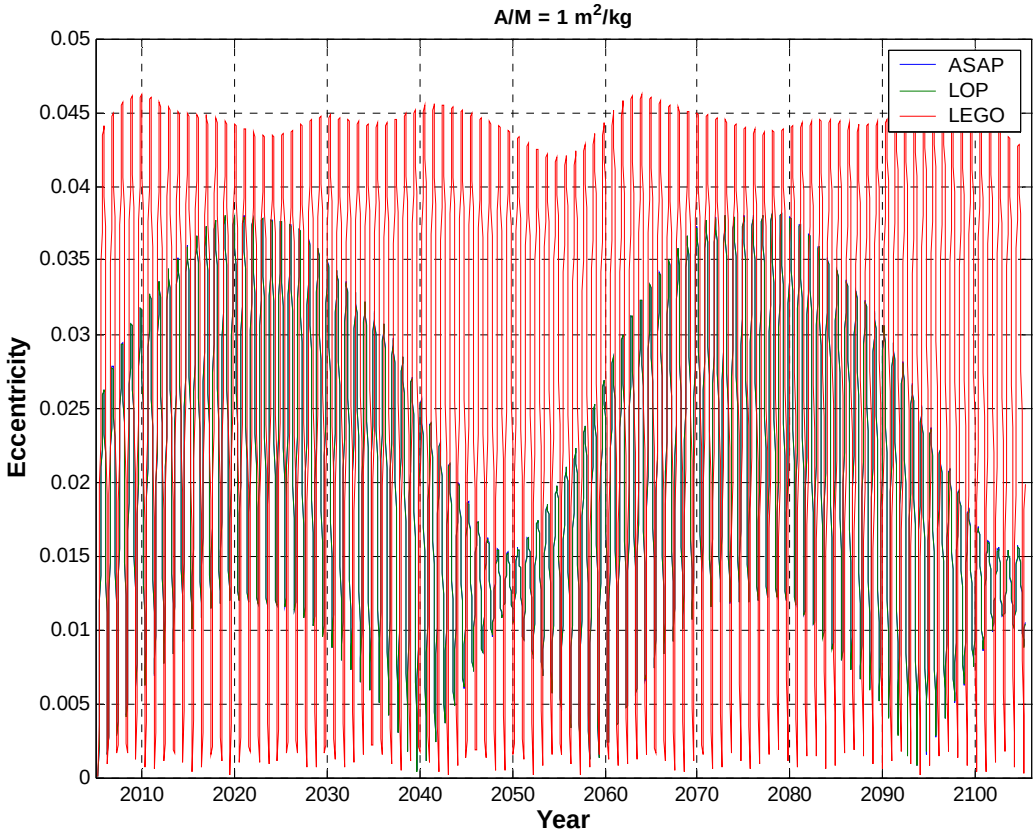

Figure 2.38

Long-term eccentricity evolution in GEO, taking into account all relevant perturbations (A/M = 1 m^2/kg). There were significant discrepancies, both qualitative and quantitative, between the predictions of LEGO and those of ASAP and LOP.

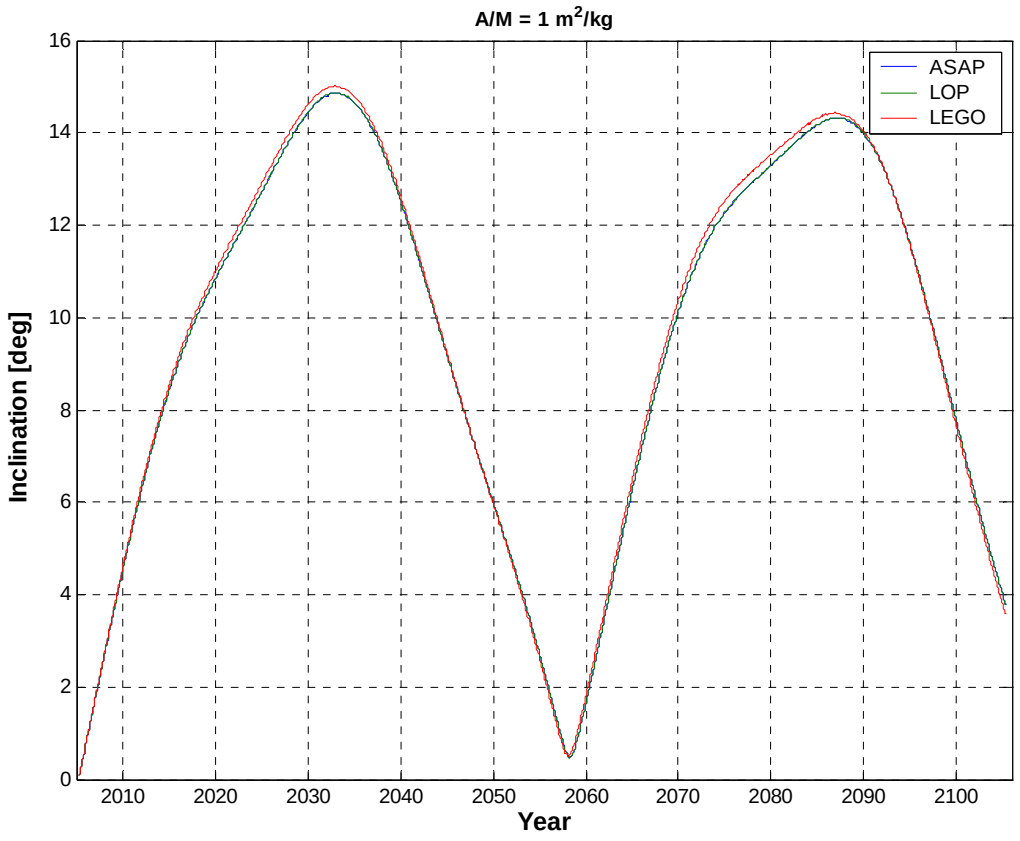

Figure 2.39

Long-term inclination evolution in GEO, taking into account all relevant perturbations (A/M = 1 m^2/kg). The LEGO predictions were in good agreement with those of ASAP and LOP.

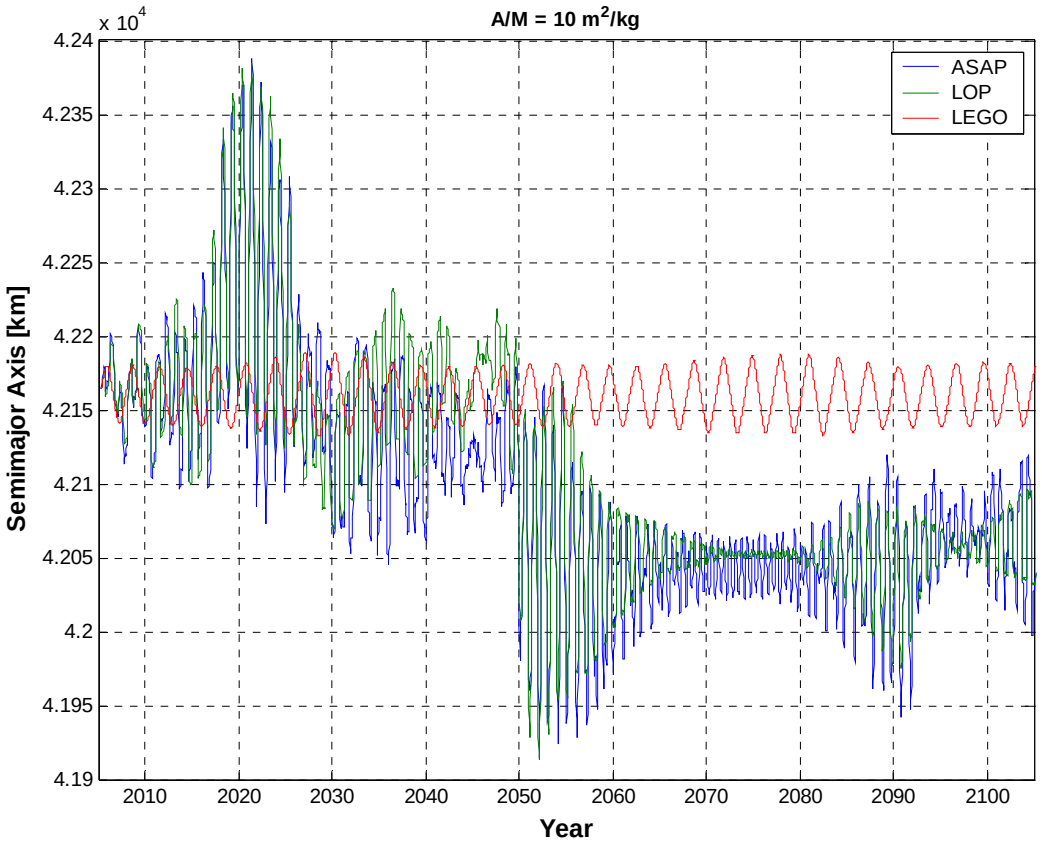

Figure 2.40

Long-term semimajor axis evolution in GEO, taking into account all relevant perturbations (A/M = 10 m^2/kg). There were significant discrepancies, both qualitative and quantitative, between the predictions of LEGO and those of ASAP and LOP, mainly because the first program ignored the eclipses.

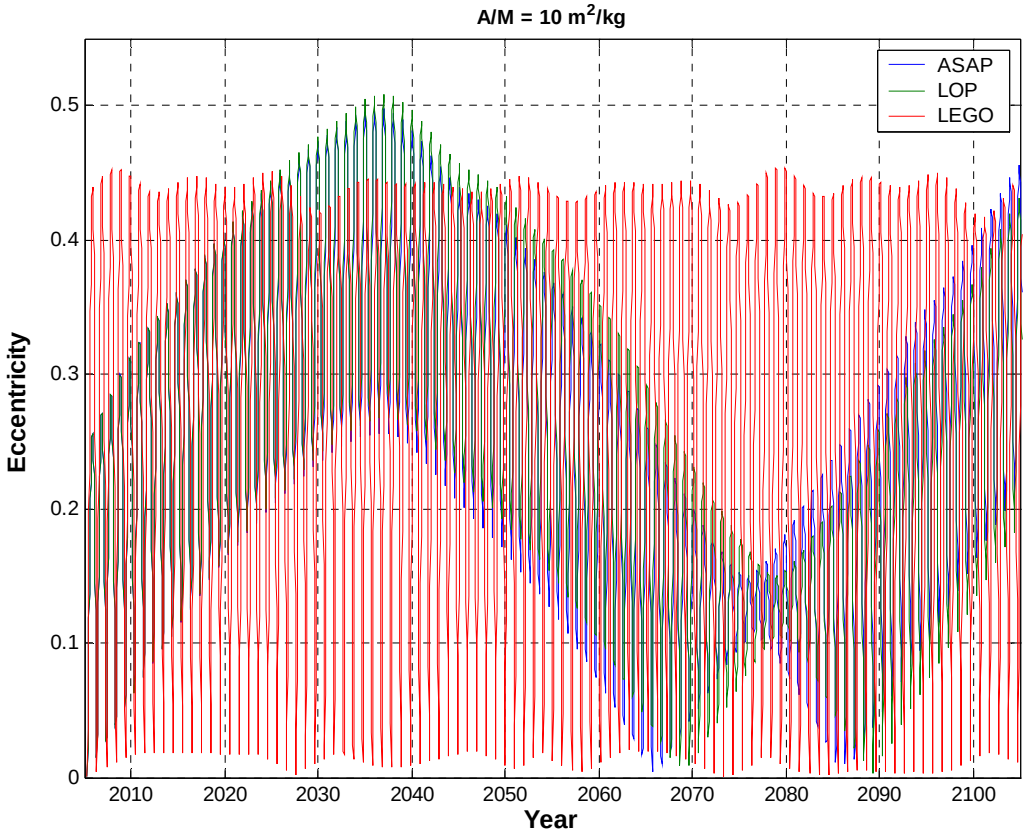

Figure 2.41

Long-term eccentricity evolution in GEO, taking into account all relevant perturbations (A/M = 10 m^2/kg). There were significant discrepancies, both qualitative and quantitative, between the predictions of LEGO and those of ASAP and LOP.

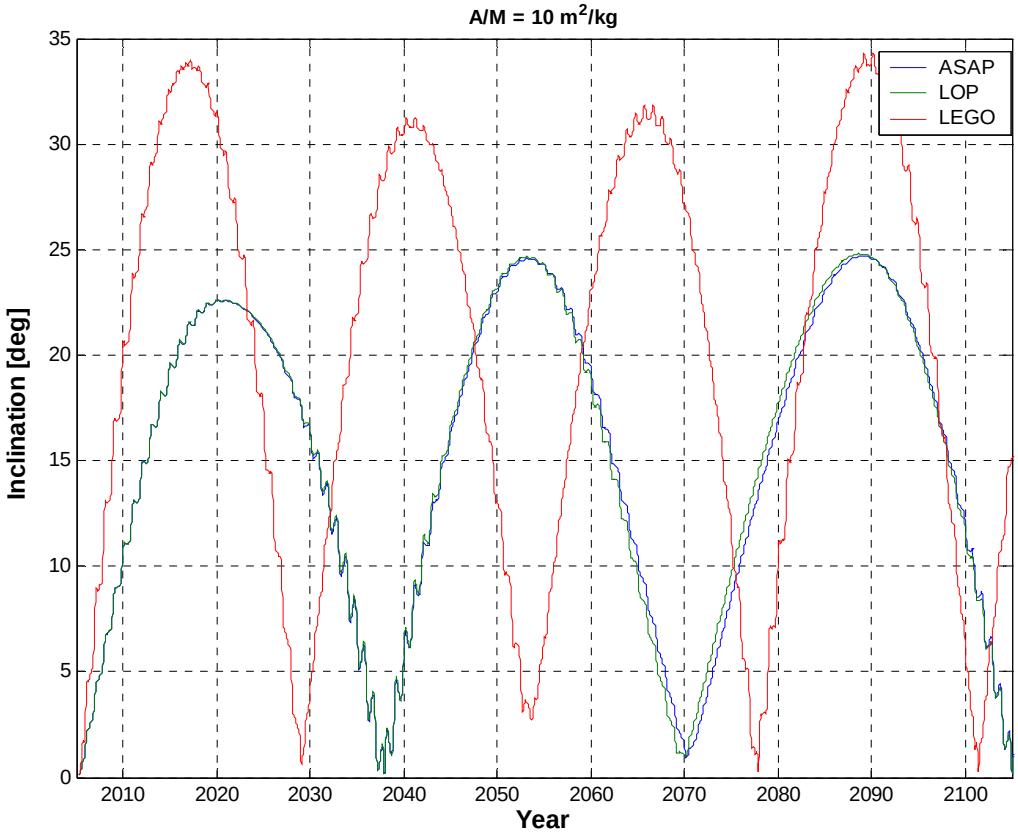

Figure 2.42

Long-term inclination evolution in GEO, taking into account all relevant perturbations (A/M = 10 m^2/kg). There were significant discrepancies, both qualitative and quantitative, between the predictions of LEGO and those of ASAP and LOP.

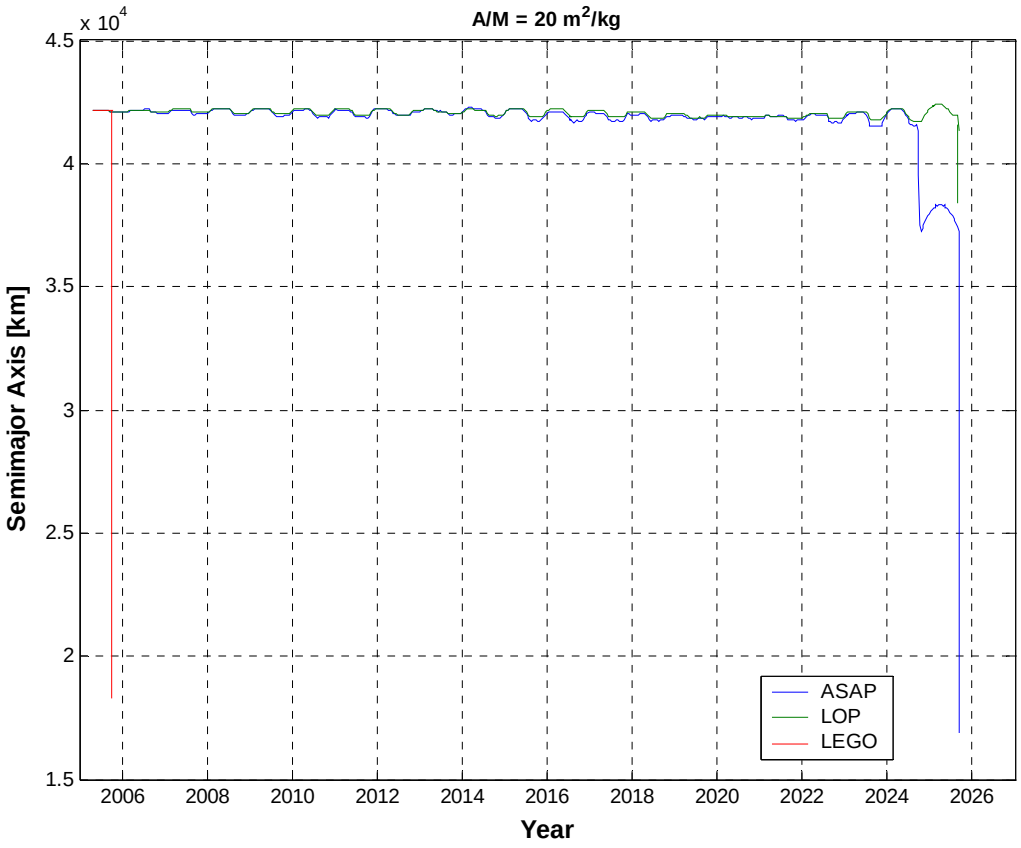

Figure 2.43

Long-term semimajor axis evolution in GEO, taking into account all relevant perturbations (A/M = 20 m^2/kg). The eccentricity computed by LEGO rapidly increased too much (see Figure 2.44), inducing an early orbital decay in just a few months.

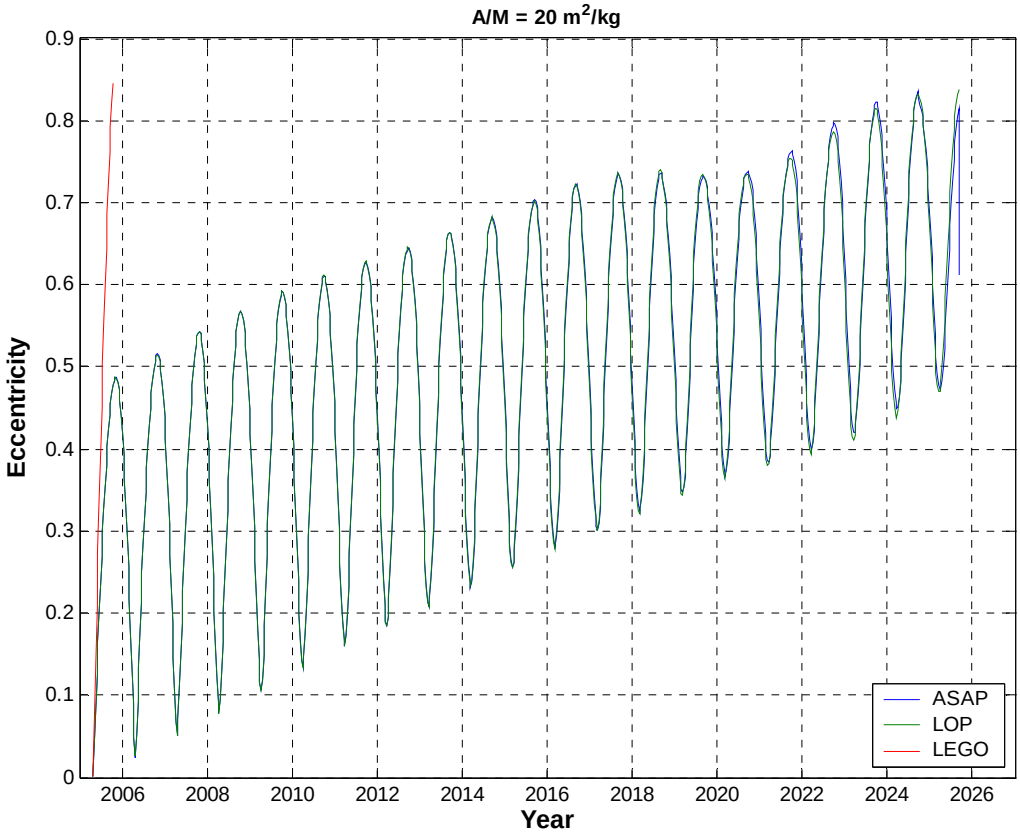

Figure 2.44

Long-term eccentricity evolution in GEO, taking into account all relevant perturbations (A/M = 20 m^2/kg). The eccentricity computed by LEGO rapidly increased too much, inducing an early orbital decay in just a few months.

Figure 2.45

Long-term inclination evolution in GEO, taking into account all relevant perturbations (A/M = 20 m^2/kg). The eccentricity computed by LEGO rapidly increased too much (see Figure 2.44), inducing an early orbital decay in just a few months.

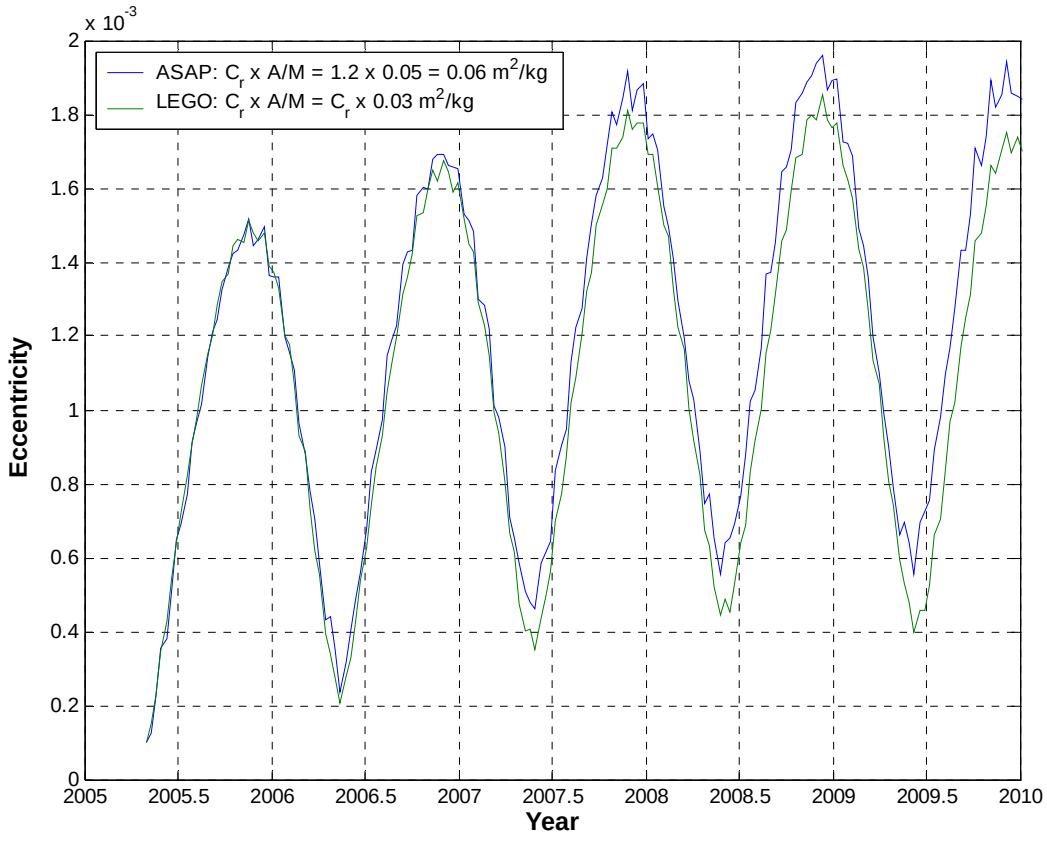

Figure 2.46

Eccentricity evolution in GEO, taking into account all relevant perturbations. A good agreement between ASAP and LEGO, at least for a few years and for relatively small area-to-mass ratios, was obtained by assuming that the fixed value $C_r = 2$ was implicitly set inside the latter software code.

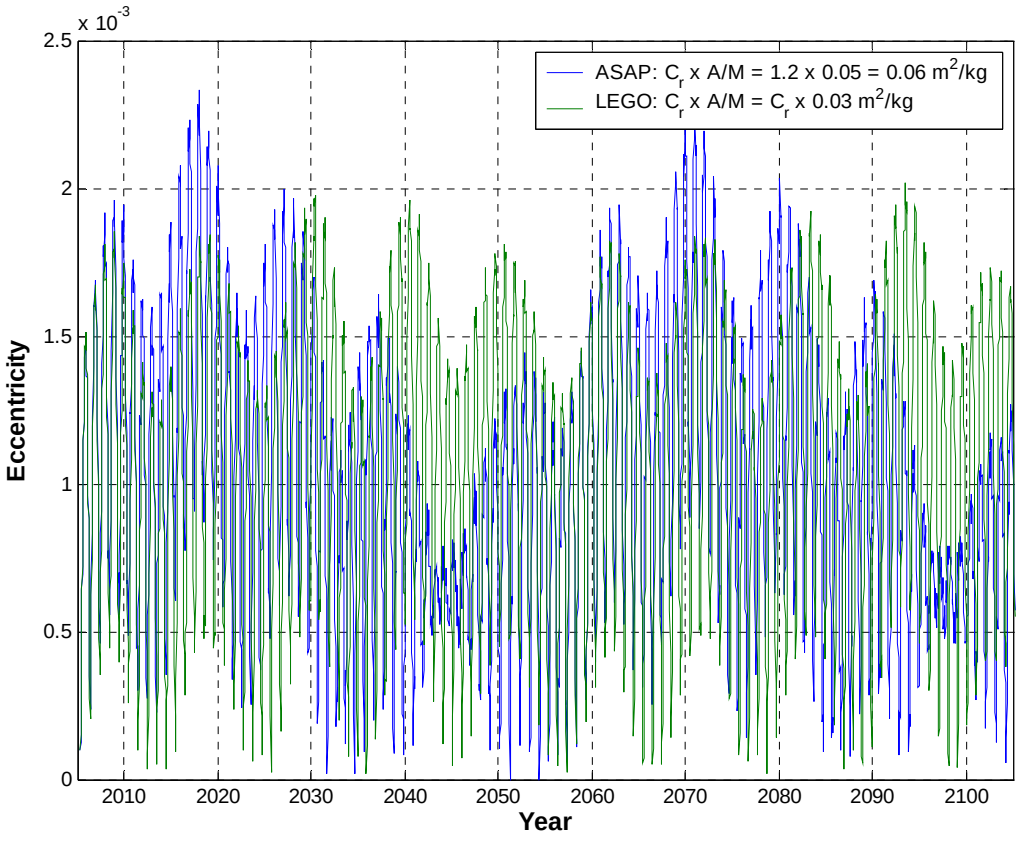

Figure 2.47

Long-term eccentricity evolution in GEO, taking into account all relevant perturbations. The best agreement between ASAP and LEGO, even though not fully satisfactory, was obtained by assuming that the fixed value $C_r = 2$ was implicitly set inside the latter software code.

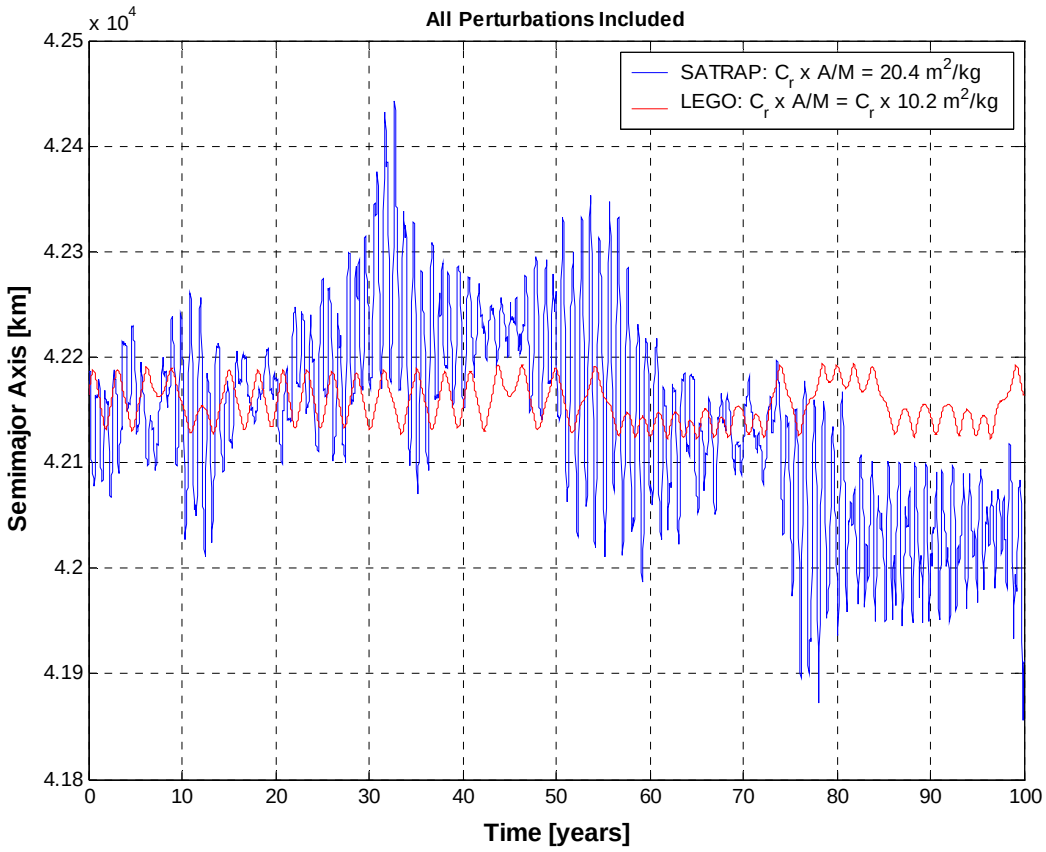

Figure 2.48

Long-term semimajor axis evolution in GEO, taking into account all relevant perturbations and putting $C_r \times A/M$ = 20.4 m^2/kg in SATRAP and A/M = 10.2 m^2/kg in LEGO. The discrepancies observed were mainly due to the fact that LEGO ignored the sunlight eclipses.

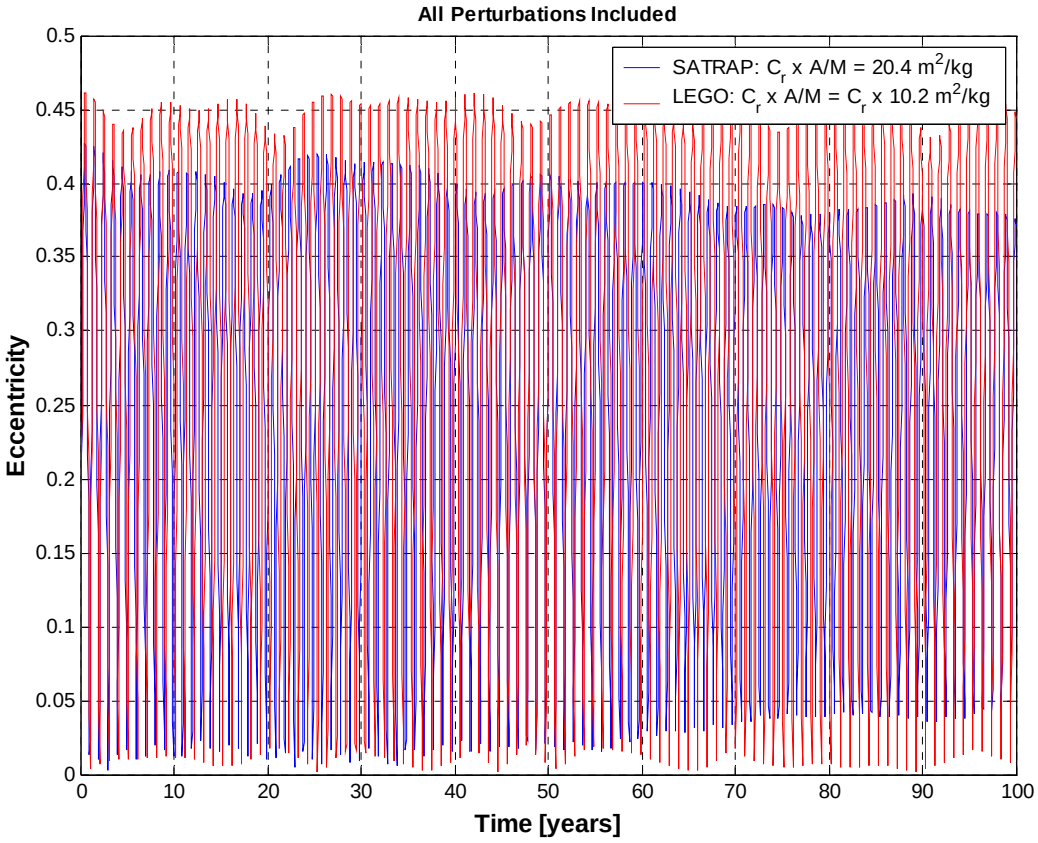

Figure 2.49

Long-term eccentricity evolution in GEO, taking into account all relevant perturbations and putting $C_r \times A/M$ = 20.4 m^2/kg in SATRAP and A/M = 10.2 m^2/kg in LEGO. A more than satisfactory long-term agreement between SATRAP and LEGO, also for this extremely large area-to-mass ratio, was obtained by assuming that the fixed value C_r = 2 was implicitly set inside the latter software code. Moreover, the LEGO eccentricity evolution was compatible with the predictions of the propagators, like the last version of SATRAP, which consider the varying Sun-Earth distance in the estimation of the radiation pressure magnitude.

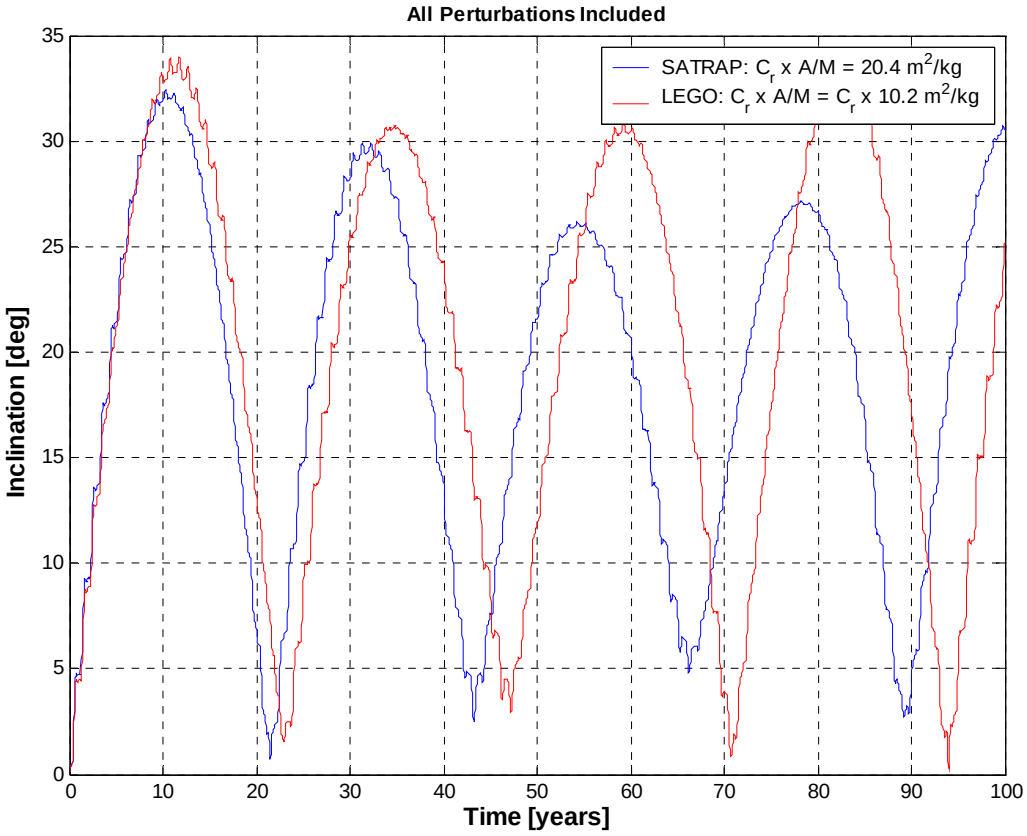

Figure 2.50

Long-term inclination evolution in GEO, taking into account all relevant perturbations and putting $C_r \times A/M$ = 20.4 m^2/kg in SATRAP and A/M = 10.2 m^2/kg in LEGO. A reasonable long-term agreement between SATRAP and LEGO, also for this extremely large area-to-mass ratio, was obtained by assuming that the fixed value C_r = 2 was implicitly set inside the latter software code.

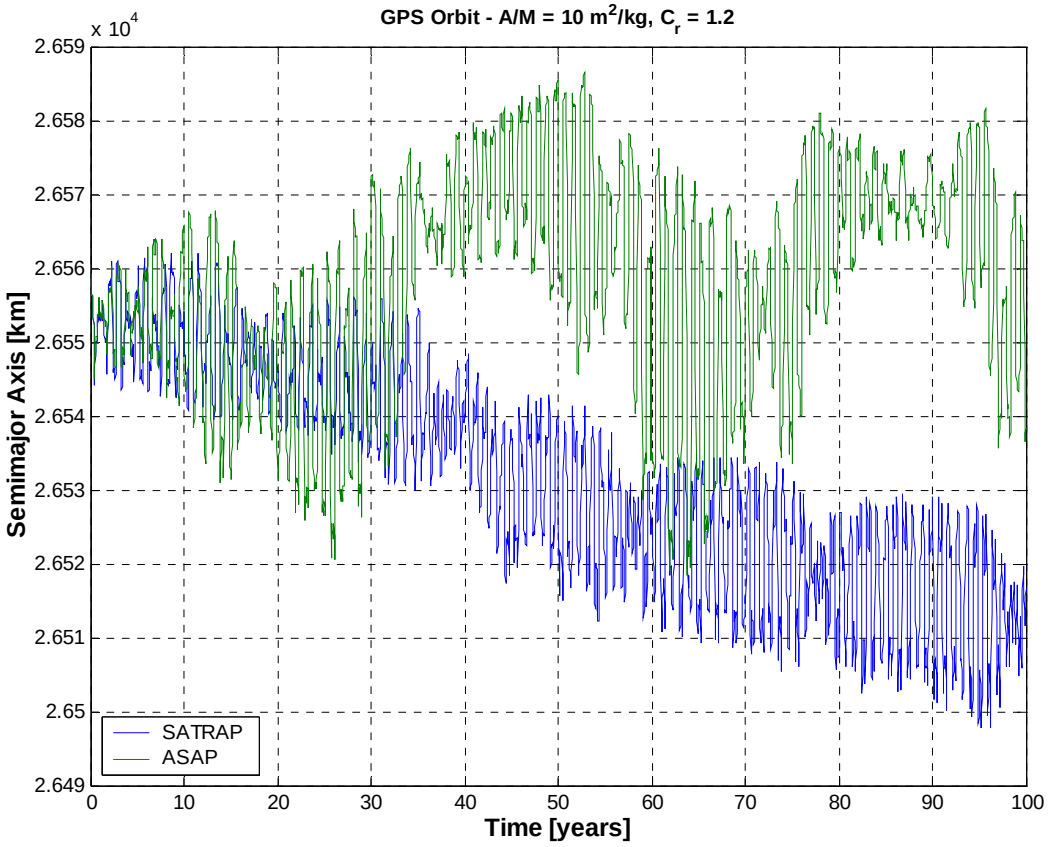

Figure 2.51

Long-term semimajor axis evolution of a GPS orbit, taking into account all relevant perturbations. In the direct solar radiation pressure model, SATRAP considered the varying Sun-Earth distance in the estimation of the perturbing acceleration magnitude, while in ASAP such a distance was fixed to 1 astronomical unit.

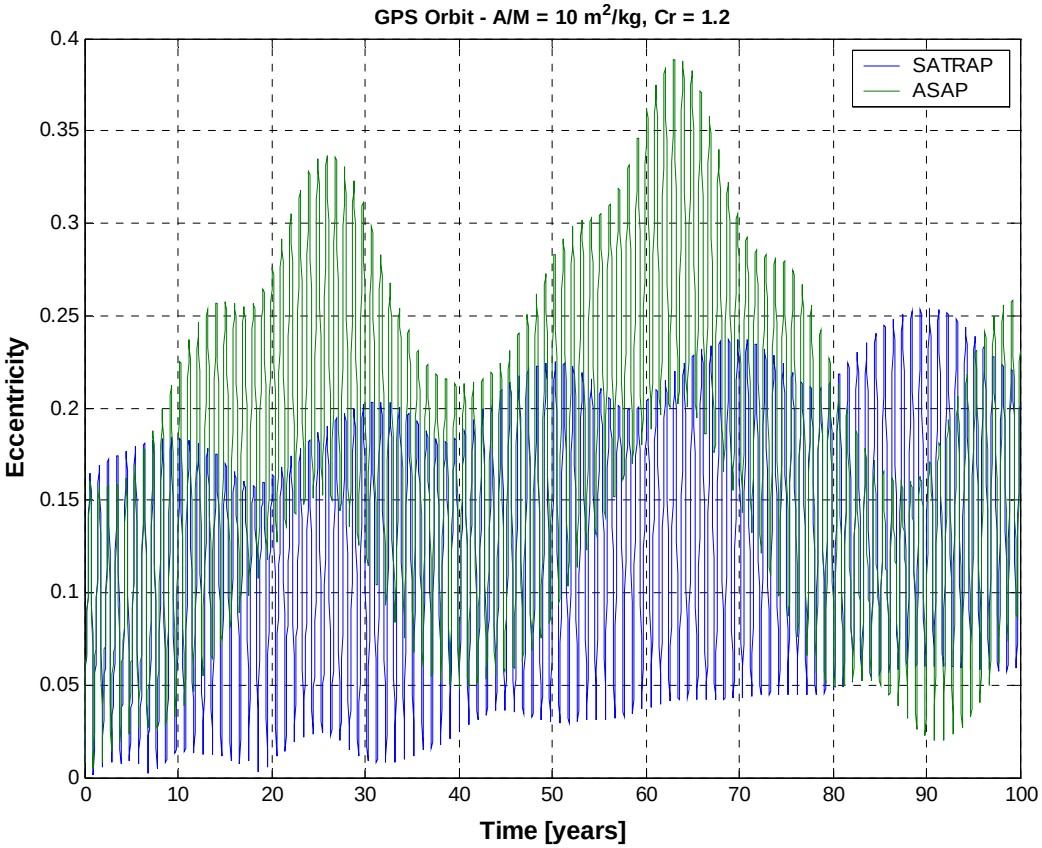

Figure 2.52

Long-term eccentricity evolution of a GPS orbit, taking into account all relevant perturbations. In the direct solar radiation pressure model, SATRAP considered the varying Sun-Earth distance in the estimation of the perturbing acceleration magnitude, while in ASAP such a distance was fixed to 1 astronomical unit. As in GEO, also in this case the latter simplifying assumption introduced significant long period effects, not observed with the more accurate model.

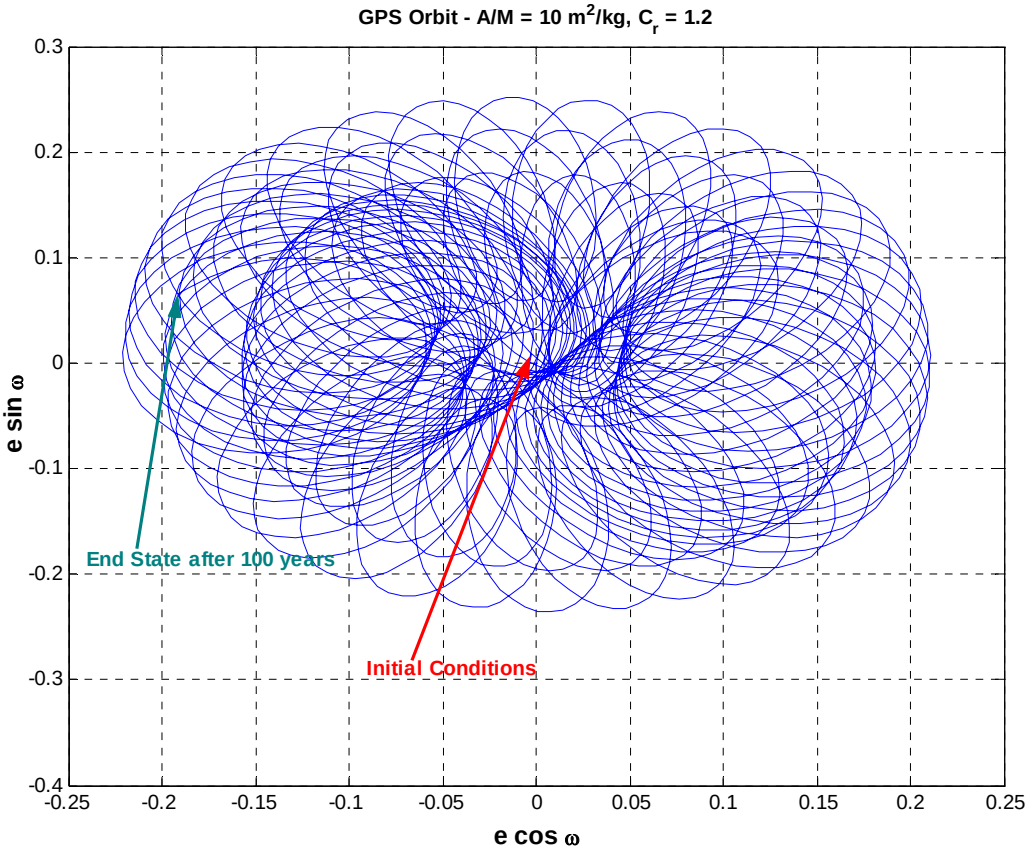

Figure 2.53

Long-term evolution of the eccentricity vector of a GPS orbit with $C_r \times A/M$ = 12 m^2/kg, taking into account all relevant perturbations and considering the varying Sun-Earth distance in the estimation of the solar radiation pressure magnitude. Basically, the vector was subjected to the combination of two anti-clockwise precessions, one with a period of one year and the other with a period of approximately 40 years.

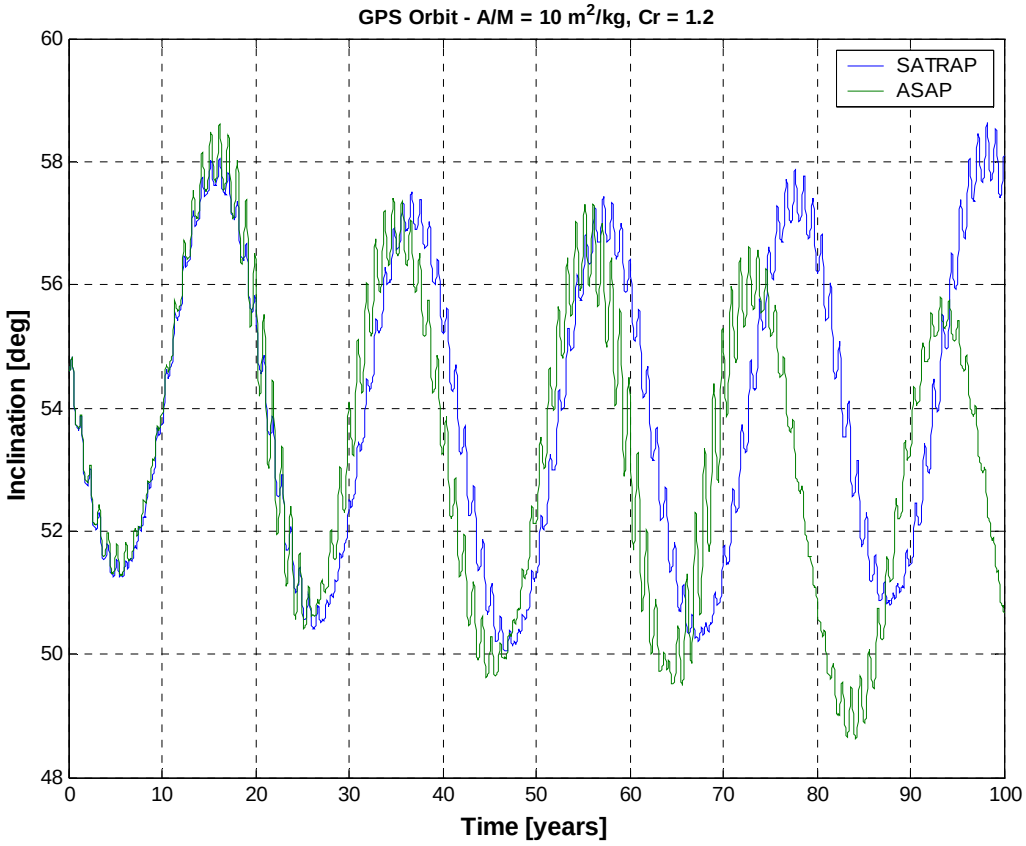

Figure 2.54

Long-term inclination evolution of a GPS orbit, taking into account all relevant perturbations. In the direct solar radiation pressure model, SATRAP considered the varying Sun-Earth distance in the estimation of the perturbing acceleration magnitude, while in ASAP such a distance was fixed to 1 astronomical unit. Noteworthy discrepancies were observed only after several decades.

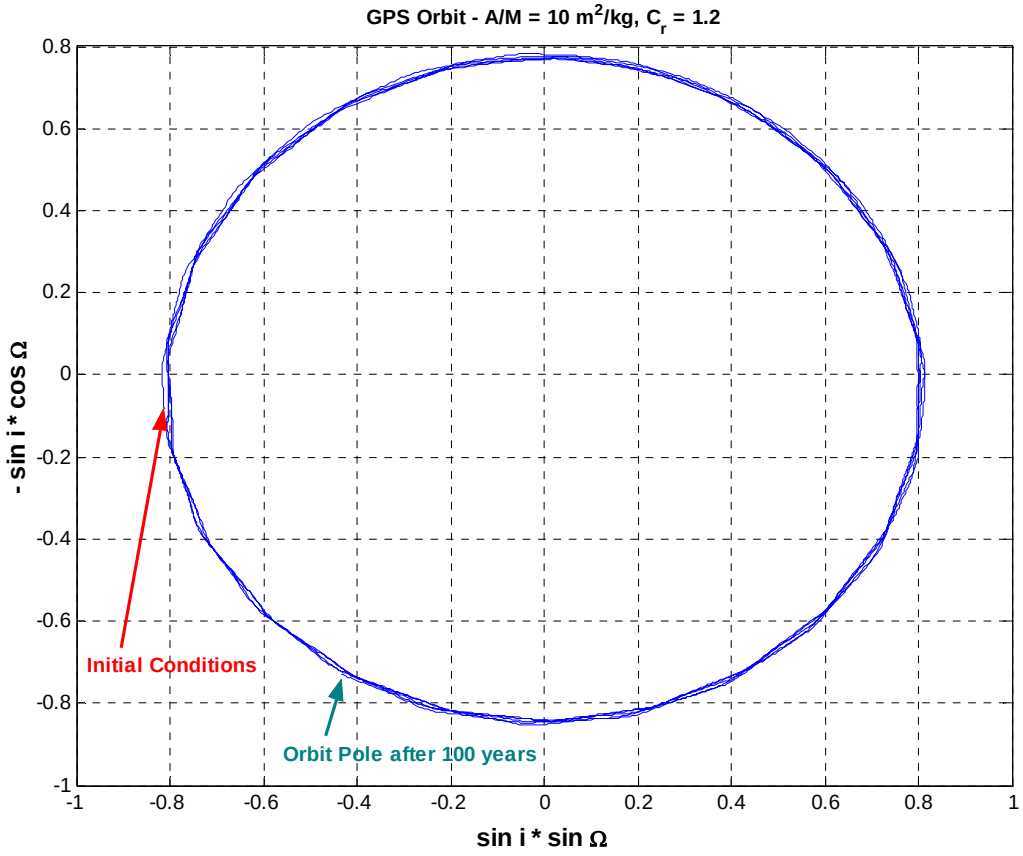

Figure 2.55

Long-term evolution of the two-dimensional inclination vector of a GPS orbit with $C_r \times A/M$ = 12 m^2/kg, taking into account all relevant perturbations and considering the varying Sun-Earth distance in the estimation of the solar radiation pressure magnitude. The orbit pole was subjected to a clockwise precession with a period of a little bit more than 20 years.

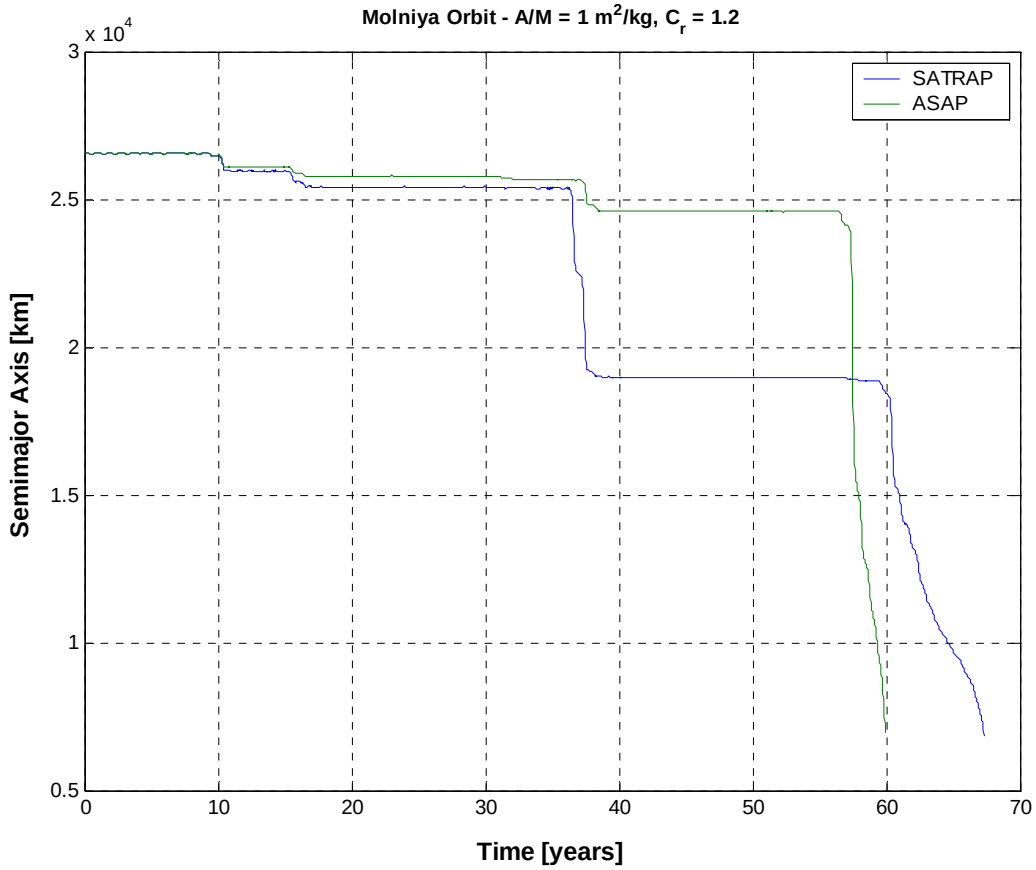

Figure 2.56

Long-term semimajor axis evolution of a Molniya orbit, taking into account all relevant perturbations. In the direct solar radiation pressure model, SATRAP considered the varying Sun-Earth distance in the estimation of the perturbing acceleration magnitude, while in ASAP such a distance was fixed to 1 astronomical unit. For more than 30 years, the agreement remained quite good. Later on, the discrepancies observed were basically a consequence of small numerical differences in the perigee altitude, leading to dissimilar apogee evolutions and orbital lifetimes.

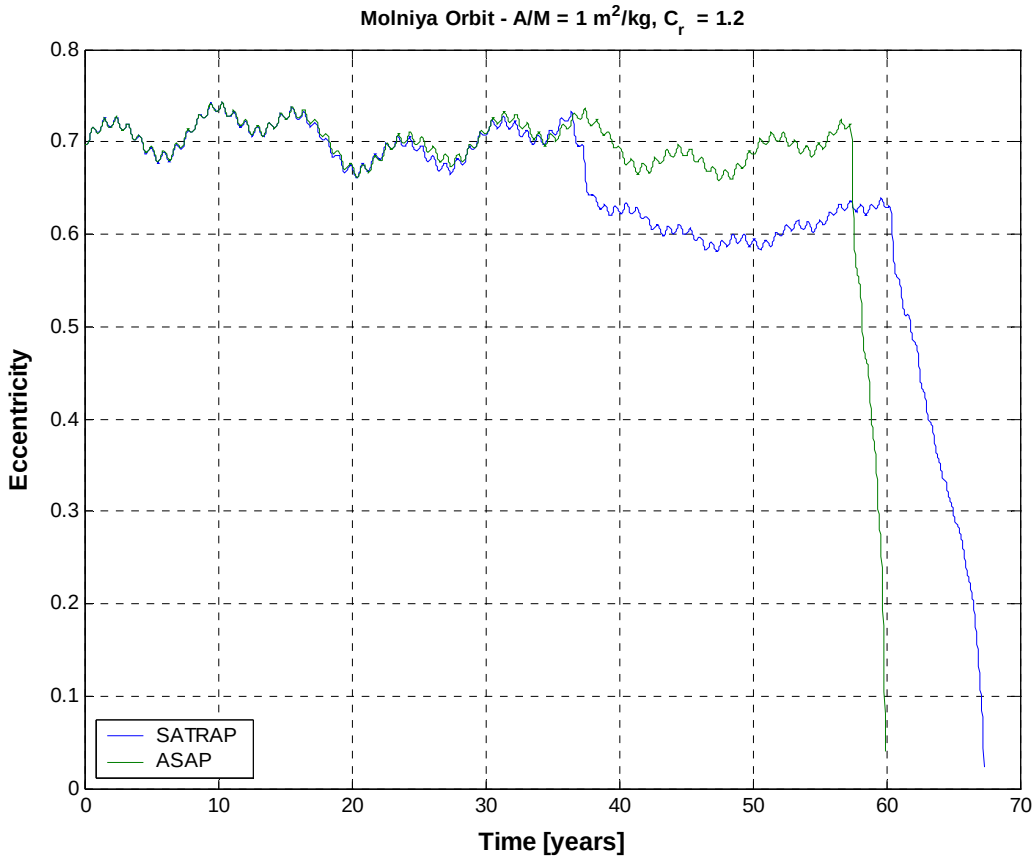

Figure 2.57

Long-term eccentricity evolution of a Molniya orbit, taking into account all relevant perturbations. In the direct solar radiation pressure model, SATRAP considered the varying Sun-Earth distance in the estimation of the perturbing acceleration magnitude, while in ASAP such a distance was fixed to 1 astronomical unit. For more than 30 years, the agreement remained quite good. Later on, the discrepancies observed were basically a consequence of small numerical differences in the perigee altitude, leading to dissimilar apogee evolutions and orbital lifetimes.

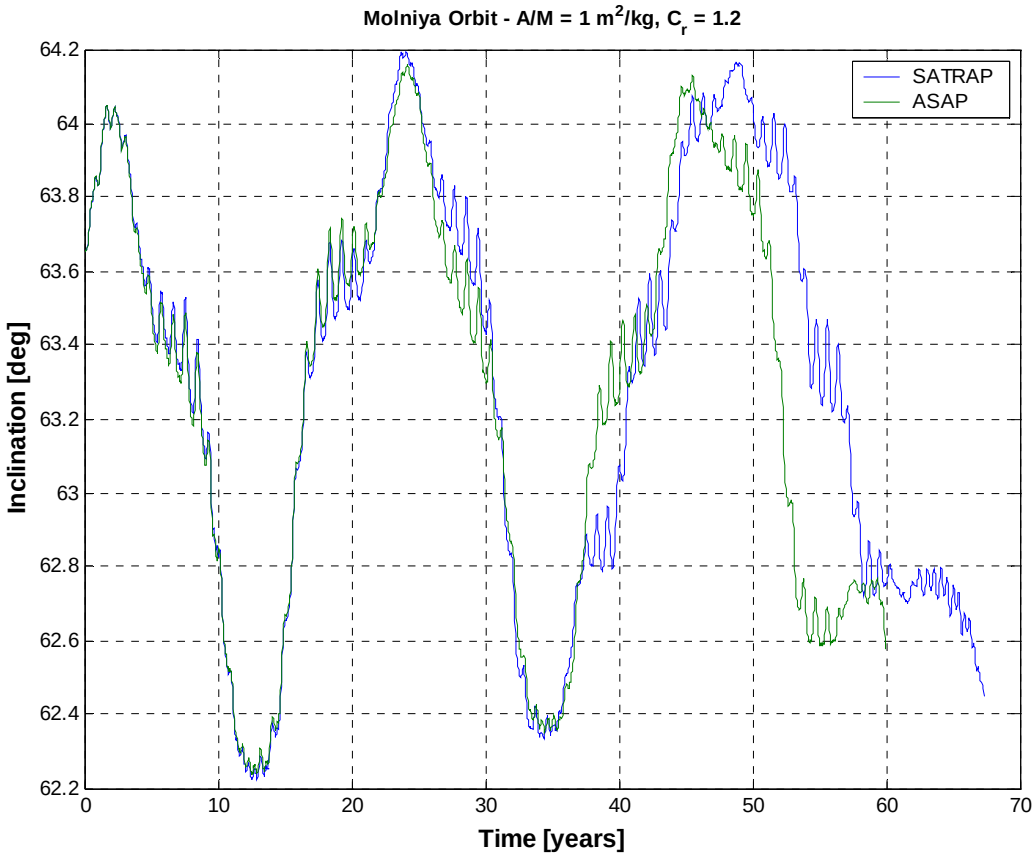

Figure 2.58

Long-term inclination evolution of a Molniya orbit, taking into account all relevant perturbations. In the direct solar radiation pressure model, SATRAP considered the varying Sun-Earth distance in the estimation of the perturbing acceleration magnitude, while in ASAP such a distance was fixed to 1 astronomical unit. For more than 30 years, the agreement remained quite good. Later on, the discrepancies observed were basically a consequence of small numerical differences in the perigee altitude, leading to dissimilar apogee evolutions and orbital lifetimes.

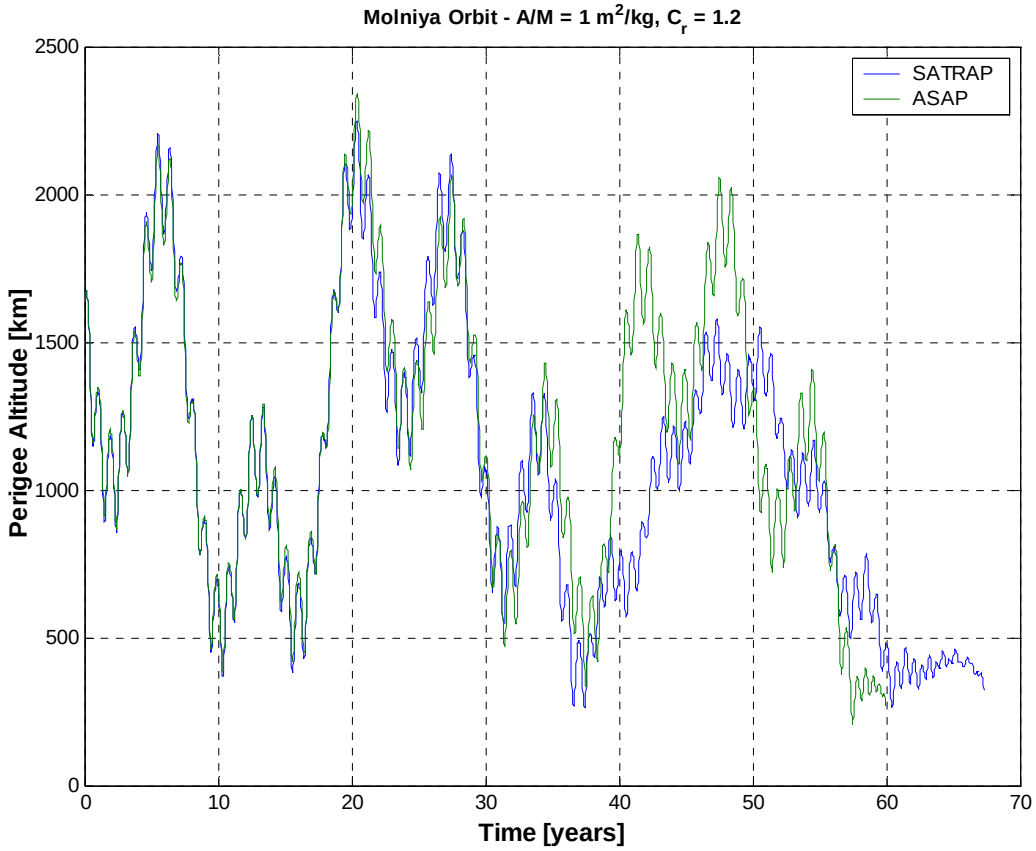

Figure 2.59

Long-term evolution of the perigee altitude of a Molniya orbit, taking into account all relevant perturbations. In the direct solar radiation pressure model, SATRAP considered the varying Sun-Earth distance in the estimation of the perturbing acceleration magnitude, while in ASAP such a distance was fixed to 1 astronomical unit. For more than 30 years, the agreement remained quite good. Later on, small numerical differences in the perigee altitude caused dissimilar apogee evolutions and orbital lifetimes.

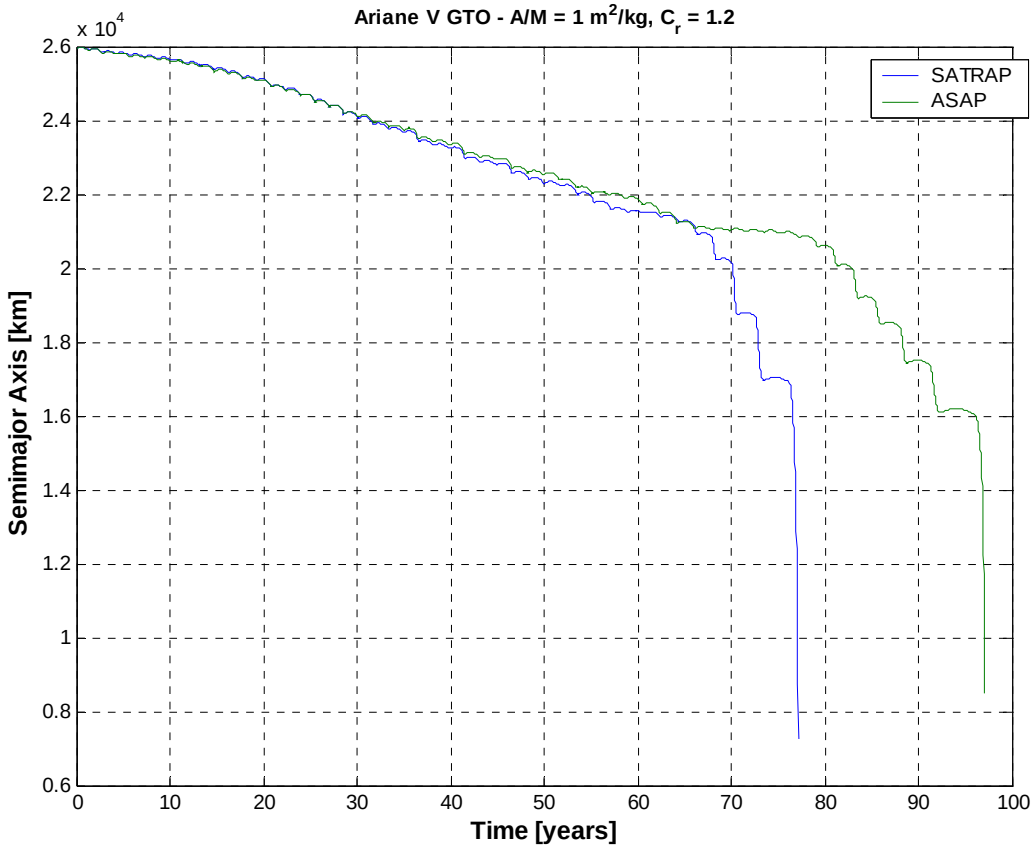

Figure 2.60

Long-term semimajor axis evolution of an Ariane V GTO, taking into account all relevant perturbations. In the direct solar radiation pressure model, SATRAP considered the varying Sun-Earth distance in the estimation of the perturbing acceleration magnitude, while in ASAP such a distance was fixed to 1 astronomical unit. For about 65 years, the agreement remained very good. Later on, the discrepancies observed were basically a consequence of small numerical differences in the perigee altitude, leading to dissimilar apogee evolutions and orbital lifetimes.

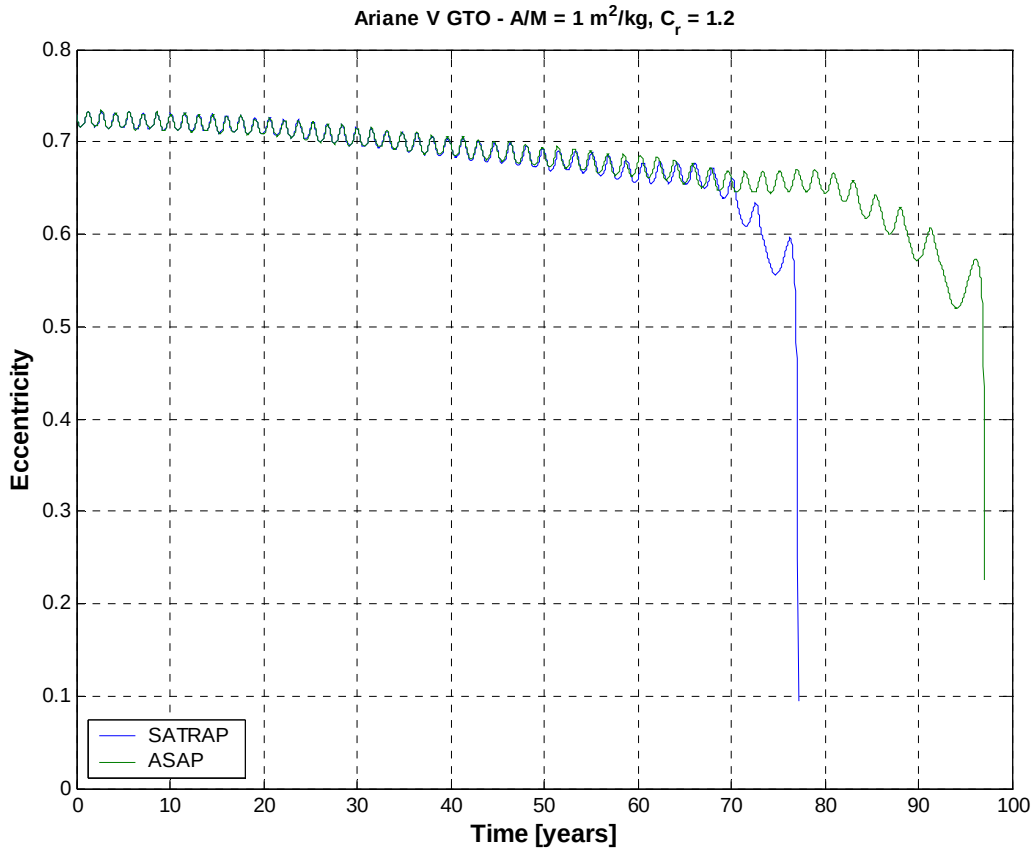

Figure 2.61

Long-term eccentricity evolution of an Ariane V GTO, taking into account all relevant perturbations. In the direct solar radiation pressure model, SATRAP considered the varying Sun-Earth distance in the estimation of the perturbing acceleration magnitude, while in ASAP such a distance was fixed to 1 astronomical unit. For about 70 years, the agreement remained very good. Later on, the discrepancies observed were basically a consequence of small numerical differences in the perigee altitude, leading to dissimilar apogee evolutions and orbital lifetimes.

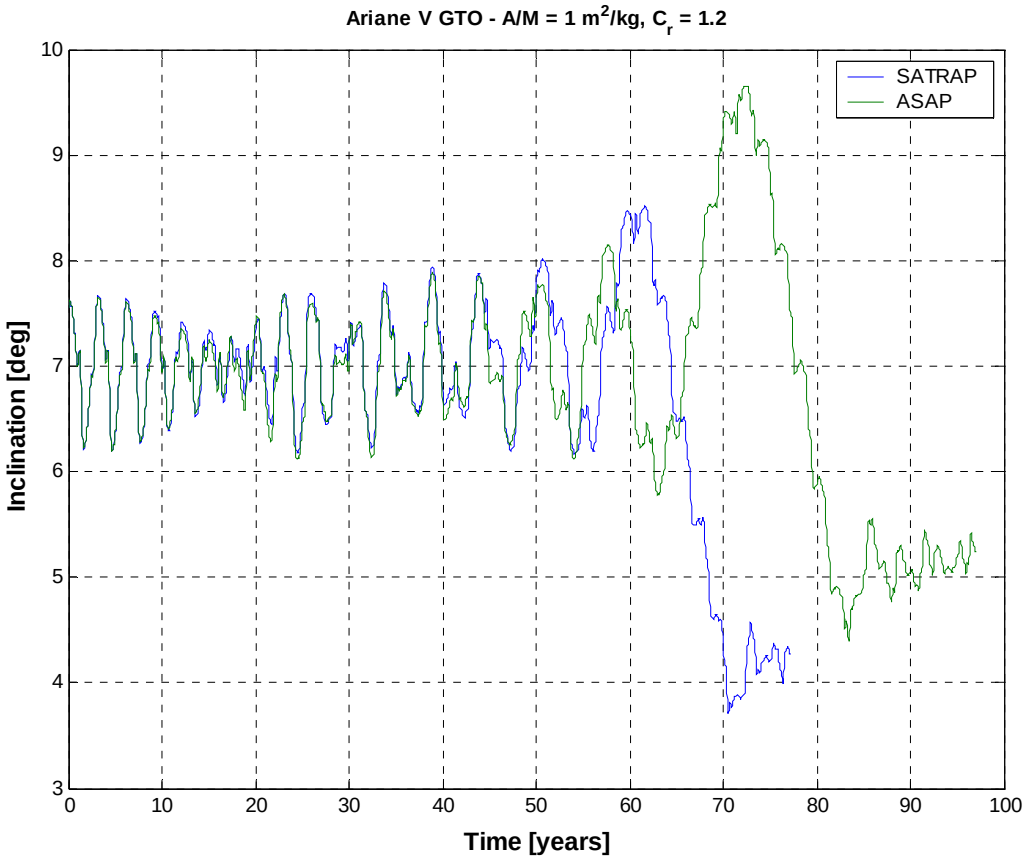

Figure 2.62

Long-term inclination evolution of an Ariane V GTO, taking into account all relevant perturbations. In the direct solar radiation pressure model, SATRAP considered the varying Sun-Earth distance in the estimation of the perturbing acceleration magnitude, while in ASAP such a distance was fixed to 1 astronomical unit. For about 50 years, the agreement remained quite good. Later on, the discrepancies observed were basically a consequence of small numerical differences in the perigee altitude, leading to dissimilar apogee evolutions and orbital lifetimes.

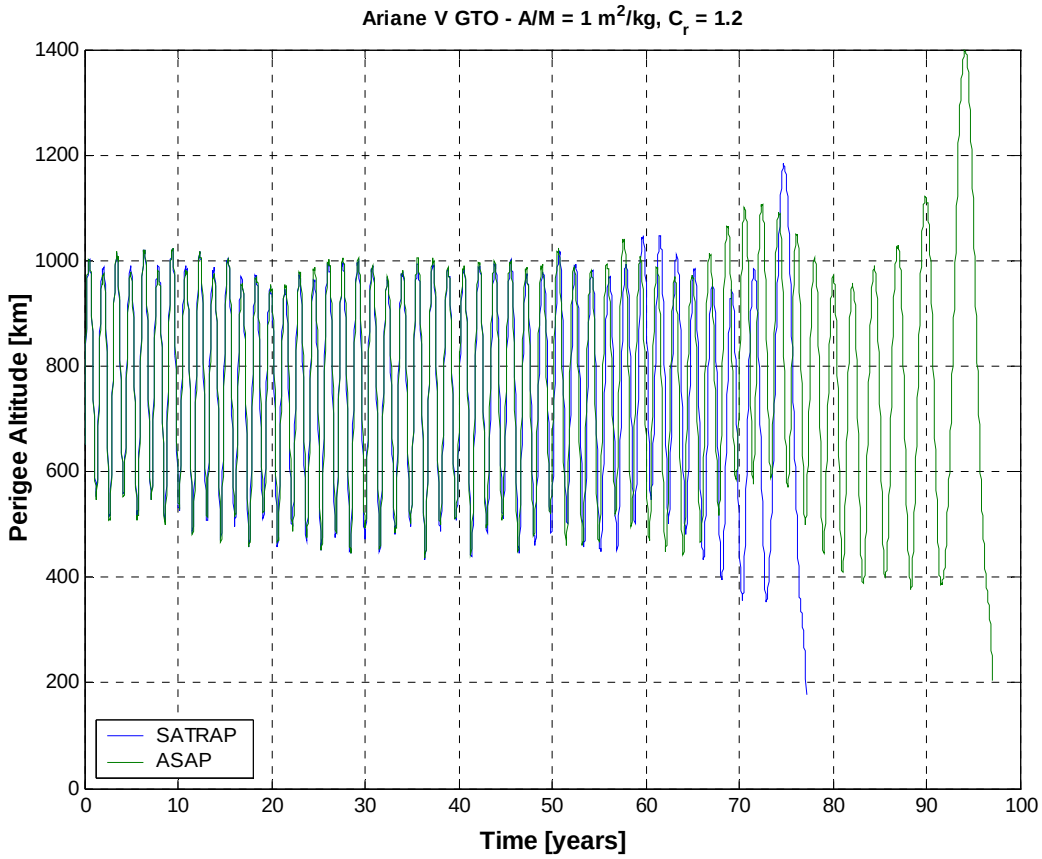

Figure 2.63

Long-term evolution of the perigee altitude of an Ariane V GTO, taking into account all relevant perturbations. In the direct solar radiation pressure model, SATRAP considered the varying Sun-Earth distance in the estimation of the perturbing acceleration magnitude, while in ASAP such a distance was fixed to 1 astronomical unit. For about 50 years, the agreement remained very good. Later on, small numerical differences in the perigee altitude caused dissimilar apogee evolutions and orbital lifetimes.

3. DYNAMICAL IMPACT OF SUNLIGHT ECLIPSES ON HIGH EARTH ORBITS

3.1 Dynamical Effects of the Earth's Shadow in GEO

The last version of SATRAP, including the direct solar radiation pressure model described by Eq. (1.2), was also used to investigate the dynamical effects induced by the Earth's shadow on high Earth orbits. For GEO, the reference orbit given in Table 2.1 was adopted as initial conditions. The time span of the simulations was 100 years, C_r = 1.2 and A/M = 17 m^2/kg, in order to enhance the effects of solar radiation pressure.

Two sets of runs were carried out: the first one, including only the direct solar radiation pressure, with and without eclipses; and the second one, taking into account all relevant perturbations, again with and without eclipses. In the latter case, the perturbations included were the geopotential, up to the 8th degree and order, luni-solar third body attraction and direct solar radiation pressure.

Figures 3.1-3.8 summarize the results obtained by considering only solar radiation pressure. As expected, the differences between the simulation in which the eclipses seasons (two per year, in GEO) were taken into account and the other, in which they were ignored, were quite small, even for a so high area-to-mass ratio. Only the evolution of the semimajor axis was qualitatively dissimilar (see Figures 3.1 and 3.2), even though the quantitative discrepancies were relatively modest. The effect of the Earth's shadow on the eccentricity vector was negligible (see Figures 3.3-3.5). Quite small was also the impact on the inclination vector (see Figures 3.6-3.8): the amplitude of the variation remained the same, but the eclipses slightly increased the period of the orbit pole precession. The main short-term oscillation, however, retained the same period (1 year) and phase resulting from the simulation without the Earth's shadow.

These conclusions were basically confirmed by the results obtained with all relevant perturbations (see Figures 3.9-3.16). Again, only the evolution of the semimajor axis was qualitatively dissimilar (see Figure 3.9), while the quantitative discrepancies were not very large, considering the huge area-to-mass ratio adopted. The effect of the Earth's shadow on the yearly eccentricity oscillations was very small, reducing a little bit the maximum ellipticity of the orbit (see Figures 3.10-3.13). Relatively small was also the impact on the inclination vector (see Figures 3.14-3.16): the eclipses, in combination with the other perturbations, slightly modified the amplitude of the orbit pole clockwise precession and increased a little bit its period. The main short-term oscillation, however, retained the same period (1 year) and phase resulting from the simulation without the Earth's shadow.

3.2 Dynamical Effects of the Earth's Shadow in GPS Orbit

In order to investigate the dynamical effects induced by the Earth's shadow on GPS orbits, the reference trajectory given in Table 2.5 was adopted as initial conditions. The time span of the simulations was 100 years, C_r = 1.2 and A/M = 10 m^2/kg, in order to enhance the effects of solar radiation pressure. The perturbations included were the geopotential, up to the 8th degree and order, luni-solar third body attraction and direct solar radiation pressure, with and without eclipses.

Figures 3.17-3.21 summarize the results obtained. In this case, the evolution of the semimajor axis (Figure 3.17), the eccentricity (Figure 3.18) and the eccentricity vector (Figure 3.19) displayed growing differences as a function of time. The Earth's shadow decreased the semimajor axis and maintained a less elliptical orbit. Concerning the inclination (Figure 3.20) and the inclination vector (Figure 3.21), the amplitude of the variation remained the same, but the eclipses slightly increased the period of the orbit pole precession. The main short-term oscillation, however, retained the same period (≅ 1 year) and phase.

3.3 Dynamical Effects of the Earth's Shadow in Molniya Orbit

In order to investigate the dynamical effects induced by the Earth's shadow on Molniya orbits, the reference trajectory given in Table 2.6 was adopted as initial conditions. The time span of the simulations was several decades, C_r = 1.2 and A/M = 1 m^2/kg, in order to enhance, as much as possible, the effects of solar radiation pressure (higher values of the area-to-mass ratio induced too short orbital lifetimes). The perturbations included were the geopotential, up to the 8th degree and order, luni-solar third body attraction, air drag, according to the parameters given in Table 1.1, and direct solar radiation pressure, with and without eclipses.

The results obtained are summarized in Figures 3.22-3.28. For approximately 35 years, the agreement between the two simulations remained very good, both qualitatively and quantitatively. Later on, the discrepancies observed were basically a consequence of small numerical differences in the perigee altitude, leading to a dissimilar apogee evolution and orbital lifetime. However, similar numerical differences were also found using different trajectory predictors with the same solar radiation pressure model [15].

3.4 Dynamical Effects of the Earth's Shadow in GTO

The long-term dynamical effects induced by the Earth's shadow were finally investigated in geosynchronous transfer orbit (GTO). The reference trajectory selected, given in Table 2.7, was an Ariane V GTO. The time span of the simulations was 100 years, C_r = 1.2 and A/M = 1 m^2/kg, in order to enhance, as much as possible, the effects of solar radiation pressure (higher values of the area-to-mass ratio induced too short orbital lifetimes). The perturbations included were the geopotential, up to the 8th degree and order, luni-solar third body attraction, air drag, according to the parameters given in Table 1.1, and direct solar radiation pressure, with and without eclipses.

The results obtained are summarized in Figures 3.29-3.35. For approximately 30 years, the agreement between the two simulations remained very good, both qualitatively and quantitatively, becoming progressively worse, but anyway satisfactory, in the following four decades. The discrepancies observed, and the accelerated decay of the orbit subjected to the effects of the Earth's shadow, were basically a consequence of small numerical differences in the minimum perigee altitude, leading to a dissimilar apogee evolution and orbital lifetime. However, similar numerical differences were also found using different trajectory predictors with the same solar radiation pressure model [15].

3.5 Summary

The last version of SATRAP, including the direct solar radiation pressure model described by Eq. (1.2), was used to investigate the dynamical effects, on high Earth orbits, of the Earth's shadow, determined according to Eqs. (1.4) and (1.5). For this purpose, the long-term evolution of objects with very high area-to-mass ratios was simulated, including all relevant perturbations, both with and without sunlight eclipses.

In general, significant differences due to shadowing effects only emerged after several years and with extremely large area-to-mass ratios. However, the analysis of the extreme conditions was merely possible for geosynchronous and GPS orbits, in which stable long-term trajectories were attainable even with huge area-to-mass ratios. The influence of the Earth's shadow was more pronounced on the lower trajectory, i.e. the GPS orbit, as far as the eccentricity vector was concerned, while the effects on the orbit pole were more conspicuous in GEO. As expected, the semimajor axis was clearly affected in both cases.

Concerning GTO and Molniya orbits, a sufficiently long lifetime was attained only with relatively smaller area-to-mass ratios. The agreement found between the simulations, with and without the eclipses, was very good during the first few decades. Later on, the discrepancies observed were basically a consequence of small numerical differences in the perigee altitude, leading to a dissimilar apogee evolution and orbital lifetime. However, similar numerical variations were also found using different trajectory predictors with the same solar radiation pressure model. The effects of the Earth's shadow were, therefore, comparable to the numerical differences between orbit propagators adopting the same force model, but distinct methods for computing the evolution of the state vector.

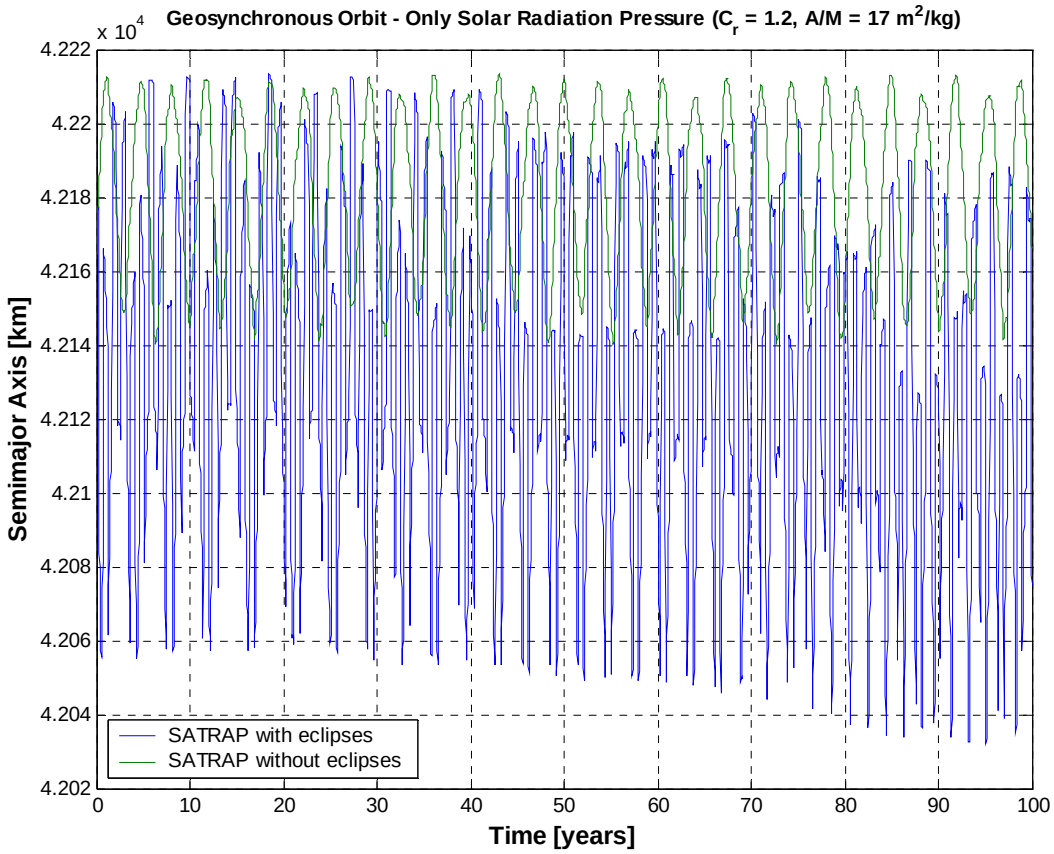

Figure 3.1

Long-term semimajor axis evolution in GEO, taking into account only solar radiation pressure, with and without eclipses. The Earth's shadow increased the oscillation amplitude of the semimajor axis, lowered its average value and introduced a small decreasing trend. However, the overall quantitative effects were relatively modest, even for a so high area-to-mass ratio ($C_r \times A/M$ = 20.4 m^2/kg).

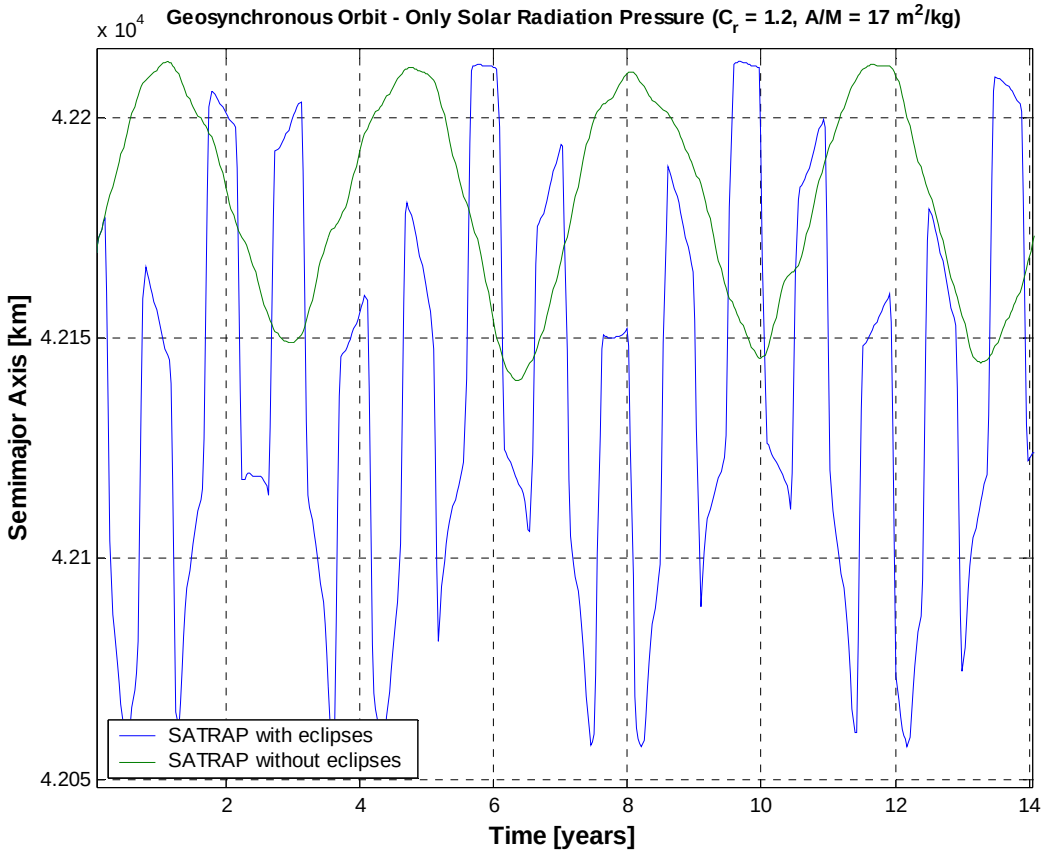

Figure 3.2

Detail of the semimajor axis evolution during the first 14 years, taking into account only solar radiation pressure, with and without eclipses. The effects of the eclipses seasons (two per year, in GEO) are evident on the blue curve.

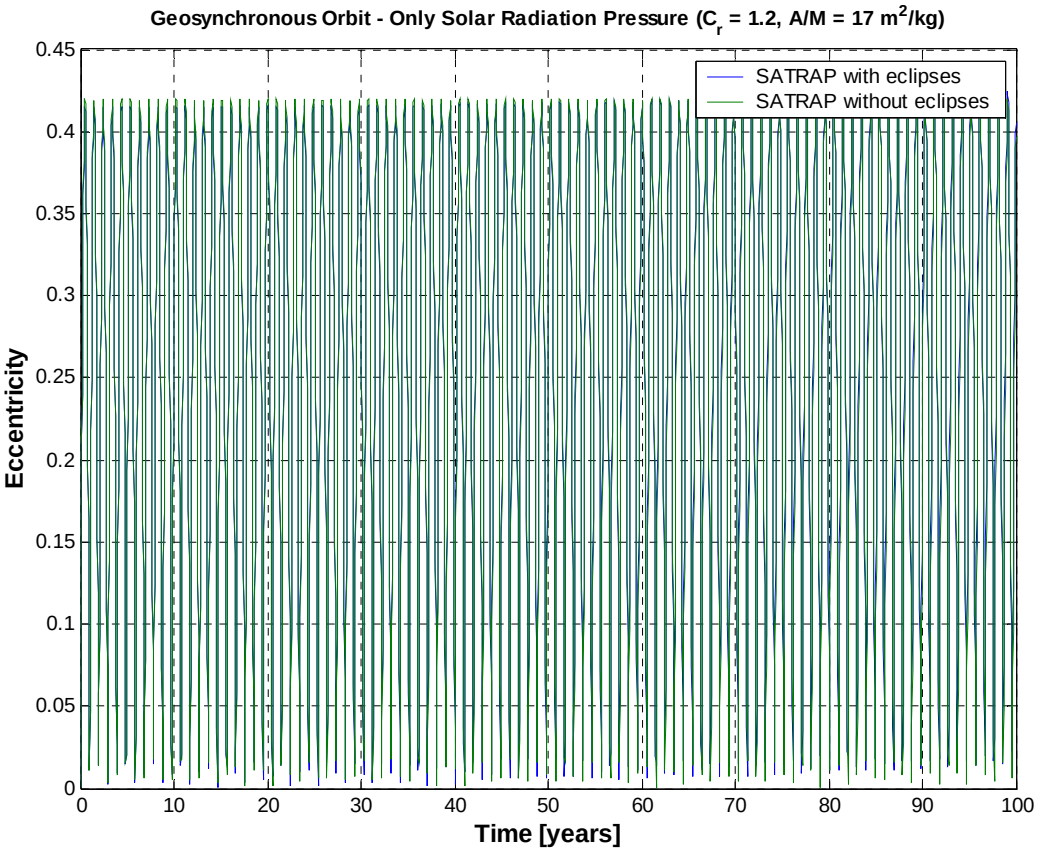

Figure 3.3

Long-term eccentricity evolution in GEO, taking into account only solar radiation pressure, with and without eclipses. The differences in the yearly oscillation and long period modulation were very small, even for a so high area-to-mass ratio ($C_r \times A/M$ = 20.4 m^2/kg).

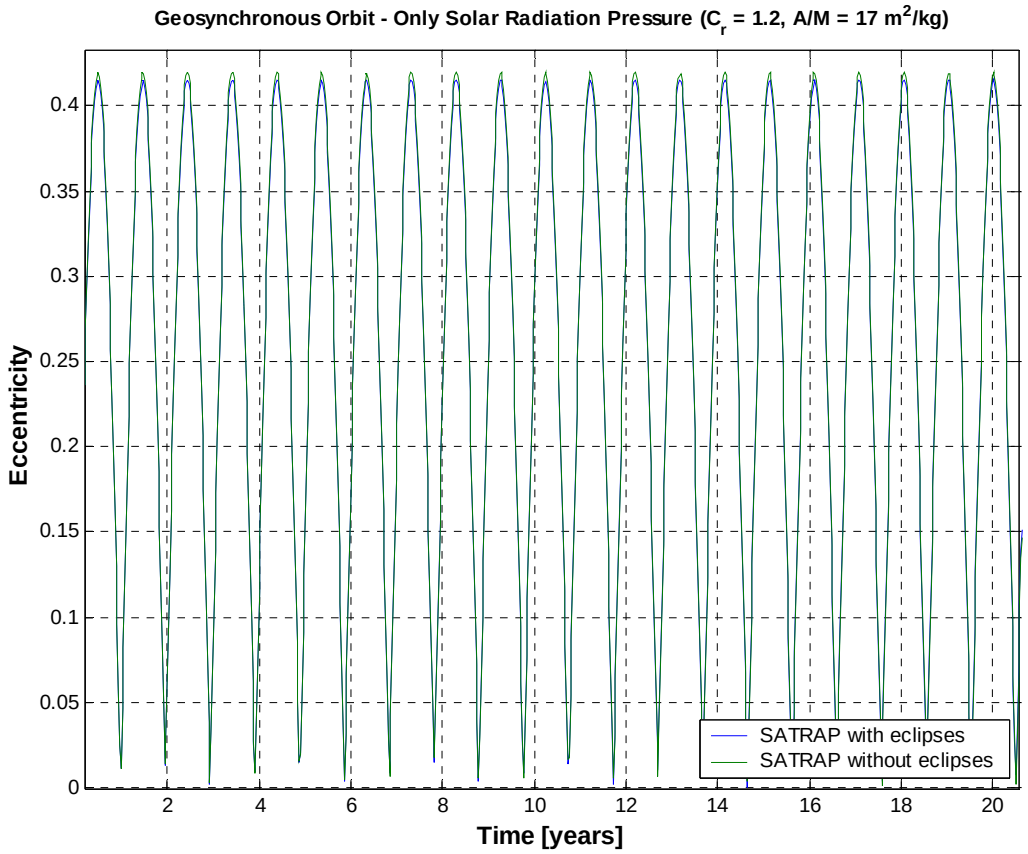

Figure 3.4

Detail of the eccentricity evolution during the first 20 years, taking into account only solar radiation pressure, with and without eclipses. The effects of the eclipses seasons (two per year, in GEO) on the yearly oscillations were negligible, even for a so high area-to-mass ratio ($C_r \times A/M$ = 20.4 m^2/kg).

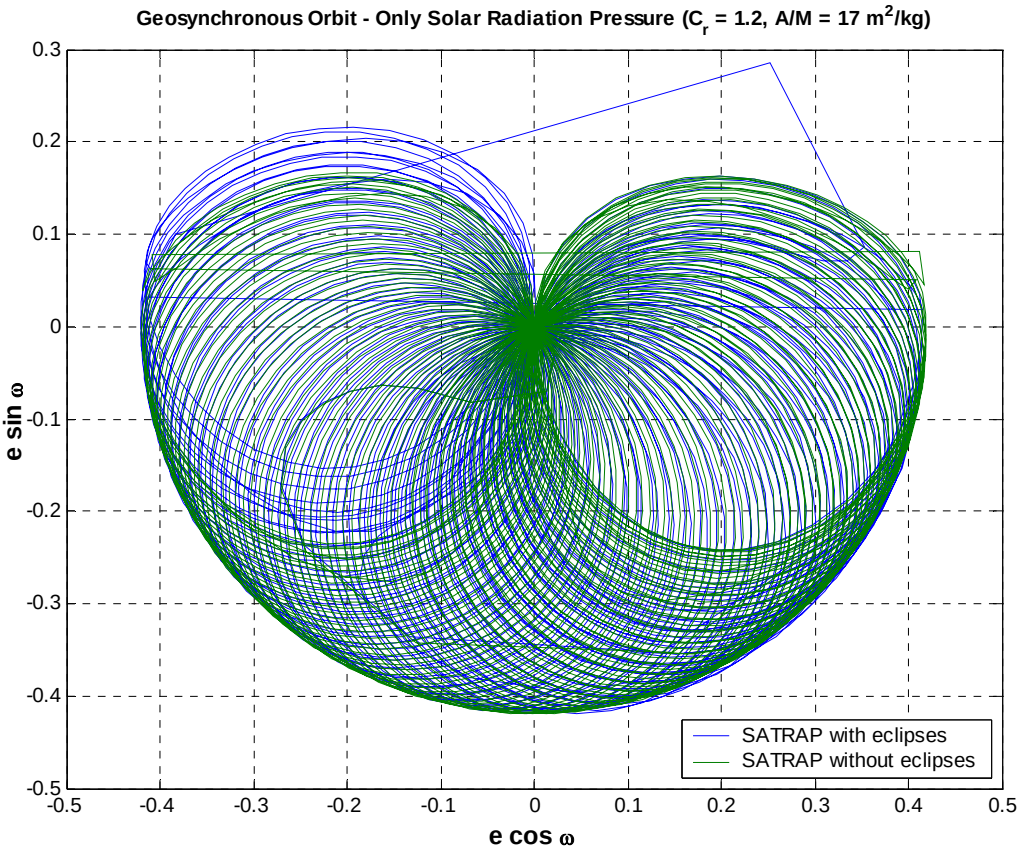

Figure 3.5

Evolution, over 100 years, of the eccentricity vector in GEO, taking into account only solar radiation pressure, with and without eclipses. The pattern observed was basically produced by the superimposition of two anti-clockwise precessions, one with a period of 1 year and the other with a period of many decades. The initial value of the eccentricity vector was ≅ [0, 0]. The differences were quite small, even for a so high area-to-mass ratio ($C_r \times A/M$ = 20.4 m^2/kg).

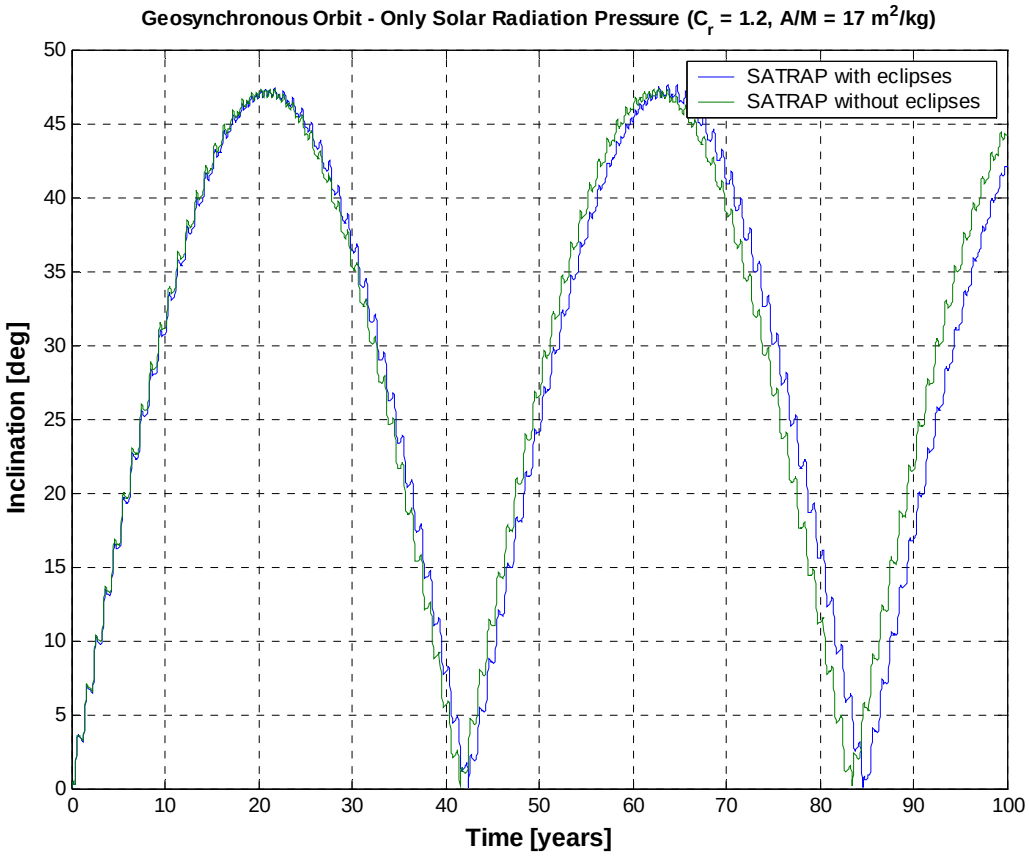

Figure 3.6

Long-term inclination evolution in GEO, taking into account only solar radiation pressure, with and without eclipses. The differences were relatively small, even for a so high area-to-mass ratio ($C_r \times A/M$ = 20.4 m^2/kg). The amplitude of the variation remained the same, but the Earth's shadow increased a little bit the period of the orbit pole precession.

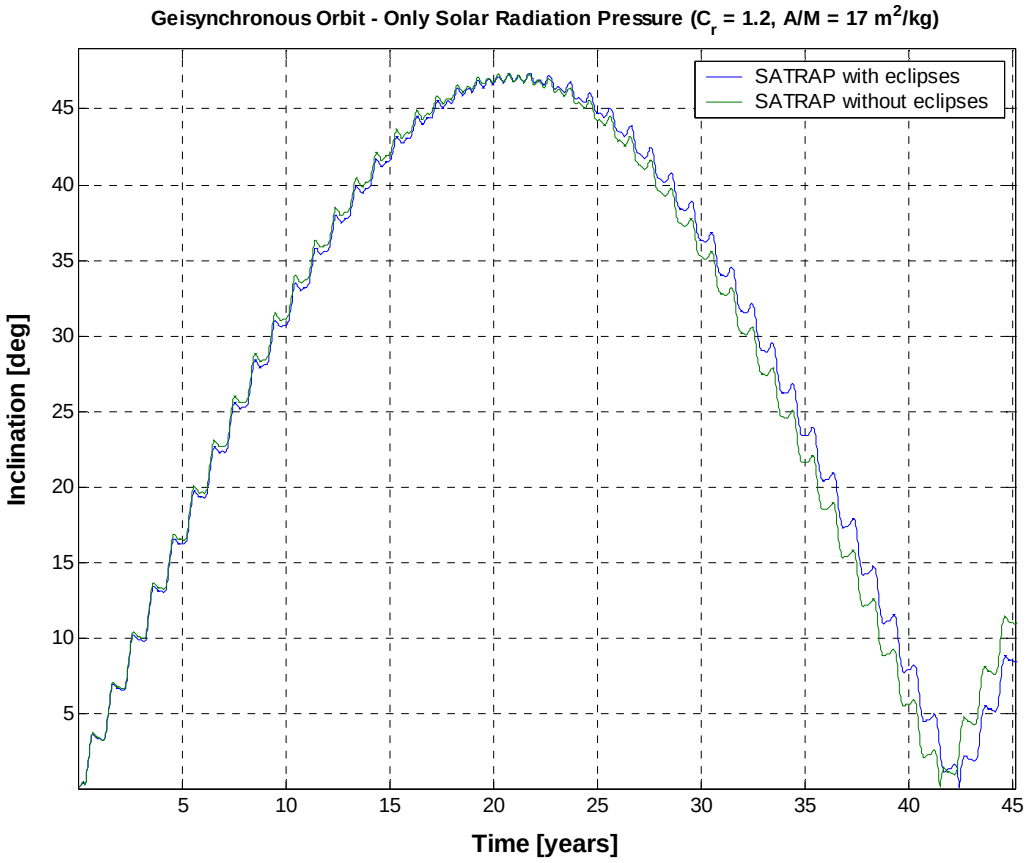

Figure 3.7

Detail of the inclination evolution during the first 45 years, taking into account only solar radiation pressure, with and without eclipses. The amplitude of the variation remained the same, but the Earth's shadow increased a little bit (by ≅ 1 year, or 2.3%) the period of the orbit pole precession. The main short-term oscillation, however, retained the same period (1 year) and phase.

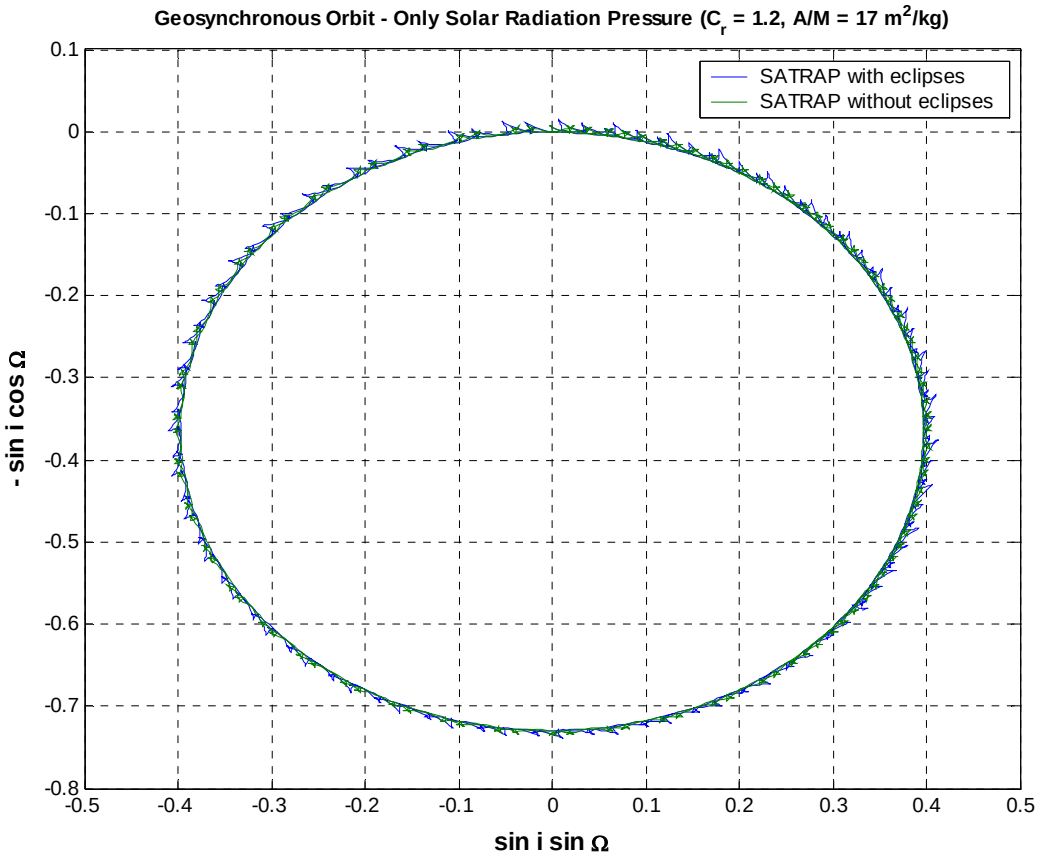

Figure 3.8

Evolution, over 100 years, of the two-dimensional inclination vector in GEO, taking into account only solar radiation pressure, with and without eclipses. The initial value of the inclination vector was ≅ [0, 0]. The differences were quite small, even for a so high area-to-mass ratio ($C_r \times A/M$ = 20.4 m^2/kg). The amplitude of the orbit pole clockwise precession remained the same, but the Earth's shadow increased a little bit its period.

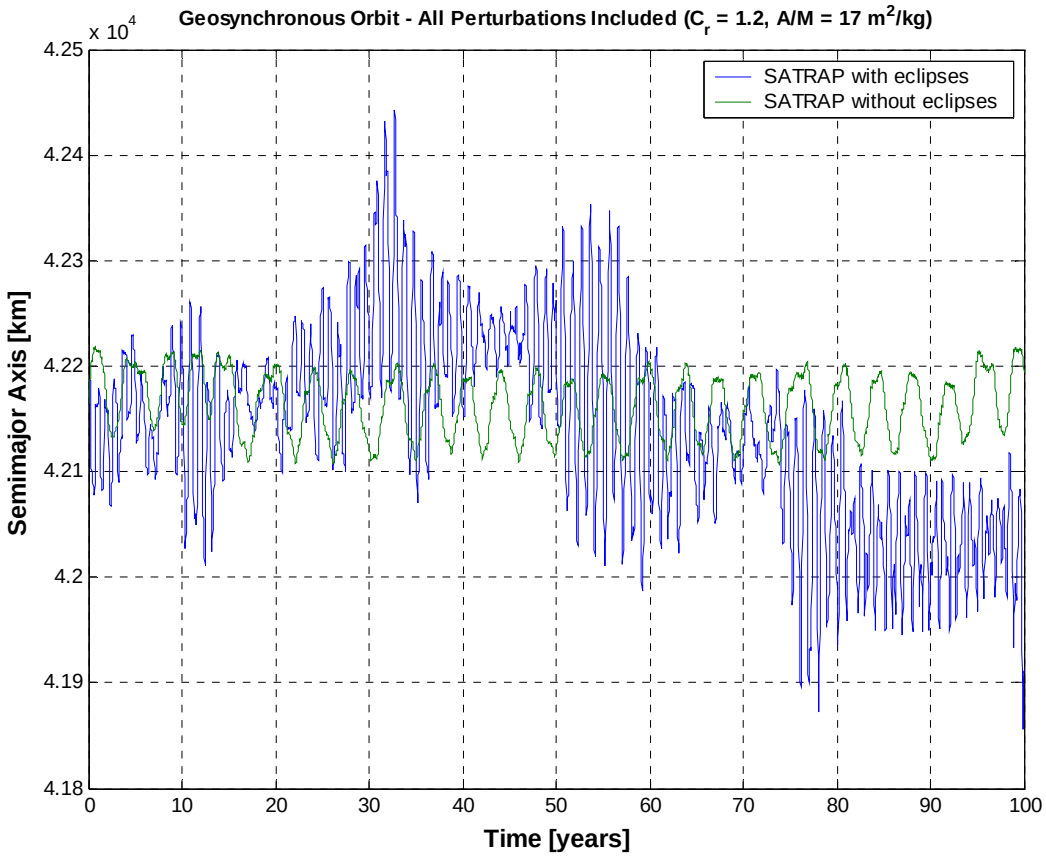

Figure 3.9

Long-term semimajor axis evolution in GEO, taking into account all relevant perturbations, with and without the Earth's shadow. The eclipses seasons (two per year, in GEO) induced yearly oscillations and long period variations. However, the quantitative differences were not very large, considering the huge area-to-mass ratio ($C_r \times A/M$ = 20.4 m^2/kg) adopted in the simulations.

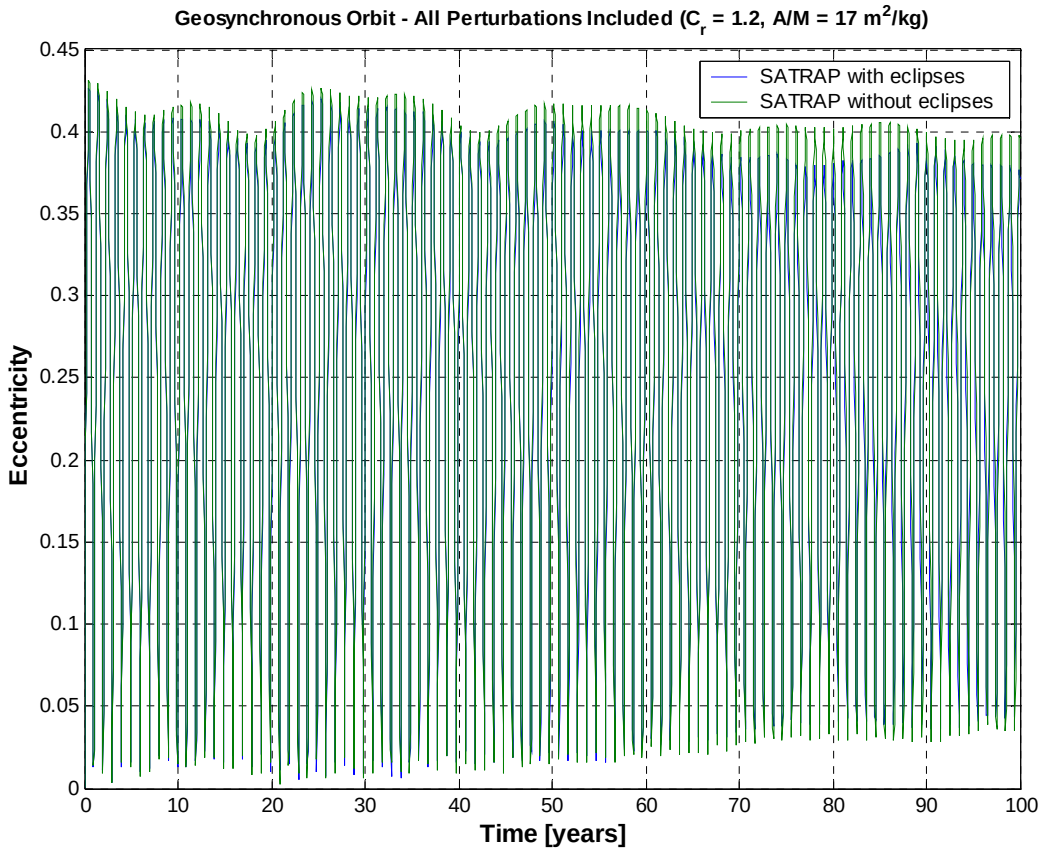

Figure 3.10

Long-term eccentricity evolution in GEO, taking into account all relevant perturbations, with and without eclipses. The differences in the yearly oscillation and long period modulation were very small, even for a so high area-to-mass ratio ($C_r \times A/M$ = 20.4 m^2/kg).

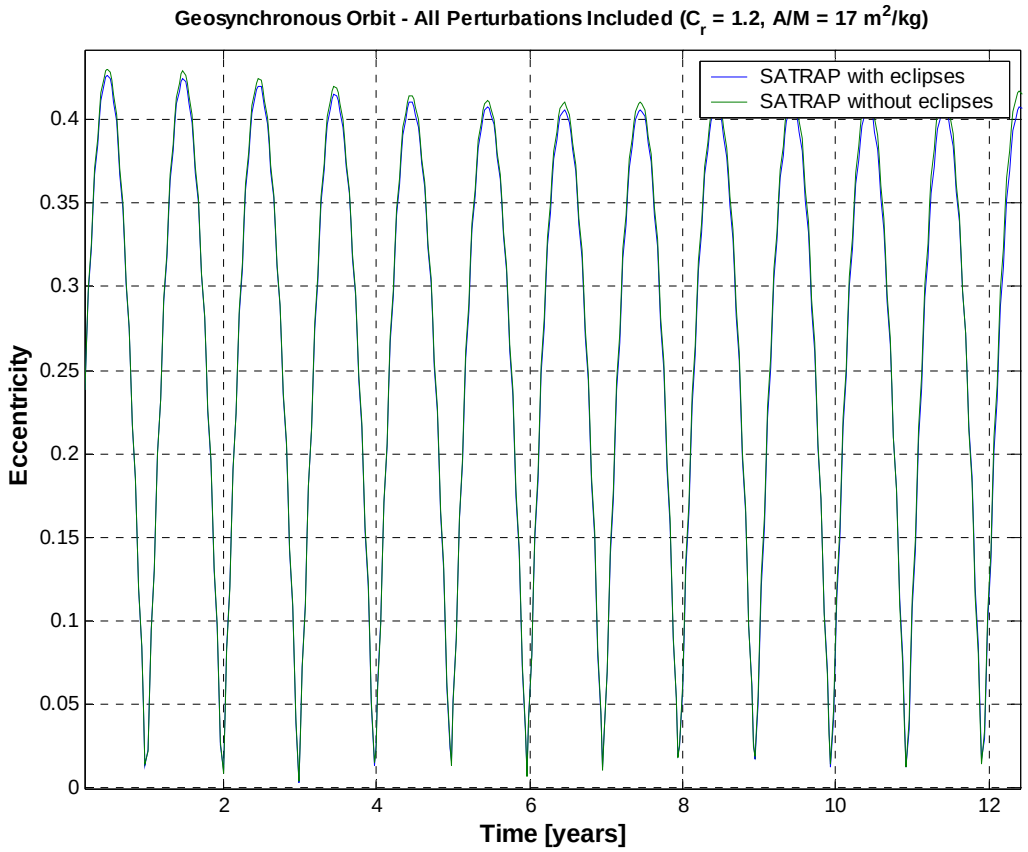

Figure 3.11

Detail of the eccentricity evolution during the first 12 years, taking into account all relevant perturbations, with and without eclipses. The effects of the eclipses seasons (two per year, in GEO) on the yearly oscillations were very small, reducing a little bit the maximum ellipticity of the orbit.

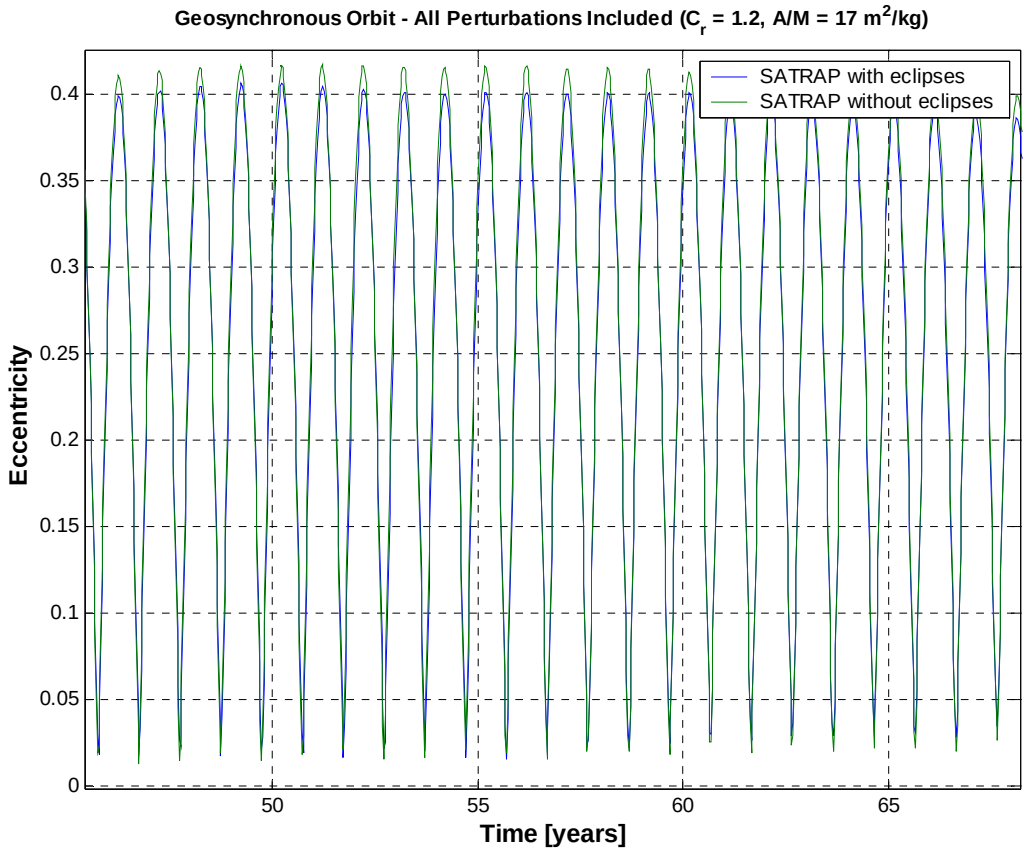

Figure 3.12

Another detail of the eccentricity long-term evolution in GEO, taking into account all relevant perturbations, with and without eclipses. The effects of the Earth's shadow on the yearly oscillations were very small, reducing a little bit the maximum ellipticity of the orbit.

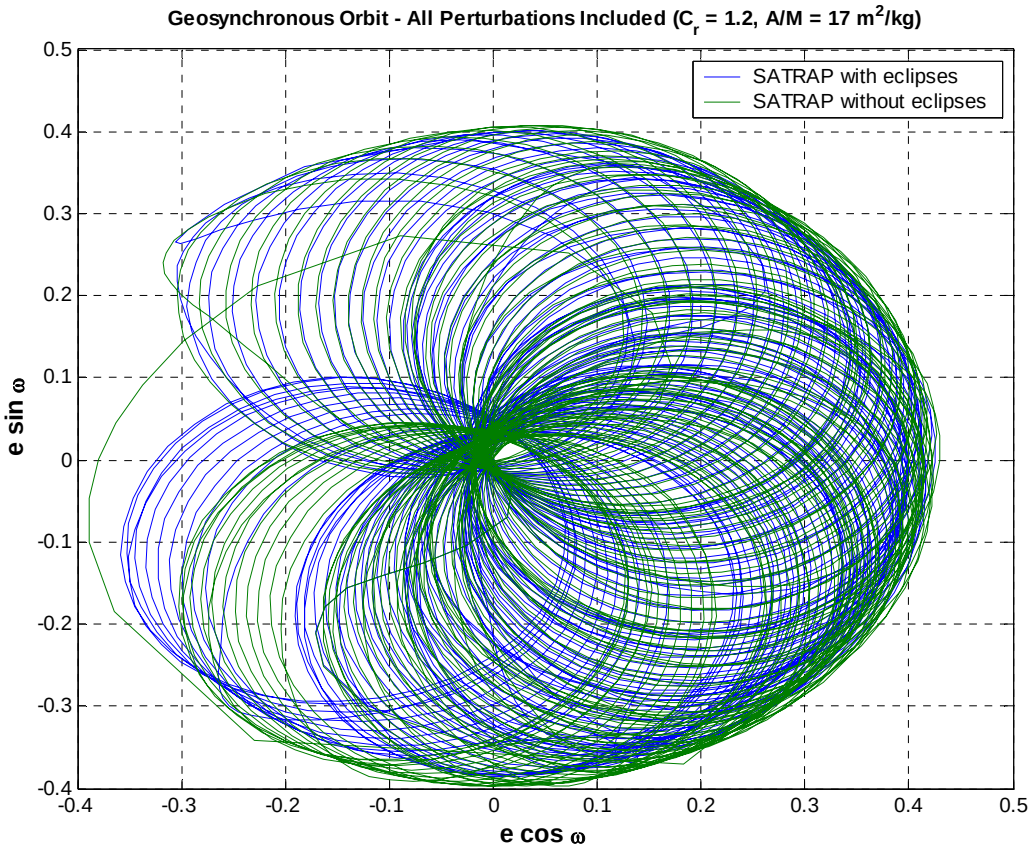

Figure 3.13

Evolution, over 100 years, of the eccentricity vector in GEO, taking into account all relevant perturbations, with and without eclipses. The pattern observed was basically produced by the superimposition of two anti-clockwise precessions, one with a period of 1 year and the other with a period of several decades. The initial value of the eccentricity vector was ≅ [0, 0]. The differences were quite small, even for a so high area-to-mass ratio ($C_r \times A/M$ = 20.4 m^2/kg).

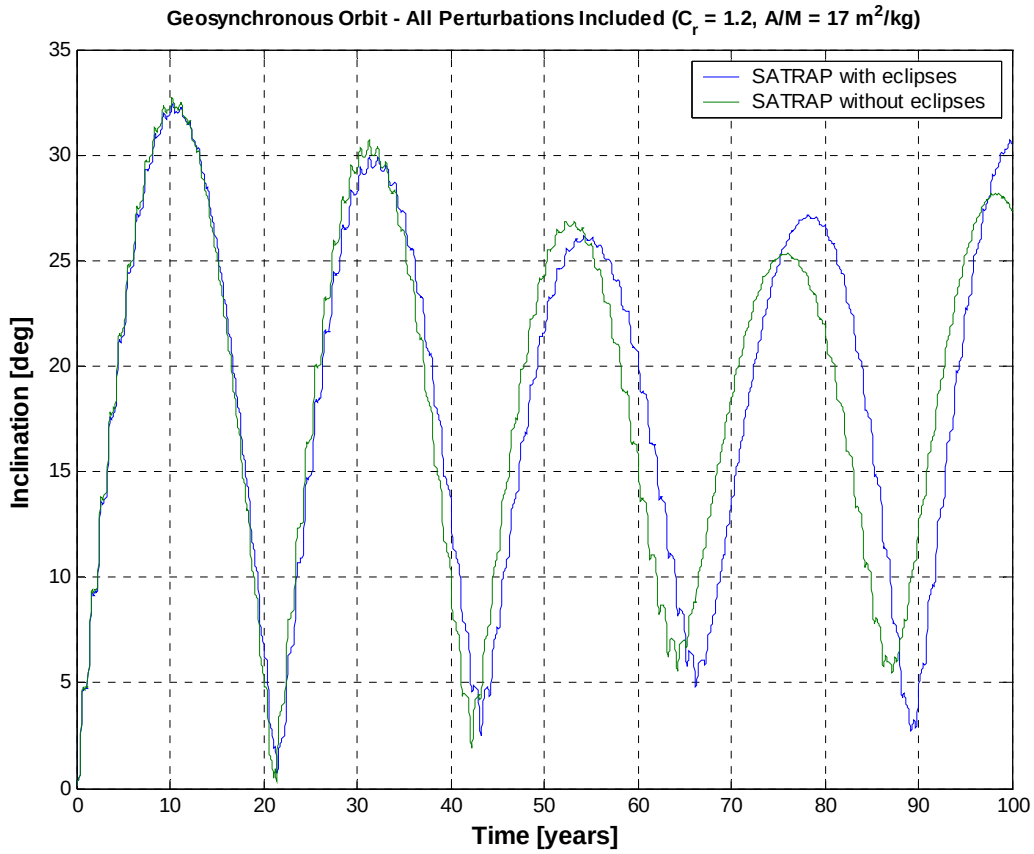

Figure 3.14

Long-term inclination evolution in GEO, taking into account all relevant perturbations, with and without eclipses. The differences were relatively small, at least during the first 50 years, even for a so high area-to-mass ratio ($C_r \times A/M$ = 20.4 m^2/kg). The amplitude of the variation remained approximately the same in first five decades, but the Earth's shadow increased a little bit the period of the orbit pole precession.

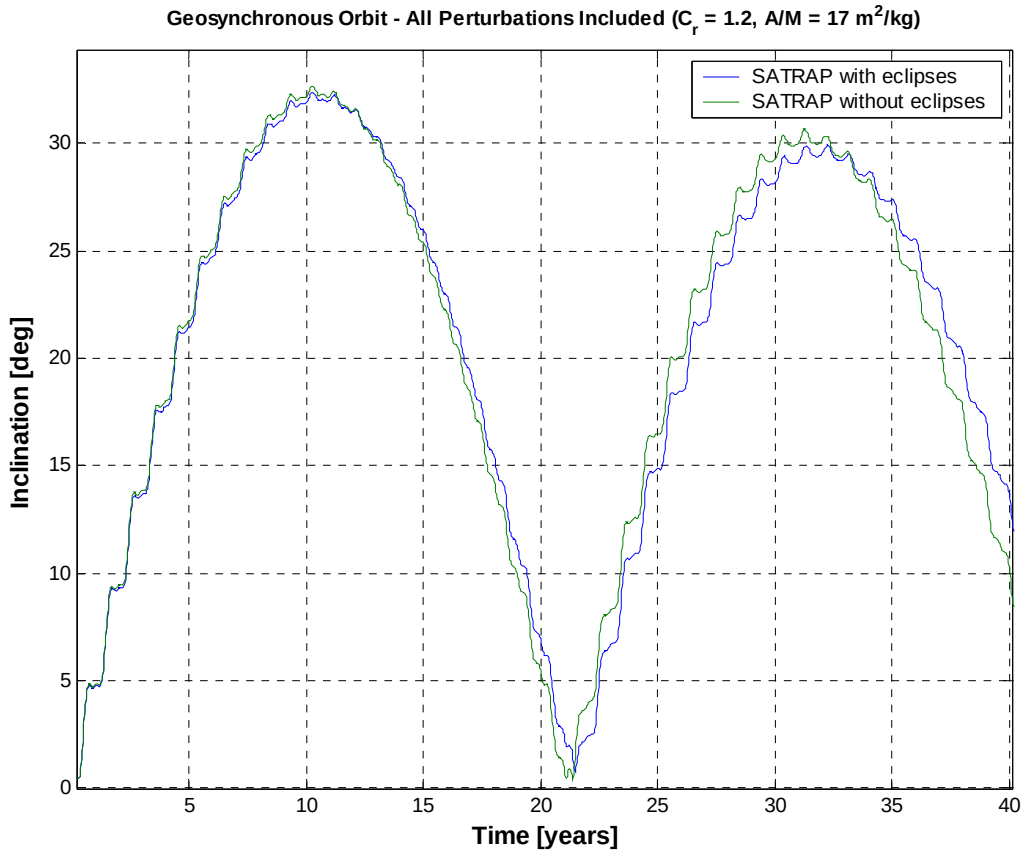

Figure 3.15

Detail of the inclination evolution during the first 40 years, taking into account all relevant perturbations, with and without eclipses. The amplitude of the variation remained approximately the same, but the Earth's shadow increased a little bit (by ~ 6 months, or 2.3%) the period of the orbit pole precession. The main short-term oscillation, however, retained the same period (1 year) and phase.

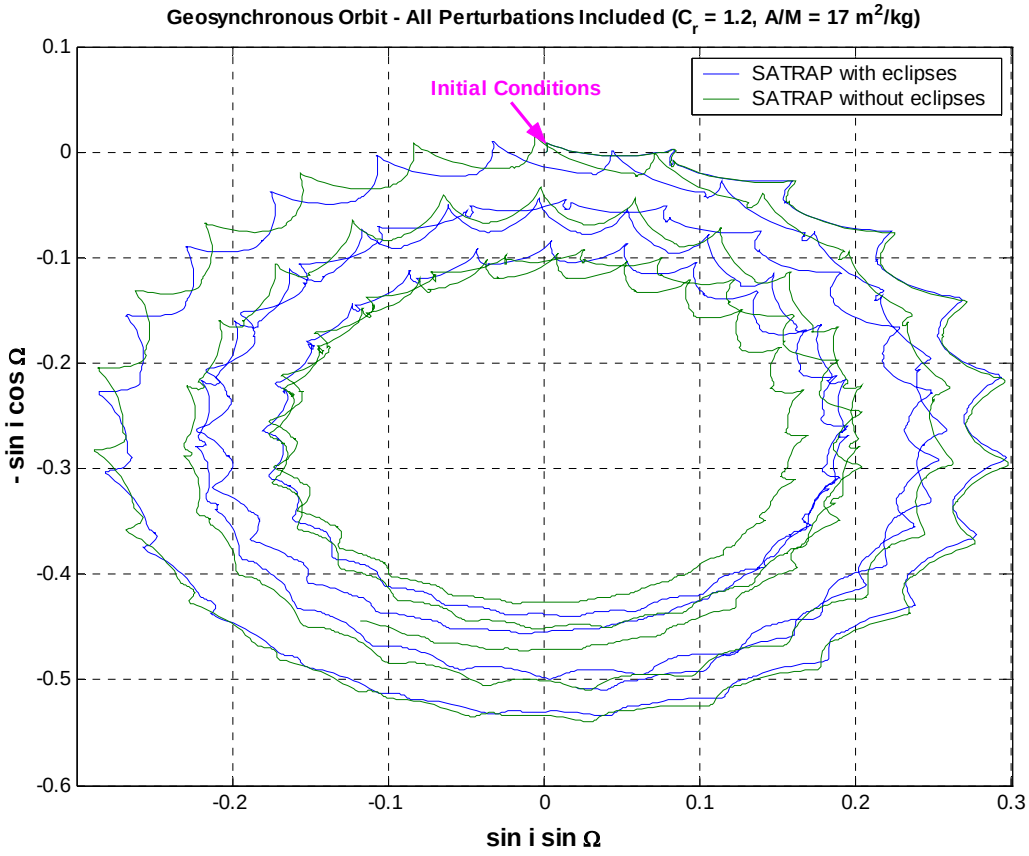

Figure 3.16

Evolution, over 100 years, of the two-dimensional inclination vector in GEO, taking into account all relevant perturbations, with and without eclipses. The initial value of the inclination vector was ≅ [0, 0]. The differences increased as a function of time, but did not become very large, considering the huge area-to-mass ratio ($C_r \times A/M$ = 20.4 m^2/kg) adopted in the simulations. The Earth's shadow, in combination with the other perturbations, slightly modified the amplitude of the orbit pole clockwise precession and increased a little bit its period. The yearly wobble of the orbit pole is also evident.

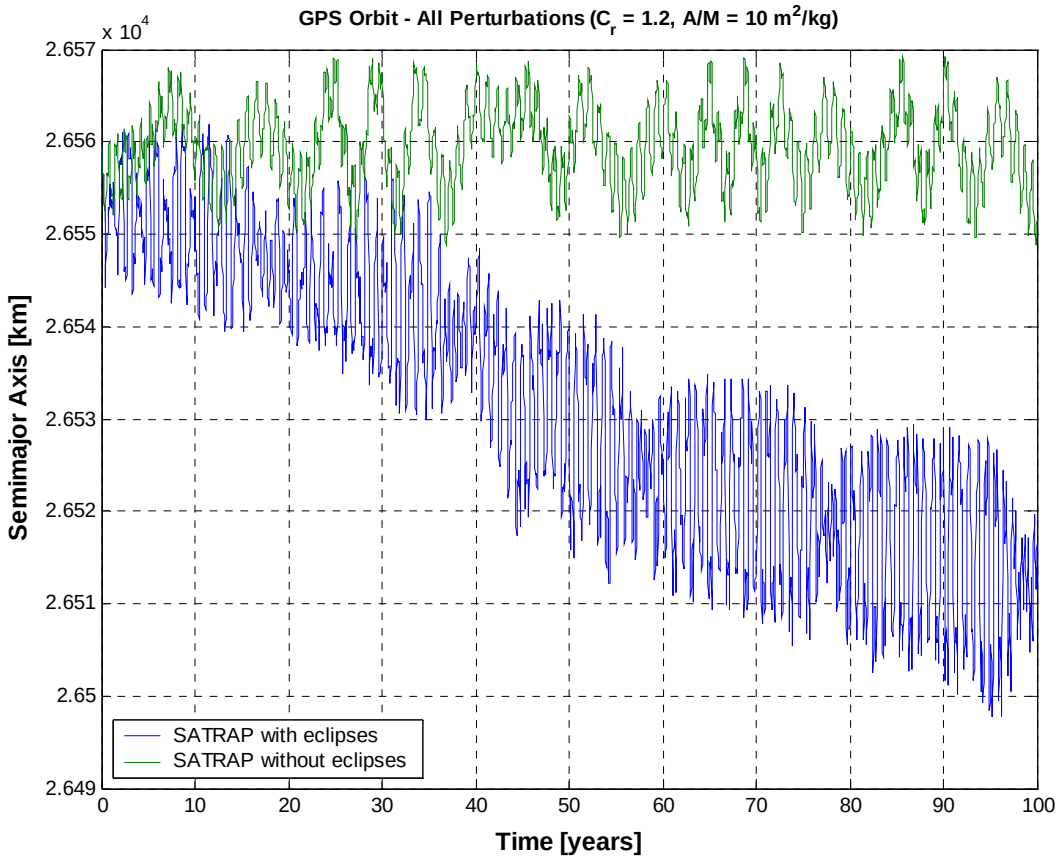

Figure 3.17

Long-term semimajor axis evolution of a GPS orbit, taking into account all relevant perturbations, with and without the Earth's shadow. The divergence increased as a function of time.

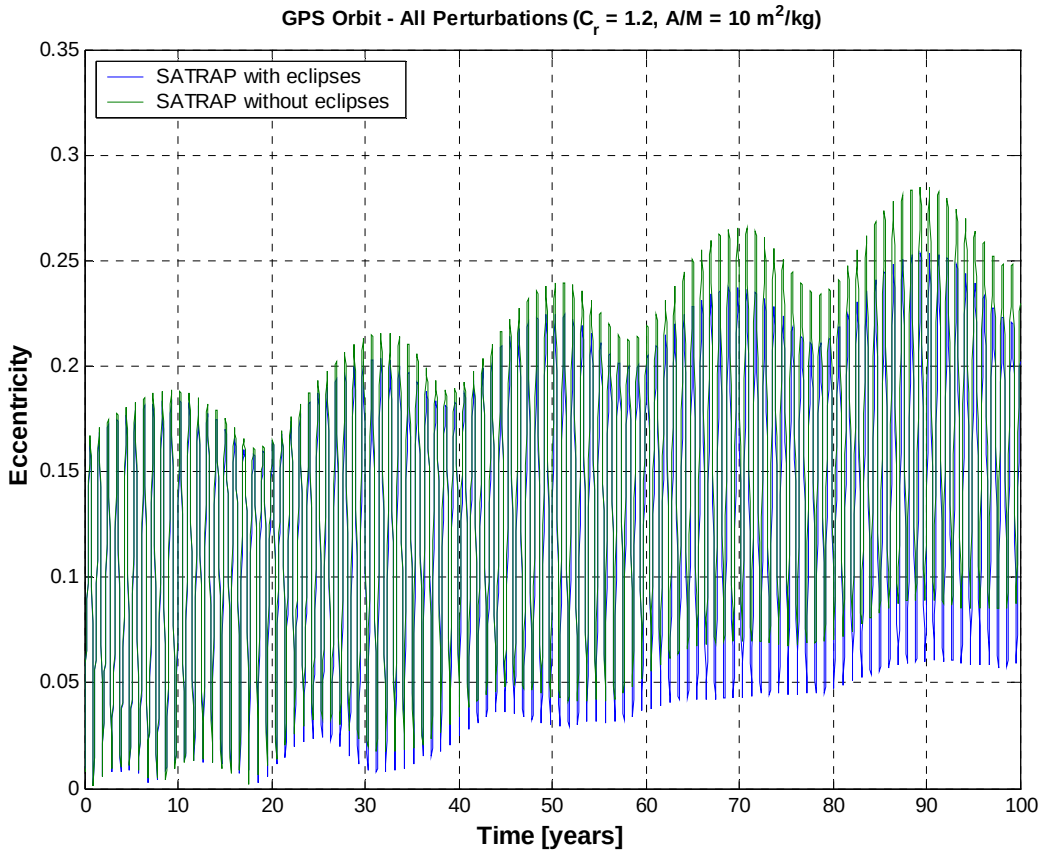

Figure 3.18

Long-term eccentricity evolution of a GPS orbit, taking into account all relevant perturbations, with and without the Earth's shadow. The differences increased as a function of time, with the Earth's shadow maintaining a slightly less elliptical orbit.

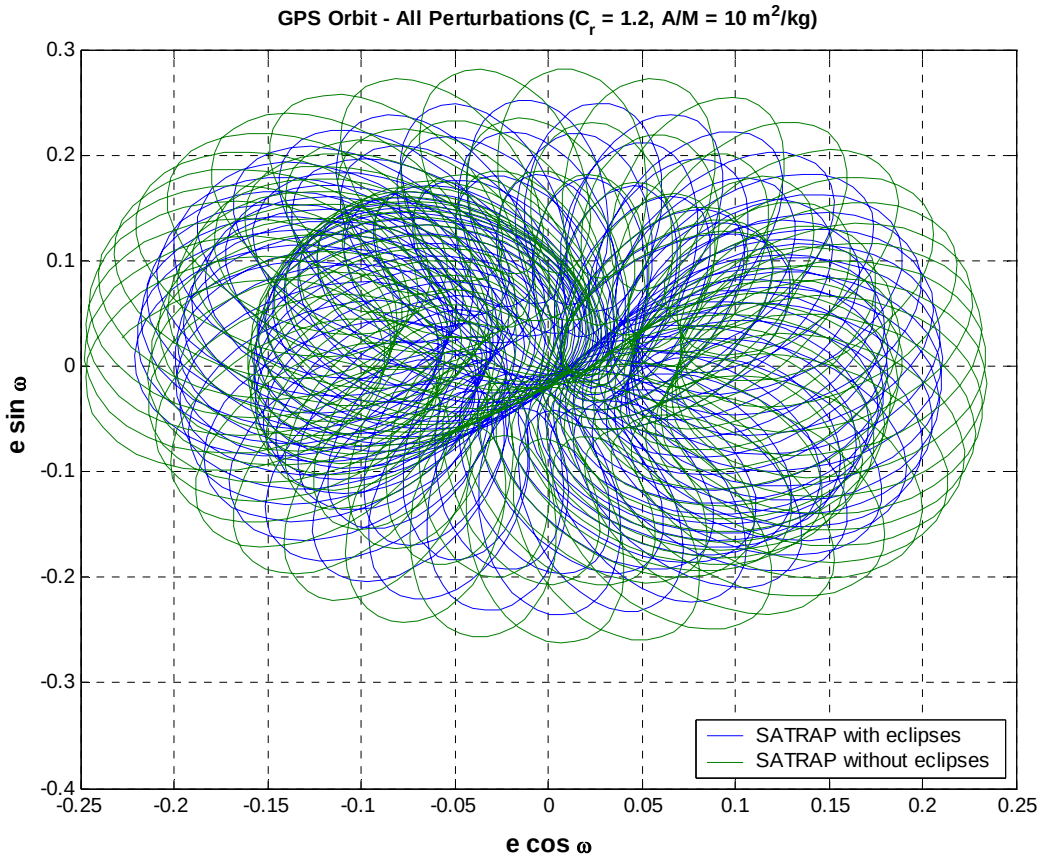

Figure 3.19

Evolution, over 100 years, of the eccentricity vector of a GPS orbit, taking into account all relevant perturbations, with and without the Earth's shadow. The pattern observed was basically produced by the superimposition of two anti-clockwise precessions, one with a period of 1 year and the other with a period of approximately 40 years. The initial value of the eccentricity vector was ≅ [0, 0]. The differences increased as a function of time, with the Earth's shadow maintaining a slightly less elliptical orbit.

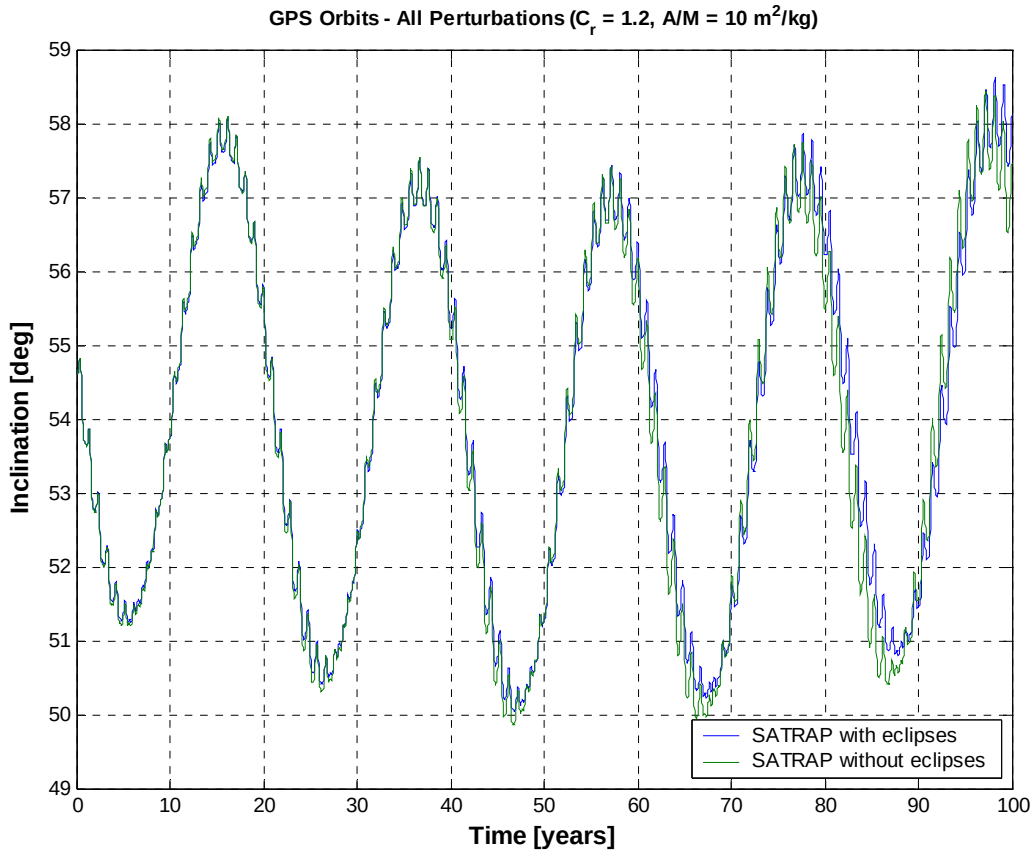

Figure 3.20

Long-term inclination evolution of a GPS orbit, taking into account all relevant perturbations, with and without the Earth's shadow. The amplitude of the variation remained the same, but the Earth's shadow increased a little bit the period of the orbit pole precession. The main short-term oscillation, however, retained the same period (≅ 1 year) and phase.

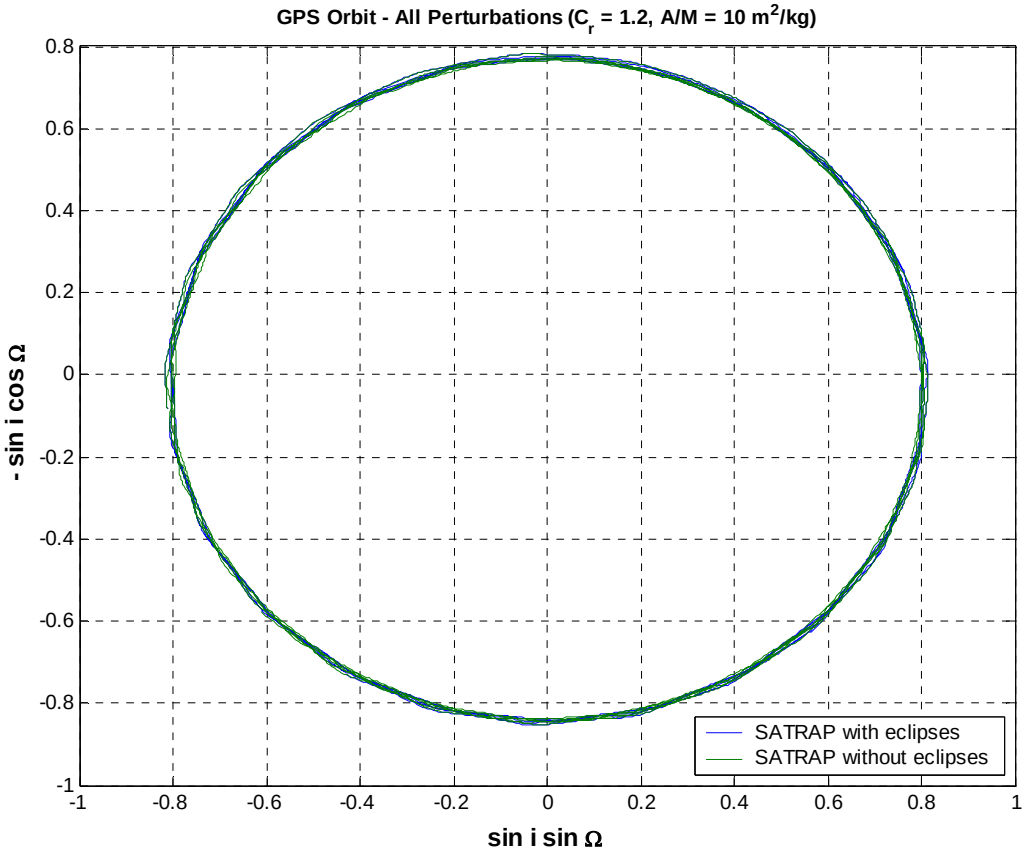

Figure 3.21

Evolution, over 100 years, of the two-dimensional inclination vector of a GPS orbit, taking into account all relevant perturbations, with and without eclipses. The initial value of the inclination vector was ≅ [0, 0] and the precession period was approximately 25 years. The amplitude of the orbit pole clockwise precession remained the same, but the Earth's shadow slightly increased its period.

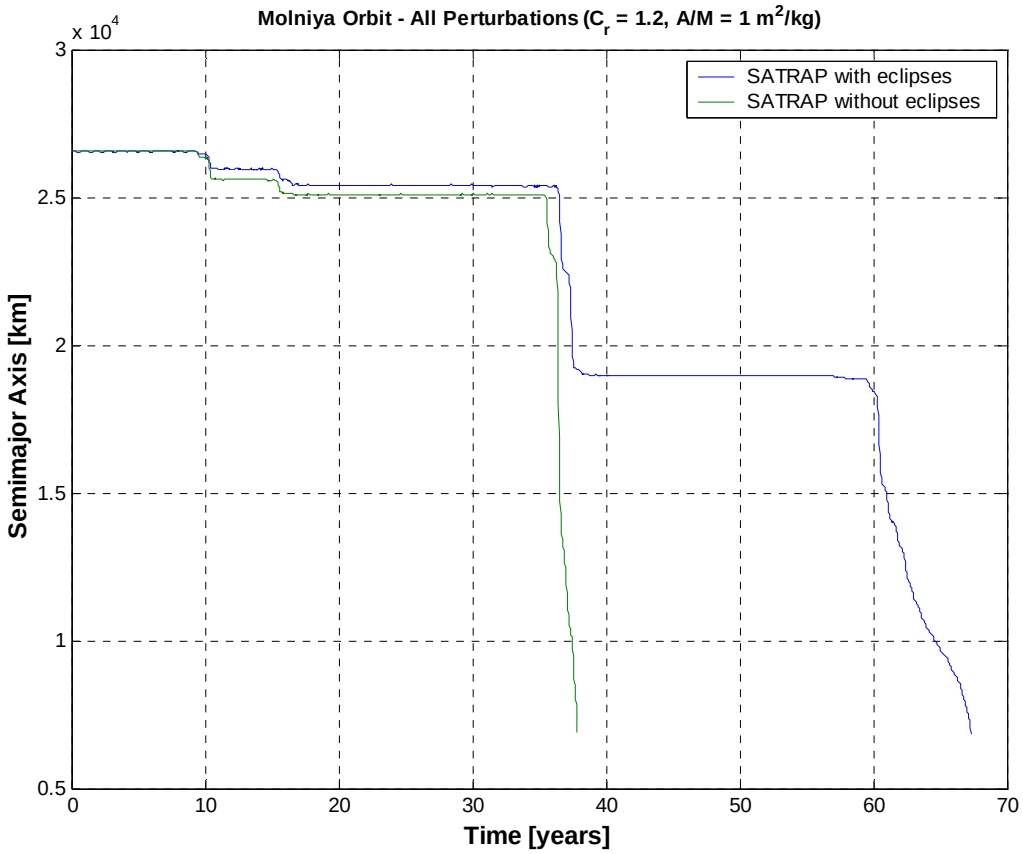

Figure 3.22

Long-term semimajor axis evolution of a Molniya orbit, taking into account all relevant perturbations, with and without the Earth's shadow. The agreement was very good during the first decade and more than acceptable in the following 25 years. The lifetime of Molniya orbits is very sensitive to small differences of the perigee height. In this example, the Earth's shadow substantially increased the lifetime, even though the orbital evolution was practically the same in both cases, until the phase of rapid decay of the orbit not subjected to sunlight eclipses.

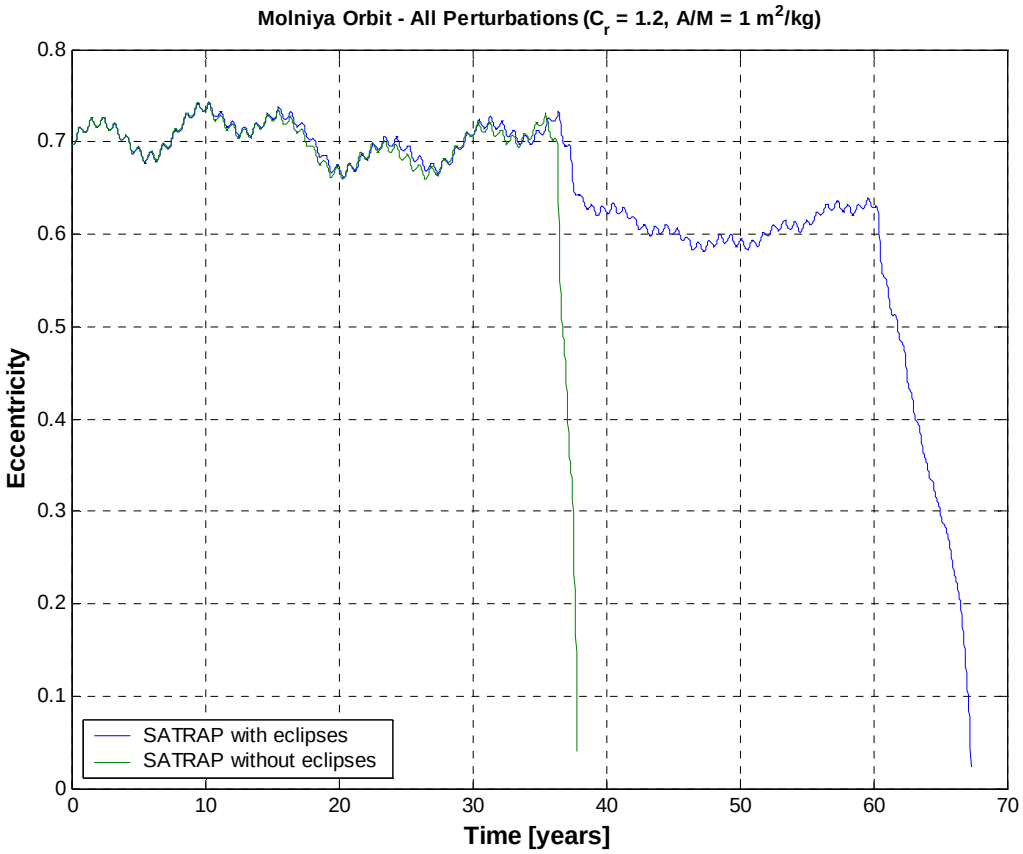

Figure 3.23

Long-term eccentricity evolution of a Molniya orbit, taking into account all relevant perturbations, with and without the Earth's shadow. The agreement was very good during the first 35 years, i.e. until the phase of rapid decay of the orbit not subjected to sunlight eclipses in this example.

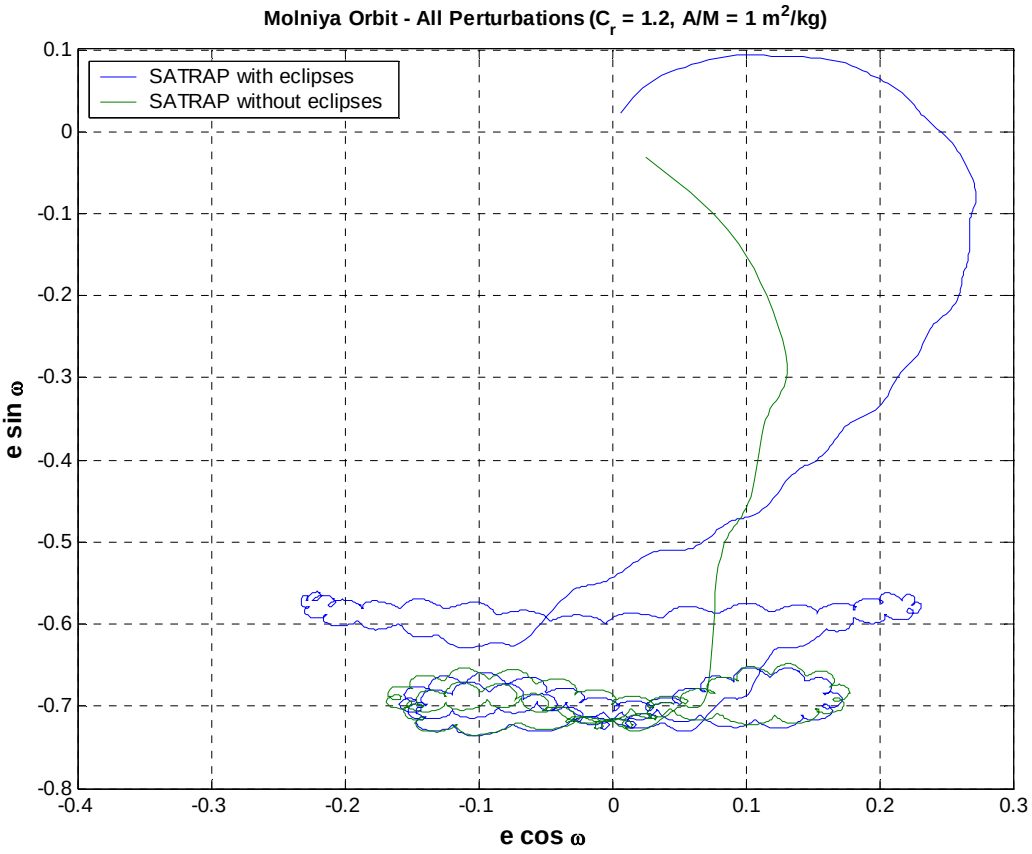

Figure 3.24

Evolution, over several decades, of the eccentricity vector of a Molniya orbit, taking into account all relevant perturbations, with and without the Earth's shadow. The initial value of the eccentricity vector was ≅ [0.046, –0.697]. The agreement was quite good during the first 35 years, i.e. until the phase of rapid decay of the orbit not subjected to sunlight eclipses in this example.

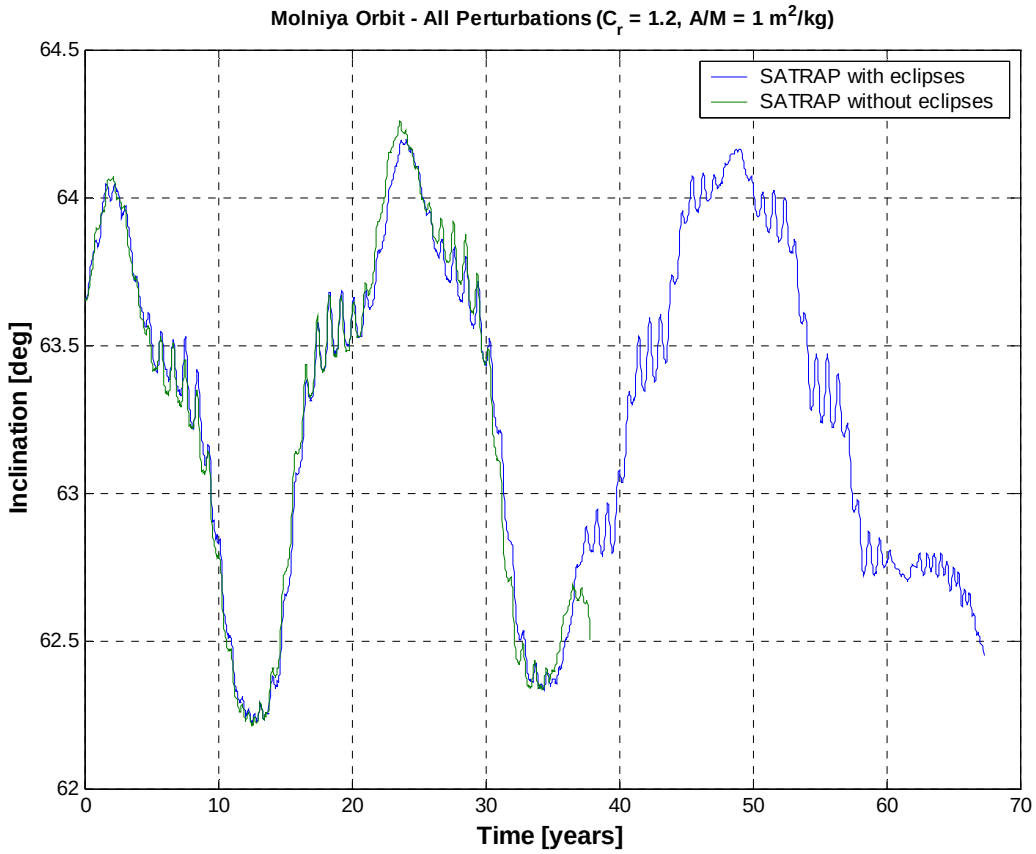

Figure 3.25

Long-term inclination evolution of a Molniya orbit, taking into account all relevant perturbations, with and without the Earth's shadow. The agreement was very good during the first 35 years, i.e. until the phase of rapid decay of the orbit not subjected to sunlight eclipses in this example.

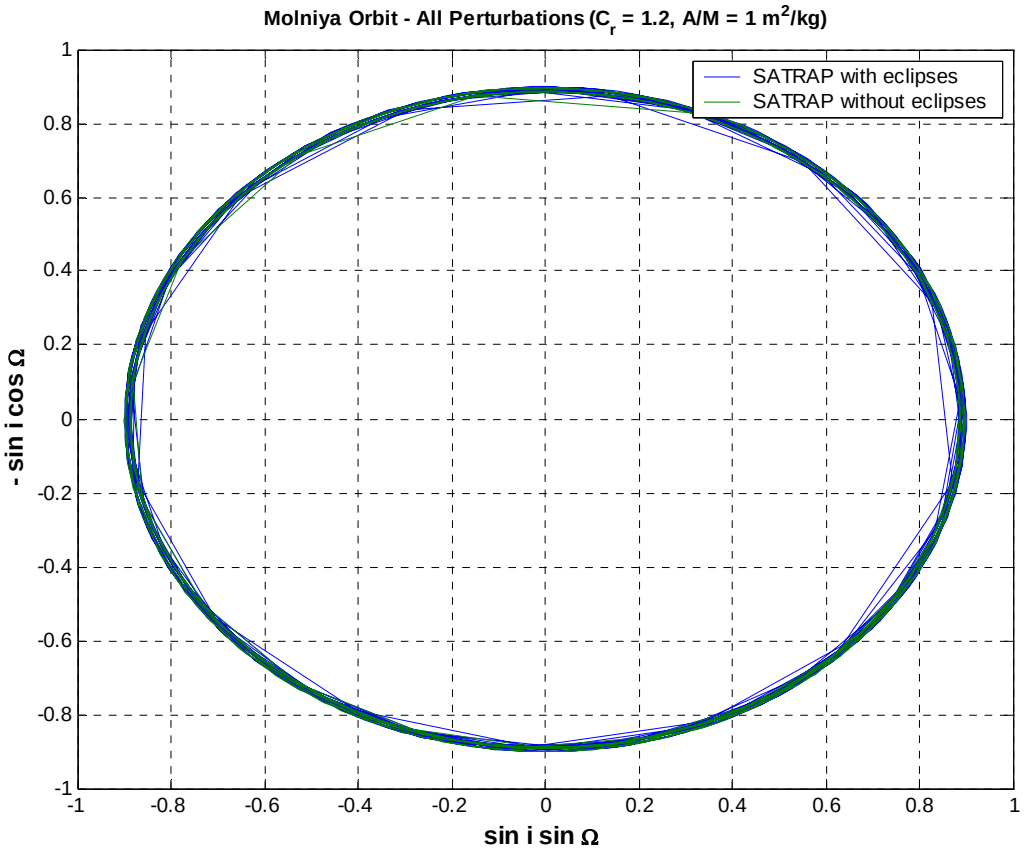

Figure 3.26

Evolution, over several decades, of the two-dimensional inclination vector of a Molniya orbit, taking into account all relevant perturbations, with and without the Earth's shadow. The initial value of the inclination vector was ≅ [0.890, 0.104]. The amplitude of the clockwise precession was practically the same in both cases.

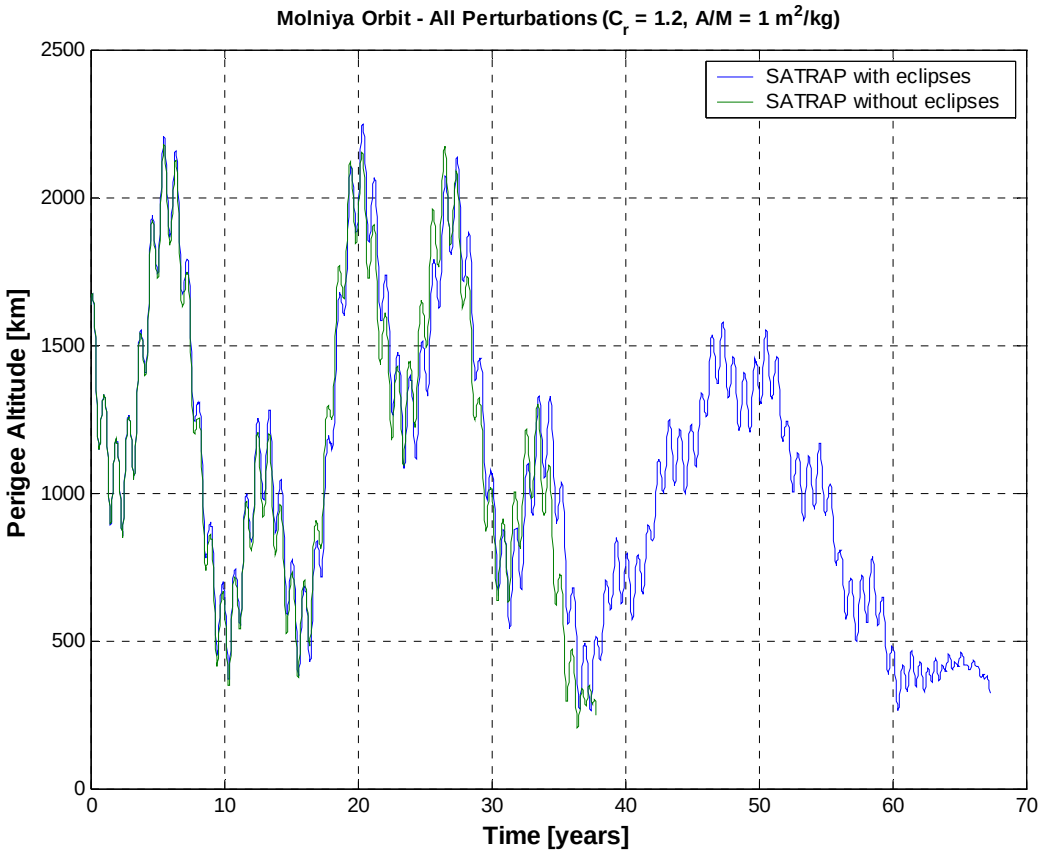

Figure 3.27

Long-term evolution of the perigee height of a Molniya orbit, taking into account all relevant perturbations, with and without the Earth's shadow. The agreement was very good during the first 35 years, but the lifetime of Molniya orbits is very sensitive to small differences of the perigee height. In this example, the Earth's shadow substantially increased the lifetime, even though the orbital evolution was practically the same in both cases, until the phase of rapid decay of the orbit not subjected to sunlight eclipses.

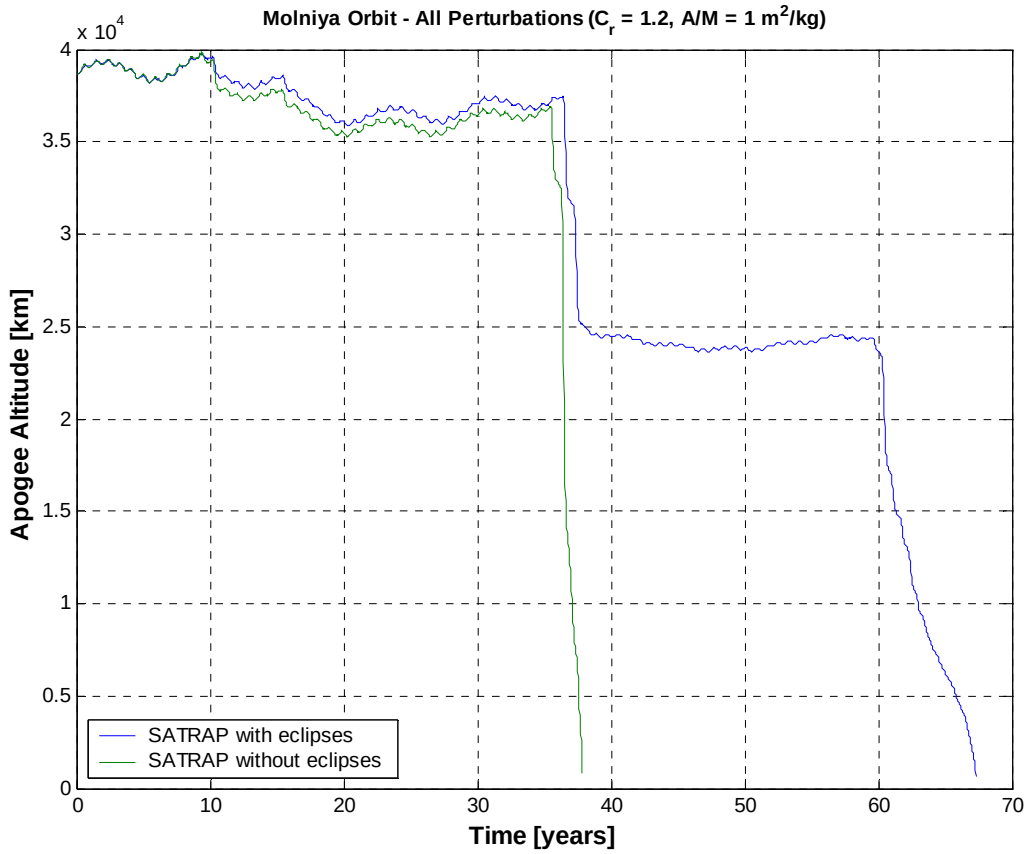

Figure 3.28

Long-term evolution of the apogee height of a Molniya orbit, taking into account all relevant perturbations, with and without the Earth's shadow. The agreement was quite good during the first 35 years, but the apogee altitude and the lifetime of Molniya orbits is very sensitive to small differences of the perigee height. In this example, the Earth's shadow substantially increased the lifetime, even though the orbital evolution was practically the same in both cases, until the phase of rapid decay of the orbit not subjected to sunlight eclipses.

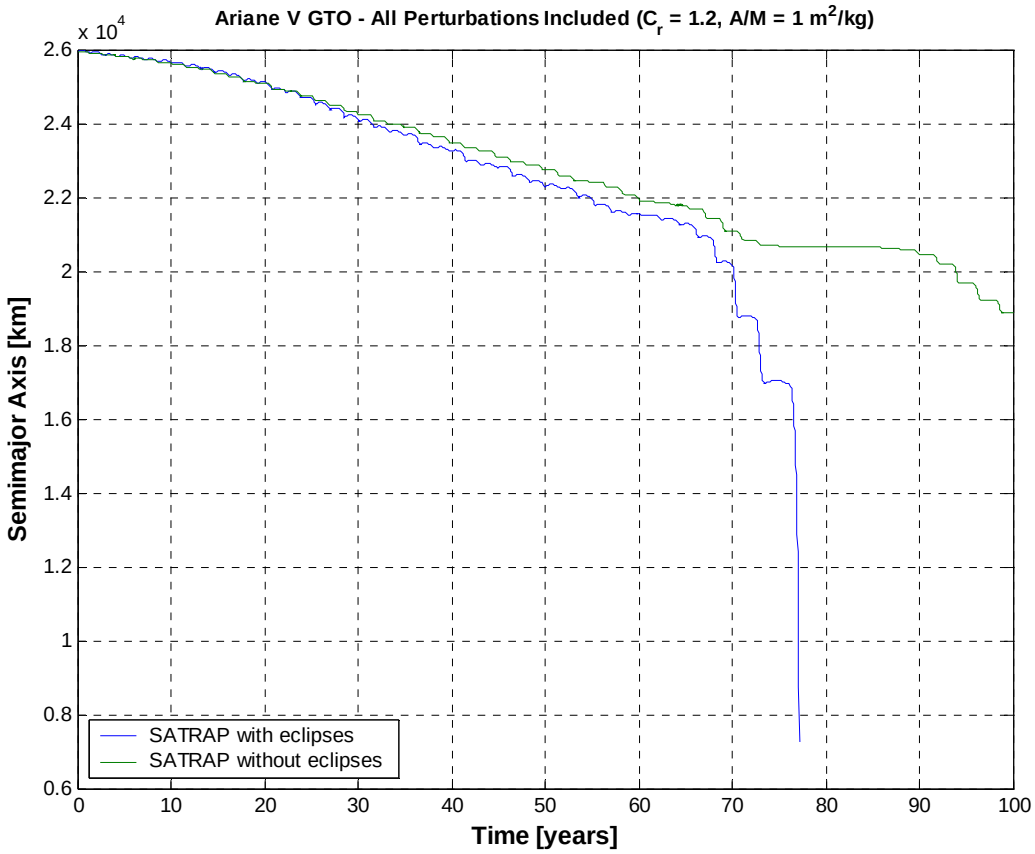

Figure 3.29

Long-term semimajor axis evolution of an Ariane V GTO, taking into account all relevant perturbations, with and without the Earth's shadow. The agreement remained reasonably good for about 70 years. However, the GTO lifetime is very sensitive to small differences of the perigee height. In this example, the Earth's shadow substantially decreased the lifetime, even though the orbital evolution was practically the same in both cases, until the phase of rapid decay of the orbit subjected to eclipses.

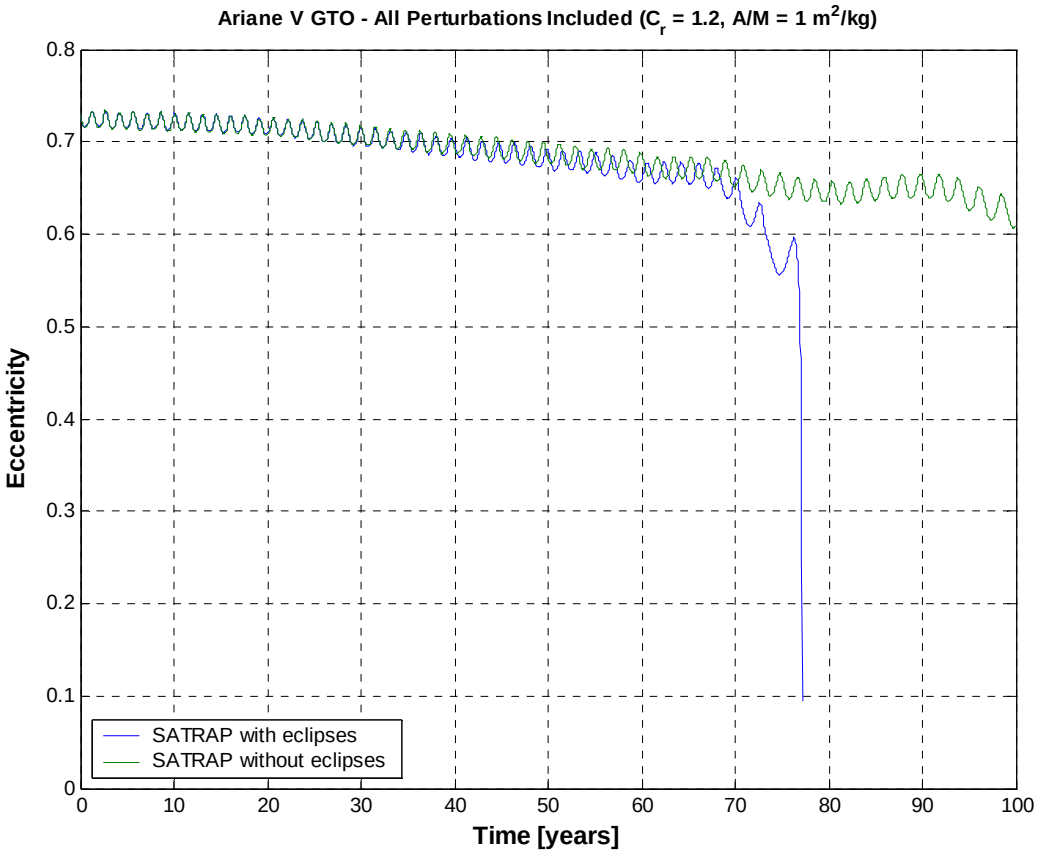

Figure 3.30

Long-term eccentricity evolution of an Ariane V GTO, taking into account all relevant perturbations, with and without the Earth's shadow. The agreement was very good during the first 30 years and more than acceptable in the following 40 years. However, the GTO lifetime is very sensitive to small differences of the perigee height. In this example, the Earth's shadow substantially decreased the lifetime, even though the orbital evolution was practically the same in both cases, until the phase of rapid decay of the orbit subjected to eclipses.

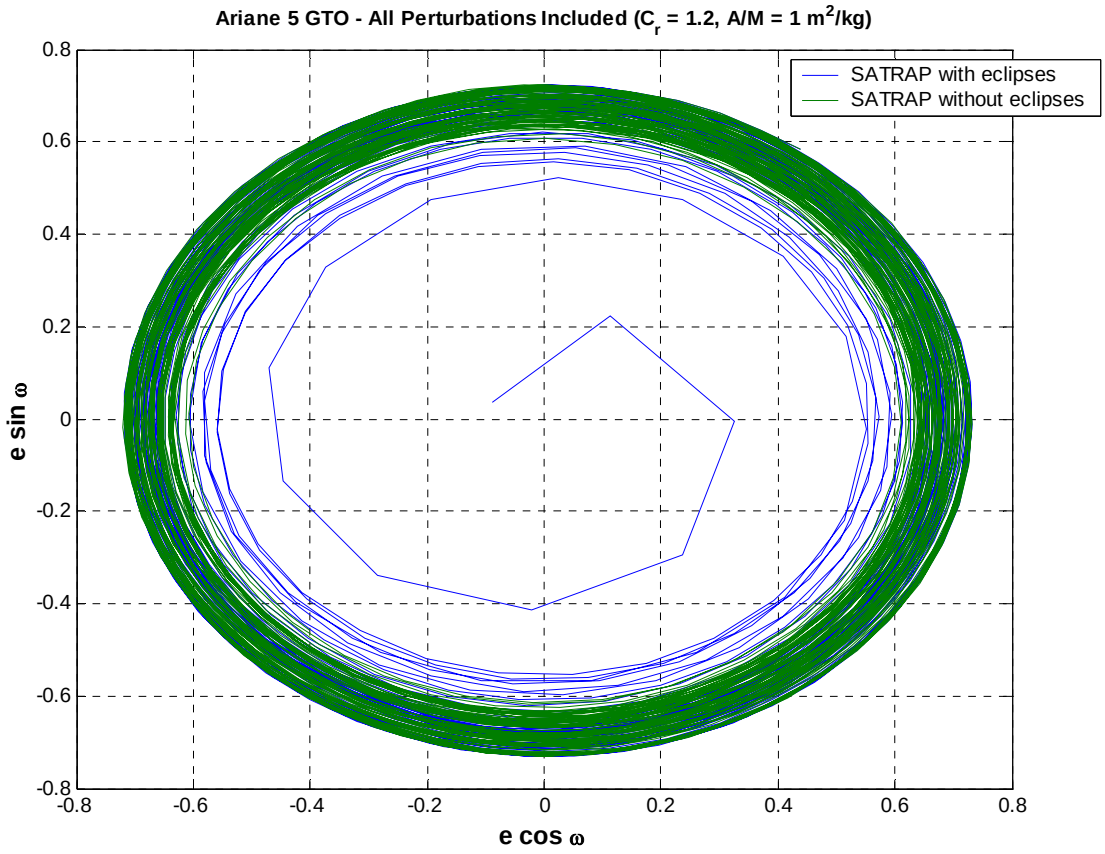

Figure 3.31

Evolution, over 100 years, of the eccentricity vector of an Ariane V GTO, taking into account all relevant perturbations, with and without the Earth's shadow. The initial value of the eccentricity vector was ≅ [0.437, 0.583]. The anti-clockwise precession was quite similar in both cases for about 70 years, i.e. until the phase of rapid decay of the orbit subjected to eclipses in this example.

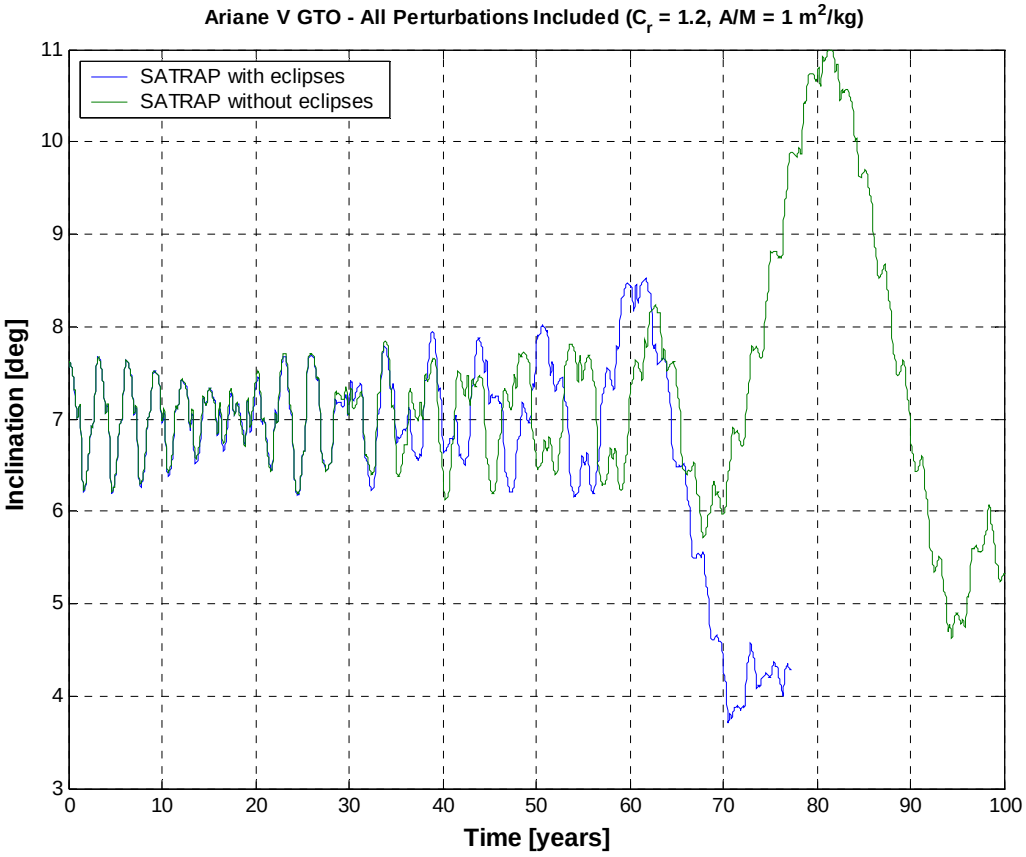

Figure 3.32

Long-term inclination evolution of an Ariane V GTO, taking into account all relevant perturbations, with and without the Earth's shadow. The agreement was very good during the first 30 years, becoming progressively worse in the following decades.

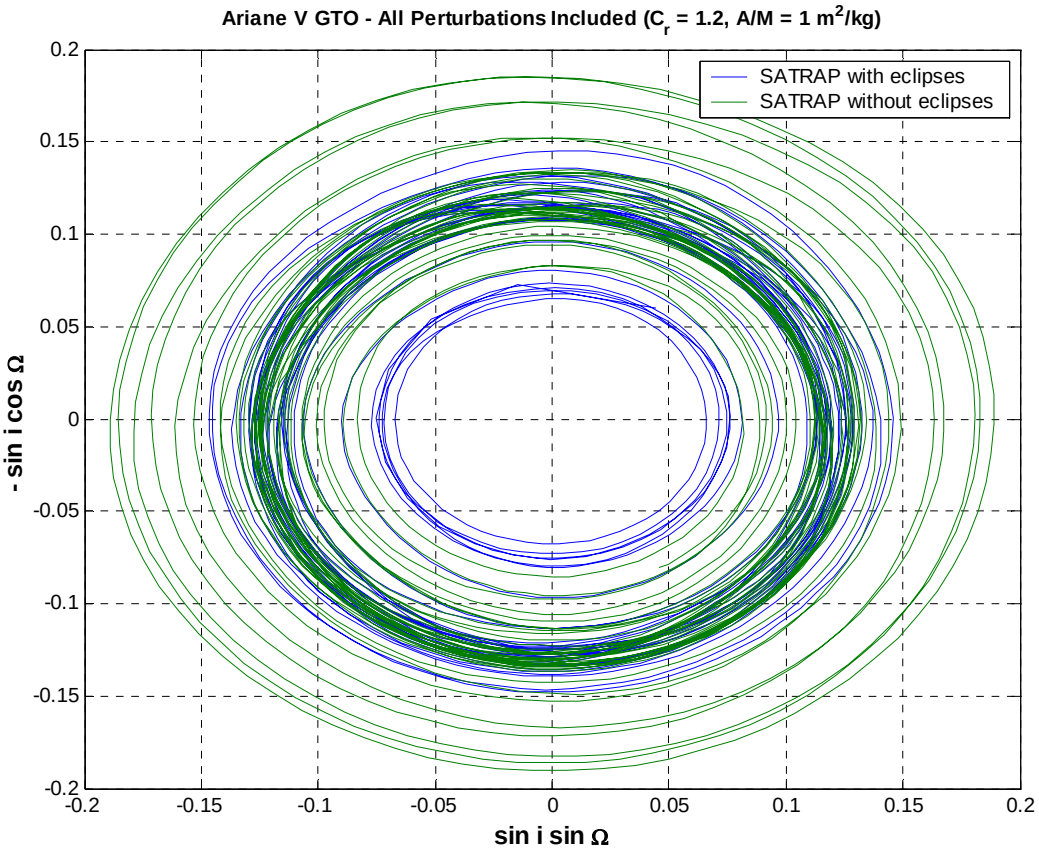

Figure 3.33

Evolution, over 100 years, of the two-dimensional inclination vector of an Ariane V GTO, taking into account all relevant perturbations, with and without the Earth's shadow. The initial value of the inclination vector was ≅ [0.009, –0.131]. In both cases, the clockwise precession was quite similar during the first 30 years, becoming progressively worse in the following decades.

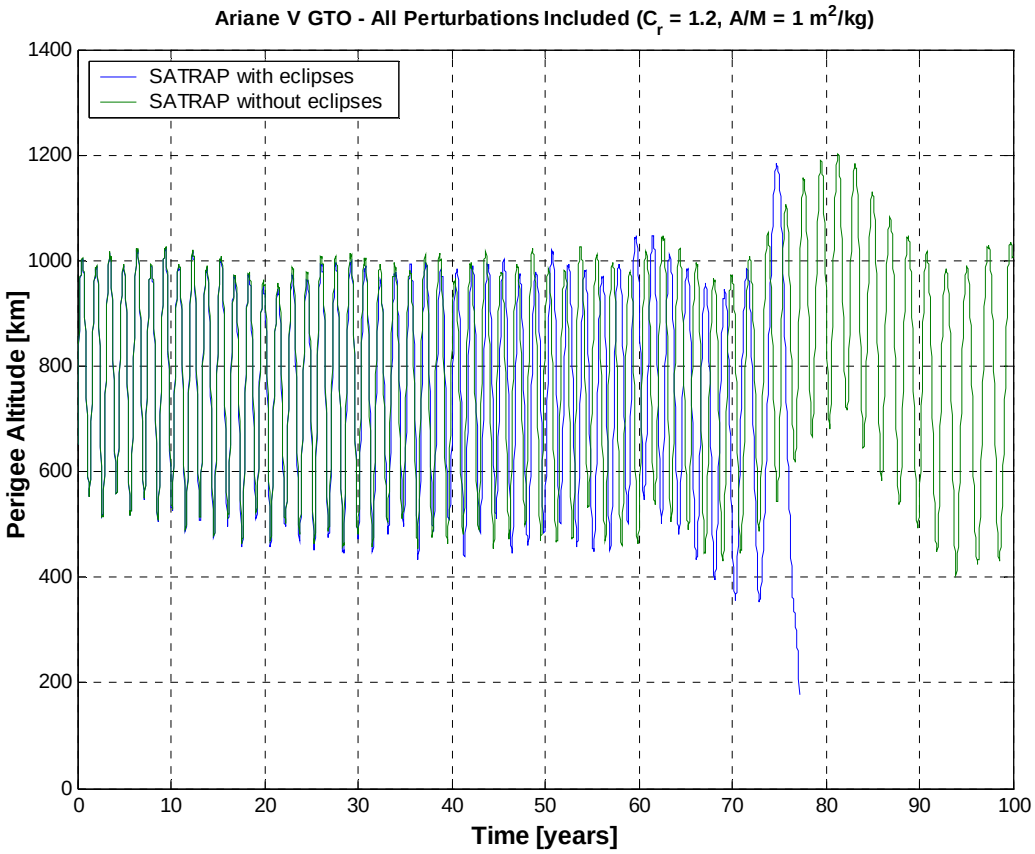

Figure 3.34

Long-term evolution of the perigee altitude of an Ariane V GTO, taking into account all relevant perturbations, with and without the Earth's shadow. The agreement remained reasonably good for about 70 years. However, the GTO lifetime is very sensitive to small differences of the perigee height. In this example, the Earth's shadow typically induced, for several decades, slightly lower minimum perigee altitudes, resulting at the end in a substantial decrease of the lifetime.

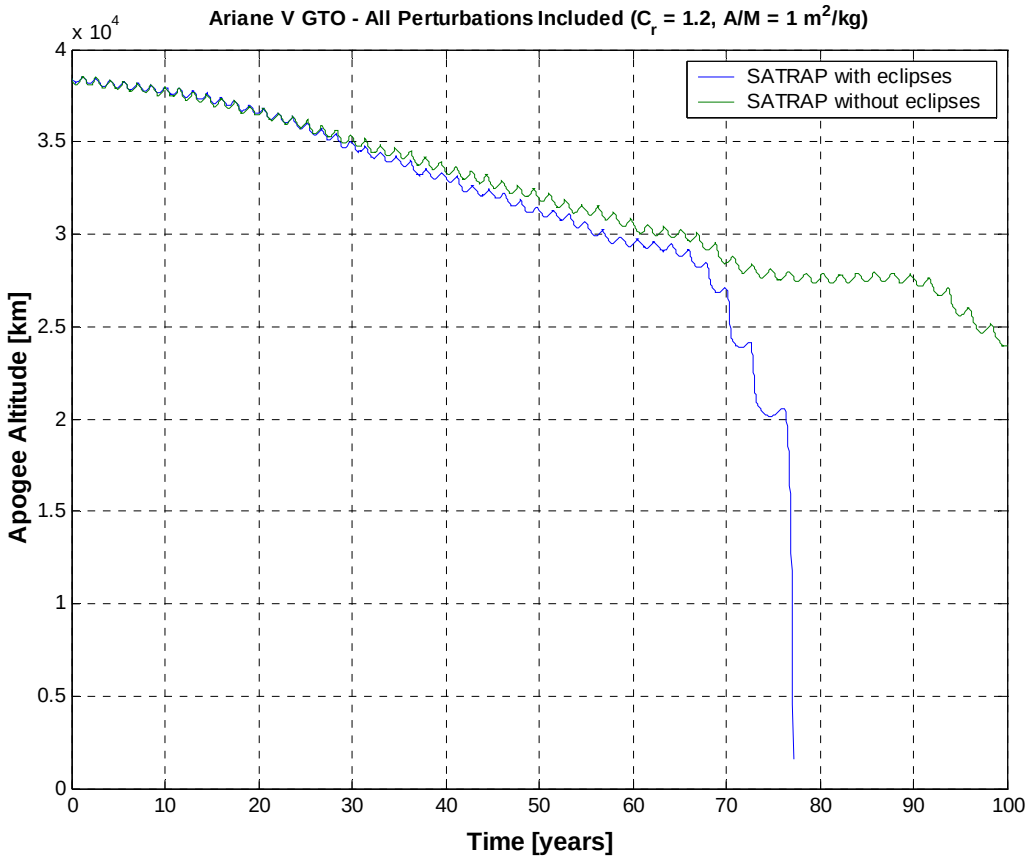

Figure 3.35

Long-term evolution of the apogee altitude of an Ariane V GTO, taking into account all relevant perturbations, with and without the Earth's shadow. The agreement remained reasonably good for about 70 years. However, the GTO apogee and lifetime are very sensitive to small differences of the perigee height. In this example, the Earth's shadow typically induced, for several decades, slightly lower minimum perigee altitudes, resulting at the end in an accelerated decrease of the apogee height and orbital lifetime.

4. EFFECTS OF PERTURBATIONS IN GEOSYNCHRONOUS ORBIT

4.1 Comparison of the Effects of Perturbations in GEO

Concluding the analysis of high Earth orbits, solar radiation pressure models and trajectory propagators outlined in the previous sections, the geosynchronous orbit was revisited with the last version of SATRAP, including the sunlight perturbing acceleration described by Eq. (1.2), in order to evaluate the relative importance of the various relevant perturbations. Again, the reference orbit adopted as initial conditions is given in Table 2.1. The time span of the simulations was 100 years, while C_r = 1.2 and A/M = 17 m^2/kg, in order to enhance the dynamical effects of solar radiation pressure, when considered.

The results obtained are summarized in the following figures, grouped in terms of the orbital perturbations considered:

1. J_2 – Figure 4.1 (semimajor axis), Figure 4.2 (eccentricity), Figure 4.3 (eccentricity vector), Figure 4.4 (inclination) and Figure 4.5 (two-dimensional inclination vector);
2. Geopotential harmonics 8 × 8 – Figure 4.6 (semimajor axis), Figure 4.7 (eccentricity), Figure 4.8 (eccentricity vector), Figure 4.9 (inclination) and Figure 4.10 (two-dimensional inclination vector);
3. Geopotential harmonics 8 × 8 + solar radiation pressure with eclipses – Figure 4.11 (semimajor axis), Figure 4.12 (eccentricity) and Figure 4.13 (inclination);
4. Comparison of third body gravitational perturbation of Moon, Sun, and Moon and Sun – Figure 4.14 (semimajor axis), Figure 4.15 (eccentricity), Figure 4.16 (eccentricity vector), Figure 4.17 (inclination) and Figures 4.18 and 4.19 (two-dimensional inclination vector);
5. Comparison of J_2 + Moon and Sun (3^{rd} body) with geopotential harmonics 8 × 8 + Moon and Sun (3^{rd} body) – Figure 4.20 (semimajor axis), Figure 4.21 (eccentricity), Figure 4.22 (eccentricity vector), Figure 4.23 (inclination), Figure 4.24 (two-dimensional inclination vector) and Figure 4.25 (perigee altitude);
6. Comparison of geopotential harmonics 2 × 2 + Moon and Sun (3^{rd} body) with geopotential harmonics 8 × 8 + Moon and Sun (3^{rd} body) – Figure 4.26 (semimajor axis), Figure 4.27 (eccentricity), Figure 4.28 (eccentricity vector), Figure 4.29 (inclination), Figure 4.30 (two-dimensional inclination vector) and Figure 4.31 (perigee altitude);
7. Geopotential harmonics 8 × 8 + Moon and Sun (3^{rd} body) + solar radiation pressure with eclipses – Figure 4.32 (semimajor axis), Figure 4.33 (eccentricity), Figures 4.34-4.36 (eccentricity vector), Figure 4.37 (inclination) and Figure 4.38 (two-dimensional inclination vector).

The evolution of the semimajor axis was mainly affected by J_{22} (see Figure 4.26) and the combined action of direct solar radiation pressure and Earth's shadow (see Figures 4.11 and 4.32).

Concerning the eccentricity, the geopotential harmonics alone induced very small short and long-term oscillations, mainly due to J_2, with amplitudes of about 6×10^{-6} (see Figures 4.2 and 4.7). The addition of luni-solar attraction introduced much more significant effects, causing a long-term oscillation with an average period of 10.4 years and amplitude of about 6×10^{-4} (see Figures 4.21 and 4.27). The inclusion of solar radiation pressure, on the other hand, induced, for $A/M = 17$ m^2/kg and $C_r = 1.2$, a yearly oscillation with amplitude of about 0.4 and long period modulations of ~ 0.05 (see Figures 4.12 and 4.33). The evolution of the eccentricity vector was basically characterized by the superimposition of two anti-clockwise precession motions, both with a radius of about 0.2 (see Figures 4.34-4.36). One precession cycle was completed in 1 year, while the other presented a significantly longer period and a more complex behavior.

Concerning the inclination evolution, the geopotential effects were negligible (see Figures 4.4 and 4.9). Only the right ascension of the ascending node was subjected to a regression of –0.0134 deg per day, largely due to J_2. The addition of luni-solar perturbations, on the other hand, induced the well-known clockwise precession of the orbit angular momentum vector, with a period of 53.3 years and a resulting maximum inclination of about 15 deg (see Figures 4.23, 4.24, 4.29 and 4.30). However, for a so high area-to-mass ratio ($C_r \times A/M = 20.4$ m^2/kg), solar radiation pressure too became very effective in perturbing the orbital plane, being able to induce – alone – long-term inclination oscillations with amplitude of 47 deg and duration of about 42.5 years, together with much smaller (< 1 deg) ripples with a period of 1 year (see Figures 3.6-3.8).

Finally, geopotential harmonics (primarily J_2), luni-solar attraction and solar radiation pressure effects combined in a non-linear way, exhibiting a quite complex evolution. The inclination, therefore, presented oscillations of varying amplitude, reaching a maximum value of 32.4 deg in one century (see Figure 4.37). The average period of these oscillations was about 22.4 years. The evolution of the orbit pole consisted of a clockwise precession motion, characterized by the same varying amplitude and duration of the dominant inclination oscillation (see Figure 4.38). A smaller wobbling motion, with amplitude of about 1 deg and period of approximately 1 year, was superimposed to the main long-term precession.

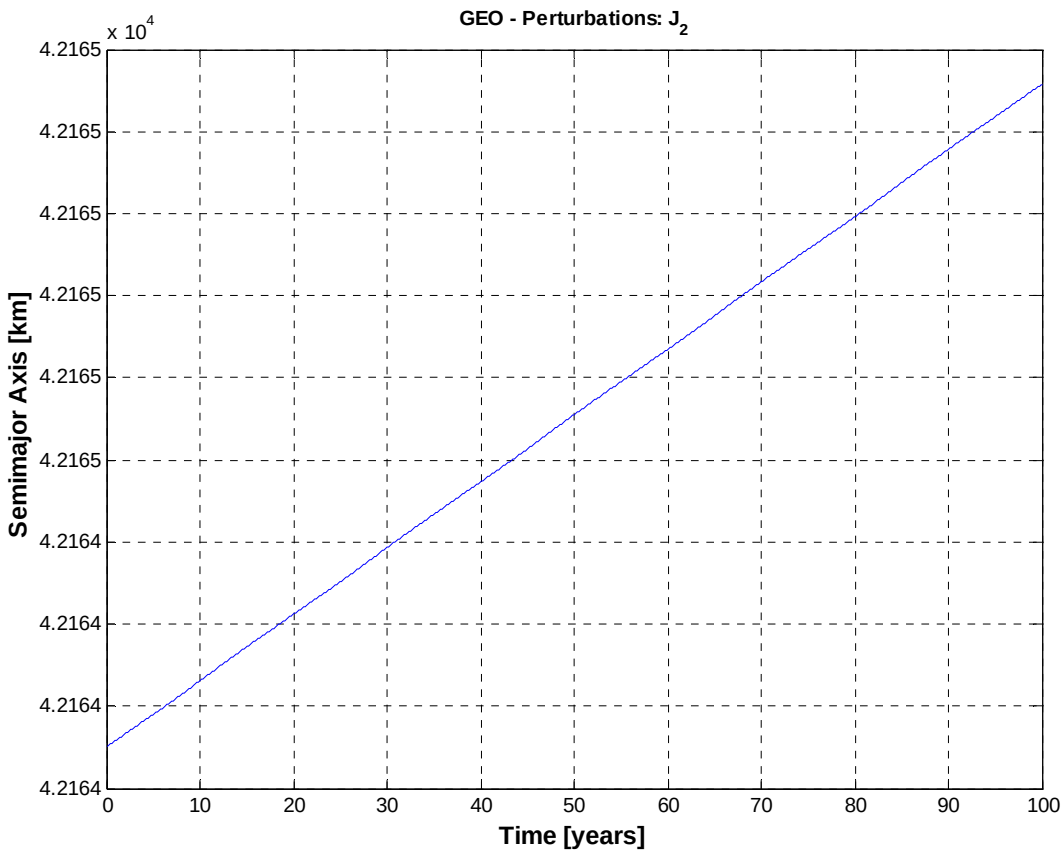

Figure 4.1

Long-term semimajor axis evolution in GEO, taking into account only J_2. As expected, it remained very close to the initial synchronous value.

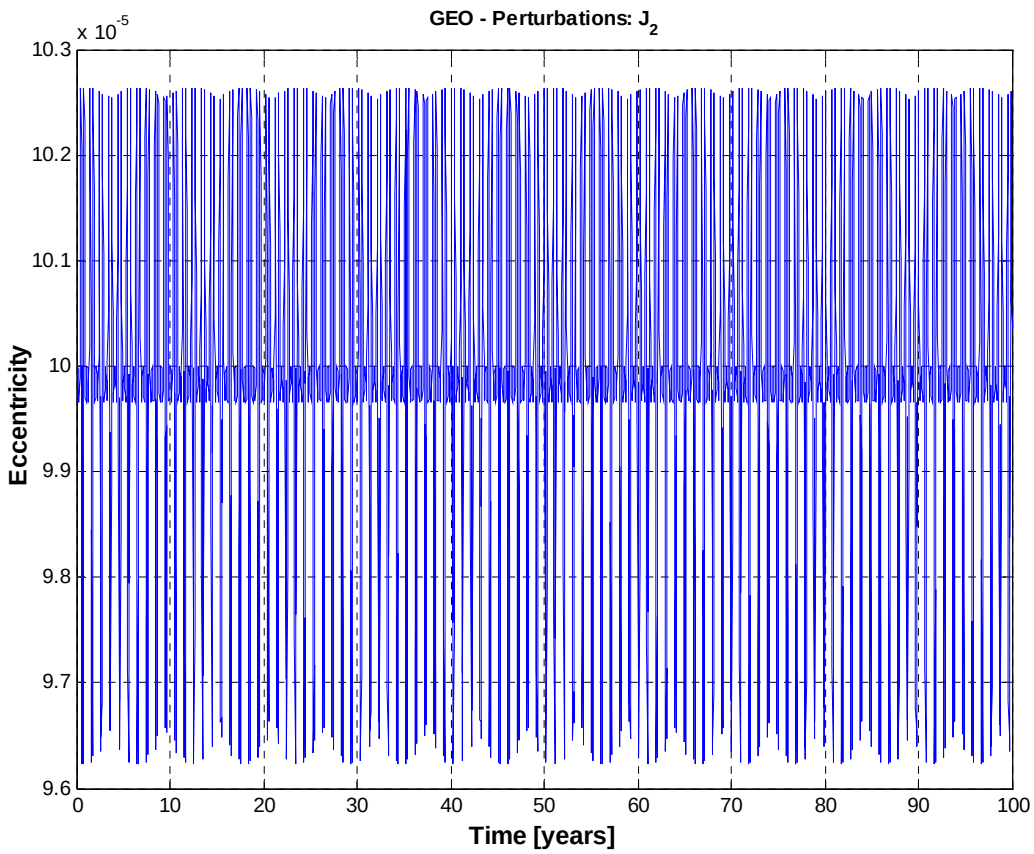

Figure 4.2

Long-term eccentricity evolution in GEO, taking into account only J_2. There was a variation, by $\pm$ 3-4 $\times$ 10^{-6}, around the initial value of 10^{-4}.

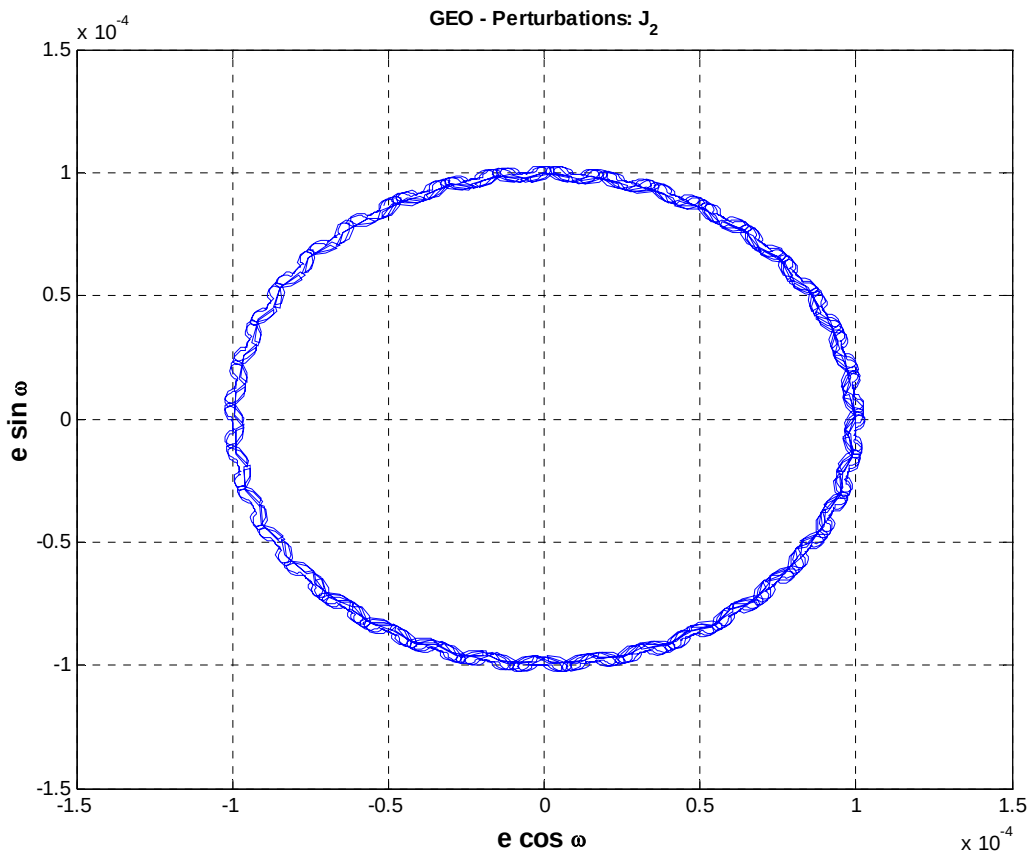

Figure 4.3

Evolution, over 100 years, of the eccentricity vector in GEO, taking into account only J_2. The initial value of the eccentricity vector was $\cong [-7.6 \times 10^{-5}, -6.4 \times 10^{-5}]$. The period of the main component of the anti-clockwise precession was about 36.8 years.

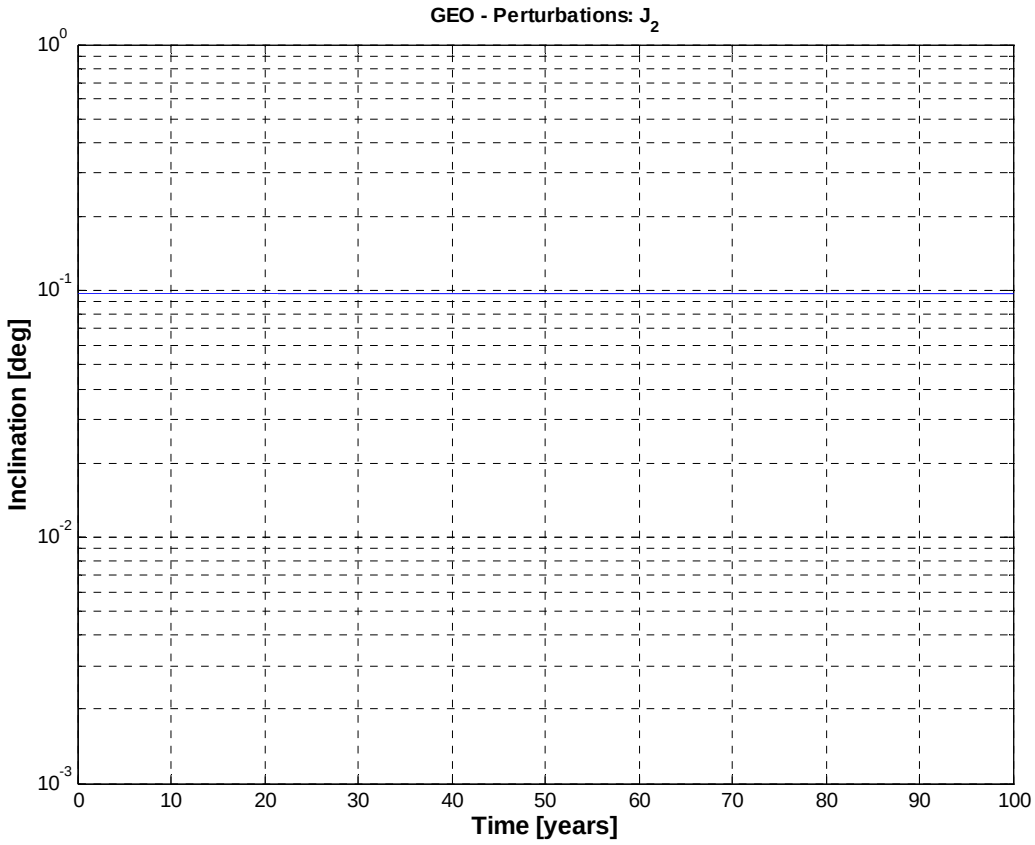

Figure 4.4

Long-term inclination evolution in GEO, taking into account only J_2. As expected, the value remained stable.

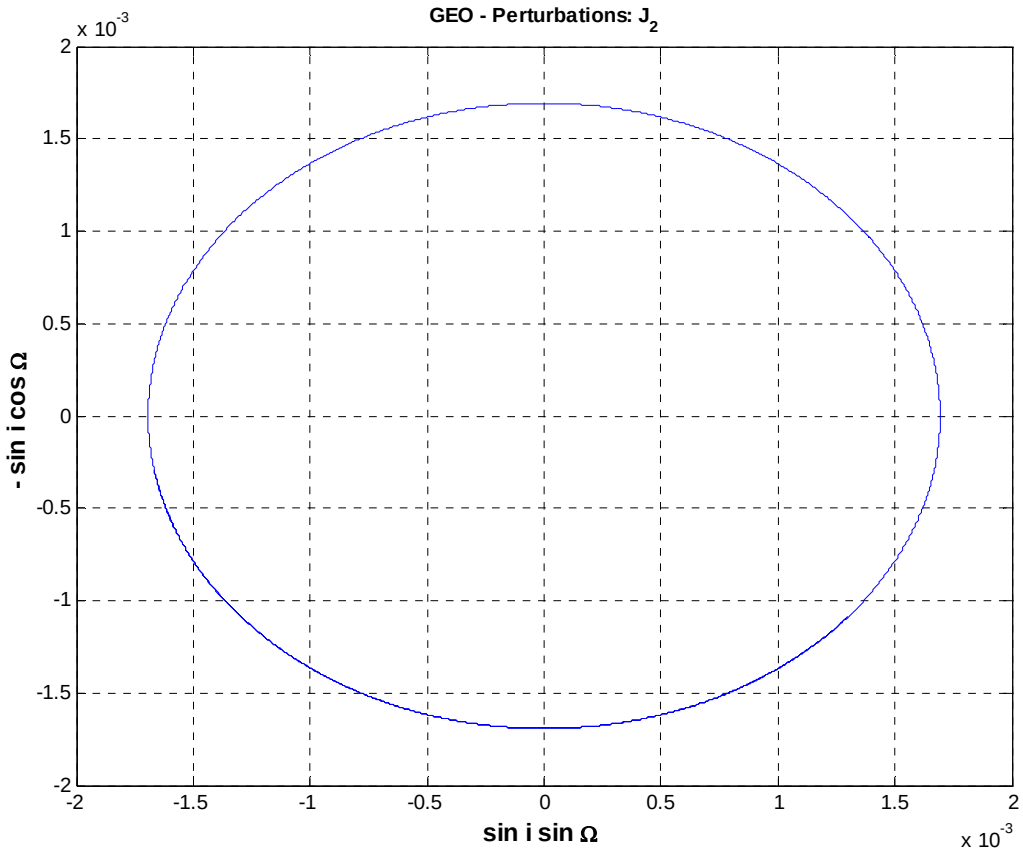

Figure 4.5

Evolution, over 100 years, of the two-dimensional inclination vector in GEO, taking into account only J_2. The initial value of the inclination vector was $\cong [1.3 \times 10^{-3}, -1.1 \times 10^{-3}]$. The period of the clockwise precession of the orbit pole was about 73.5 years.

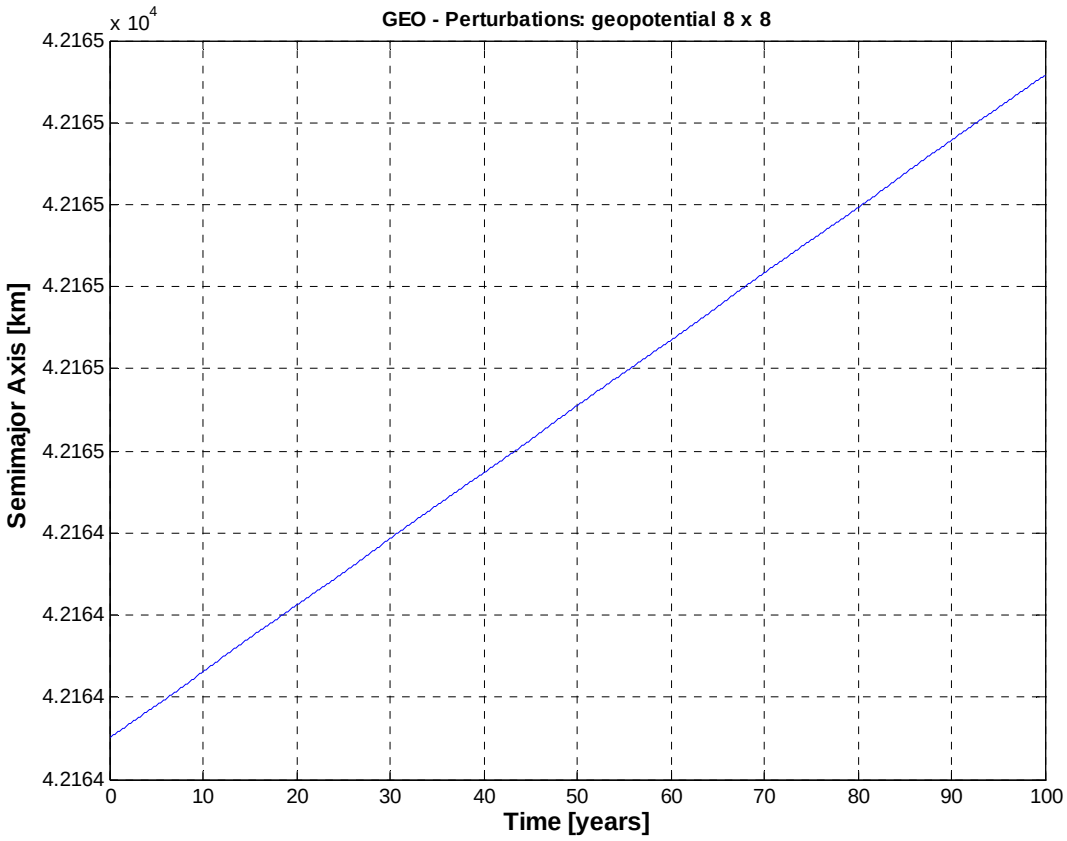

Figure 4.6

Long-term semimajor axis evolution in GEO, taking into account the geopotential harmonics, up to the 8th degree and order. No substantial difference was observed with respect to the case considering only J_2.

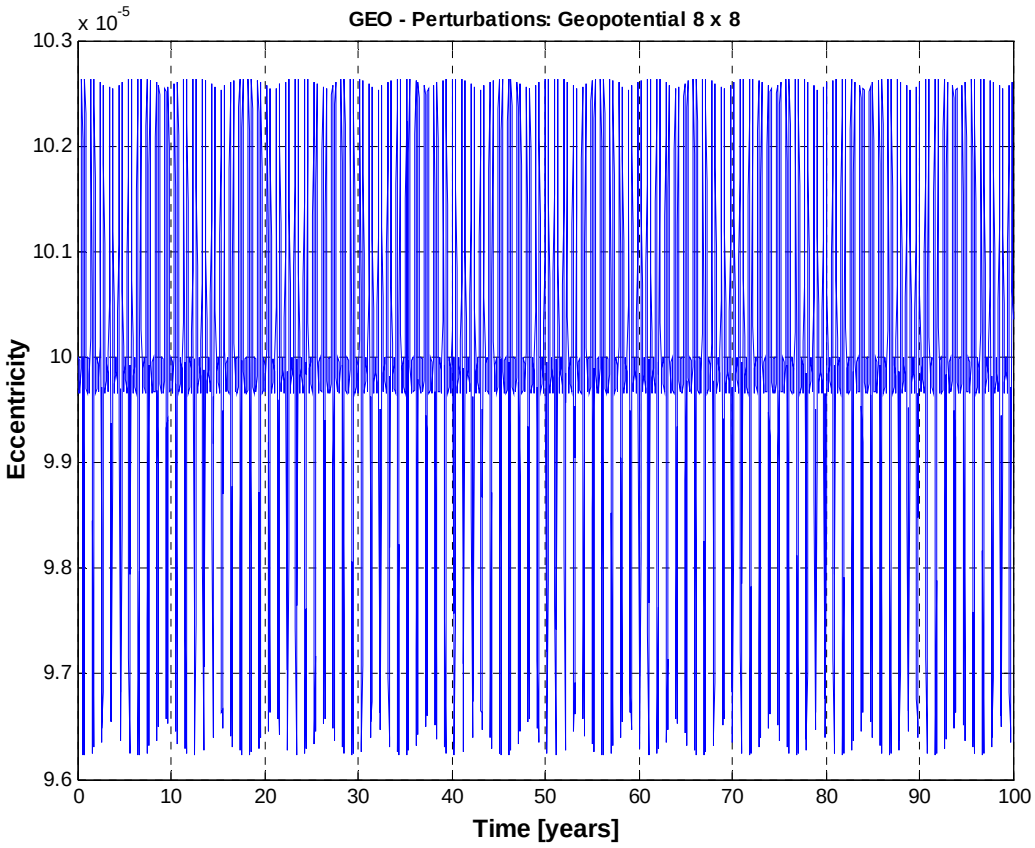

Figure 4.7

Long-term eccentricity evolution in GEO, taking into account the geopotential harmonics, up to the 8th degree and order. No substantial difference was observed with respect to the case considering only J_2.

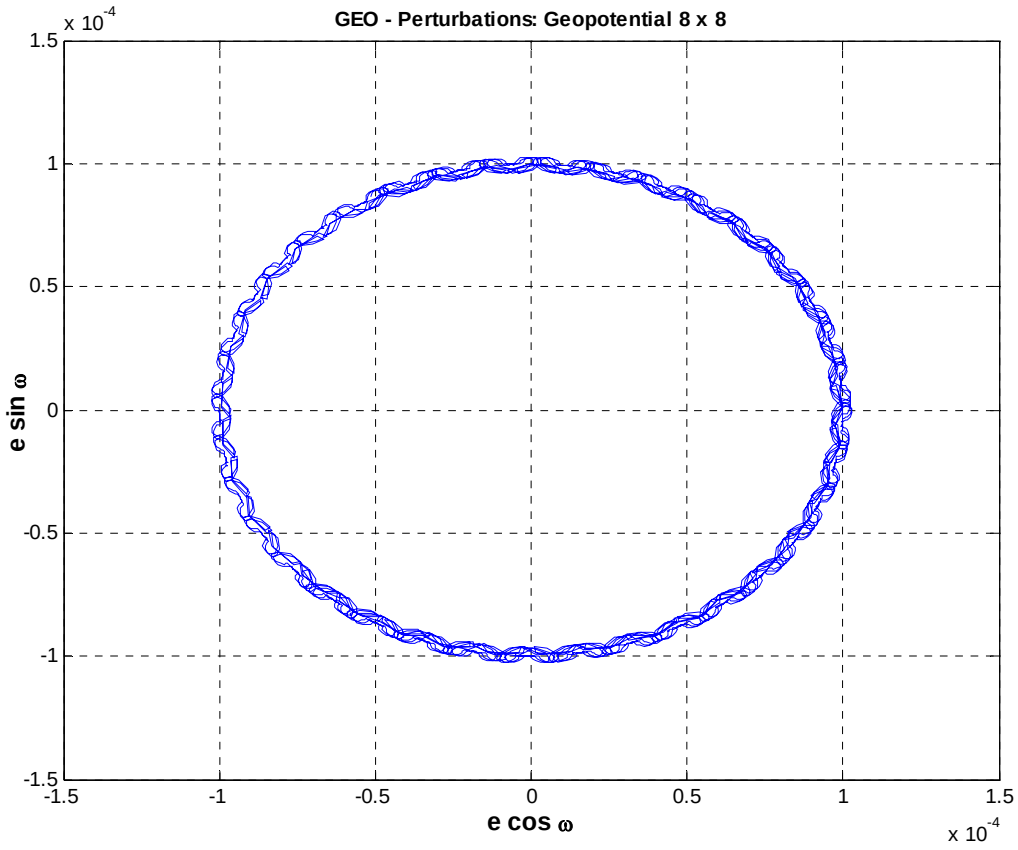

Figure 4.8

Evolution, over 100 years, of the eccentricity vector in GEO, taking into account the geopotential harmonics, up to the 8th degree and order. The initial value of the eccentricity vector was $\cong [-7.6 \times 10^{-5}, -6.4 \times 10^{-5}]$. No substantial difference was observed with respect to the case considering only J_2.

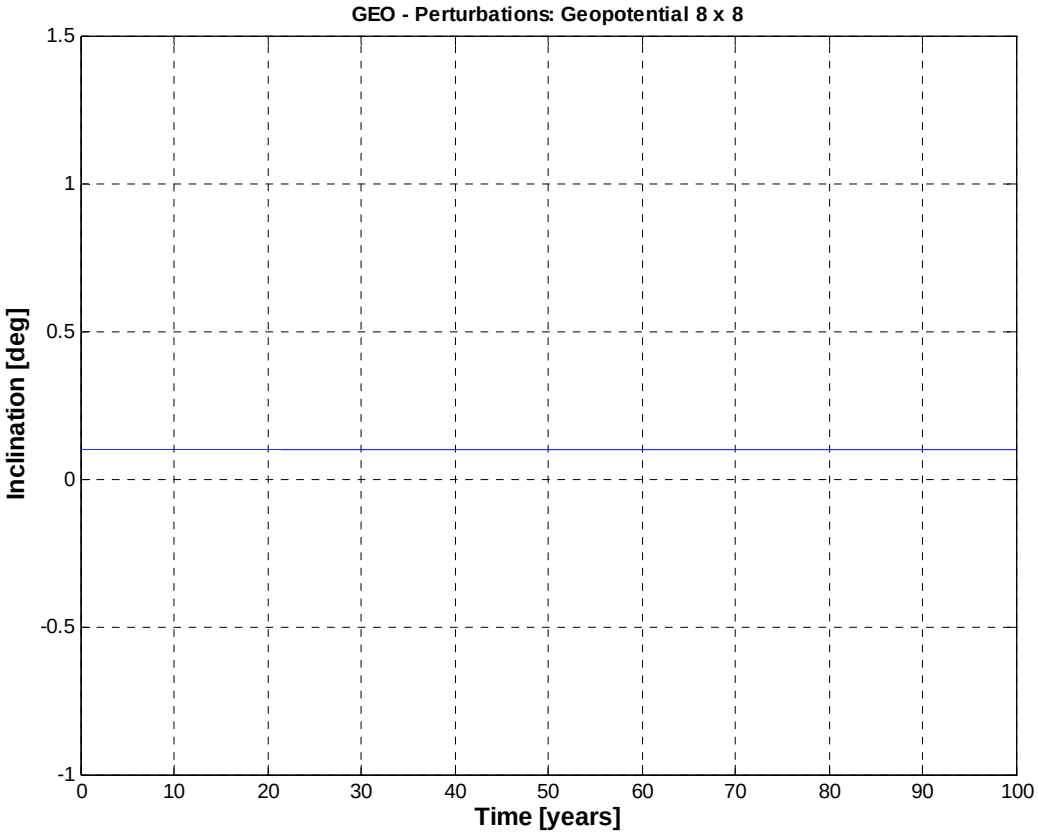

Figure 4.9

Long-term inclination evolution in GEO, taking into account the geopotential harmonics, up to the 8th degree and order. As in the case considering only J_2, the value remained stable.

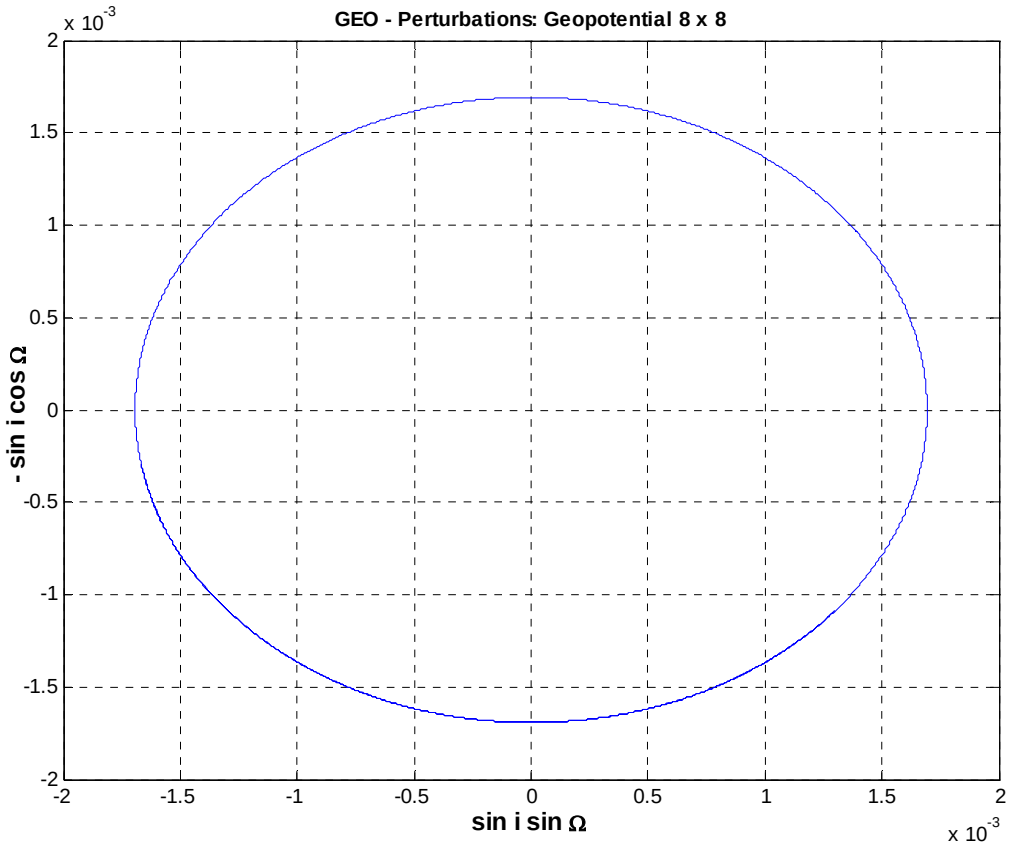

Figure 4.10

Evolution, over 100 years, of the two-dimensional inclination vector in GEO, taking into account the geopotential harmonics, up to the 8th degree and order. The initial value of the inclination vector was $\cong [1.3 \times 10^{-3}, -1.1 \times 10^{-3}]$. No substantial difference was observed with respect to the case considering only J_2.

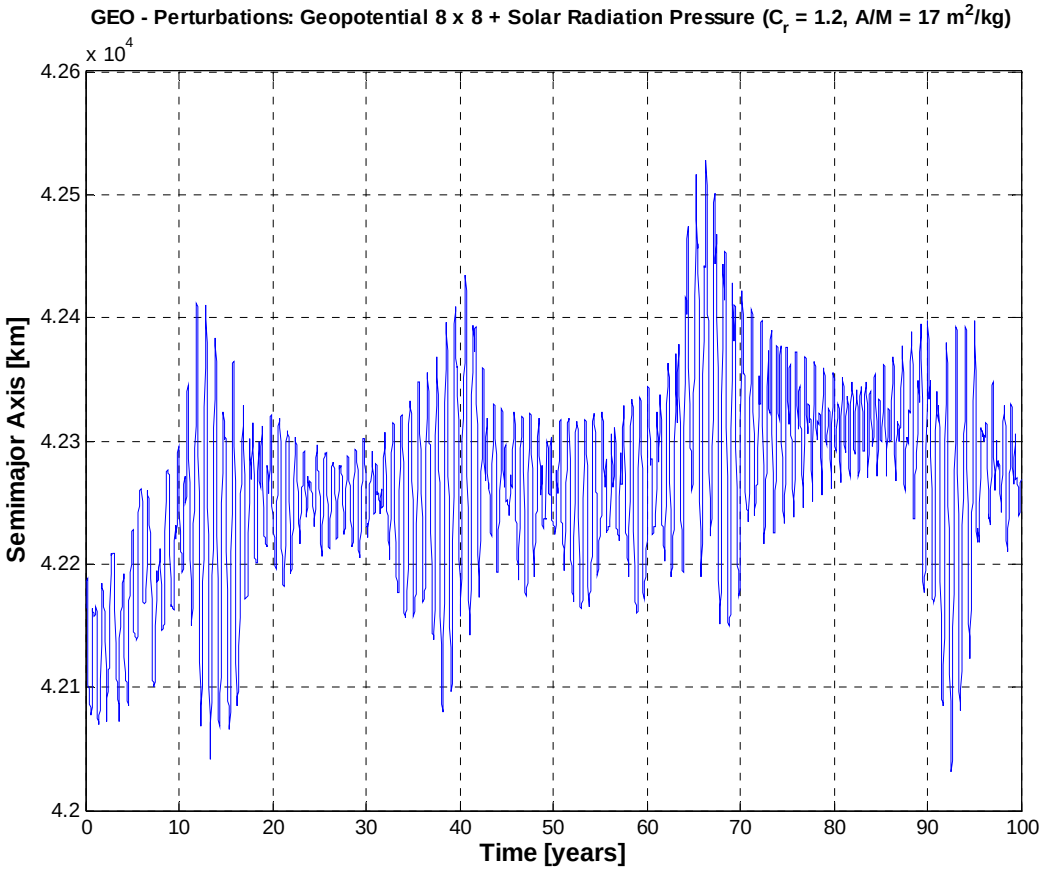

Figure 4.11

Long-term semimajor axis evolution in GEO, taking into account the geopotential harmonics, up to the 8th degree and order, and direct solar radiation pressure with eclipses. The oscillations with a period of about 1 year, induced by the combined effects of solar radiation pressure and Earth's shadow, are very evident in this example with $C_r \times A/M = 20.4$ m^2/kg.

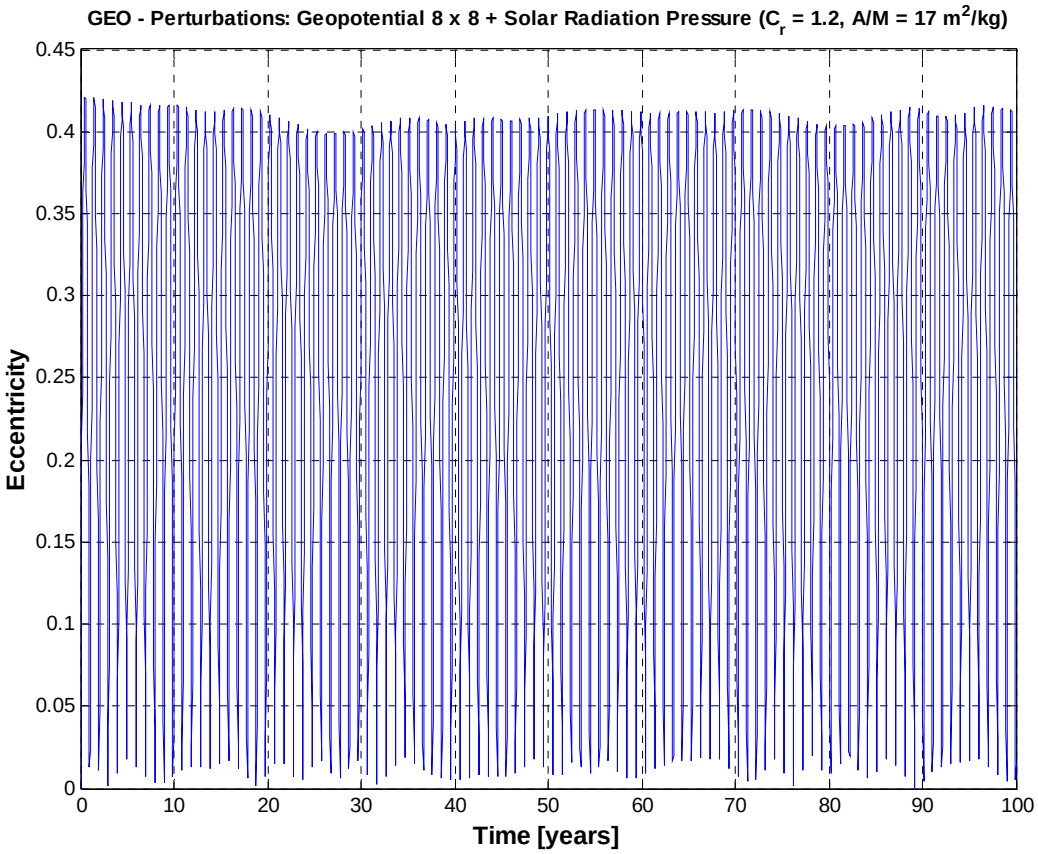

Figure 4.12

Long-term eccentricity evolution in GEO, taking into account the geopotential harmonics, up to the 8th degree and order, and direct solar radiation pressure with eclipses. The large oscillations, with a period of about 1 year, were due to solar radiation pressure, in this example with $C_r \times A/M = 20.4$ m^2/kg.

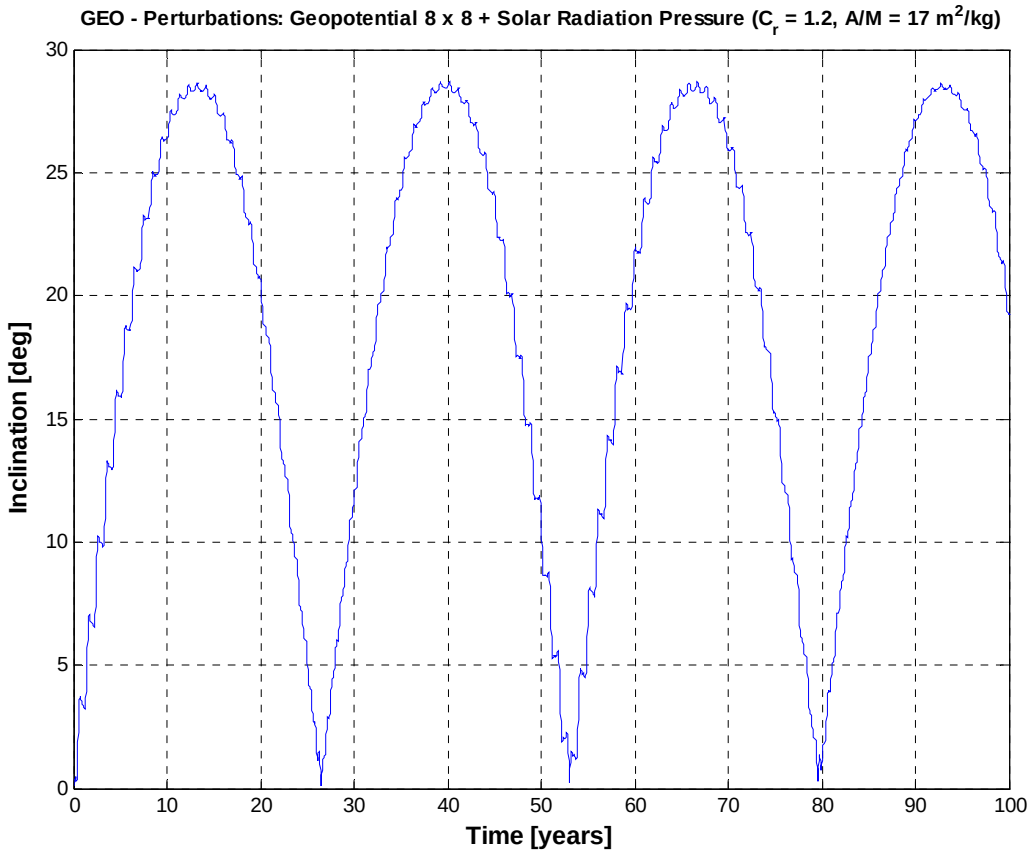

Figure 4.13

Long-term inclination evolution in GEO, taking into account the geopotential harmonics, up to the 8th degree and order, and direct solar radiation pressure with eclipses. The large oscillations, with a period of about 26.5 years, were due to solar radiation pressure, in this example with $C_r \times A/M = 20.4$ m^2/kg.

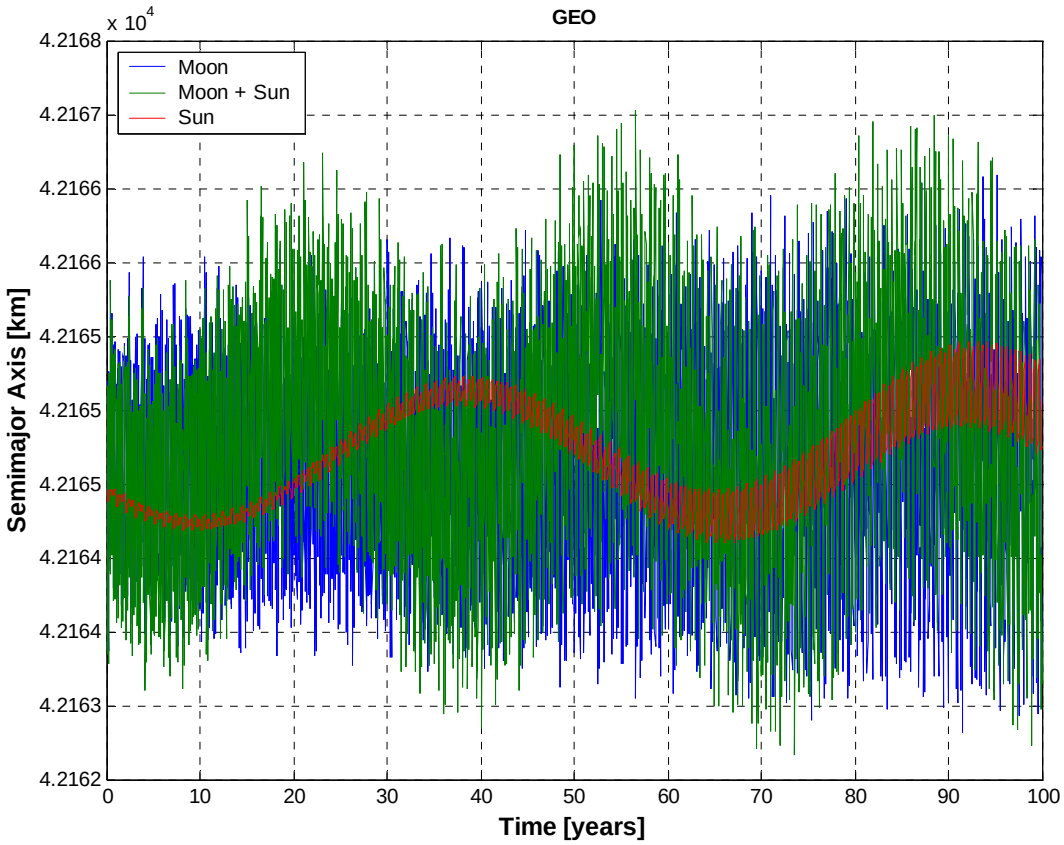

Figure 4.14

Long-term semimajor axis evolution in GEO, taking into account the third body attraction of the Moon, of the Sun, and of Moon and Sun combined. In addition to the long-term variations, the Sun induced small oscillations with a period of about 6 months, while the Moon produced larger oscillations with a period of approximately 1 month. The combined effect of Moon and Sun was more complex, but the semimajor axis variation remained very small (± 2-3 km with respect to the initial value).

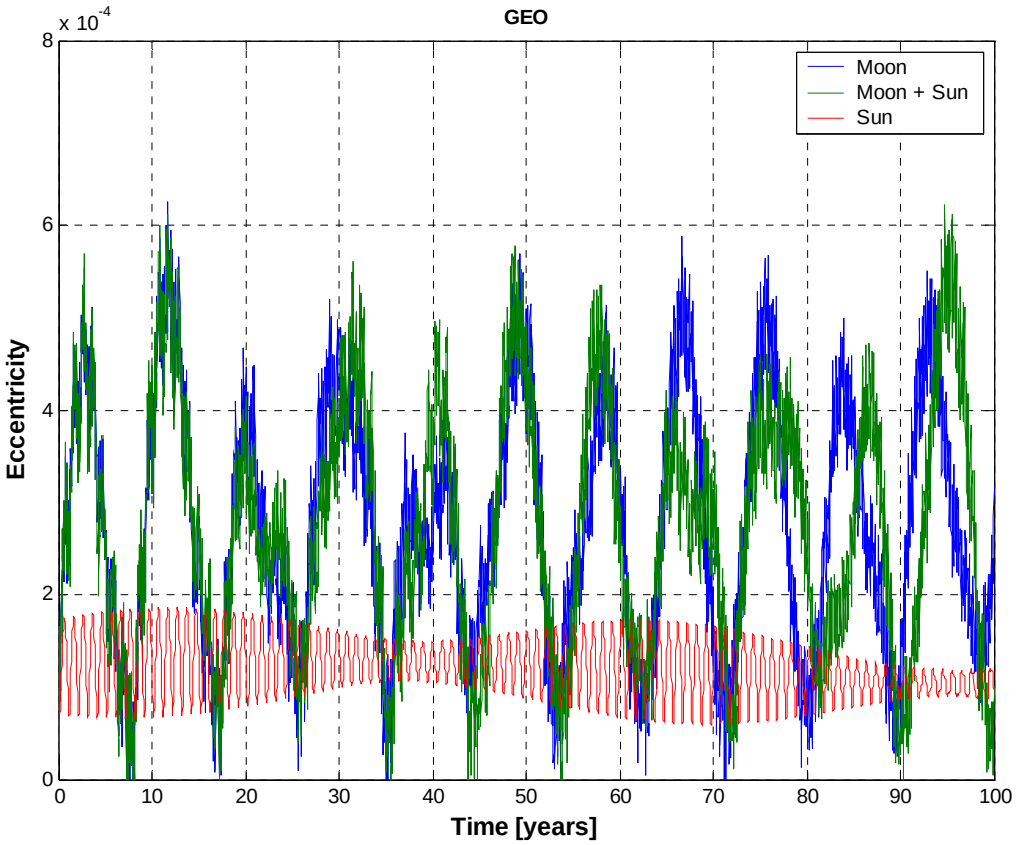

Figure 4.15

Long-term eccentricity evolution in GEO, taking into account the third body attraction of the Moon, of the Sun, and of Moon and Sun combined. In addition to a long-term modulation, the Sun induced oscillations with a period of about 1 year and amplitude of ~ 10^{-4}. The Moon as well produced short-term oscillations of similar amplitude and approximately monthly period, but the main effect was a periodic variation with an amplitude of ~ 5×10^{-4} and a period of about 8.9 years (close to the precession period of the argument of the lunar periapsis). The combined effect was dominated by the Moon component and the period of the main oscillation became almost 9 years.

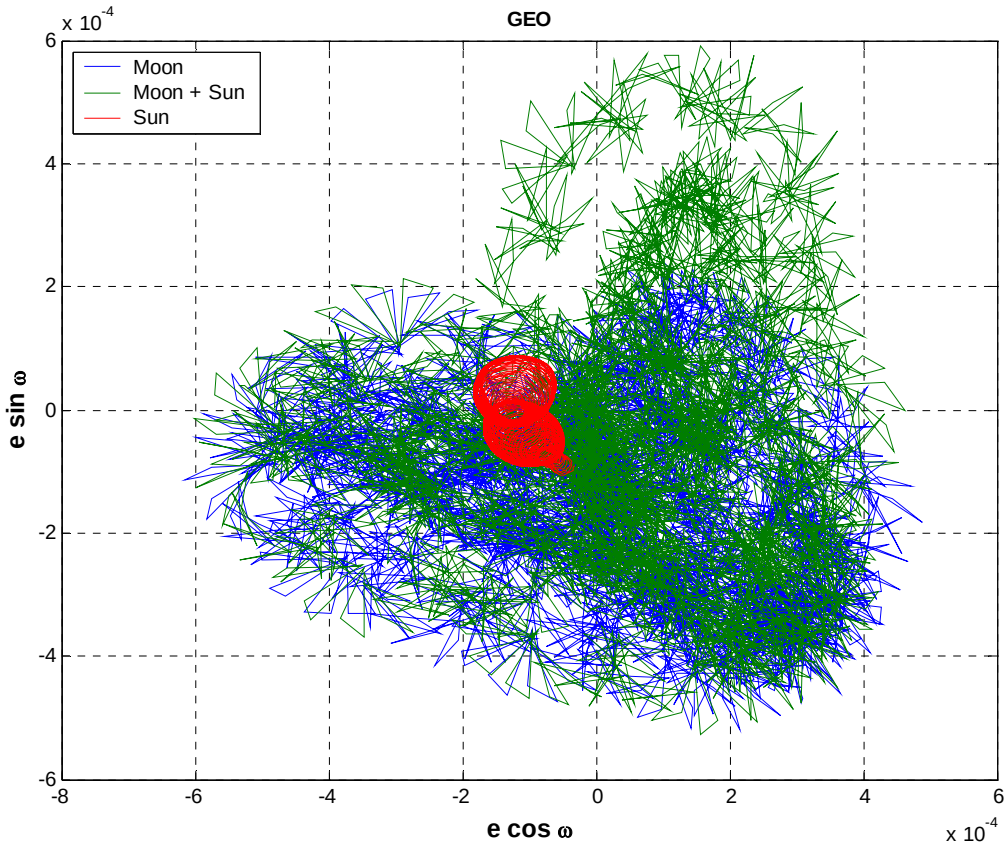

Figure 4.16

Evolution, over 100 years, of the eccentricity vector in GEO, taking into account the third body attraction of the Moon, of the Sun, and of Moon and Sun combined. The initial value of the eccentricity vector was $\cong [-7.6 \times 10^{-5}, -6.4 \times 10^{-5}]$. The precessional motion was quite complicated, but the combined effect was dominated by the Moon component.

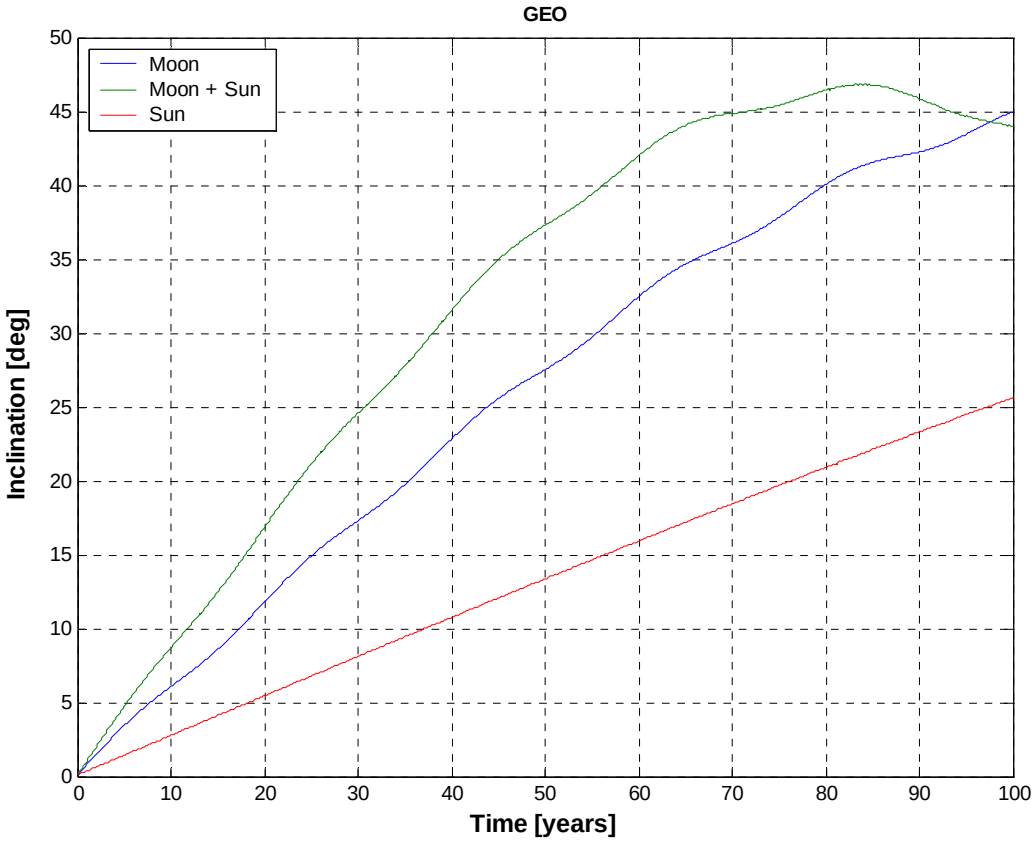

Figure 4.17

Long-term inclination evolution in GEO, taking into account the third body attraction of the Moon, of the Sun, and of Moon and Sun combined.

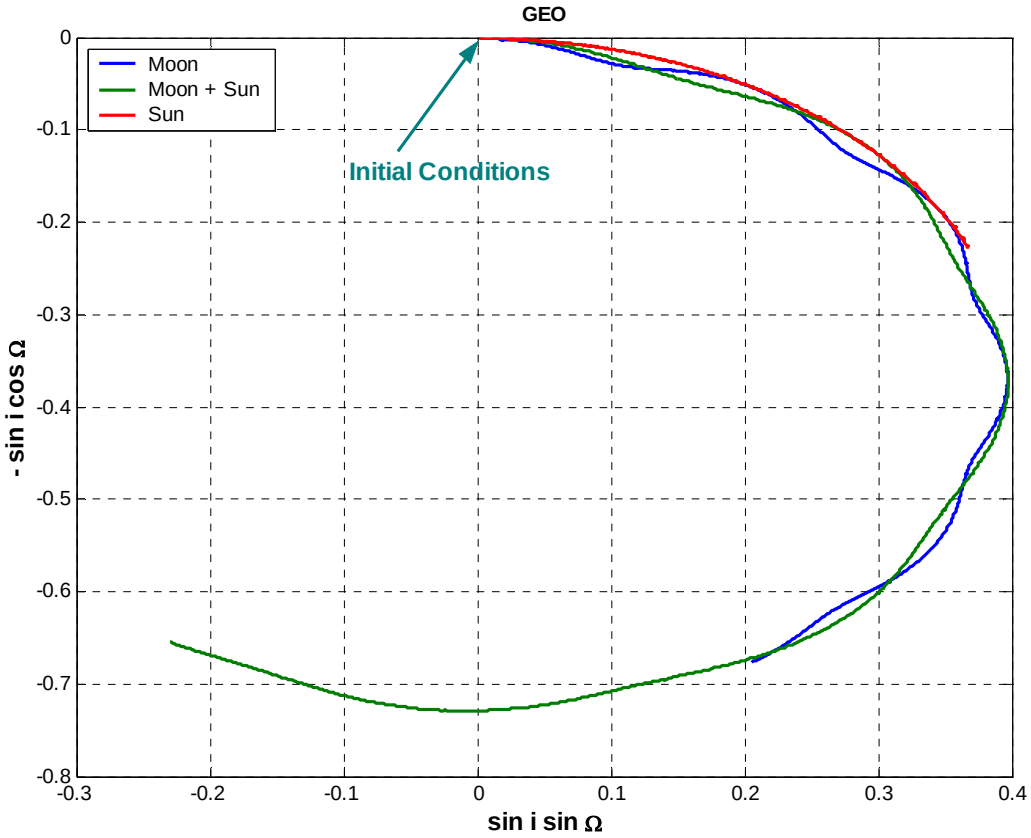

Figure 4.18

Evolution, over 100 years, of the two-dimensional inclination vector in GEO, taking into account the third body attraction of the Moon, of the Sun, and of Moon and Sun combined. All three cases induced a clockwise precession of the orbit pole with similar amplitudes, corresponding to a half-cone aperture of 20-23 deg, but markedly different periods: more than 500 years with the Sun, about 250 years with the Moon and almost 170 years with Moon and Sun combined.

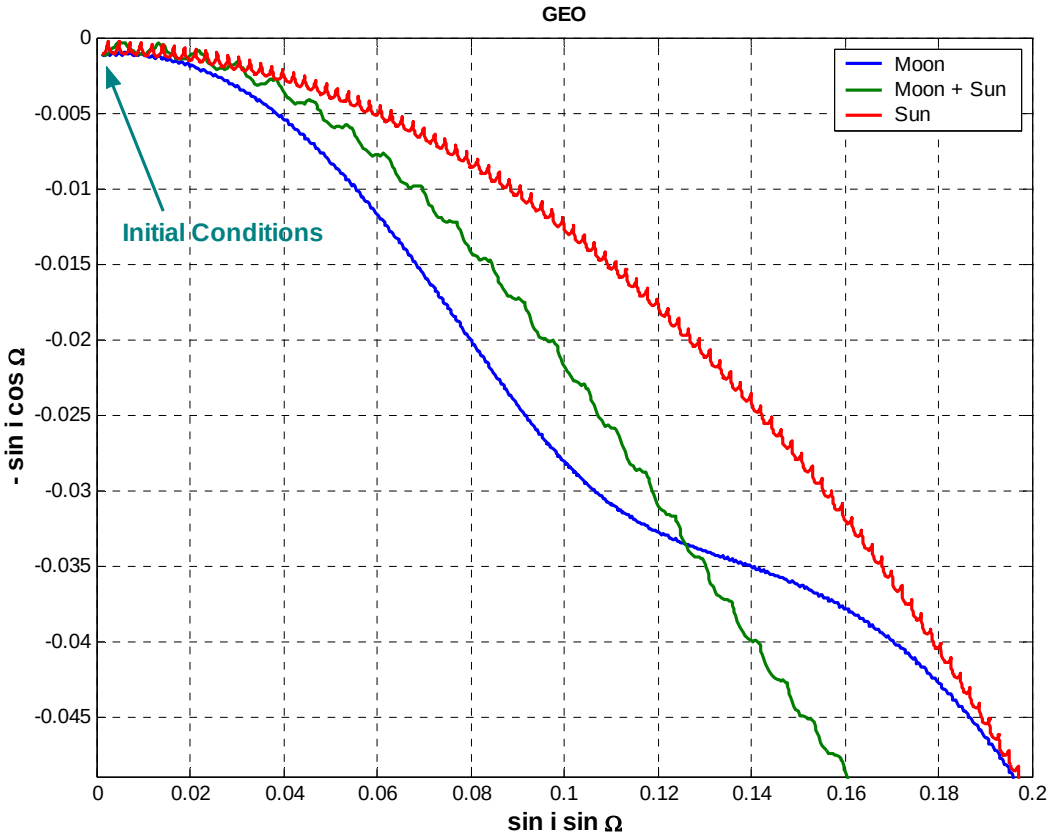

Figure 4.19

Detail of the evolution of the two-dimensional inclination vector in GEO, taking into account the third body attraction of the Moon, of the Sun, and of Moon and Sun combined. At this scale, the small wobble induced by the Sun, with a period of about 6 months, is clearly discernible in the red and green curves. The analogous short-term oscillations due to the Moon are smaller by approximately one order of magnitude and cannot be easily identified in the blue curve.

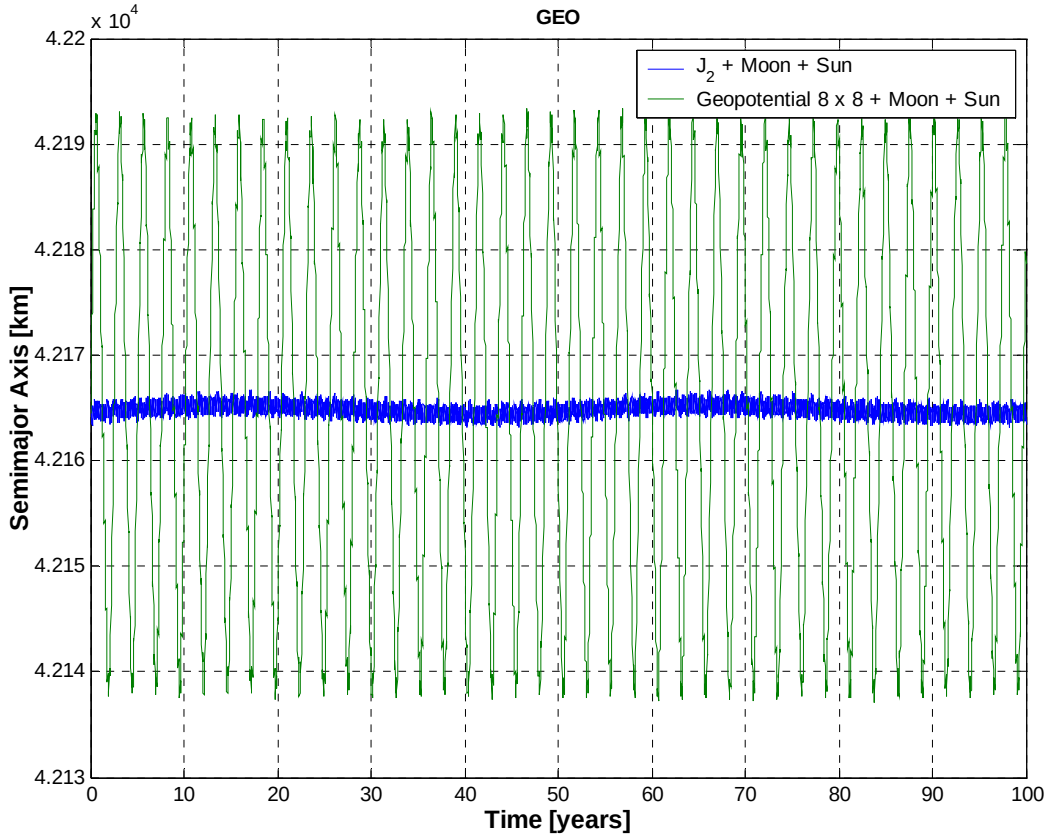

Figure 4.20

Long-term semimajor axis evolution in GEO, taking into account the geopotential harmonics, either J_2 or 8×8, and the combined Moon and Sun third body attraction. The impact of the resonant tesseral harmonics, in particular J_{22}, is evident.

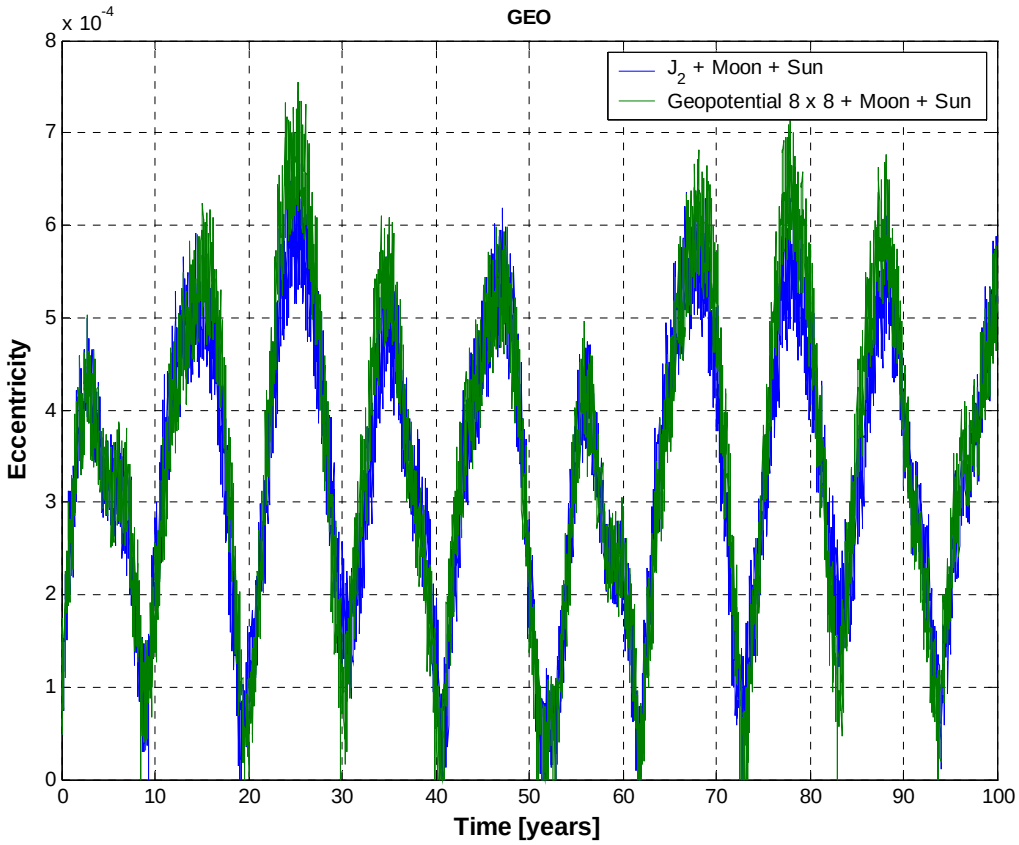

Figure 4.21

Long-term eccentricity evolution in GEO, taking into account the geopotential harmonics, either J_2 or 8×8, and the combined Moon and Sun third body attraction. The main effect, driven by the Moon, was an oscillation with an amplitude of $\sim 6 \times 10^{-4}$ and a period of about 10.4 years.

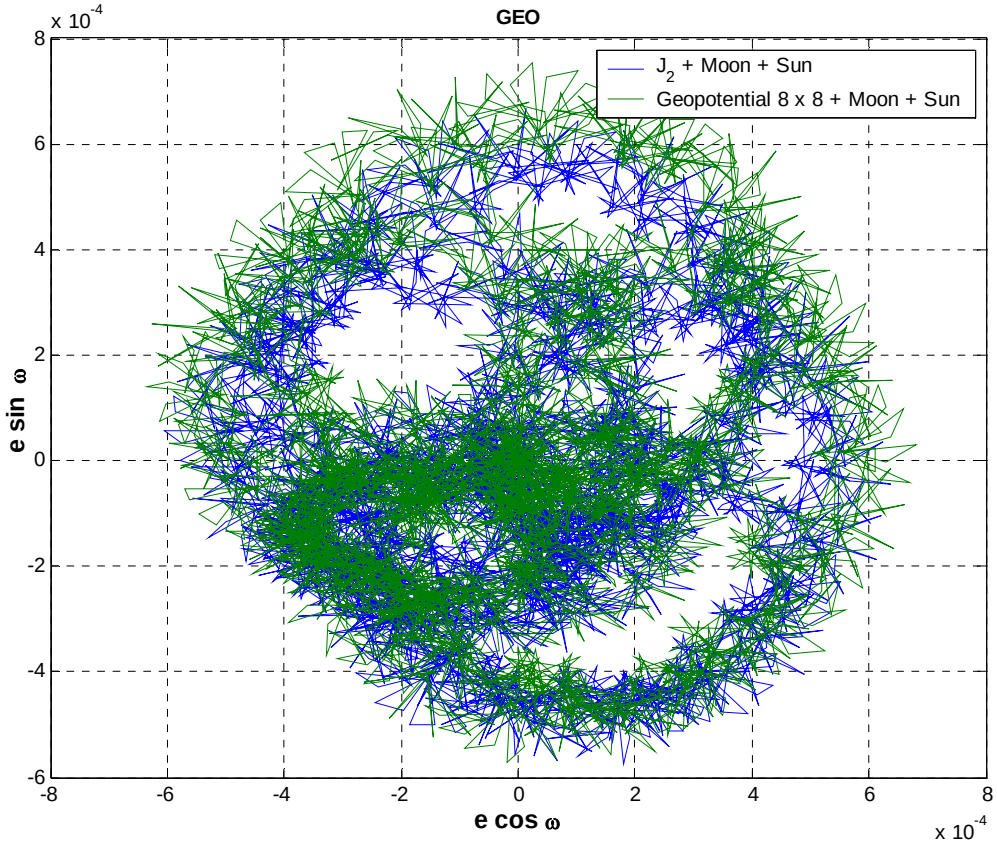

Figure 4.22

Evolution, over 100 years, of the eccentricity vector in GEO, taking into account the geopotential harmonics, either J_2 or 8 × 8, and the combined Moon and Sun third body attraction. The initial value of the eccentricity vector was ≅ [−7.6 × 10^{-5}, −6.4 × 10^{-5}]. The precessional motion was quite complicated, but was dominated by the Moon third body perturbation.

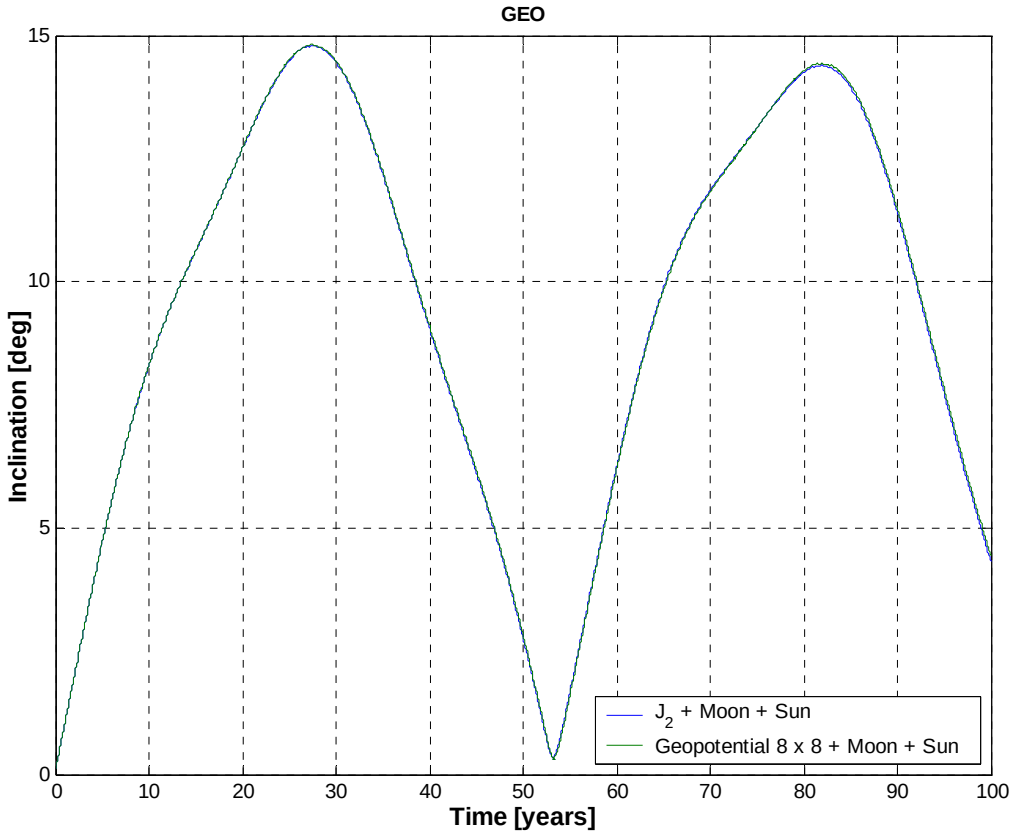

Figure 4.23

Long-term inclination evolution in GEO, taking into account the geopotential harmonics, either J_2 or 8×8, and the combined Moon and Sun third body attraction. The main effect, well known in the case of abandoned geosynchronous satellites, was the long-term oscillation of the inclination, with a maximum value of almost 15 deg and a period of 53.3 years. This evolution was driven by the combined action of the Earth's oblateness (J_2) and luni-solar third body attraction.

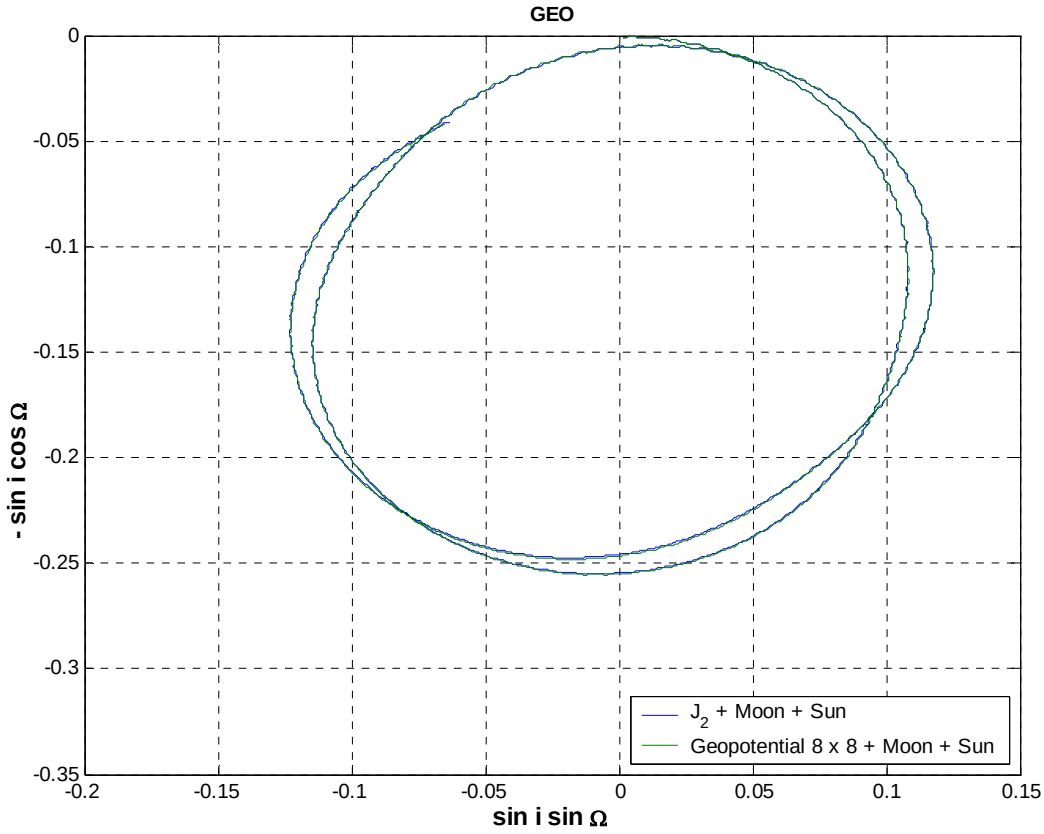

Figure 4.24

Evolution, over 100 years, of the two-dimensional inclination vector in GEO, taking into account the geopotential harmonics, either J_2 or 8×8, and the combined Moon and Sun third body attraction. The initial value of the inclination vector was $\cong [1.3 \times 10^{-3}, -1.1 \times 10^{-3}]$. The foremost effect, well known in the case of abandoned geosynchronous satellites, was the clockwise orbit pole precession, with a period of 53.3 years. This evolution was driven by the combined action of the Earth's oblateness (J_2) and luni-solar third body attraction. In addition, a small wobbling motion, with a period of about 6 months, was superimposed to the main precession.

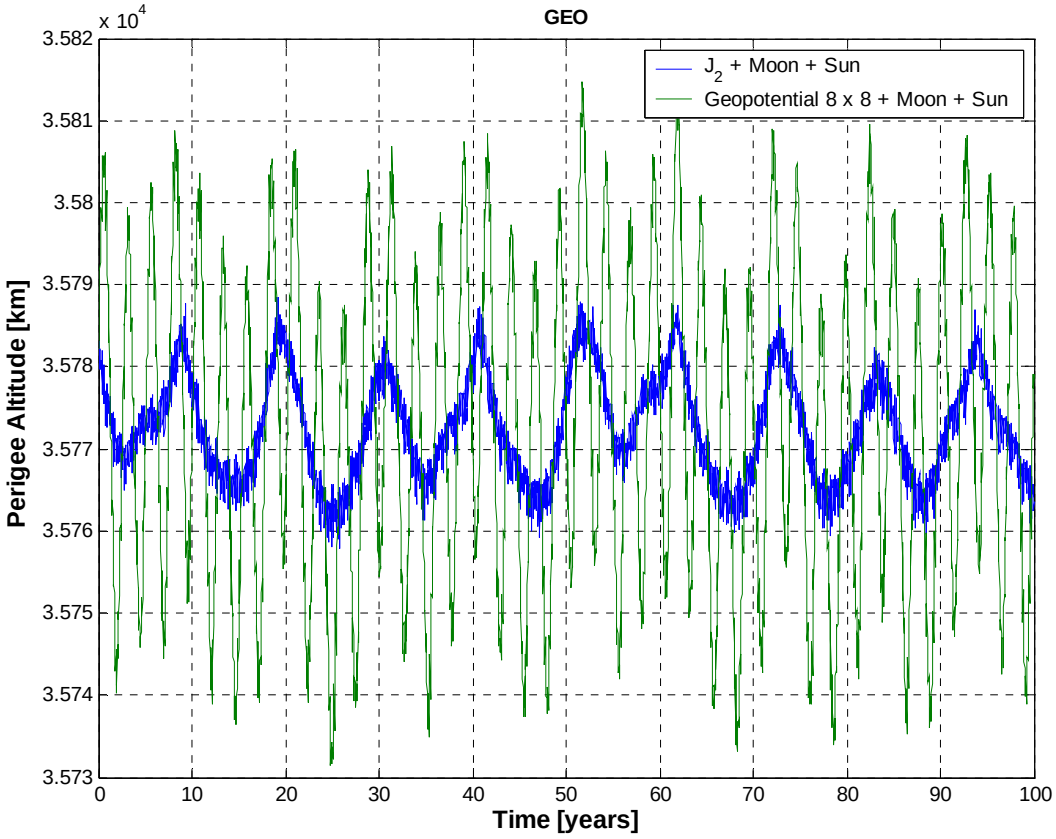

Figure 4.25

Long-term evolution of the perigee altitude in GEO, taking into account the geopotential harmonics, either J_2 or 8×8, and the combined Moon and Sun third body attraction. The impact of the resonant tesseral harmonics, in particular J_{22}, is evident.

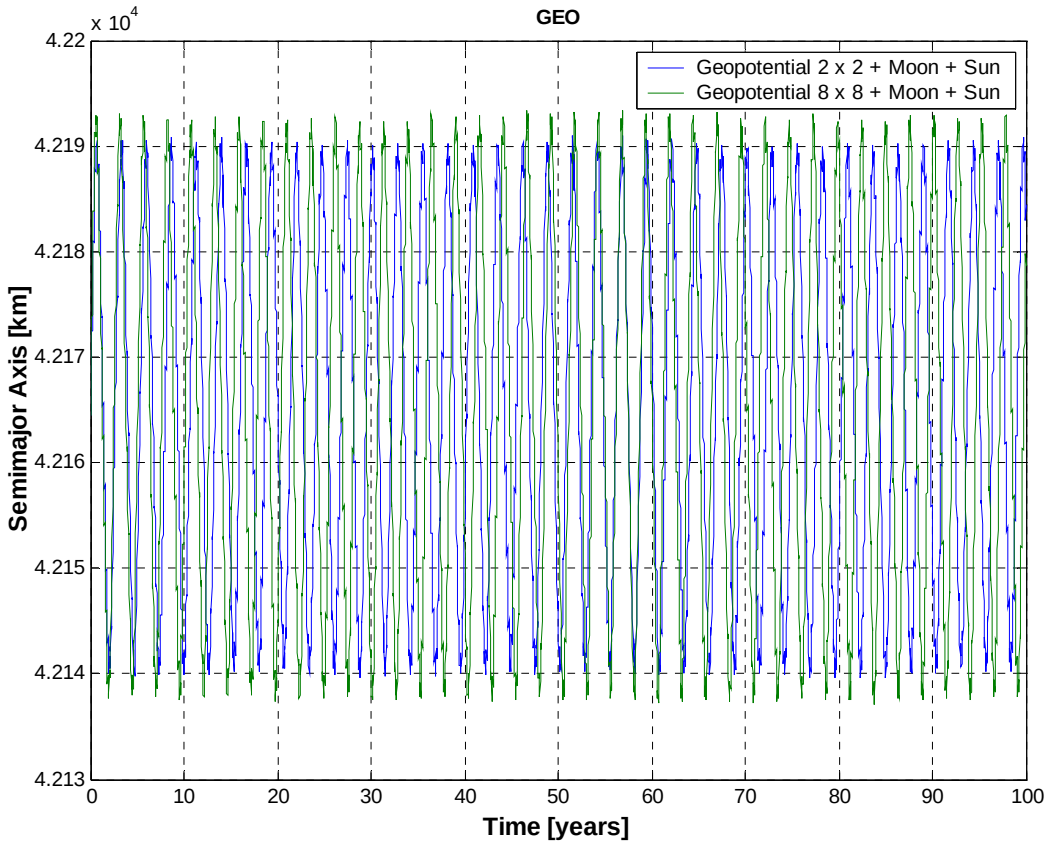

Figure 4.26

Long-term semimajor axis evolution in GEO, taking into account the geopotential harmonics, either 2×2 or 8×8, and the combined Moon and Sun third body attraction. The differences were very small, due to the dominant influence of J_{22}.

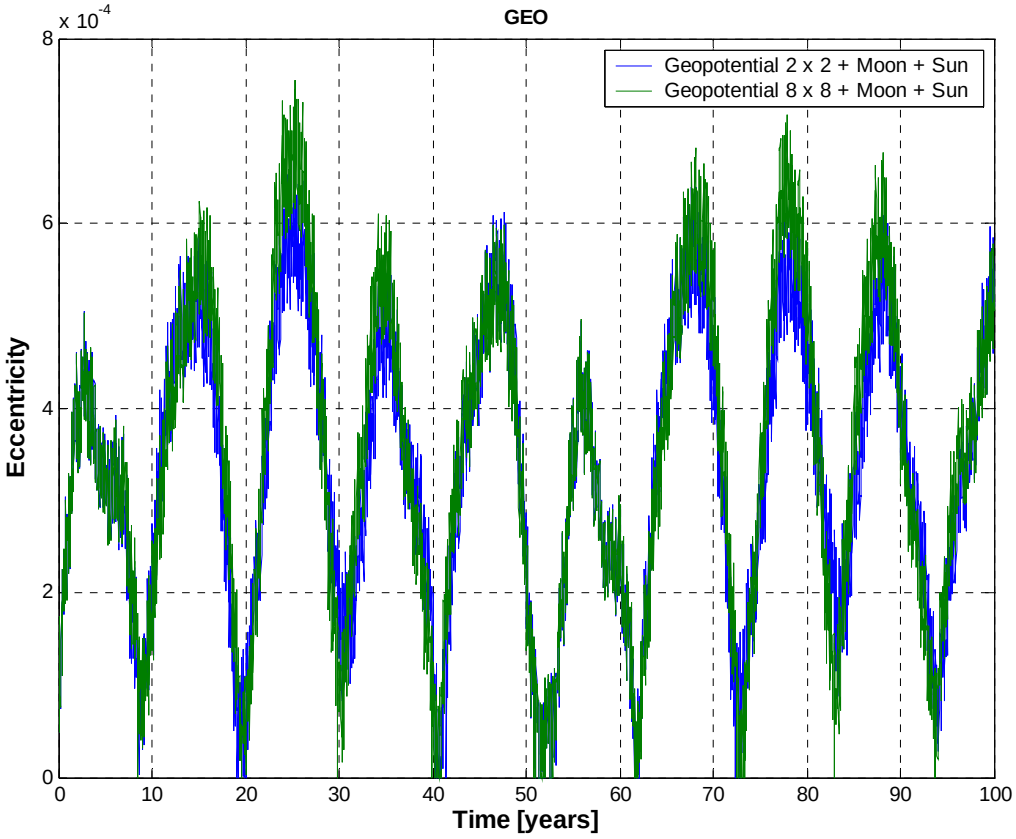

Figure 4.27

Long-term eccentricity evolution in GEO, taking into account the geopotential harmonics, either 2×2 or 8×8, and the combined Moon and Sun third body attraction. There were no appreciable differences between the results obtained with the 2×2 harmonics or with J_2 (see Figure 4.21).

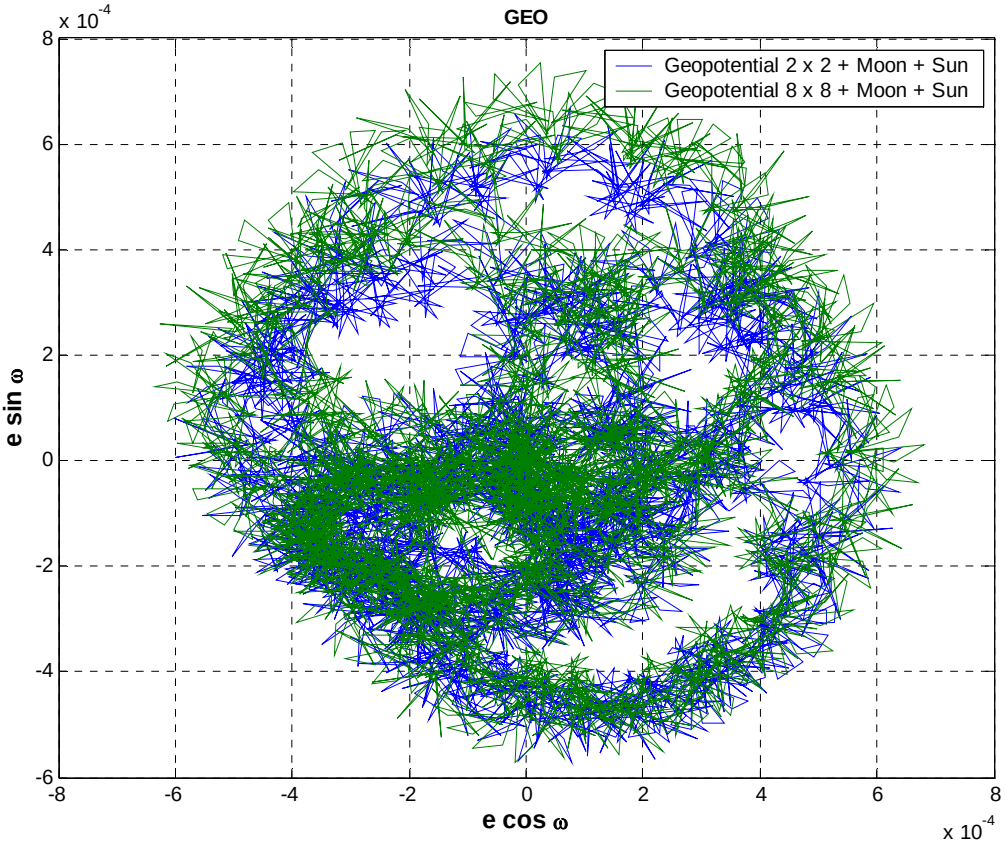

Figure 4.28

Evolution, over 100 years, of the eccentricity vector in GEO, taking into account the geopotential harmonics, either 2 × 2 or 8 × 8, and the combined Moon and Sun third body attraction. The initial value of the eccentricity vector was ≅ [-7.6×10^{-5}, -6.4×10^{-5}]. There were no significant differences between the results obtained with the 2 × 2 harmonics or with J_2 (see Figure 4.22).

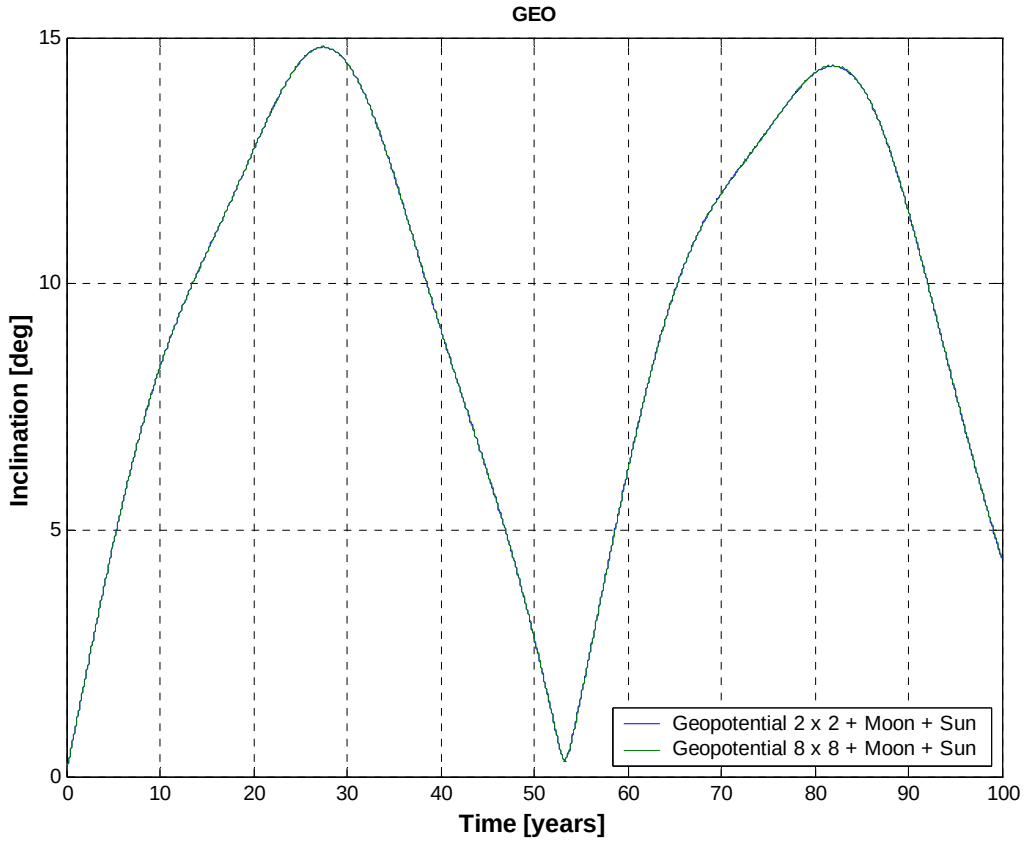

Figure 4.29

Long-term inclination evolution in GEO, taking into account the geopotential harmonics, either 2×2 or 8×8, and the combined Moon and Sun third body attraction. Being the evolution driven by the combined action of the Earth's oblateness (J_2) and luni-solar third body attraction, there was no appreciable difference between the two curves and the results obtained with J_2 (see Figure 4.23).

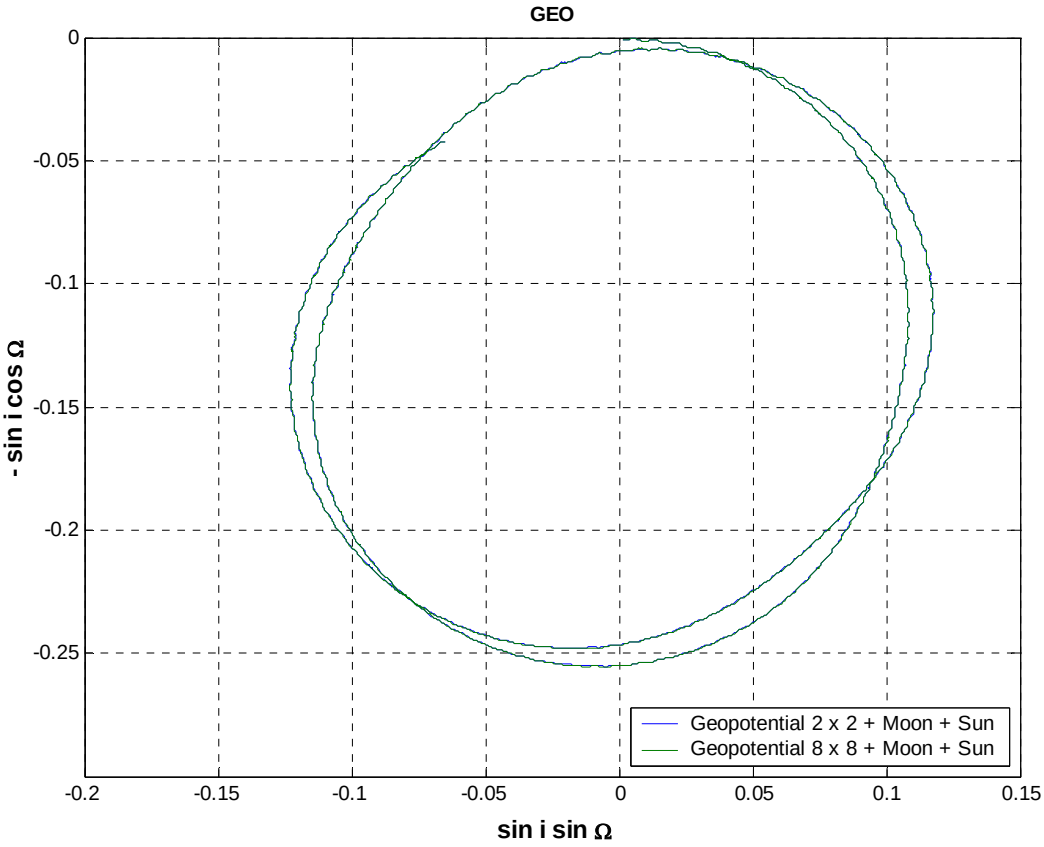

Figure 4.30

Evolution, over 100 years, of the two-dimensional inclination vector in GEO, taking into account the geopotential harmonics, either 2 × 2 or 8 × 8, and the combined Moon and Sun third body attraction. The initial value of the inclination vector was $\cong [1.3 \times 10^{-3}, -1.1 \times 10^{-3}]$. Being the evolution driven by the combined action of the Earth's oblateness (J_2) and luni-solar third body attraction, there was no appreciable difference between the two curves and the results obtained with J_2 (see Figure 4.24).

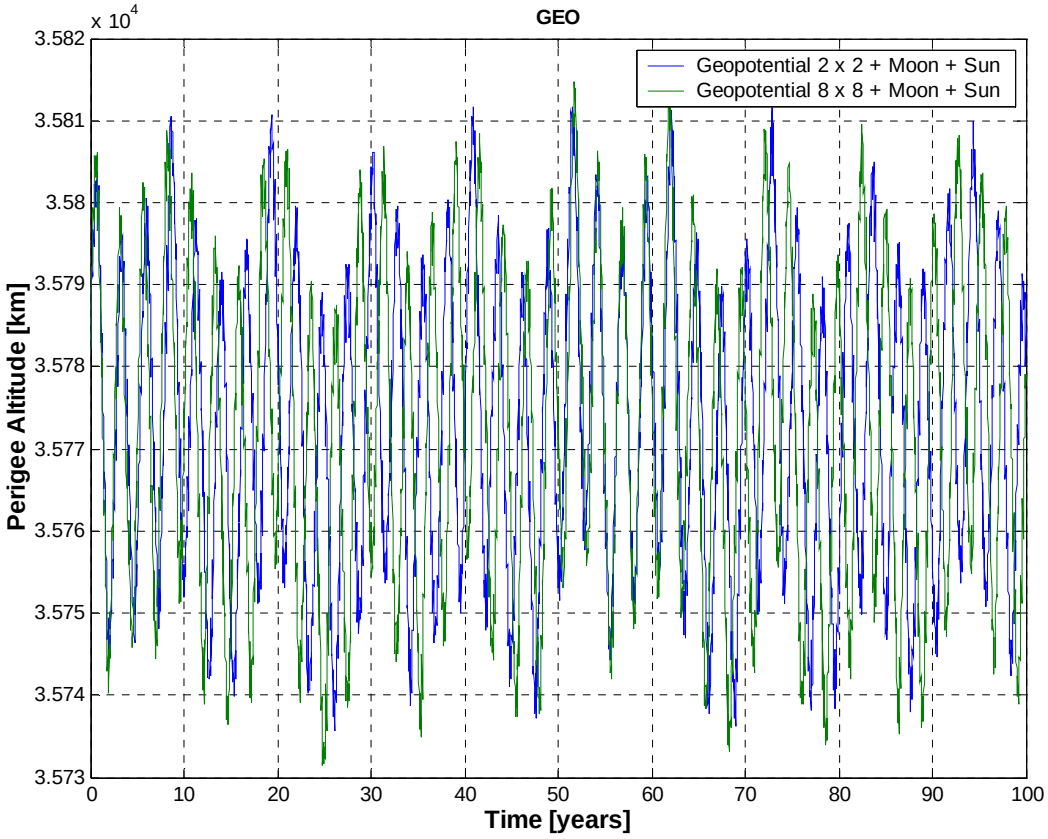

Figure 4.31

Long-term evolution of the perigee altitude in GEO, taking into account the geopotential harmonics, either 2 × 2 or 8 × 8, and the combined Moon and Sun third body attraction. The differences were very small, due to the dominant influence of J_{22}.

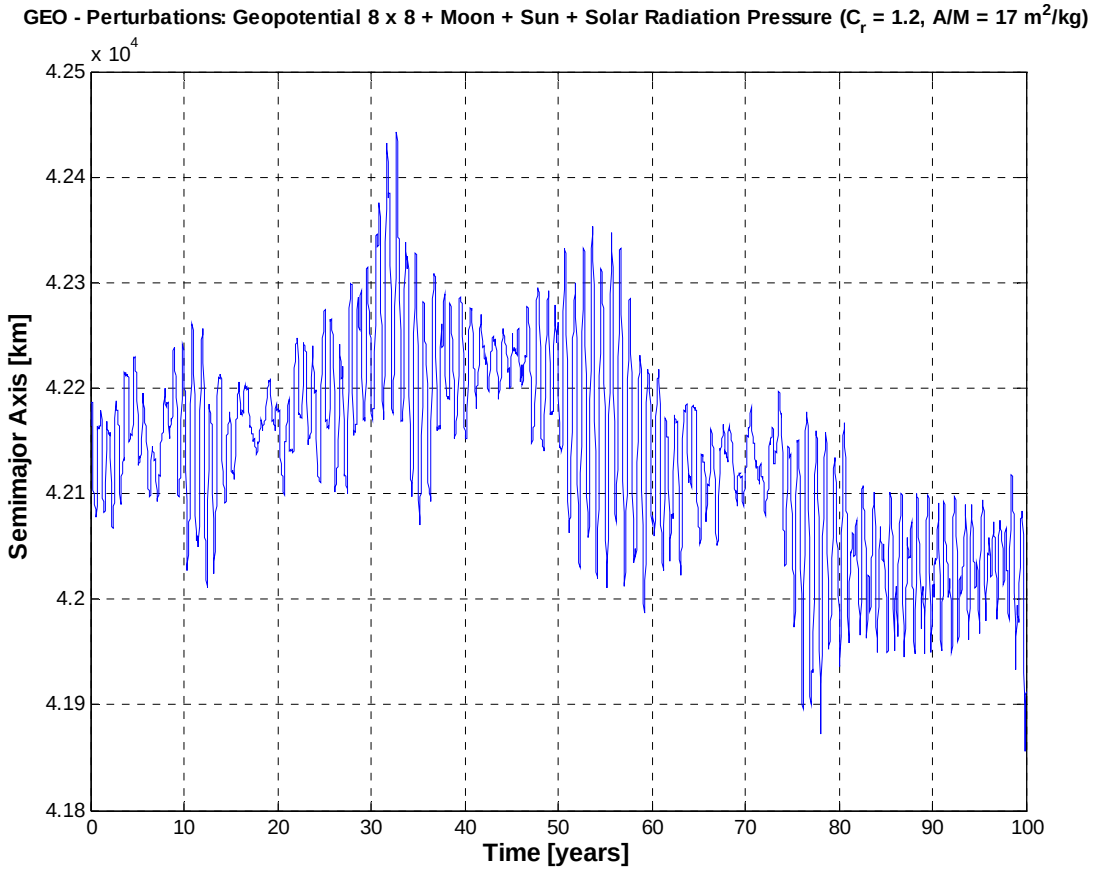

Figure 4.32

Long-term semimajor axis evolution in GEO, taking into account the geopotential harmonics, up to the 8th degree and order, the combined Moon and Sun third body attraction and direct solar radiation pressure, with eclipses. The oscillations with a period of about 1 year, induced by the combined effects of solar radiation pressure and Earth's shadow, are very evident in this example with $C_r \times A/M = 20.4$ m^2/kg.

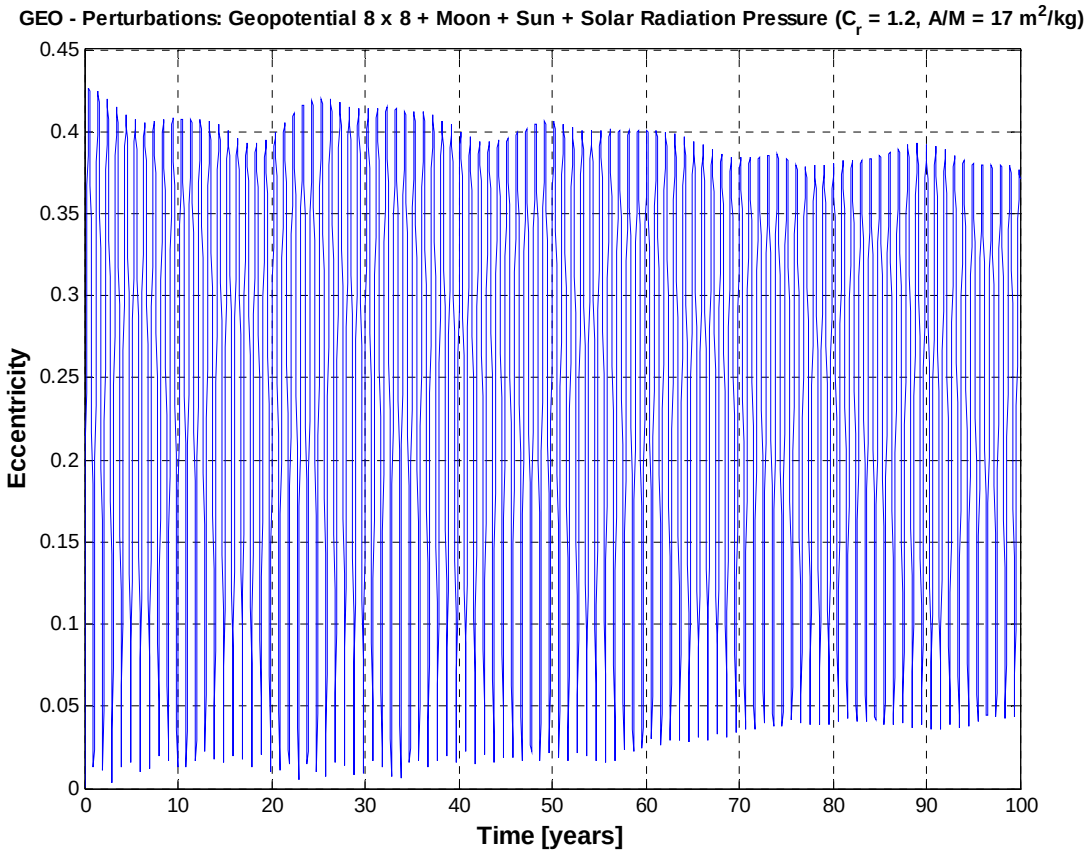

Figure 4.33

Long-term semimajor axis evolution in GEO, taking into account the geopotential harmonics, up to the 8th degree and order, the combined Moon and Sun third body attraction and direct solar radiation pressure, with eclipses. The large oscillations, with a period of about 1 year, were due to solar radiation pressure, in this example with $C_r \times A/M = 20.4$ m^2/kg.

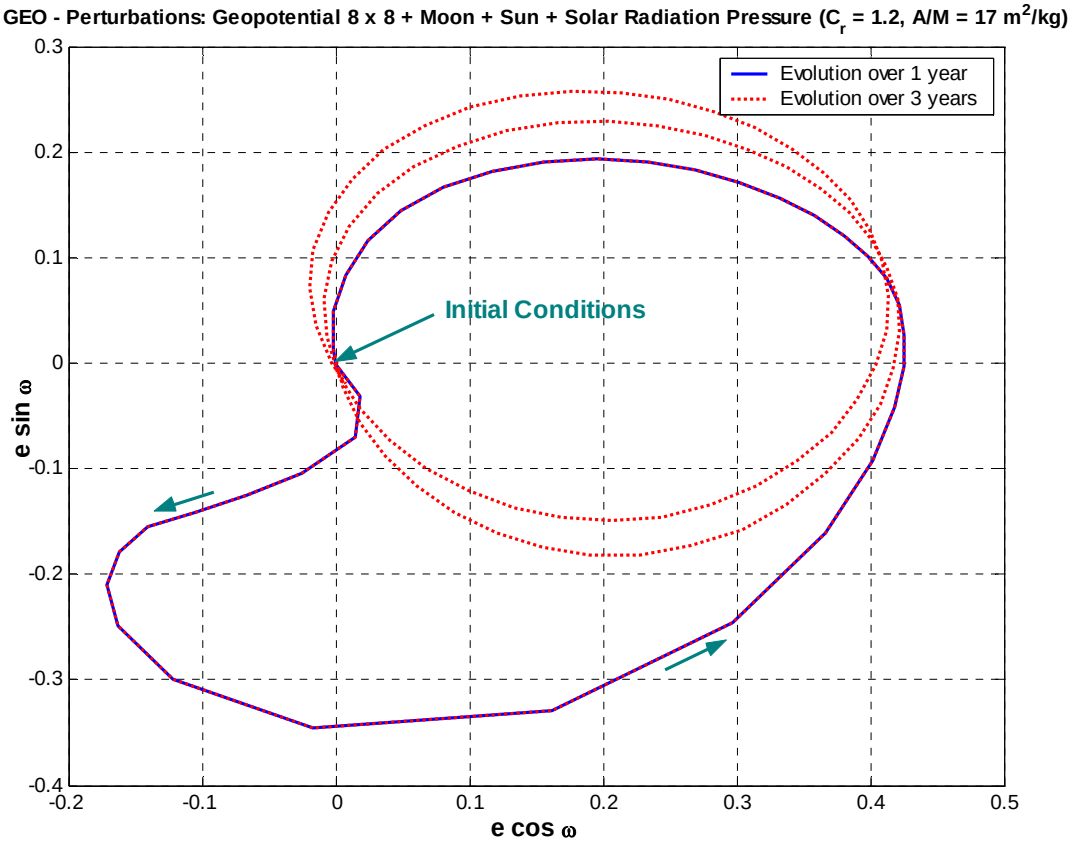

Figure 4.34

Evolution of the eccentricity vector in GEO, taking into account the geopotential harmonics, up to the 8th degree and order, the combined Moon and Sun third body attraction and direct solar radiation pressure, with eclipses. The presence of a very intense solar radiation pressure ($C_r \times A/M$ = 20.4 m^2/kg) induced two anti-clockwise precessions, one with a period of about 1 year and the other with a much longer duration.

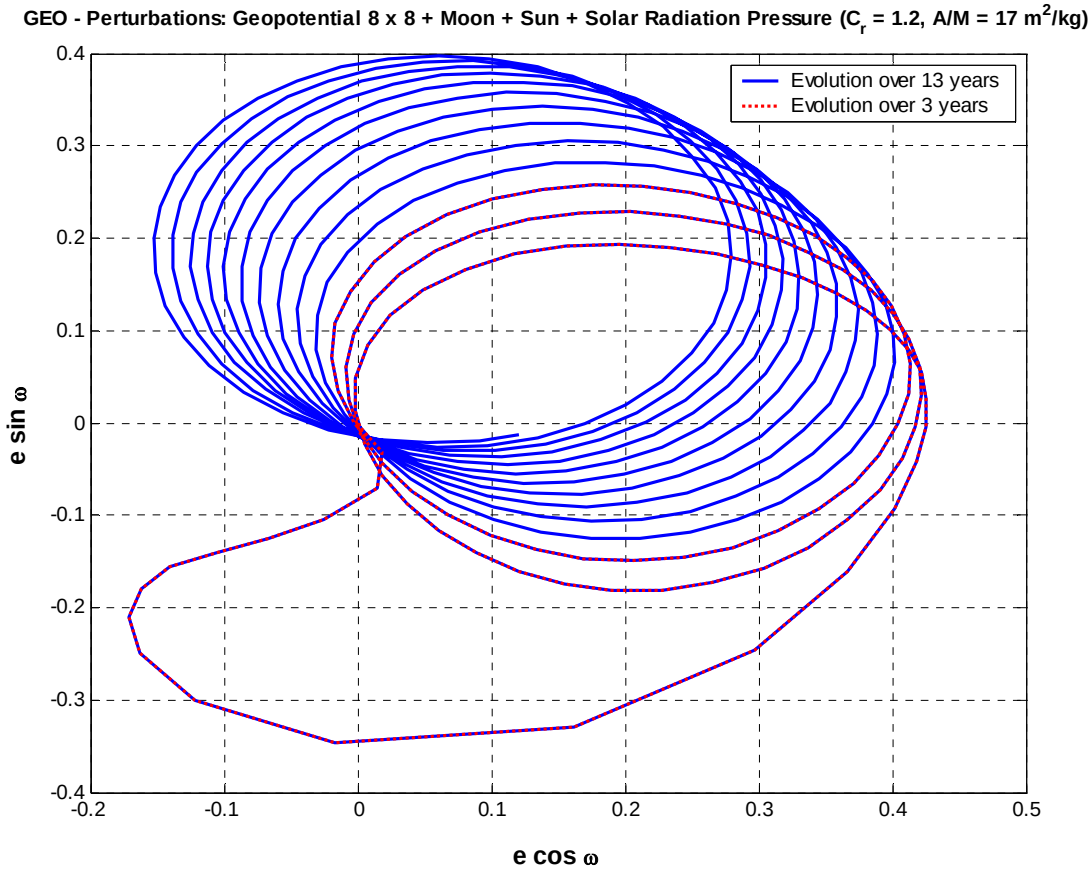

Figure 4.35

Evolution of the eccentricity vector in GEO, taking into account the geopotential harmonics, up to the 8th degree and order, the combined Moon and Sun third body attraction and direct solar radiation pressure, with eclipses. The initial value of the eccentricity vector was ≅ [–7.6 × 10^{-5}, –6.4 × 10^{-5}]. The presence of a very intense solar radiation pressure ($C_r \times A/M$ = 20.4 m^2/kg) induced two anti-clockwise precessions, one with a period of about 1 year and the other with a much longer duration.

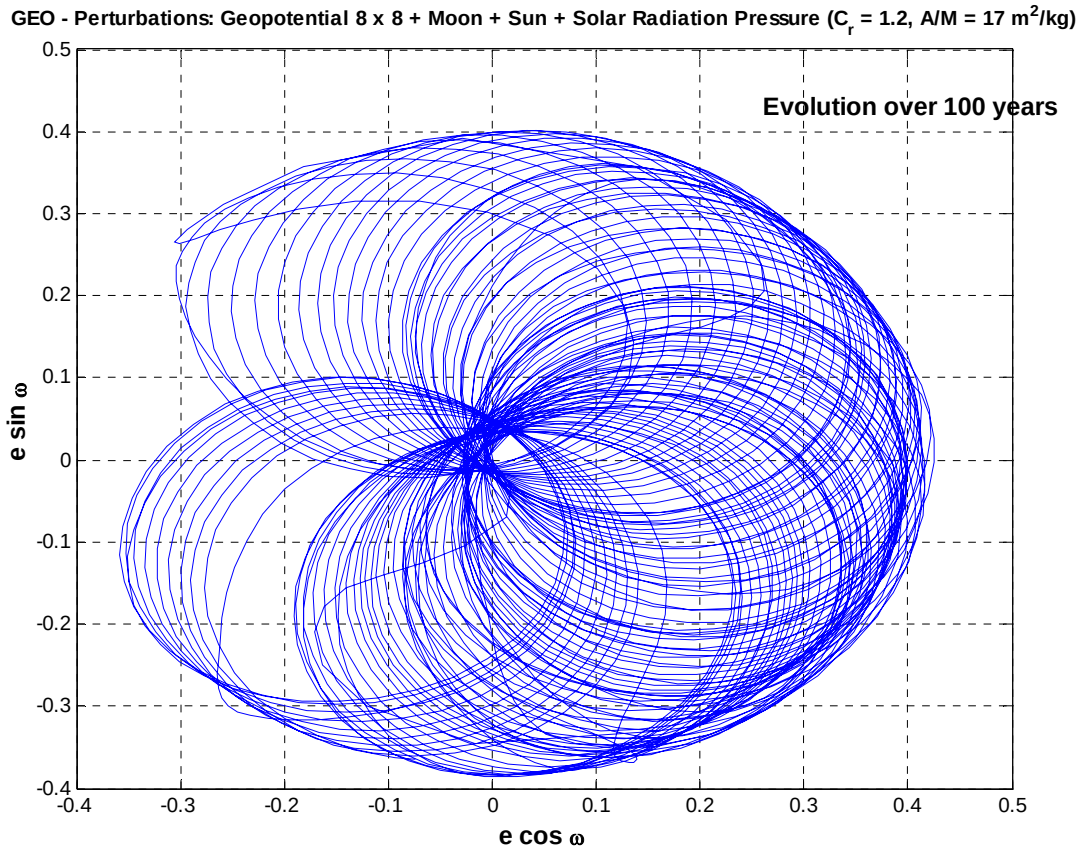

Figure 4.36

Evolution, over 100 years, of the eccentricity vector in GEO, taking into account the geopotential harmonics, up to the 8th degree and order, the combined Moon and Sun third body attraction and direct solar radiation pressure, with eclipses. The initial value of the eccentricity vector was $\cong [-7.6 \times 10^{-5}, -6.4 \times 10^{-5}]$. The presence of a very intense solar radiation pressure ($C_r \times A/M$ = 20.4 m^2/kg) basically induced two anti-clockwise precessions of similar amplitude, one with a period of about 1 year and the other with a period of many decades.

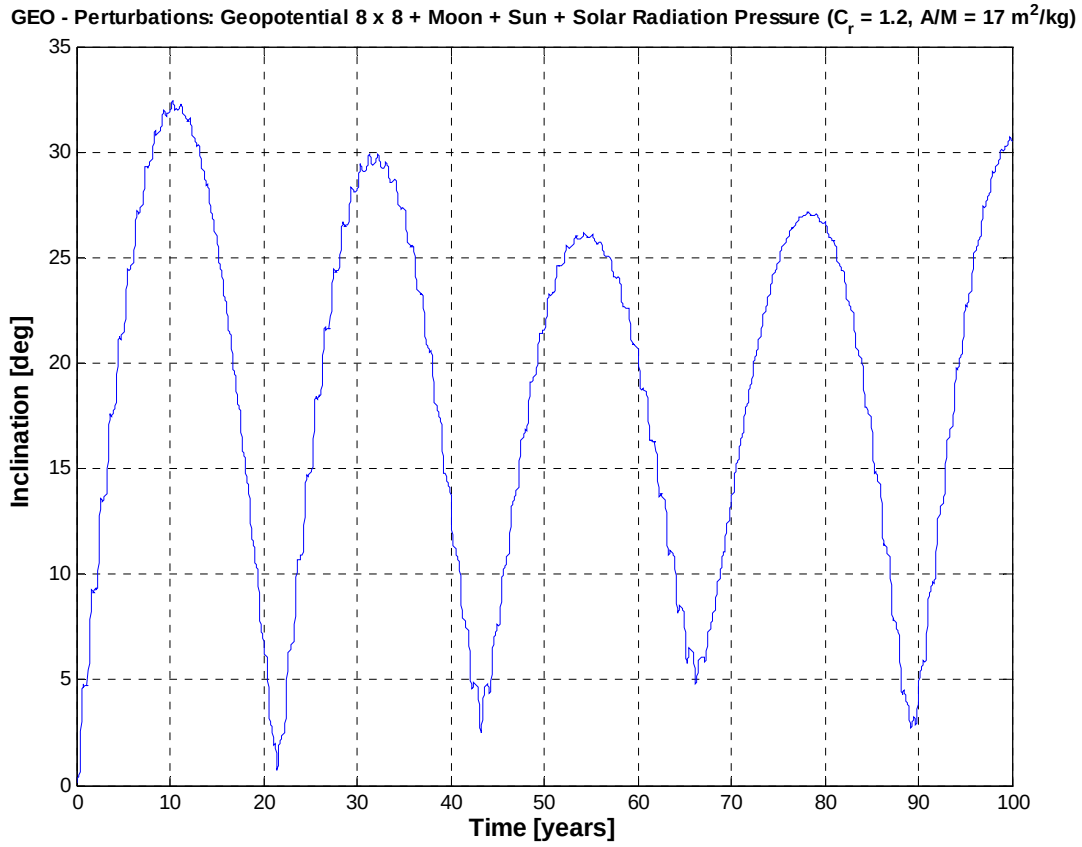

Figure 4.37

Long-term inclination evolution in GEO, taking into account the geopotential harmonics, up to the 8th degree and order, the combined Moon and Sun third body attraction and direct solar radiation pressure, with eclipses. The action of a considerable solar radiation pressure ($C_r \times A/M$ = 20.4 m^2/kg), combined with the Earth's oblateness (J_2) and luni-solar third body attraction, substantially modified the inclination evolution, increasing the amplitude of the oscillation (up to more than 30 deg) and reducing its period (to about 22 years).

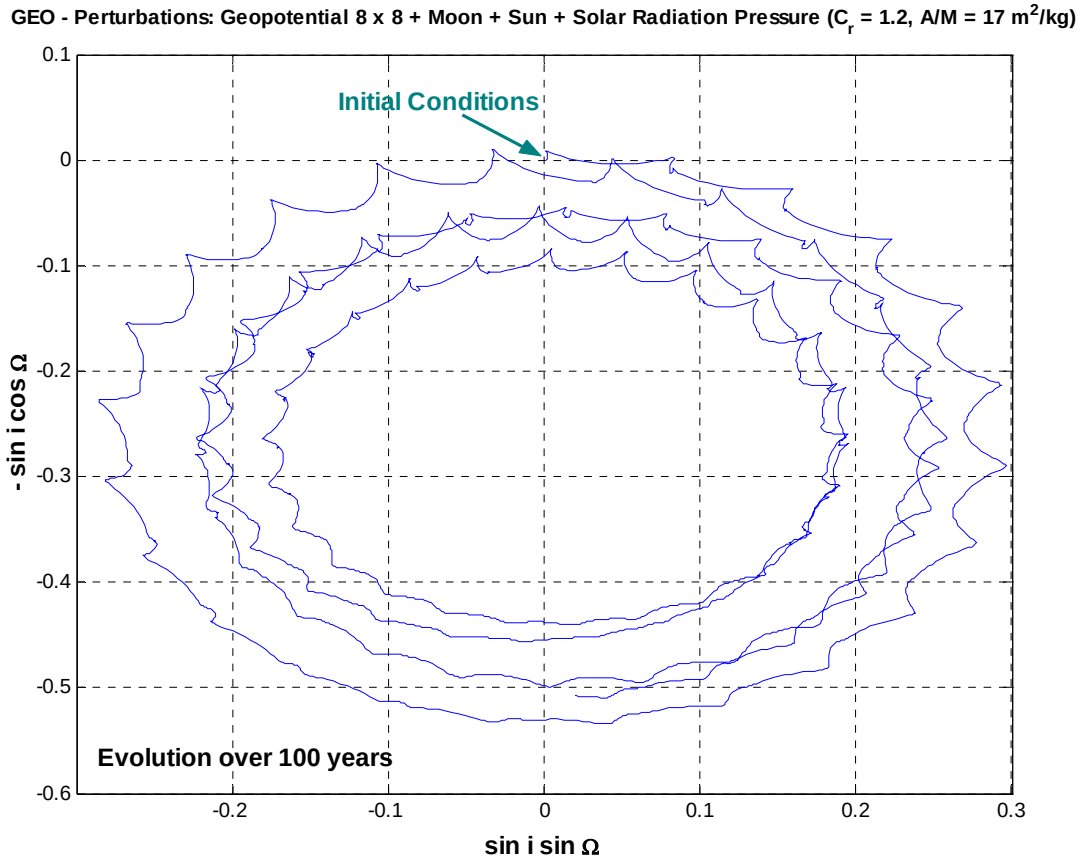

Figure 4.38

Evolution, over 100 years, of the two-dimensional inclination vector in GEO, taking into account the geopotential harmonics, up to the 8th degree and order, the combined Moon and Sun third body attraction and direct solar radiation pressure, with eclipses. The action of a fairly large solar radiation pressure ($C_r \times A/M$ = 20.4 m^2/kg), combined with the Earth's oblateness (J_2) and luni-solar third body attraction, substantially modified the classic clockwise orbit pole precession (see Figures 4.24 and 4.30), increasing its amplitude and reducing its period (to about 22 years, in this example). A small wobble, with a period of approximately 1 year, is also clearly present.

GLOSSARY

A/M	Area-to-Mass ratio
ASAP	Artificial Satellite Analysis Program
CNR	Consiglio Nazionale delle Ricerche (Italian National Research Council)
CPU	Central Processing Unit
e	Eccentricity of the orbit
ESA	European Space Agency
ESOC	European Space Operations Centre
GEO	GEosynchronous Orbit
GPS	Global Positioning System
GTO	Geosynchronous Transfer Orbit
i	Inclination of the orbit with respect to the Earth's equator
ISTI	Istituto di Scienza e Tecnologie dell'Informazione "Alessandro Faedo"
JPL	Jet Propulsion Laboratory
LEGO	Long-term Evolution of Geostationary and near-geostationary Orbit propagator
LOP	Long-term Orbit Predictor
SATORB	SATellite ORBit propagator
SATRAP	SATellite Reentry Analysis Program
WB1/COWELL	Orbital Work Bench, Version 1.0 (Cowell numerical propagator)
ω	Argument of perigee of the orbit
Ω	Right ascension of the ascending node of the orbit

REFERENCES

1. Kwok, J.H., The Artificial Satellite Analysis Program (ASAP), Version 2.0, JPL NPO-17522, Jet Propulsion Laboratory (JPL), Pasadena, California, USA, 20 April 1987.
2. Beutler, G., *Methods of Celestial Mechanics*, Springer, Heidelberg, Germany, 2005.
3. Pardini, C. and Anselmo, L., SATRAP: Satellite Reentry Analysis Program, Internal Report C94-17, CNUCE Institute, Consiglio Nazionale delle Ricerche (CNR), Pisa, Italy, 30 August 1994.
4. Anonymous, Orbital Workbench – Version 1.0 – Program Description & User's Manual, MS-DOS Edition, Cygnus Engineering, Sunnyvale, California, USA, 1990.
5. Anonymous, Orbital Workbench – Version 1.1 – Program Description & User's Manual, Professional Edition for MS-DOS, Cygnus Engineering, Cupertino, California, USA, 1992.
6. Van Der Ha J.C., Very Long Term Orbit Evolution of a Geostationary Satellite, MAO Working Paper No. 122, ESA/ESOC, Darmstadt, Germany, March 1980.
7. Kwok J.H., The Long-Term Orbit Predictor (LOP), Version 2.0, NPO-17052, Jet Propulsion Laboratory, Pasadena, California, USA, June 1986.
8. Valk, S., Solar Radiation Pressure Modeling. Comparison with SATRAP: Eccentricity Dynamics, Presentation handout, Facultés Universitaires Notre-Dame de la Paix, Unité de Systèmes Dynamiques et Mécanique Céleste, Namur, Belgium, 9 February 2007.
9. Anselmo, L., Long-Term Evolution of Geosynchronous Orbits with High Area-to-Mass Ratio: SATRAP-1 vs. SATRAP-2, Presentation handout, Istituto di Scienza e Tecnologie dell'Informazione "Alessandro Faedo", Consiglio Nazionale delle Ricerche (CNR), Pisa, Italy, 15 February 2007.
10. Anselmo, L. and Pardini, C., Orbital Evolution of Geosynchronous Objects with High Area-to-Mass Ratios, Proceedings of the Fourth European Conference on Space Debris, ESA SP-587, ESA Publication Division, Noordwijk, The Netherlands, August 2005, pp. 279-284.
11. Pardini, C. and Anselmo, L., Long-Term Evolution of Geosynchronous Orbital Debris with High Area-to-Mass Ratios, Proceedings of the 25th International Symposium on Space Technology and Science (Selected Papers), Japan Society for Aeronautical and Space Sciences and Organizing Committee of the 25th ISTS, Kanazawa, Japan, 2006, pp. 1322-1327.
12. Pardini, C. and Anselmo, L., Long-Term Evolution of Geosynchronous Orbital Debris with High Area-to-Mass Ratios, ISTI Technical Report 2007-TR-03, Istituto di Scienza e Tecnologie dell'Informazione "Alessandro Faedo", Consiglio Nazionale delle Ricerche (CNR), Pisa, Italy, 5 March 2007.
13. Anselmo, L., Effects of Perturbations on the Long-Term Evolution of Geosynchronous Orbits, Presentation handout, Istituto di Scienza e Tecnologie dell'Informazione "Alessandro Faedo", Consiglio Nazionale delle Ricerche (CNR), Pisa, Italy, 11 July 2006.

14. Anselmo, L., Long-Term Evolution of Geosynchronous Objects with High Area-to-Mass Ratio: Additional Tests with SATRAP and SATORB, Presentation handout, Istituto di Scienza e Tecnologie dell'Informazione "Alessandro Faedo", Consiglio Nazionale delle Ricerche (CNR), Pisa, Italy, 20 November 2006.
15. Anselmo, L., Long-Term Simulations of Objects in High-Earth Orbits, ISTI Project Report 2005-PR-05, Istituto di Scienza e Tecnologie dell'Informazione "Alessandro Faedo", Consiglio Nazionale delle Ricerche (CNR), Pisa, Italy, 6 December 2005.
16. Martinot, V., LEGO: An Orbit Propagator for Long-Term Evolution of Geostationary and Near-Geostationary Orbits, MAS Technical Note No. 3, Mission Analysis Section, Mission Operations Department, ESA/ESOC, Darmstadt, Germany, March 2006.